



MULTIDISCIPLINARY CENTER FOR EARTHQUAKE ENGINEERING RESEARCH
A National Center of Excellence in Advanced Technology Applications

ISSN 1520-295X

Property Modification Factors for Seismic Isolation Bearings

by

Michael C. Constantinou, Panos Tsopelas,
Amarnath Kasalanati and Eric D. Wolff
University at Buffalo, State University of New York
Department of Civil, Structural and Environmental Engineering
Ketter Hall
Buffalo, New York 14260

Technical Report MCEER-99-0012

July 20, 1999

This research was conducted at the University at Buffalo, State University of New York and was supported by the Federal Highway Administration under contract number DTFH61-92-C-00106.

@Seismicisolation

Telegram Channel: @Seismicisolation

NOTICE

This report was prepared by University at Buffalo, State University of New York as a result of research sponsored by the Multidisciplinary Center for Earthquake Engineering Research (MCEER) through a contract from the Federal Highway Administration. Neither MCEER, associates of MCEER, its sponsors, University at Buffalo, State University of New York, nor any person acting on their behalf:

- a. makes any warranty, express or implied, with respect to the use of any information, apparatus, method, or process disclosed in this report or that such use may not infringe upon privately owned rights; or
- b. assumes any liabilities of whatsoever kind with respect to the use of, or the damage resulting from the use of, any information, apparatus, method, or process disclosed in this report.

Any opinions, findings, and conclusions or recommendations expressed in this publication are those of the author(s) and do not necessarily reflect the views of MCEER or the Federal Highway Administration.



Telegram Channel: [@Seismicisolation](https://t.me/Seismicisolation)



Property Modification Factors for Seismic Isolation Bearings

by

Michael C. Constantinou¹, Panos Tsopelas², Amarnath Kasalanati³
and Eric D. Wolff⁴

Publication Date: July 20, 1999
Submittal Date: February 19, 1999

Technical Report MCEER-99-0012

Task Number 106-F-4.2.1(a)

FHWA Contract Number DTFH61-92-C-00106

- 1 Professor, Department of Civil, Structural and Environmental Engineering, University at Buffalo, State University of New York
- 2 Assistant Professor, Department of Civil Engineering, The Catholic University of America; former Research Scientist, Department of Civil, Structural and Environmental Engineering, University at Buffalo, State University of New York
- 3 Project Engineer, DIS, Inc.; former Graduate Research Assistant, Department of Civil, Structural and Environmental Engineering, University at Buffalo, State University of New York
- 4 Graduate Research Assistant, Department of Civil, Structural and Environmental Engineering, University at Buffalo, State University of New York

MULTIDISCIPLINARY CENTER FOR EARTHQUAKE ENGINEERING RESEARCH
University at Buffalo, State University of New York
Red Jacket Quadrangle, Buffalo, NY 14261

@Seismicisolation

Telegram Channel: @Seismicisolation

Preface

The Multidisciplinary Center for Earthquake Engineering Research (MCEER) is a national center of excellence in advanced technology applications that is dedicated to the reduction of earthquake losses nationwide. Headquartered at the University at Buffalo, State University of New York, the Center was originally established by the National Science Foundation in 1986, as the National Center for Earthquake Engineering Research (NCEER).

Comprising a consortium of researchers from numerous disciplines and institutions throughout the United States, the Center's mission is to reduce earthquake losses through research and the application of advanced technologies that improve engineering, pre-earthquake planning and post-earthquake recovery strategies. Toward this end, the Center coordinates a nationwide program of multidisciplinary team research, education and outreach activities.

MCEER's research is conducted under the sponsorship of two major federal agencies, the National Science Foundation (NSF) and the Federal Highway Administration (FHWA), and the State of New York. Significant support is also derived from the Federal Emergency Management Agency (FEMA), other state governments, academic institutions, foreign governments and private industry.

The Center's FHWA-sponsored Highway Project develops retrofit and evaluation methodologies for existing bridges and other highway structures (including tunnels, retaining structures, slopes, culverts, and pavements), and improved seismic design criteria and procedures for bridges and other highway structures. Specifically, tasks are being conducted to:

- assess the vulnerability of highway systems, structures and components;
- develop concepts for retrofitting vulnerable highway structures and components;
- develop improved design and analysis methodologies for bridges, tunnels, and retaining structures, which include consideration of soil-structure interaction mechanisms and their influence on structural response;
- review and recommend improved seismic design and performance criteria for new highway systems and structures.

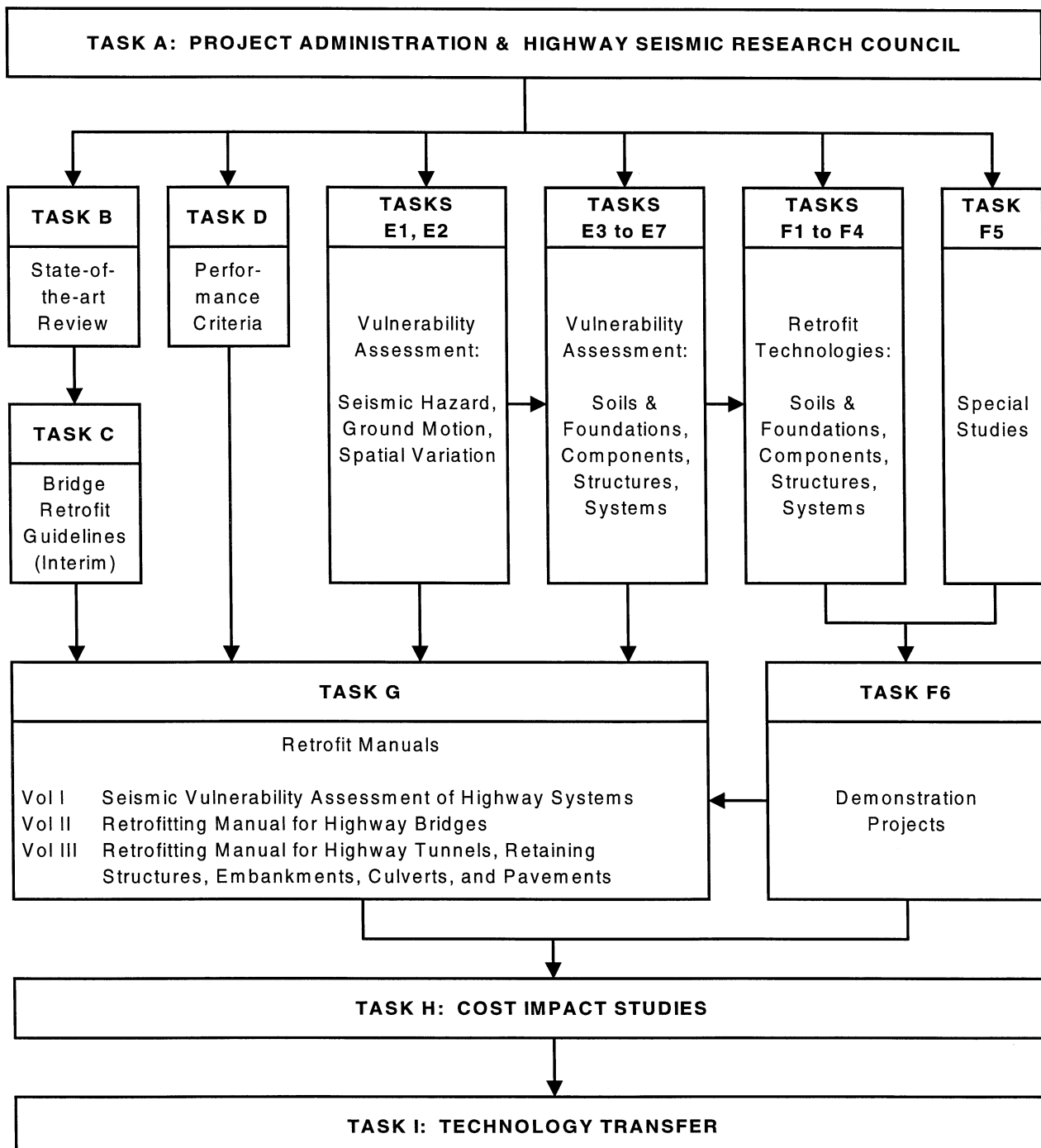
Highway Project research focuses on two distinct areas: the development of improved design criteria and philosophies for new or future highway construction, and the development of improved analysis and retrofitting methodologies for existing highway systems and structures. The research discussed in this report is a result of work conducted under the existing highway structures project, and was performed within Task 106-F-4.2.1(a), "Longevity and Reliability of Sliding Seismic Isolation Systems" of that project as shown in the flowchart on the following page.

The overall objective of this task was to develop an improved understanding of the expected performance and behavior of sliding isolation systems; evaluate their functionality, reliability, and longevity; and assist in the development of improved codes and specifications for their use. This report deals with the problem of establishing upper and lower bound values of properties

of seismic isolation bearings for use in the analysis and design of seismically isolated bridges. These bounding values of properties are determined by using system property modification factors or λ -factors.

On the basis of experimental results and an understanding of the basic behavior of seismic isolation bearings, λ -factor values are presented for several of these properties, including the effects of aging, contamination, travel, temperature and scrapping for selected sliding interfaces and elastomeric bearings. The concepts presented and the values of the λ -factors represent the basis on which bounding analysis is described in the new 1999 "AASHTO Guide Specifications for Seismic Isolation Design."

SEISMIC VULNERABILITY OF EXISTING HIGHWAY CONSTRUCTION
FHWA Contract DTFH61-92-C-00106



ABSTRACT

This report deals with the problem of establishing upper and lower bound values of properties of seismic isolation bearings for use in the analysis and design of seismically isolated bridges. These bounding values of properties are determined with the use of system property modification factors or λ -factors.

The λ -factors account for the effects of the history of loading, the environmental conditions, and aging on the properties of seismic isolation bearings. While it appears that these factors can be established by testing, and indeed some of them can be so determined, the procedure requires that the mechanical behavior of the bearings be well understood both at the macroscopic and microscopic levels. Accordingly, this report devotes a major part to the subjects of aging in elastomeric and in sliding bearings, and to the nature of friction in sliding bearings.

On the basis of experimental results and an understanding of the basic behavior of seismic isolation bearings, λ -factor values are presented for the effects of aging, contamination, travel, temperature, and scragging for selected sliding interfaces and elastomeric bearings. The concepts presented and the values of the λ -factors represent the basis on which bounding analysis is described in the new 1999 AASHTO Guide Specifications for Seismic Isolation Design.

ACKNOWLEDGEMENTS

This work was funded by the Highway Project, Task 106-F-4.2.1(a) of the Multidisciplinary Center for Earthquake Engineering Research (when the research started the center was called National Center for Earthquake Engineering Research).

The members of the T-3 Task group, who wrote the 1999 AASHTO Guide Specifications for Seismic Isolation Design and who endorsed the λ -factor approach, are J.F. Roberts, R. Lacalle and L-H Sheng of Caltrans, M.M. Lwin of Washington State DOT, R.E. Anderson of Illinois State DOT, H. Ghasemi of FHWA, J.F. Stanton of the University of Washington, J.M. Kelly and I. Aiken of the University of California, Berkeley, R.L. Mayes of DIS, Inc., V.A. Zayas of Earthquake Protection Systems, Inc., P. Bradford of R.J. Watson, Inc., and the first author of this report.

Special thanks are due to Professor John F. Stanton for his thorough review of this report.

TABLE OF CONTENTS

SECTION	TITLE	PAGE
1	INTRODUCTION	1
2	AGING OF SEISMIC ISOLATION HARDWARE	3
2.1	Introduction	3
2.2	Elastomeric Bearings	4
2.3	Sliding Bearings	9
2.4	Summary	13
3	THE NATURE OF FRICTION IN SELECTED SLIDING INTERFACES	15
3.1	Introduction	15
3.2	Friction	15
3.3	Basic Mechanisms of Friction	15
3.4	Static (or Breakaway) and Sliding (or Kinetic) Friction	17
3.5	Stick-Slip Motion	19
3.6	Friction in PTFE-Polished Stainless Steel Interfaces	24
3.6.1	Dependency on Velocity of Sliding and Pressure	24
3.6.2	Effect of Temperature	30
3.6.3	Effect of Time of Loading (Load Dwell)	31
3.7	Friction in Bimetallic Interfaces	34
3.8	Frictional Heating	36
3.8.1	Theory	36
3.8.2	Test Results on Temperature Rise Histories due to Frictional Heating	51
3.8.3	Example of Temperature Rise Calculation in Bi-directional Sliding Motion	54
3.8.4	Concluding Remarks on Frictional Heating	60
3.9	Summary	60
4	FRICTIONAL PROPERTIES OF PTFE-POLISHED STAINLESS STEEL INTERFACES	63
4.1	Introduction	63
4.2	Effect of Load Dwell on Breakaway (or Static) Friction	65
4.3	Effect of Apparent Pressure and Sliding Velocity	70
4.4	Effect of Temperature	79
4.5	Effect of Cumulative Movement	92
4.6	Effect of Surface Roughness of Stainless Steel	101
4.7	Corrosion of Stainless Steel	102
4.8	Effect of Contamination	109
4.9	Effect of Lubrication	111
4.10	Summary	113

TABLE OF CONTENTS (CONT'D)

SECTION	TITLE	PAGE
5	SYSTEM PROPERTY MODIFICATION FACTORS	115
5.1	Introduction	115
5.2	The Concept of System Property Modification Factor	115
5.3	System Property Adjustment Factors	116
5.4	Proposed System Property Modification Factors for Sliding Bearings	117
5.4.1	Effect of Aging	118
5.4.2	Effect of Contamination	119
5.4.3	Effect of Wear (Travel)	119
5.4.4	Effect of Temperature	121
5.5	Other Applications of System Property Modification Factors	121
5.6	System Property Modification Factors for Elastomeric Isolation Systems	122
5.6.1	Effect of Aging	122
5.6.2	Effect of Scragging	123
5.6.3	Effect of Temperature	127
5.7	Generation of Heat in Elastomeric Bearings during Testing	129
5.7.1	High Damping Rubber Bearings	129
5.7.2	Lead-Rubber Bearings	131
5.8	Summary	136
6	CONCLUSIONS	137
7	REFERENCES	139
APPENDIX A	Sample of Experimental Results in Testing of Sliding Interfaces for Determining Temperature Effects on Frictional Properties	147

LIST OF ILLUSTRATIONS

FIGURE	TITLE	PAGE
2-1	Idealized Force-Displacement Relation of Typical Seismic Isolation Bearing	3
2-2	Arrhenius Plot for Time to Degradation of a Rubber Compound (Increase of Shear Modulus by 15-percent)	8
3-1	View of Interface Showing Apparent and Real (True) Areas of Contact	16
3-2	Typical Friction Force-Sliding Displacement Loop of PTFE-Stainless Steel Interface (Pressure=20.7 MPa, Peak Velocity=2.5 mm/sec)	18
3-3	Machine Used in Testing of Sliding Bearing	20
3-4	Simplified Diagram of Testing Machine	21
3-5	Histories of Imposed Motion and Axial Load on Tested Sliding Bearing	21
3-6	Recorded Friction Force-Displacement Loops in Testing of Sliding Bearing	22
3-7	Friction Force and Spring Force-Displacement Plots Following Reversal of Motion	23
3-8	Dependency of Coefficient of Friction of PTFE-Polished Stainless Steel Interface on Sliding Velocity and Normal Load	25
3-9	Variation of Real Area of Contact, Pressure at Contact Area and Coefficient of Sliding Friction with Increasing Normal Load	27
3-10	Relation Between Inverse of Sliding Coefficient of Friction and Apparent Pressure	28
3-11	Effect of Temperature on the Frictional Properties of PTFE-Polished Stainless Steel Interfaces	31
3-12	Schematic of Two Bodies in Sliding Contact	37
3-13	Semi-infinite Solid with Constant Heat Flux at $x=0$	39
3-14	Calculated Distribution of Temperature Rise with Depth of Stainless Steel Plate at Conclusion of Testing	43
3-15	History of Heat Flux Input in Periodic Constant Velocity Motion of Large Amplitude	45
3-16	Heat Flux Input at Various Positions of Steel Body in Uni-directional Periodic Constant Velocity Motion	49
3-17	Heat Flux Input at Various Positions of Steel Body in Multi-directional Constant Velocity Motion	50
3-18	Recorded and Predicted Histories of Temperature at Middle Thermocouple (Depth of 1.5 mm) in Small Amplitude Tests	52
3-19	Recorded and Predicted Histories of Temperature at Middle Thermocouple (Dept of 1.5 mm) in Large Amplitude Tests	53
3-20	FPS Bearing for the Benicia-Martinez Bridge, California	54

LIST OF ILLUSTRATIONS (CONT'D)

FIGURE	TITLE	PAGE
3-21	Calculated Histories of Vertical Load and Bi-directional Horizontal Motion of FPS Bearing for Benicia-Martinez Bridge, California	55
3-22	Displacement Path in Bi-directional Motion and Actual and Equivalent Apparent Contact Areas	56
3-23	Histories of Heat Flux	58
3-24	Predicted Histories of Temperature Rise at the Surface and at Depth of 1.5 mm of Stainless Steel Overlay at its Center	59
4-1	Testing Arrangement Used in Testing of Sliding Bearings	64
4-2	Recorded Loops of Friction Force Divided by Normal Load Versus Displacement in Load Dwell Tests at 6.9 MPa Apparent Pressure	68
4-3	Recorded Loops of Friction Force Divided by Normal Load Versus Displacement in Load Dwell Tests at 20.7 MPa Apparent Pressure	69
4-4	Recorded Response of Sliding Bearings in Shake Table	
4-5	Testing of a Model Bridge Structure by Constantinou et al. (1993)	71
4-5	Close-up View of Recorded Response of Sliding Bearings in Shake Table Testing of a Model Bridge Structure by Constantinou et al. (1993)	73
4-6	Recorded Response of Sliding Bearings in Shake Table Testing of a Model Bridge Structure by Tsopelas et al. (1994)	74
4-7	Close-up View of recorded Response of Sliding Bearings in Shake Table Testing of a Model Bridge Structure by Tsopelas et al. (1994)	75
4-8	Coefficient of Sliding Friction of Unfilled PTFE-Polished Stainless Steel Interfaces ($0.03 \mu\text{m Ra}$). Ambient Temperature is about 20°C	77
4-9	Coefficient of Sliding Friction of Composite No. 1 -Polished Stainless Steel Interfaces. Ambient Temperature is about 20°C (all tests conducted under normal load of about 35 kN)	78
4-10	Effect of Parameter α on Variation of Coefficient of Friction with Velocity	80
4-11	Imposed Displacement History in Testing of Sliding Interfaces for Determining Temperature Effects on Frictional Properties	81
4-12	Example of Determination of Frictional Properties	82
4-13	Breakaway (or Static) Friction of Unfilled PTFE-Polished Stainless Steel Interfaces as Function of Temperature and Sequence of Testing	85
4-14	Friction of Unfilled PTFE-Polished Stainless Steel Interfaces as Function of Temperature	86

LIST OF ILLUSTRATIONS (CONT'D)

FIGURE	TITLE	PAGE
4-15	Friction of Unfilled PTFE-Polished Stainless Steel Interfaces at Various Temperatures as Function of Sliding Velocity	87
4-16	Breakaway (or Static) Friction of PTFE-based Composite-Polished Stainless Steel Interfaces as Function of Temperature and Sequence of Testing	89
4-17	Friction of PTFE-based Composite-Polished Stainless Steel Interfaces as Function of Temperature	90
4-18	Friction of PTFE-based Composite-Polished Stainless Steel Interfaces at Various Temperatures as Function of Sliding Velocity	91
4-19	Effect of Cumulative Movement (Travel) on Sliding Coefficient of Friction of PTFE Composite in Contact with Polished Stainless Steel	96
4-20	Effect of Cumulative Movement (Travel) on Sliding Coefficient of Friction of Unfilled PTFE in Contact with Polished Stainless Steel	98
4-21	Recorded Loops of Friction Force/Normal Load vs Displacement of Unfilled PTFE-Polished Stainless Steel Interfaces Following Travel of 0.5 m to 510 m. Testing Conducted with Motion of Fig. 4-11 and Frequency of 2 Hz.	99
4-22	Views of PTFE Composite Material Following Travel of 500 in (left), Following Short Travel and High Amplitude Motion (center) and Prior to Testing (right)	100
4-23	Effect of Surface Roughness of Stainless Steel on the Sliding Friction of Unfilled PTFE	103
4-24	Effect of Surface Roughness of Stainless Steel on the Sliding Friction of PTFE	104
5-1	Lateral Force-Lateral Displacement Loops of a Small Scale High Damping Elastomeric Bearing (all test are at frequency of 1.0 Hz)	124
5-2	Time-dependent Low Temperature Behavior of Elastomers	127
5-3	Energy Dissipation Per Cycle in a Lead-Rubber Bearing	133
5-4	Appropriate Model for Problem of Heat Conduction in Lead-Rubber Bearings	133

LIST OF TABLES

TABLE	TITLE	PAGE
3-1	Thermal Properties of PTFE and Stainless Steel	38
3-2	Comparison of Measured and Calculated Maximum Rise in Temperature in Unfilled PTFE-Polished Stainless Steel (Type 304) Interfaces	42
4-1	Test Results on Effect of Load Dwell on Static (Breakaway) Friction of Unfilled PTFE in Contact with Polished Stainless at Apparent Pressure of 6.9 MPa	66
4-2	Test results on Effect of Load Dwell on Static (Breakaway) Friction of Unfilled PTFE in Contact with Polished Stainless Steel at Apparent Pressure of 20.7 MPa	67
4-3	Effect of Temperature on the Breakaway and the Sliding Coefficient of Friction ($v = 1$ mm/s) of Unfilled PTFE in Contact with Highly Polished Stainless Steel at Apparent Pressure of 20.7 MPa (from Campbell et al., 1991)	80
4-4	Information on Performance of Austenitic Stainless Steels in Various Atmospheric Environments	106
4-5	Suggested Surface Roughness Values (in μm arithmetic average) of Type 304 Austenitic Stainless Steel (originally polished to roughness of $0.03 \mu\text{m}$ arithmetic average) After 30 Years of Exposure Within Unlubricated Sliding Bearings	108
4-6	Proposed Factors for Increasing the High Velocity Sliding Coefficient of Friction (f_{\max}) of Unlubricated Unfilled PTFE and PTFE Composites in Contact with Type 304 Austenitic Stainless After 30 Years of Exposure in Various Environments	108
4-7	Coefficient of Sliding Friction of Lubricated Unfilled PTFE-Stainless Steel Interfaces (data from Campbell and Kong, 1989). Values of Friction are for First Cycle of Movement	112
4-8	Coefficient of Sliding Friction of Lubricated Unfilled PTFE-Stainless Steel Interfaces after 50 Cycles of Movement (2 m of Travel) and Velocity of 20 mm/s (from Campbell and Kong, 1989)	112
5-1	System Property Modification Factor for Effects of Aging ($\lambda_{\max, a}$) on the Coefficient of Friction of Sliding Bearings	119
5-2	System Property Modification Factor for Effects of Contamination ($\lambda_{\max, c}$) on the Coefficient of Friction of Sliding Bearing	120
5-3	System Property Modification Factor for Effects of Wear (Travel) ($\lambda_{\max, tr}$) on the Coefficient of Friction of Sliding Bearings	120

LIST OF TABLES (CONT'D)

FIGURE	TITLE	PAGE
5-4	System Property Modification Factor for Effects of Temperature ($\lambda_{max, t}$) on the Coefficient of Friction of Sliding Bearings	121
5-5	System Property Modification Factor for Effects of Aging ($\lambda_{max, a}$) on the Properties of Elastomeric Bearings	123
5-6	System Property Modification Factor for Effects of Scrapping-Recovery ($\lambda_{max, scrag}$) on the Properties of Elastomeric Bearings	125
5-7	System Property Modification Factor for Effects of Temperature ($\lambda_{max, t}$) on the Properties of Elastomeric Bearings	129
5-8	Thermal and Other Properties of Lead, Steel and Rubber	134

SECTION 1 INTRODUCTION

The prediction of dynamic response and the design of seismically isolated structures is currently based on data obtained from testing of newly-fabricated seismic isolation hardware. Often the condition that this hardware may be in after years of service is not considered in the initial design. That is, the effect of changes in the mechanical properties of the seismic isolation hardware on the response of the isolated structure are typically neglected. However, in some projects these effects have been considered either based on assumptions or based on limited testing. It may be stated that these considerations are not based on a systematic analysis of the probable condition (or conditions) of the hardware and that testing does not truly assess this probable condition of the hardware. That is, the current state-of-practice either completely neglects probable changes in the properties of the isolation hardware or considers changes in a non-systematic and likely optimistic way.

The design of isolated structures requires analysis utilizing bounding values of properties of the seismic isolation hardware. Determination of these bounding values requires consideration of environmental effects (e.g., temperature), history of loading, aging, etc., and consideration of the likelihood that these effects occur simultaneously with the design basis earthquake. Some of these effects can be easily determined by testing (e.g., effect of temperature), whereas others are extremely difficult to assess. For example, the aging effects on seismic isolation hardware cannot be easily predicted, nor is there a simple test that can provide useful information on these effects.

The safest guide to the aging characteristics of a particular seismic isolation hardware is previous experience. Given, however, the rather recent origin of the seismic isolation technology, there is a complete lack of data on aged seismic isolation bearings (e.g., Taylor et al., 1992). Yet, at the start of this project there was a widespread belief that elastomeric isolation bearings have good aging characteristics, whereas sliding isolation bearings do not. Based on this notion, a project under the title “Longevity and Reliability of Sliding Seismic Isolation Systems”, task 106-F-4.2.1(a), began at the University at Buffalo, State University of New York in 1993 with support from the NCEER Highway Project. The objectives of this task were: (a) to collect laboratory and field performance data of sliding bearings with emphasis on factors affecting their long-term service life, (b) to provide a physical interpretation of the phenomenon of friction of sliding bearings, and (c) to utilize this interpretation for the qualitative prediction of the long-term frictional properties of sliding bearings and for the proposal and verification of testing procedures for assessing these properties.

In the course of this research effort it becomes apparent that there was a nearly complete lack of data on the dynamic frictional properties of sliding seismic isolation bearings (that is, under high velocity motion) for a range of conditions of interest in the analysis and design. These included, in addition to the effects aging, the effects of temperature, contamination and history of loading (e.g., following loading without movement for prolonged time or following significant movement caused by traffic and temperature variations).



Telegram Channel: [@Seismicisolation](https://t.me/Seismicisolation)

Moreover, one of the authors participated in the development of the 1999 AASHTO Guide Specifications for Seismic Isolation Design (American Association of State Highway and Transportation Officials, 1999). This development effort was carried out by a specially-appointed Task Group on behalf of the AASHTO Highway Subcommittee on Bridges and Structures, T-3 Seismic Design Technical Committee. A specific challenge for the T-3 Task Group has been the development of a procedure for determining bounding values of isolator properties for analysis and design. The determination of bounding values of isolator properties requires consideration of the aforementioned effects of aging, history of loading, temperature, etc. Moreover, it requires the development of an understanding of the origin of these effects in order to specify factors for the modification of properties of isolators that account for the conditions of construction, installation and environment.

Based on these needs the objectives of task 106-F-4.2.1(a) of the NCEER Highway Project have been modified to include the development of a procedure for establishing bounding values of frictional properties of sliding bearings for use in the design of seismically isolated bridges. The effort culminated in the establishment of System Property Modification Factors or λ -factors and the inclusion of these factors in the 1999 AASHTO Guide Specifications for Seismic Isolation Design.

This report presents the λ -factor approach and the background information that led to the establishment of λ -factor values for sliding seismic isolation bearings. Since the λ -factor approach is also applicable to elastomeric isolation bearings, background information and λ -factor values are briefly presented for elastomeric systems. The report starts with a section on aging and proceeds with a section on the nature of friction of sliding interfaces. This section attempts to provide a physical and mathematical characterization of the phenomenon of friction in selected sliding interfaces. Subsequently, collected and newly generated experimental results on the frictional properties of selected sliding interfaces are presented. A section is devoted to a presentation of the λ -factor approach. Proposed λ -factor values for sliding interfaces and elastomeric bearings are presented last.



Telegram Channel: [@Seismicisolation](https://t.me/Seismicisolation)

SECTION 2

AGING OF SEISMIC ISOLATION HARDWARE

2.1 Introduction

Aging is the degradation or change of properties with time. Herein we are primarily concerned with changes in the mechanical properties that characterize the stiffness and energy dissipation capability of seismic isolation hardware. For example, Figure 2-1 illustrates a typical lateral force-displacement loop of a seismic isolation bearing. The important mechanical properties that describe the behavior of this bearing are the characteristic strength Q_b and the post-yielding (or post-elastic) stiffness K_b . The characteristic strength is directly related to the energy dissipation capability of the bearing. For a sliding bearing, quantity Q_b is the friction force under dynamic conditions, that is, it is the product of the sliding coefficient of friction and axial load.

The mechanical properties of characteristic strength and stiffness can be affected by aging and other effects. The analysis and design of isolated structures should be based on considerations of these effects. Specifically, lower bound values of these properties should be utilized in determining the isolator displacement response, whereas upper bound values should be utilized in determining the substructure and/or superstructure force response.

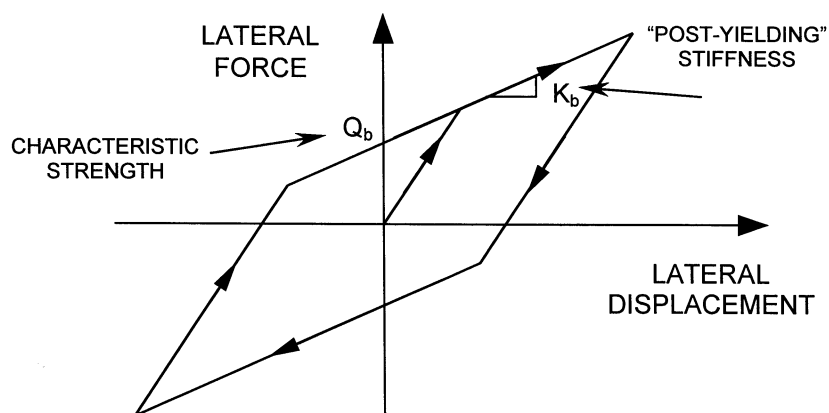


FIGURE 2-1 Idealized Force-Displacement Relation of Typical Seismic Isolation Bearing

Aging and other factors may also affect the ability of the isolation hardware to sustain stress, strain, force or deformation, leading therefore, to a requirement to consider these effects in the design of the isolation hardware.

This section contains a brief review of published information on the aging characteristics of elastomeric and sliding seismic isolation bearings. It primarily deals with field observations of the performance of bearings used in non-seismic applications and with laboratory studies of artificially aged specimens.

2.2 Elastomeric Bearings

There are several reports on the field performance of elastomeric bearings used in non-seismic bridge applications. These reports provide little information on the aging characteristics of these bearings. Rather, some of these reports deal with non-specific reports of failures (e.g., Stanton and Roeder, 1982; Manning and Bassi, 1986; and Taylor et al., 1992). Accurate data on these failures are not available due to the litigious risks of revealing such data. However, these failures are attributed to elastomer debonding, misalignment, excessive creep, surface cracking, improper installation, etc. Nearly, all of these problems may be attributed to poor quality of manufacturing. If one excludes problems attributed to poor quality (in principle, they can be prevented with a rigorous quality control and inspection program), the in-service record of elastomeric bridge bearings is very good.

Few reports contain information that can provide further insight into the performance of rubber bearings. Malik (1991) reported on the condition of twenty-year old natural rubber bearings that were removed from a bridge in New York State. The mechanical properties of the bearings at the time of installation were not known. However, the bearings were subjected to standard physical tests and found to meet all currently applicable requirements except those of the compression tests (per ASTM D395).

Malik (1991) also reports that some of the removed bearings developed significant cracks so that the steel reinforcement was exposed. Similar problems have been reported in Ontario (Manning and Bassi, 1986). In both cases the authors report that the bearings could safely carry the loads and thermal displacements. If these bearings were seismic isolation bearings, the existing large cracks would have been significant defects when the bearings are subjected to earthquake-induced large displacements. However, it is likely that these old bearings had insufficient anti-oxidants in the rubber compound that led to the observed cracking. Modern elastomeric bearings are typically provided with sufficient anti-oxidants.

Stevenson and Price (1986) reported a study on twenty-year old natural rubber bearings that were removed from a bridge in England. The bearings were in good condition and their physical properties were found to meet the requirements for new bridge bearings. The bearings were also subjected to combined compression and shear. Data on the lateral stiffness of the bearings at the time of installation were not known. However, the design called for stiffness in the range of 1.36 to 2.04 kN/mm (1.7 kN/mm \pm 20%). The measured value of the lateral stiffness of one pair of twenty-year old bearings has been reported to be 1.8 kN/mm. That is, the lateral stiffness may have increased by as much as 32-percent or may have decreased by as much as 12-percent of the bounding design values.

The most relevant information on the effect of aging on the mechanical properties of seismic isolation bearings have been recently reported by Clark et al. (1996). Lead-rubber and high-damping rubber bearings tested in 1983 in conjunction with the construction of the Foothill Communities Law and Justice Center in California were re-tested after 12 and 13 years. Moreover, a pair of high-damping rubber bearings were

removed from the building and re-tested after 12 years of service. The original tests and the re-tests were done with different machine configurations and probably different rates of loading. Moreover, no data were recorded for the bearings under unscragged conditions and the original data were not available in digitized form. That is, there was uncertainty in the original data, and interpretation of the results of the comparison study is difficult.

The data on the testing of lead-rubber bearings show insignificant changes in the characteristic strength and some minor increase in the effective stiffness of the bearings. The data on high damping rubber bearings indicate a possible increase in effective stiffness at shear strains of 50 to 100-percent by a factor of about 1.25. No data are provided for the energy dissipated per cycle, characteristic strength and post-yielding stiffness (see Fig. 2-1). However, some information could be obtained from reported force-displacement loops in half-cycle tests (note that this is not a fully reversed cycle of lateral movement) at shear strain of 100-percent. Increases in both the characteristic strength and post-yielding stiffness (K_b in Fig. 2-1) by factors of about 1.2 to 1.3 may be inferred.

It is evident that data on the mechanical properties of in-situ aged elastomeric bearings are extremely scarce. Yet it is possible to conclude that:

- (a) Aging may cause an increase in both the characteristic strength and stiffness of elastomeric bearings.
- (b) This increase is dependent on the rubber compound. It is expected to be least for standard low damping compounds and greatest for the high damping compounds.
- (c) Except for improperly cured bearings, this increase is expected to be modest. Likely, it is of the order of 10-percent for low damping natural rubber bearings and of the order of 20-percent for high damping natural rubber bearings (effective damping of about 0.10) over a period of approximately 30 years.

Data on the aging characteristics of high damping rubber bearings with high effective damping (exceeding 15-percent) do not exist. It is known that very high damping can be achieved by incomplete curing of the elastomer. Insufficiently cured bearings exhibit also large differences between unscragged and scragged properties, and recovery (that is, they recover, either fully or partially, their unscragged properties after some time). Recovery implies continuation of chemical processes in the rubber, and therefore, it suggests that significant potential for age hardening exists. It is, thus, reasonable to expect that such bearings would exhibit increases in their mechanical properties over time that are more than those of bearings with low effective damping.

Manufacturers of high damping rubber bearings have claimed insignificant changes in the mechanical properties of their bearings over time. Particularly, Kojima and Fukahori (1989) presented data for the Bridgestone high damping rubber bearings that show changes of less than 10-percent over a period of 60 years. It is of importance to review the basis and relevance of these results.

The results are based on accelerated aging of rubber specimens at high temperature and prediction of “lifetime” by the Arrhenius procedure. Accelerated aging of rubber is based on exposure of rubber samples (typically, dumbbell specimens per ASTM Standard D412) to high temperatures (typically in the range of 60° to 80°C), in vacuum and for short time periods (up to 45 days). The procedure explores the known degradation of rubber at high temperatures in order to produce indirect data on the effect of time on rubber bearings. The results of such tests cannot provide any substantial evidence on the long-term properties of elastomeric bearings for the following reasons:

- (a) The relationship between short-term accelerated testing of small specimens and the long-term in-situ performance of elastomeric bearings is not understood.
- (b) Such tests cannot reveal the effect of creep deflections, static loading, and history of motion and loading on the long-term properties of elastomeric bearings.
- (c) There is complete lack of data on the properties of in-situ aged high damping rubber bearings, so that verification of the predictions is not possible.

The Arrhenius method explores the degradation of rubber at high temperatures. Tests on small rubber specimens are conducted after exposure to at least three different high temperatures. Information is obtained on the time needed for a particular event to occur at each temperature (e.g., failure, increase of shear modulus by 15-percent of the original value, reduction of the elongation at break by 15-percent, etc.). This information is then used to extrapolate and obtain the time needed for the same particular event to occur at the normal temperature of operation of the specimen.

The Arrhenius method clearly relates degradation due to aging to degradation due to temperature. It cannot provide conclusive evidence on the long-term properties of in-situ aged elastomeric bearings for the reasons stated earlier in this section. However, the Arrhenius method provides additional information above that provided by the other methods, that is, “life expectancy”. Apart from the poorly understood relation between in-situ aging and temperature-induced degradation, the Arrhenius method makes use of a further assumption to arrive at estimates of “life expectancy”. This is done by the use of the Arrhenius rate law (Nelson, 1990).

According to Arrhenius law, the rate of a simple, first order chemical reaction is related to the Kelvin temperature, T, as follows

$$(rate) = A' \exp\left[-\frac{E}{kT}\right] \quad (2-1)$$

where A' = constant that is characteristic of test conditions and of the “failure” or degradation mechanism of the specimen, E = activation energy and k = Boltzmann’s constant. Equation (2-1) also describes metal diffusion.

Based on the simple view that rubber degradation is due to such a simple, first order chemical reaction, one can assume that the specimen degraded when some critical amount of the material has reacted or

$$(\text{critical amount}) = (\text{rate}) \times (\text{time to specific degradation}) \quad (2-2)$$

From (2-2) one can express the time to specific degradation, τ , as

$$\tau = \frac{(\text{critical amount})}{(\text{rate})} \quad (2-3)$$

and using (2-1)

$$\tau = A \exp\left[\frac{E}{kT}\right] \quad (2-4)$$

where A is a constant depending on specimen geometry, size, test method, etc. Equation (2-4) is known as the Arrhenius life relationship. The logarithm (base 10) of (2-4) is

$$\log(\tau) = a_0 + \frac{a_1}{T} \quad (2-5)$$

and thus $\log(\tau)$ is linearly dependent on the inverse of the Kelvin temperature.

As an example, the Arrhenius method is used to predict the time to degradation of the shear modulus of a particular high-damping rubber compound. In this case, degradation is defined as the increase in the shear modulus by 15-percent. The method is used to predict the time for a 15-percent increase in the effective stiffness of a bearing made of the same compound. Specimens of the rubber were maintained in vacuum at temperatures of 60°, 70° and 80°C and periodically tested to measure the shear modulus. The times were determined by interpolation to be 45, 13.5 and 4.5 days, respectively for the three temperatures. Figure 2-2 shows the Arrhenius plot for this case. Extrapolation determines the expected time to an increase of the modulus by 15-percent at the normal temperature of 15°C. It is 29,000 days or 79.5 years. This is a disturbing prediction because it is based on extrapolation of data over a period of 45 days to a range that is 650 times larger. Even more disturbing is the prediction of life expectancy of 160,500 days or 440 years if the bearing were at the temperature of 5°C. The fallacy of such a prediction is apparent.

The Arrhenius method is useful in the evaluation of materials on a laboratory basis. However, its use for the prediction of life expectancy of elastomeric bearings is problematic for the following reasons:

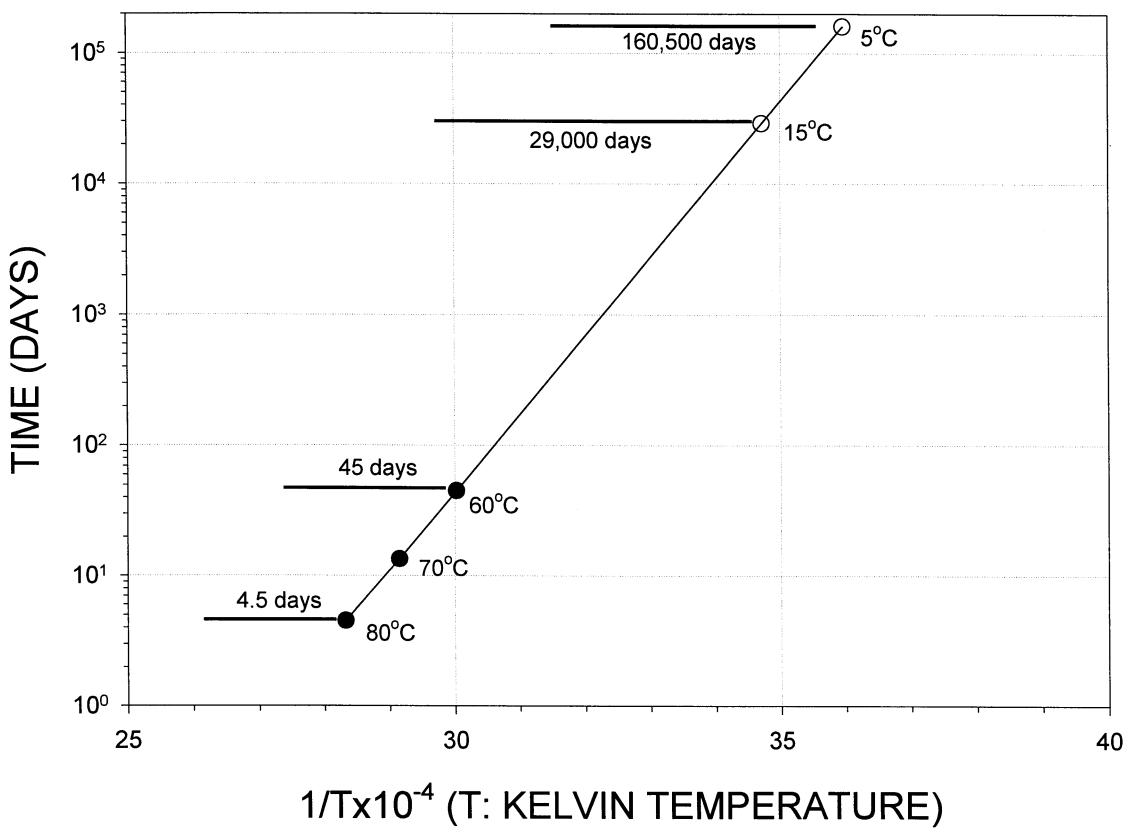


FIGURE 2-2 Arrhenius Plot for Time to Degradation of a Rubber Compound (Increase of Shear Modulus by 15-percent)

- (a) The method is based on artificial aging of rubber at elevated temperatures. As we have already discussed, the relationship between short-term accelerated aging and long-term in-situ aging is not understood. Furthermore, the effects of creep, static loading and history of loading are not accounted for in the artificial aging.
- (b) The harmful effects of atmospheric gasses are excluded when a vacuum is used, although they are known to be influential.
- (c) The long-term prediction of the method is based on the Arrhenius rate law which applies to simple, first order chemical reactions.
- (d) Lifetime predictions are based on extrapolation of accelerated aging data over ranges which are several hundred times larger than the range of the available data. Confirmation of such predictions is apparently impossible.

2.3 Sliding Bearings

In the past, the bearings used in bridges for non-seismic applications consisted primarily of rockers, rollers and sliding plates. All these types of devices experienced problems such as flattening of rollers, tilting of rockers and, more commonly, severe corrosion of contact surfaces. The latter problem, which is typically the result of the use of unsuitable materials in the presence of leaking expansion joints, may have been the prime contributor to the development of a perception among many engineers that sliding bearings exhibit bad aging characteristics.

The presentation in this section concentrates on modern sliding bearings that have very different characteristics, and also different aging problems, than those deficient old types of bearings. Modern sliding bearings consist of a sliding interface and a rotational element that is needed for maintaining full contact at the sliding interface. The rotational element may take various forms such as in the pot bearing, the spherical bearing, the disc bearing, the articulated slider in the Friction Pendulum (FPS) bearings or an elastomeric bearing (Campbell and Kong, 1987; Mokha et al., 1988; Constantinou, et al., 1993). The sliding interface may take a variety of forms, but those of interest in this presentation are those that found application in seismic isolation bearings. These are:

- (1) PTFE (polytetrafluoroethylene) in contact with polished stainless steel, either under dry or under lubricated conditions,
- (2) Various forms of composites (which typically contain some PTFE) in contact with polished stainless steel as used in the FPS bearings, and
- (3) Certain forms of bimetallic interfaces that consist of stainless steel in contact with bronze which is impregnated with a lubricant such as lead, PTFE or graphite.

A number of reports provide information on the field performance of modern sliding bearings used in non-seismic bridge applications (e.g., Lee, 1981; Manning and Bassi, 1986; Transportation Research Board, 1989). Moreover, other publications provide related general information on sliding bearings (e.g., Campbell and Kong, 1987; Kauschke and Baigent, 1986). As in the case of elastomeric bearings, these reports deal with non-specific reports of failures or problems. Nevertheless, it is possible to classify the observed problems as follows:

- (1) A significant number of problems occurred due to leakage of the elastomer in pot bearings. Typically, this problem is the result of inferior bearing design (especially the seals), improper installation, miscalculation of bearing rotation, or inappropriate use (e.g., use in locations where live loads cause significant fluctuation in the axial load on the bearing).
- (2) Metal-to-metal contact due to excessive bearing rotation. Excessive rotations are often the result of improper bearing installation or of underestimation of the bridge movement.

- (3) PTFE deforming and squeezing out. This problem has been observed in early designs in which the PTFE was either not bonded or not recessed, or the recess had inadequate depth, or the free height of PTFE was excessive, or the stainless steel surface was not flat.
- (4) Corrosion. Corrosion of external metal parts with inadequate corrosion protection has been often reported. In some cases crevice corrosion between the stainless steel and its backing steel plate has been reported. This problem is easily prevented by continuous welding around the perimeter of the stainless steel plate. Chrome-plated structural steel has been tried in Germany in place of stainless steel but the surface developed in time small pockets of rust. The authors also observed this for chrome-plated steel after about one year of outside exposure. Reports on corrosion of stainless steel (particularly ASTM 240, Type 304 or better) in sliding bearings could not be found. However, the authors located several studies on corrosion of metals that document corrosion of stainless steel (e.g., Davison et al., 1987). The authors have also observed mild corrosion on ASTM 240, Type 304 stainless steel on one of their bearings after about nine years of indoor exposure. The bearing was extensively tested during this period and stored disassembled. The stainless steel exhibited mild corrosion over a small portion of the surface. This had an effect of increased surface roughness and, thus, could affect the friction coefficient. The issue of corrosion is further discussed later in this report.
- (5) Contamination. Significant increases in friction and even seizure have been reported in bearings contaminated by ferrous and cementitious materials (Lee, 1981; Tyler, 1977; Campbell and Fatemi, 1989). All these cases were either observed in the laboratory where contaminants were artificially introduced or in the field when the bearings were disassembled prior to installation. Contamination of bearings in service in dust-laden environments is unlikely and any dust that settles on the stainless steel plate is likely to be swept off by the moving PTFE part. Nevertheless, it is not impossible for some contaminants to enter the sliding interface, particularly in lubricated bearings, during service.
- (6) Total Sliding Movement. Bearings of bridges carrying heavy live loads experience significant total movements that may amount to several kilometers over their lifetime. Wear reduces the useful thickness of the PTFE and limits the operational lifetime of the bearings. Moreover, the coefficient of friction is affected by the total sliding movement experienced by the bearing. Laboratory studies have produced mixed results. Studies of German origin (summarized in Kauschke and Baigent, 1986) show substantial increases in the very low velocity coefficient of friction of lubricated PTFE bearings after 20 km travel. More recent studies by Campbell and Kong (1989) on lubricated PTFE bearings show similar results over the shorter travels of 0.5 to 0.75 km. Studies by the authors (reported later in this report) on unlubricated bearings made of either PTFE or PTFE composites and highly polished stainless steel demonstrated small changes in the sliding coefficient of friction at very low (0.4 mm/s) and at high (160 mm/s) velocities over a 0.5 km travel.

The discussed reports deal primarily with sliding interfaces consisting of PTFE in contact with stainless steel because this has been by far the most frequently used interface. An interesting report related to another sliding interfaces has been found. It reports on the frictional properties of a bimetallic interface utilized in the seismic isolation bearings of the Koeberg nuclear power station in South Africa (Lee, 1993). This interface consisted of stainless steel in contact with leaded bronze. Following 14 years in service, sixty out of a total of 1829 of these bearings were removed and tested. The bearings did not show any noticeable corrosion or contamination and have not been subjected to any movement during service. On the average, the bearings exhibited a 68-percent increase in the initial (static or breakaway) coefficient of friction. It appears that this increase in friction is the result of the motionless state of the bearings. Corroboration for this idea is provided by field observations of graphite-impregnated bronze bearings in Illinois (Jacobsen, 1977).

The effect of dwell of load (that is, loading without movement) is of interest in sliding seismic isolation bearings. While this is primarily an issue for building applications, there are cases in bridge applications in which a sliding bearing may not experience any movement for prolonged periods of time. The case may arise in bearings on top of flexible piers, which can accommodate thermal and traffic-induced movement by deformation of the pier rather than by sliding of the bearing. Tests performed on PTFE-stainless steel interfaces following a two-year load dwell (Mokha et al., 1991), resulted in no increase of the static coefficient of friction. The difference between this observation and that of Lee (1993) on bimetallic interfaces is, we will claim later in this report, likely the result of the very different mechanisms of friction in the two interfaces. That is, bimetallic interfaces are susceptible to the effects of load dwell, whereas PTFE-stainless steel interfaces are likely not.

In summary, we can group the potential problems of sliding bearings in the following categories:

- (1) Problems that can be prevented through the use of detailed specification requirements and quality control for the design, material selection, manufacture and installation of the bearings. These problems are those of corrosion of external parts, crevice corrosion, metal-to-metal contact, squeezing out of PTFE, contamination at the site (by disassembly) and some of the problems related to leakage in pot bearings.
- (2) Problems that may not affect the performance of the bearings but which may limit their operational lifetime. These problems include wear at the sliding interface that reduces the useful thickness of PTFE, and wear of the rotational part. This part may actually be the weakest part in some types of bearings under certain conditions. The reader may find interesting to read in Mayrbaurl (1986) about the tests conducted on the replacement bearings for the Manhattan Bridge. These bearings are subjected to an average of 500 train crossings per day, which induce sliding, rotation, and uplift. Testing under the actual conditions resulted in unacceptable performance of the rotational part of pot bearings. Disc bearings performed well. However, the estimated operational lifetime of the rotational part, after extrapolation of test data over the equivalent of about 6 years of service, was a mere 13.5 years. This was in

sharp contrast with the expected lifetime of the sliding interface, which showed only minor wear.

- (3) Certain conditions that are likely to occur are either known or are potentially capable of affecting the frictional properties of the sliding interface. Therefore, they have to be considered in the analysis and design of structures incorporating sliding bearings. These conditions include (a) corrosion of stainless steel, (b) contamination of the sliding interface while the bearing is in service, (c) accumulated movement (travel), and (d) loading without movement. The effects of these conditions are further investigated later in this report.

As we have done in the case of elastomeric bearings, it is of interest to review attempts at obtaining information on the “lifetime” of sliding bearings in the laboratory environment. These attempts may be classified as follows:

- (1) Testing of full size bearings under the actual conditions of loading except applied at an increased rate. A notable example of such testing is that of the Manhattan bridge bearings (Mayrbaurl, 1986). The bearings were subjected to the actual cycle of loading (as monitored at the bridge) at a rate of about 360 cycles per hour, whereas the actual rate was about 20 cycles per hour. It was thus possible to conduct testing over few months that was equivalent to about 6 years of actual service. It is time consuming and expensive testing which may be performed only in rare cases. However, it can produce very useful results provided that the interpretation is done carefully. Application of the load at an increased rate may accelerate fatigue (particularly in the rotational part) and wear. On the other hand, it does not fully account for the effects of time.
- (2) Testing of either full size or reduced size bearings under artificial conditions that may provide information on a particular effect. This has been the approach followed by the writers in generating some results on the effects of corrosion, travel, load dwell and temperature on the frictional properties of sliding bearings. It is also expected to be the procedure for establishing λ -factors for isolation bearings. The procedure is complicated by the fact that the generation of an artificial condition (a) requires understanding of the fundamental behavior of the materials that make up the bearing, (b) may require complex analysis for interpretation of the results, and (c) does not truly account for the actual, in-service conditions. These issues will become apparent when the results of the authors are presented and interpreted.

Another concern with this type of testing is the use of results generated by accelerated testing to predict lifetime by extrapolation. For example, consider that testing is performed in order to establish the lifetime of a bearing as related to wear of the PTFE. Apart from the apparent complexities in determining representative histories of loading and movement, let us say that testing is conducted over a specific length of travel. A direct result of this test is a measurement of wear and coefficient of friction, which is useful information for the tested travel. Another result may be the wear rate (i.e., wear per unit of travel) or the wear factor (Predicting Bearing Wear, 1968).

Could this information be used to predict the condition of the bearing after travel significantly longer than the tested one? That is, do the wear rate and wear factor remain unchanged? In the opinion of these authors, extrapolation of experimental results without a solid physical interpretation is unacceptable.

- (3) The writers have noted the recent appearance of testing requirements for seismic isolation bearings that include some form of artificial aging. Particularly, the State of New York specified testing of bearings following exposure for 1000 hours in a salt spray chamber (per ASTM B117) under the title "Environmental Aging". The purpose of the test is described as "to verify performance of the selected bearing assembly in a salt spray environment such as that encountered over a long period of time under an expansion deck joint which is subject to salting". It is apparently an attempt to induce accelerated corrosion of the stainless steel surface of sliding bearings. However, the salt spray fog does not truly simulate the environment of a bearing over say a period of 30 years in service. What about the effects of loading, movement, temperature, and, more importantly, the various chemicals in the atmosphere and on the road? The authors have observed specimens of stainless steel to be in excellent condition following salt spray chamber testing. They have also collected information (to be presented later in this report) that even the most corrosion-resistant stainless steel can suffer some atmospheric corrosion in the right environment. It appears that a single, simple test to assess the aging characteristics of a bearing can not provide much information, other than perhaps to increase the confidence of the engineer in the use of the selected product.

2.4 Summary

Seismic isolation bearings are likely to experience changes of their mechanical properties over time. Depending on the bearing type, materials used, design procedures, installation procedures, loading history, and environment, these changes may be significant enough to limit the operational life of the bearing.

Based on a review of reports of performance of elastomeric bearings in non-seismic bridge applications, it appears that these bearings have shown very good performance. A number of problems, including failures, of these bearings may be attributed to poor quality of manufacturing. Based on a small number of reports it was possible to conclude the changes in the mechanical properties (specifically the effective lateral stiffness) of elastomeric bearings due to aging are likely to be small for the low damping compounds. However, the changes for the high damping compounds are likely to be progressively larger as damping is increased.

Sliding bearings have experienced problems, such as corrosion, metal-to-metal contact, squeezing out of PTFE, contamination and failure of the rotational part. Currently, there is sufficient knowledge and experience in the design, material selection, manufacture and installation of these bearings to prevent or minimize the potential for these problems. Elimination or minimization of these potential problems would require the use of detailed specification requirements and rigorous quality control. Nevertheless, it should be

recognized that sliding bearings are complex structural arrangements that are likely to be sensitive to the quality of manufacturing.

Changes in the mechanical properties of sliding bearings (specifically the coefficient of friction) may be caused by corrosion of the stainless steel, contamination of the sliding interface while in service, history of movement, and loading without movement (load dwell).

SECTION 3

THE NATURE OF FRICTION IN SELECTED SLIDING INTERFACES

3.1 Introduction

The establishment of λ -factor values for sliding bearings requires the collection of experimental data on the frictional properties of sliding interfaces under conditions of relevance to seismic applications, that is, under conditions of high velocity motion. Moreover, it requires that an understanding of the nature of friction in these interfaces is developed so that the results are properly interpreted.

This section presents (or attempts to present) a physical and mathematical characterization of the phenomenon of friction in selected sliding interfaces. It deals primarily with PTFE-stainless steel interfaces and it is presumed that composites containing PTFE exhibit similar behavior. Moreover, bimetallic interfaces are discussed. The presentation is limited to certain aspects of frictional behavior that are relevant to the interpretation of experimental results at the macroscopic level.

3.2. Friction

Friction is the resistance to movement of one body relative to another. Our interest is for sliding movements between solid bodies, that is, *sliding solid friction*. Moreover, we have an interest in the description of the frictional behavior of sliding interfaces as they are used in sliding bearings for structural applications. We will refer to this as friction at the macroscopic level, as opposed to friction at the microscopic and at the atomic levels.

The frictional force, F , at the sliding interface of a bearing will be described as

$$F = \mu N \quad (3-1)$$

where μ is the coefficient of friction and N is the normal load on the interface. We will distinguish between sliding coefficient of friction and static (or breakaway) coefficient of friction, the latter been defined as the ratio F/N at initiation of movement. The classical laws of friction (named for Coulomb who built his work on earlier works by Amontons and Leonardo da Vinci) postulate a friction coefficient that is independent of sliding velocity and contact area. While these laws are applicable in many cases, they do not, in general, apply to sliding bearings. Nevertheless, there is value in the use of (3-1) with the coefficient of friction being dependent on the most influential parameters, that is, velocity of sliding and apparent pressure.

3.3 Basic Mechanisms of Friction

Our interest is the understanding of the basic mechanisms of friction, that is, the microscopic events that cause friction. The overview given in this section is limited to those aspects that may provide physical insight into the frictional behavior of sliding

bearings. It is largely based on the work of Bowden and Tabor (1950, 1964, 1973) and their Cambridge University students, and others over the past half century (American Society for Metals, 1992).

Historically, the basic mechanisms of friction were proposed and studied before an understanding of the atomic nature of friction was achieved. Actually, the study of friction at the atomic level, or nanotribology, is of very recent origin given that experimental techniques to measure the frictional force of one-atom-thick films were developed in the 1980s. The atomic nature of sliding contact is not yet known. Even if it was completely known, tribologists are still, today, unable to predict the friction force at the contact (Krim, 1996).

Various mechanisms of friction have been proposed over the past several years. It is believed that all these mechanisms contribute in the generation of friction in various degrees depending on the particular situation. These mechanisms are:

(a) Adhesion

When two clean solid materials come into contact they form intimate atomic bonds across the contact interface. These regions of contact are called *junctions*, and the sum of the areas of all the junctions constitute the real (or true) area of contact. By comparison to the apparent area of contact, the real area of contact is very small (Figure 3-1). The junctions are characterized by interfacial forces caused by adhesion. That is, the friction force is given by the product of the real area of contact, A_r , and the shear strength of the junctions, s :

$$F_a = sA_r \quad (3-2)$$

Adhesion between sliding interfaces is dominant for very clean surfaces in high vacuum. It is now generally recognized that adhesion does not contribute a clearly separate component of friction. Rather, it is thought to be a component of the deformation of asperities on the sliding surfaces.

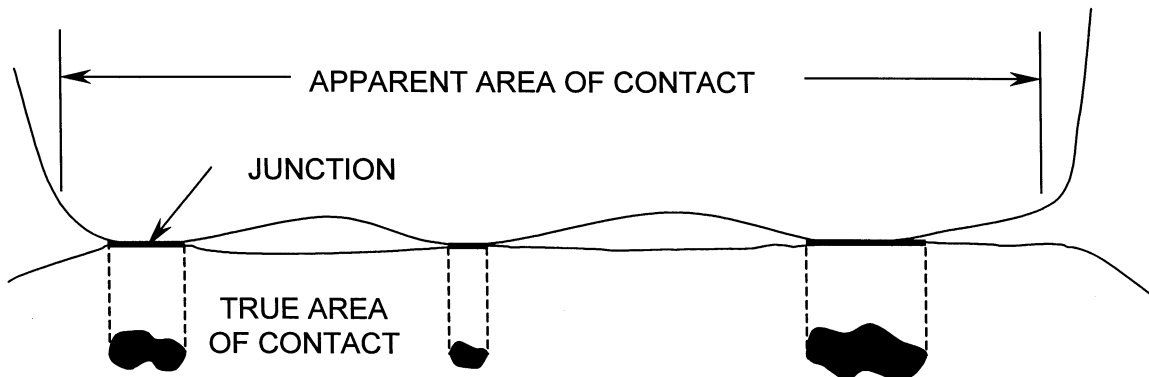


FIGURE 3-1 View of Interface Showing Apparent and Real (True) Areas of Contact

(b) Plowing

Surfaces are characterized by asperities. When in contact these asperities undergo elastic and plastic deformations. The plowing component of friction is due to energy dissipation during plastic deformation. This is better explained by considering a hard spherical asperity over a softer flat surface. On application of axial load on the asperity the softer surface below yields, junctions are formed and the asperity sticks to the surface below. On application of a shear force, the asperity moves horizontally pushing a wall (or bow wave) of softer material in its path and creating a groove. The plowing component of friction results from the effort to push the wall of material.

(c) Third-Body Effects

Wear debris and contaminants at the sliding interface contribute an additional term to the friction force. The contribution is due to plastic deformation as agglomerates of debris and contaminants roll between the surfaces or as they indent these surfaces.

(d) Viscoelastic Effects

Polymers, such as PTFE, exhibit viscoelastic behavior. As asperities of a harder material slide over a viscoelastic material, energy is dissipated due to viscoelastic deformation, contributing thus an additional component to friction.

In general, it is believed that several mechanisms contribute to friction. Their relative roles are the subject of much debate. However, we shall recognize that adhesion and mechanical deformation (elastic, plastic or viscoelastic) are collectively responsible for friction. Moreover, we shall recognize that the real area of contact is of paramount importance in the qualitative description of friction at the macroscopic scale.

3.4 Static (or Breakaway) and Sliding (or Kinetic) Friction

The static friction is the maximum force that must be overcome to initiate macroscopic motion. Accordingly, these authors prefer to call this force breakaway friction. Upon initiation of motion is most often observed that the friction drops. That is, typically the static friction is higher than the sliding friction force, the latter being measured at very low velocity of sliding (immediately following initiation of motion).

Figure 3-2 shows a typical result obtained in the testing of a sliding bearing consisting of unfilled PTFE in contact with mirror finish stainless steel. The interface was at constant average pressure of 20.7 MPa (normal load divided by apparent area) and the temperature at the start of the experiment was 19°C. A cycle of sinusoidal motion of 12.5 mm amplitude at frequency of 0.0318 Hz was imposed (peak velocity of 2.5 mm/sec). The recorded friction force was divided by the normal load and plotted against the sliding displacement. The difference between the static and sliding values of the coefficient of friction are apparent.

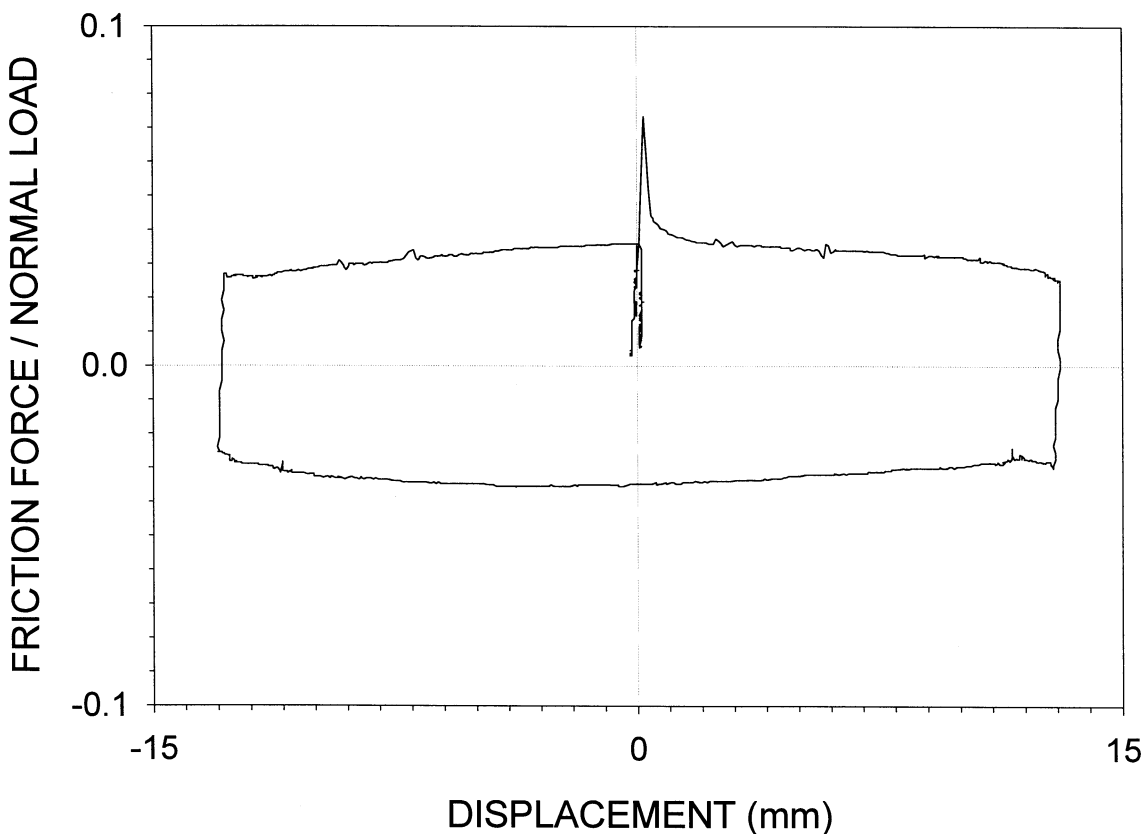


FIGURE 3-2 Typical Friction Force-Sliding Displacement Loop of PTFE-Stainless Steel Interface (Pressure=20.7 MPa, Peak Velocity=2.5 mm/sec)

The static friction is real but can also be a product of the experimental technique employed or the measuring system utilized. Often in civil engineering applications the experimental technique involves a system in which motion is imposed in a displacement controlled experiment – the motion being either a sine wave or a saw-tooth wave (constant velocity motion with reversal). In either case, initiation of motion requires an abrupt change of velocity from zero to a high value within extremely short time. This situation is unrealistic given that in actual applications motion initiates at essentially quasi-static conditions. This is corroborated by observations in the shake table testing of seismically isolated structures (e.g., Mokha et al., 1990; Constantinou et al., 1990; Constantinou et al., 1993; Al-Hussaini et al., 1994). That is, while breakaway friction exists, it does not have any measurable effect because the sliding value of friction is much higher at the velocities attained under seismic conditions. In fact the concept of static friction is meaningless when the sliding friction exhibits a substantial increase with increasing velocity of sliding (Rabinowicz 1995). It is thus important to measure the breakaway friction under quasi-static conditions.

The origin of the difference between static and sliding friction may be explained by the presumption of either a rapid drop in the real area of contact or the strength of the

junctions following initiation of sliding. In the case of PTFE this is likely caused by the transfer of a very thin film of PTFE on the stainless steel plate.

3.5 Stick-Slip Motion

It is common experience that jerky motion sometimes results when one object slides on another (e.g., squeaky door hinges, sound of a violin string, and, yes, earthquakes). In displacement controlled testing of a sliding bearing (i.e., motion is imposed by an actuator and measurement of the friction force is made), stick-slip behavior is manifested as fluctuation in the recorded friction force versus time. Conversely, in a force controlled test the behavior is manifested as motion with stops.

Stick-slip may be an intrinsic property of the sliding interface or more often is the result of inertia effects and the flexibility in the testing arrangement, although the phenomenon may be aggravated by the frictional behavior of the interface. Figure 3-3 illustrates a testing machine that the authors used in some of their experiments. A simplified diagram of the machine is shown in Figure 3-4. The testing arrangement is characterized by mass (hence inertia effects) and finite stiffness, both of which may affect the measurement of friction.

As an example, Figure 3-5 shows the histories of movement and axial load imposed in the testing of a sliding bearing with an unfilled PTFE-polished stainless steel interface. Recorded friction force-displacement loops are shown in Figure 3-6. In the loop at the top the friction force was measured by the reaction load cell so that the inertia effects of the large mass are excluded. It may be observed that the friction force is smooth except following reversals of motion (where displacement is maximum) where some small fluctuation in the force is seen. This is true stick-slip motion at the sliding interface. It is manifested by the flexibility of the supporting part of the sliding interface (the bearing contains a flexible element to accommodate rotation – this element allows for some very small translational movement).

When the actuator load cell is used to measure friction, the recorded loops exhibit significant fluctuations that result from the inertia effects. An attempt was made to correct for the inertia effects by utilizing records of acceleration of the moving mass (bottom figure). While this succeeded in removing much of the fluctuations, it did not so at the start of the experiment where the corrected friction force exhibits wild fluctuations. These fluctuations could be mistakenly interpreted as stick-slip.

Let us return to the top loop of Figure 3-6 and concentrate on the observed small fluctuation of the friction force following reversals of motion. We note that what we truly measure is not the friction force at the sliding interface but it is force in the spring (see Fig. 3-4) representing the bearing and load cell body. On reversal of motion the interface undergoes a momentary stop (movement changes direction). On initiation of motion the static (or breakaway) friction is mobilized. This is illustrated as point A on

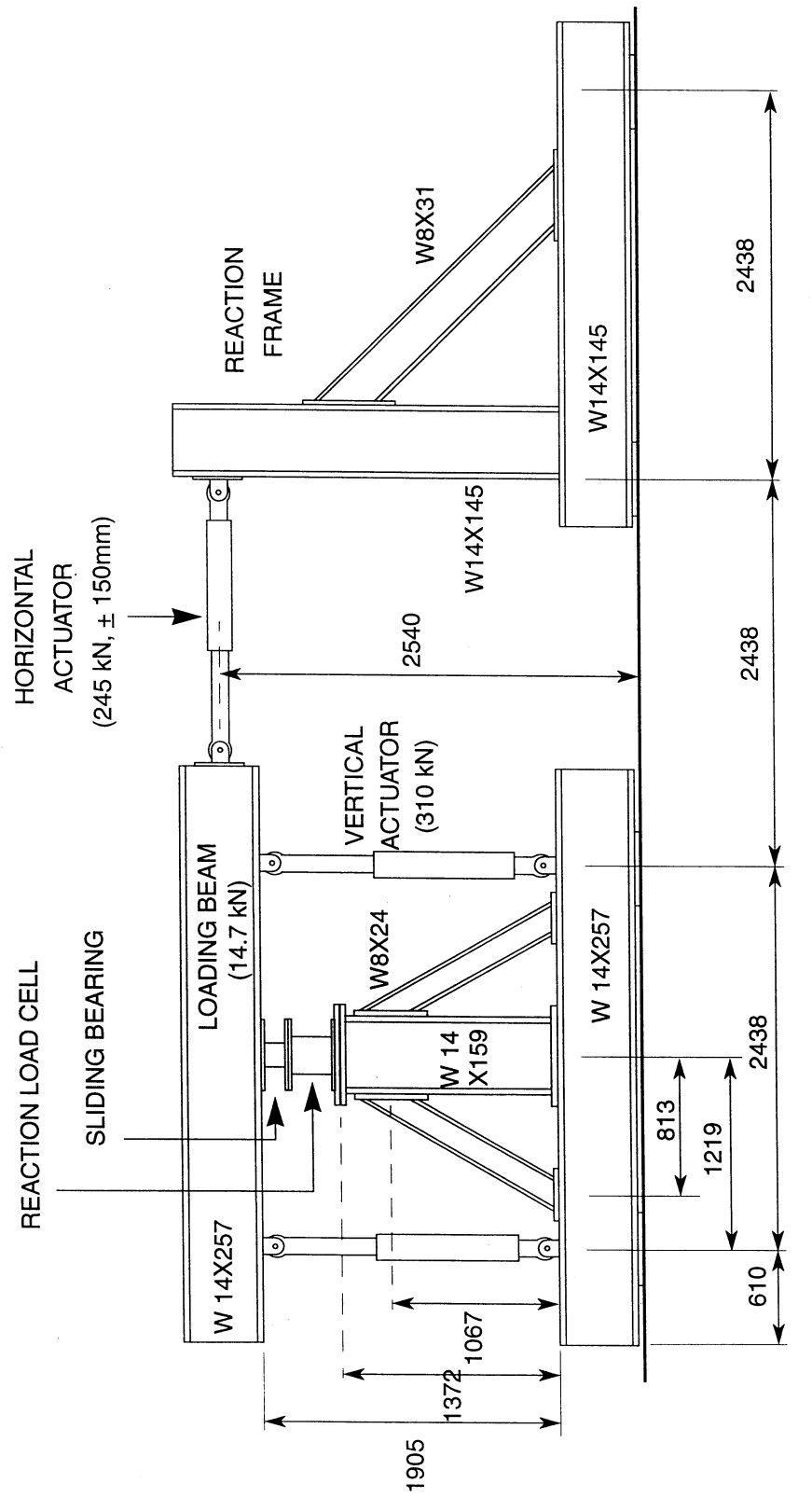


FIGURE 3-3 Machine Used in Testing of Sliding Bearing

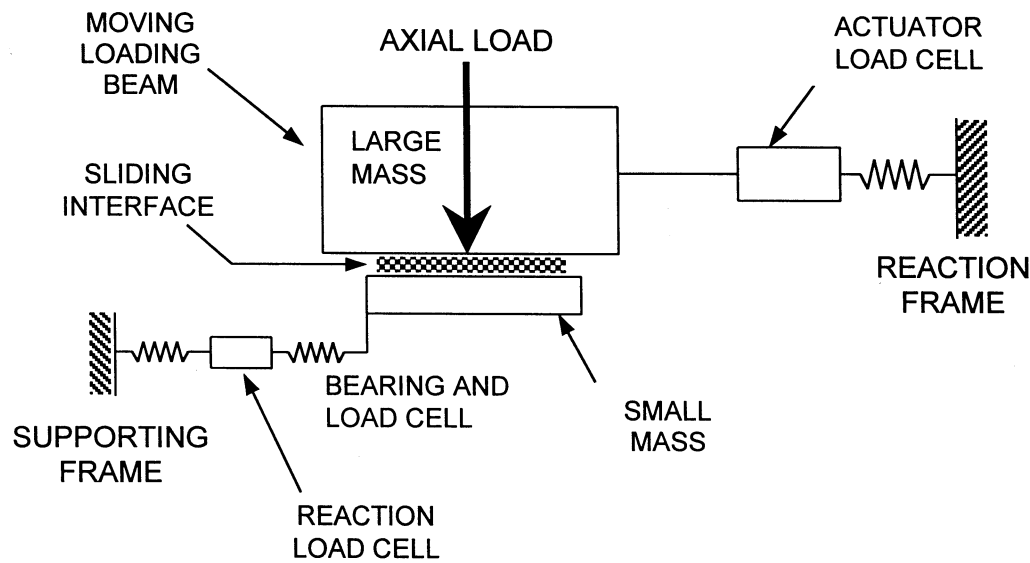


FIGURE 3-4 Simplified Diagram of Testing Machine

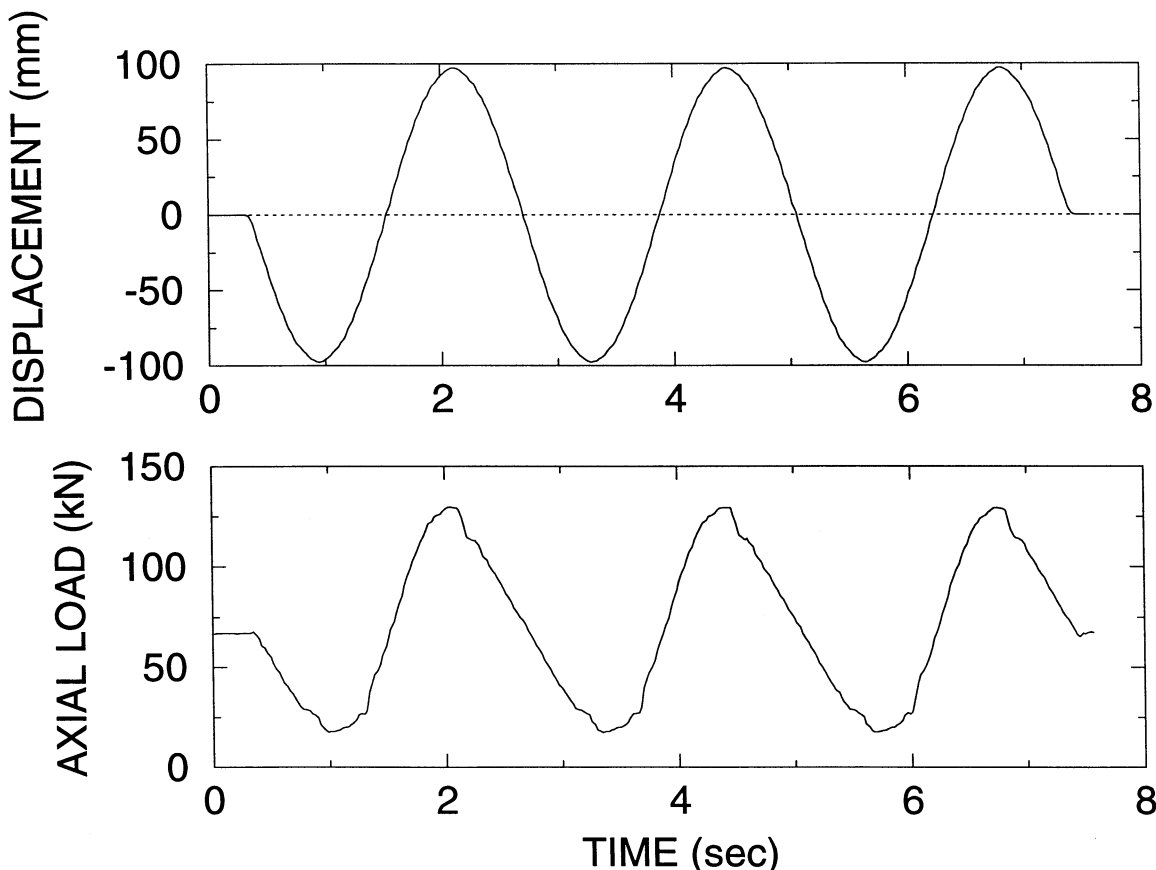


FIGURE 3-5 Histories of Imposed Motion and Axial Load on Tested Sliding Bearing

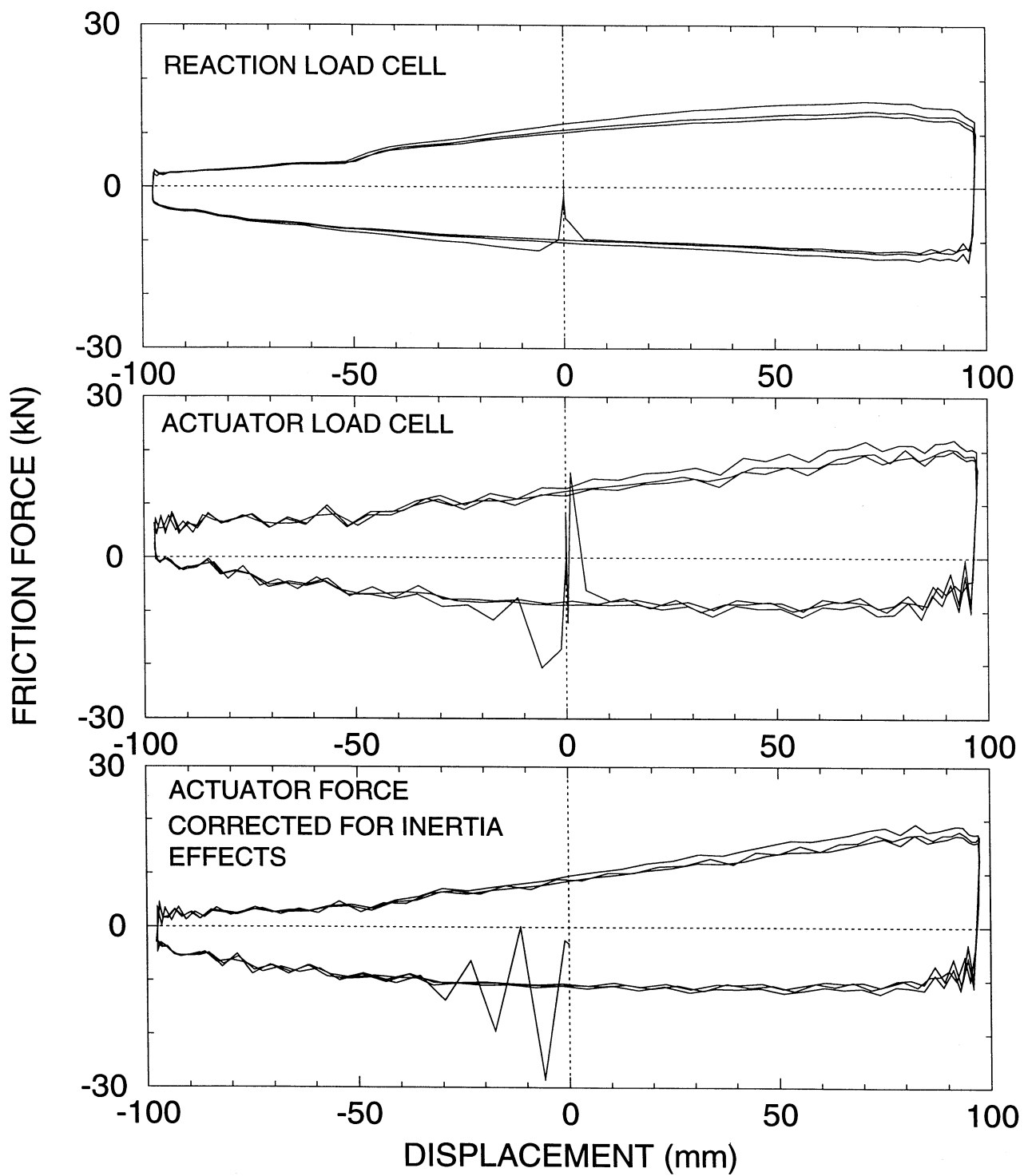


FIGURE 3-6 Recorded Friction Force-Displacement Loops in Testing of Sliding Bearing

the force-displacement plot of Figure 3-7. Subsequently, the friction force drops (smoothly) with increasing displacement (sliding friction) and later on it increases due to increases in the velocity of sliding (a property of PTFE-stainless steel interfaces). The spring cannot adjust its position accordingly. Rather it follows the straight dashed line that represents its stiffness. The excess energy, represented by the shaded area, is kinetic energy of the supporting part of the sliding interface. That is, the supporting part is set into motion until point B is reached, when all the kinetic energy is used up. The result is an abrupt drop in the spring force and a subsequent increase in this force.

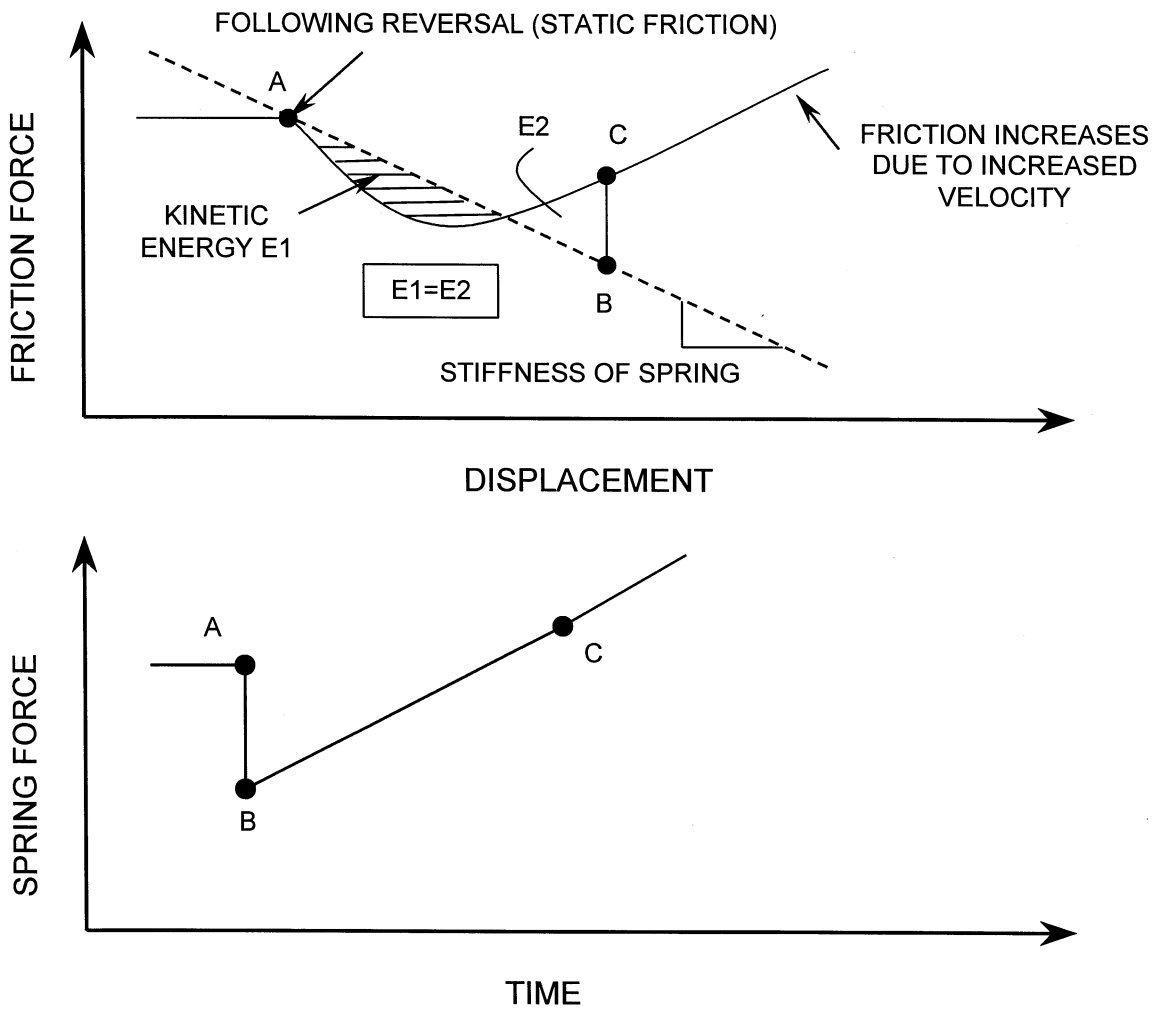


FIGURE 3-7 Friction Force and Spring Force-Displacement Plots Following Reversal of Motion

It is important to note that the phenomenon is manifested by the finite stiffness of the sliding bearing and the load cell below it (that is, the testing arrangement), as well as the actual frictional characteristics of the interface. The magnitude of the drop in the spring force is dependent on the stiffness, the difference between static and sliding friction and the rate of increase of the sliding friction with velocity. Note that if there was no increase

in the friction with increasing velocity, the same phenomenon would have been observed but with a larger drop AB in the spring force.

The presented explanation of stick-slip motion is the classical one, which until very recently was considered to be the only one. Recent studies (Yoshizawa and Israelachvili, 1993) demonstrated the possibility for another, truly intrinsic mechanism for stick-slip motion. When an interface is characterized by a thin interfacial film of polymeric fluid, phase transition between liquid-like and solid-like states of the film are possible. That is, abrupt changes in the flow characteristics of the film produce stick-slip motion.

The described stick-slip phenomenon is different, although related, to the phenomenon of motion with stops of a frictional oscillator driven by a dynamic force. Den Hartog (1931) demonstrated in a classic paper that motion with an arbitrarily large number of stops is possible. This phenomenon is the result of the requirements for dynamic equilibrium and it is completely unrelated to variations in the frictional force. Actually the stick-slip phenomenon can occur only when there is a natural variation in the friction force, whereas the analysis of Den Hartog was based on the assumption of constant friction. Makris and Constantinou (1991) have demonstrated that the motion of a frictional oscillator exhibits a substantially smaller number of stops when the friction force reduces with decreasing velocity of sliding.

3.6 Friction in PTFE-Polished Stainless Steel Interfaces

We will provide in this section a brief description of the macroscopic frictional properties of PTFE-polished stainless steel interfaces and we will attempt to provide a physical interpretation of these properties. It should be noted that PTFE or PTFE-based materials in contact with polished stainless steel represent, by far, the most frequently used interface in sliding bearings.

3.6.1 Dependency on Velocity of Sliding and Pressure

Figure 3-8 illustrates the dependencies of the coefficient of friction (friction force divided by normal load) on the velocity of sliding and normal load. The shown behavior is characteristic of clean, non-lubricated interfaces at normal ambient temperature ($\sim 20^{\circ}\text{C}$). The static (or breakaway) value, f_s , is shown at zero velocity of sliding (these should be the conditions at which the breakaway friction is determined). The sliding value is characterized by a low value immediately following initiation of sliding, f_{\min} , and a progressively increasing value as velocity increases. At large velocities the sliding value attains a constant value, f_{\max} . Increases in normal load result in reduction of the coefficient of friction- this reduction eventually diminishing at some limiting value of the normal load. It should be noted that the illustrated behavior is obtained in testing of sliding bearings under cyclic harmonic displacement and that measurements of the sliding friction are obtained within the first cycle at the first instant in which the peak sliding velocity is attained. The sliding friction is known to decrease with increasing number of cycles as a result of heating of the interface. The effect of temperature will be discussed later in this section.

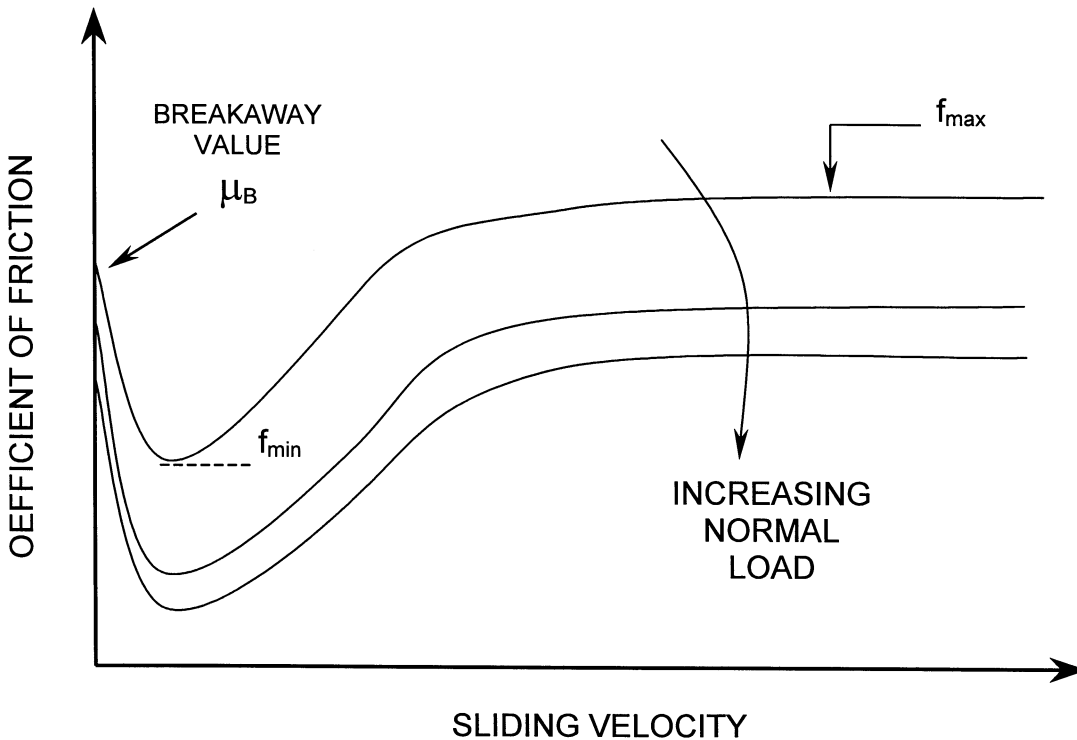


FIGURE 3-8 Dependency of Coefficient of Friction of PTFE-Polished Stainless Steel Interface on Sliding Velocity and Normal Load

In discussing this behavior it is important to note that (a) the PTFE is in the form of a large sheet (typically larger than 250 mm in diameter) with small thickness (confined within a recess and projecting out about 2 mm) and compressed by a larger size rigid stainless steel plate, (b) the stainless steel is highly polished with a surface roughness of about 0.05 μm on the arithmetic average scale, and (c) the PTFE is very soft by comparison to steel. We may assume that the PTFE surface is covered by asperities which, on application of the normal load, deform to form junctions with the stainless steel. Due to the very soft nature of PTFE, the real contact area will be large (by comparison, in metal to metal contact the true area of contact is much smaller than the apparent area).

Friction in this interface is primarily the result of adhesion, with the plowing contribution being insignificant. While in polymers the tendency is to shear in their bulk, PTFE is one of the few marked exceptions in which sliding occurs truly at the interface (Tabor, 1981). We may write as before

$$F = s A_r \quad (3-3)$$

where s is the shear strength of the interface. To a first approximation, the shear strength is a linear function of the actual pressure (pressure over the real area of contact) (Tabor, 1981)

$$s = s_0 + \alpha p_r \quad (3-4)$$

Then, the coefficient of friction is

$$\mu = \frac{F}{N} = \frac{(s_o + \alpha p_r) A_r}{p_r A_r} = \frac{s_o}{p_r} + \alpha \quad (3-5)$$

In discussing (3-5) we utilize results on the real area of contact (Bowden and Tabor, 1964). Assuming elastic deformation of asperities, the real area of contact is proportional to some power $\eta < 1$ of the normal load N

$$A_r = kN^\eta \quad (3-6)$$

As load increases the deformation may be mainly plastic and the real area of contact will be

$$A_r = \frac{N}{p} \quad (3-7)$$

where p is the resistance of PTFE to plastic flow in bulk compression. If plastic deformation occurs, the actual pressure remains constant ($=p$) and the real area of contact increases in proportion to the normal load. Thus by considering only elastic and plastic deformation of the PTFE asperities, it is possible to explain the reduction in the coefficient of friction with increasing normal load and the eventual attainment of a nearly constant value (Mokha et al., 1988; Campbell and Kong, 1987; Taylor, 1972). Figure 3-9 illustrates the variation of real area of contact, contact pressure and coefficient of friction with normal load as determined by (3-5) to (3-7).

While this theory provides an explanation for the observed dependency of the coefficient of friction on normal load, we can find a number of arguments against it. Specifically:

- (a) The interface consists of a large highly polished stainless steel surface in contact with a soft material having also a large smooth surface. The conditions are ideal for elastic contact with very large contact area (Rabinowicz, 1995).
- (b) The PTFE is essentially under conditions of hydrostatic compression, which should greatly increase its resistance to plastic flow in compression.
- (c) The PTFE exhibits viscoelastic behavior with the real area of contact expected to grow with time.

It should be noted that experimental results on friction are obtained following compression of the sliding bearing for several minutes to several hours. Accordingly, very large contact areas can be produced.

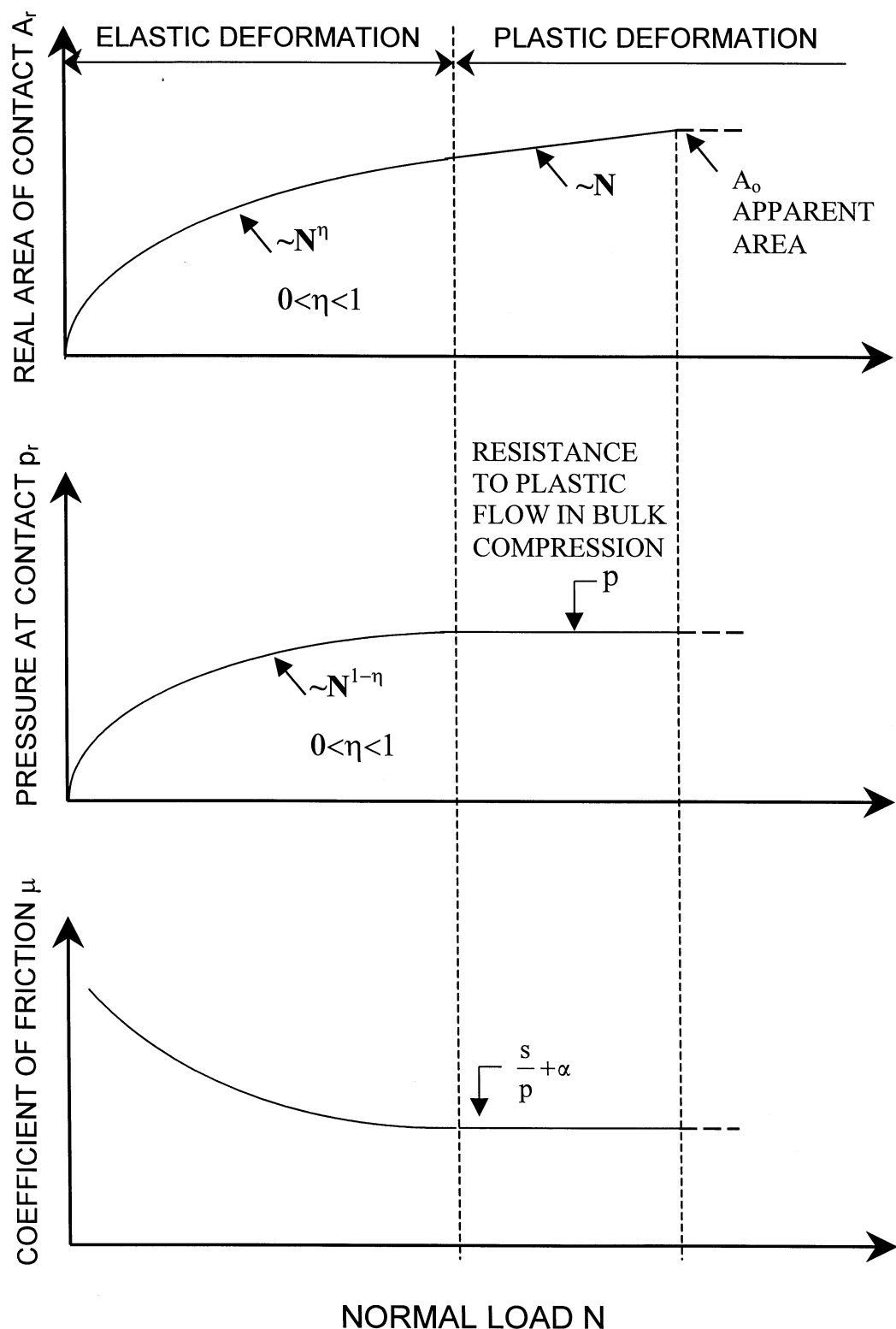


FIGURE 3-9 Variation of Real Area of Contact, Pressure at Contact Area and Coefficient of Sliding Friction with Increasing Normal Load

Therefore, it is possible that the real area of contact is essentially equal to the apparent area of the bearing, A_o . That is, $A_r \approx A_o$ and $p_r \approx N/A_o$. Equation (3-5) can then be written as

$$\mu = \frac{A_o S_o}{N} + \alpha \quad (3-8)$$

Considering that α is small by comparison to the other term in (3-8), equation (3-8) predicts that $1/\mu$ is essentially a linear function of the normal load. Indeed, this behavior is systematically consistent with experimental results. Figure 3-10 presents the inverse of the coefficient of sliding friction at very low velocity of sliding (f_{min} in Fig. 3-8) versus the apparent pressure (N/A_o) from four different experimental studies (Thompson et al., 1955, Mokha et al., 1988; Campbell et al., 1991 and Hwang et al., 1990). The presented data are for unlubricated PTFE in contact with polished stainless steel with a surface roughness of about $0.05 \mu\text{m}$ or less on the arithmetic average scale. The data clearly demonstrate a linear relation between the inverse of the sliding coefficient of friction and the normal load.

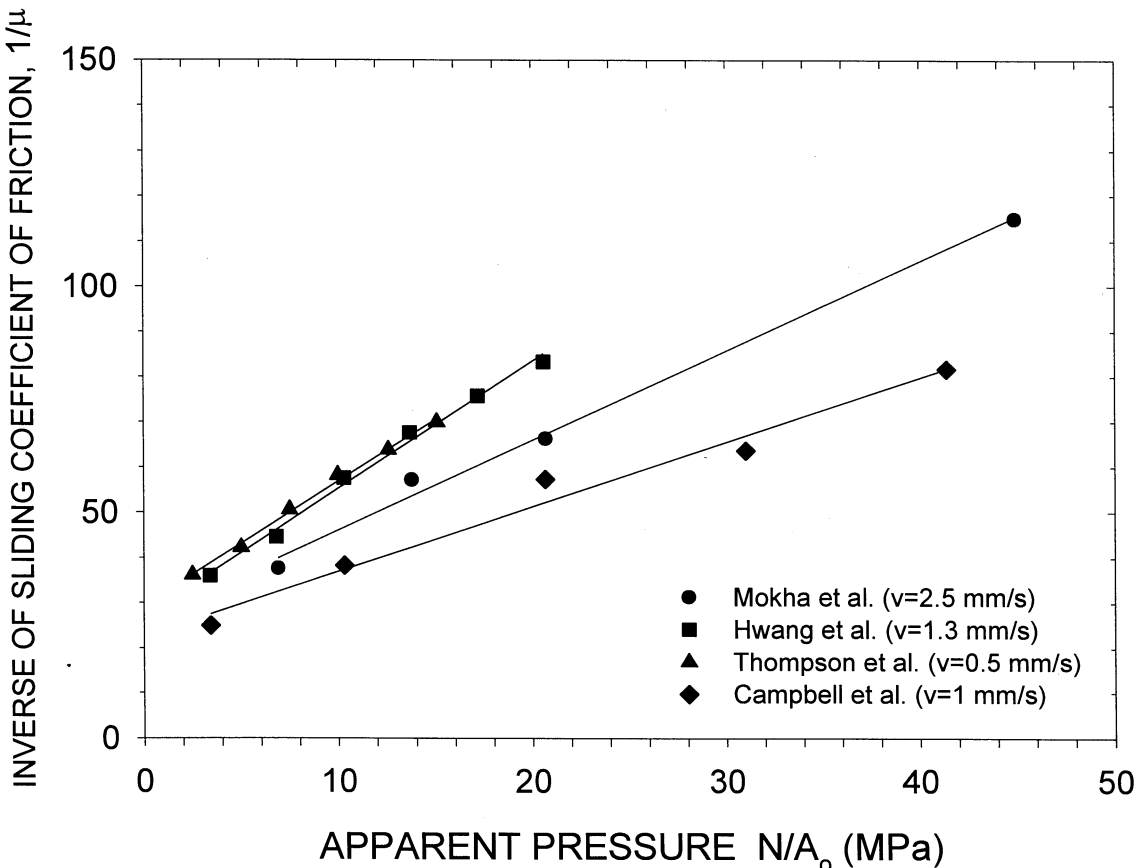


FIGURE 3-10 Relation Between Inverse of Sliding Coefficient of Friction and Apparent Pressure

This linear relation has been first observed by Hwang et al. (1990) who included in their study data from Taylor (1972) and Long (1974) on the breakaway (or static) friction, as

well as data for rougher stainless steel surfaces (roughness of up to 0.25 μm on the arithmetic average scale). That is, the linear relation is valid for a range of conditions which include the velocity and apparent pressure ranges indicated in Figure 3-10, surface roughness of up to 0.25 μm on the arithmetic average scale and specimen size (on this we note that the data in Fig. 3-10 were generated from PTFE specimens having area of between 887 mm^2 and 50,670 mm^2).

At this point it is of interest to review the work of other authors on the dependency of the friction coefficient on normal load. Taylor (1972), Long (1974) and Campbell and Kong (1989) have observed that

$$\mu = Q \left(\frac{N}{A_o} \right)^{\eta-1} \quad (3-9)$$

in which η is generally small (Taylor, 1972 reports 0.58, Long, 1974 reports 0.50, and Campbell and Kong, 1989 report values of 0.13 to 0.45 for normal temperature). Indeed, the adhesion theory of friction predicts for elastic contact (see equations 3-5 and 3-6 with $\alpha = 0$)

$$\mu = k s_o N^{\eta-1} \quad (3-10)$$

However, the theory predicts also that η is larger than 0.67 (when asperities are spherical) and close to unity when the asperities have complex or random shapes (Bowden and Tabor, 1964). Specifically, if we concentrate on the conditions of highly polished stainless steel, normal temperature and very low velocity (conditions for which the adhesion component of friction is expected to dominate), Campbell and Kong (1989) report a value $\eta = 0.13$. This is inconsistent with the theory of elastic or plastic deformation of asperities ($0.67 \leq \eta \leq 1.0$).

Concluding, it appears that (3-8) is in agreement with experimental data and it is consistent with the theory of adhesion. This implies that the real area of contact is approximately equal to the apparent area of the bearing.

Before proceeding with a discussion on the effects of sliding velocity, it is necessary to discuss the origin of the very low value of the sliding coefficient of friction at very low speed. For example, for the conditions of the test data in Figure 3-10, the value of the coefficient of friction is in the range of 0.01 to 0.03. It was once thought that this low friction is due to poor adhesion. In reality the junctions are firmly attached to the surface (hence, the higher static or breakaway friction). However, on sliding a very thin (of the order of a few hundred Angstrom) highly oriented and crystalline film of PTFE is deposited on the stainless steel surface. Sliding occurs at the interface of this film and the bulk of PTFE. The low friction is attributed to the easy shear of this thin film under tangential traction (Makison and Tabor, 1964; Sarkar, 1980).

The coefficient of sliding friction increases with increasing velocity of sliding. The increase above the low velocity value (f_{\min} in Fig. 3-9) is dependent on the velocity of sliding and it is approximately 5 to 6 times of f_{\min} at speeds of interest in seismic applications (500 mm/s or larger). Under these conditions of intense loading, there is considerable frictional heating. When heating is extensive some local melting of PTFE may occur and under these conditions friction should reduce considerably. Thus while not shown in Figure 3-9, there must be some very high velocity for which the coefficient of friction drops.

Frictional heating is not responsible for the increase in friction because it is not observed in low velocity tests that are carried out at high temperatures (Bowden and Tabor, 1964). Rather, the viscoelastic properties of PTFE and the massive transfer of PTFE are responsible for the observed increase in friction (Makison and Tabor, 1964). As the speed of sliding is increased, the force needed to shear the very thin film of PTFE increases. This process continues until the shear force exceeds the strength of the boundaries between crystals of PTFE and massive transfer of PTFE occurs. At this stage, the friction exhibits small increases with increasing velocity due, likely, to the fact that the strain rate in the bulk of PTFE is much smaller than that at the very thin film on the stainless steel surface.

3.6.2 Effect of Temperature

Figure 3-11 illustrates the coefficient of friction as function of the sliding velocity for various temperatures. This is the temperature at the interface at the start of the experiment, or otherwise is the temperature in the bulk of the testing arrangement far away of the sliding interface. Results of the form of Figure 3-11 have been produced by the authors and will be presented in more detail in Section 4. These results are in general agreement with results obtained at low velocity of sliding by Campbell et al. (1991).

Temperature has a dramatic effect on the static (or breakaway) and the very low velocity coefficients of friction (respectively, μ_B and f_{\min} in Fig. 3-11). For unfilled PTFE there is approximately a 7-fold increase in these friction values between the temperatures of 50°C and -40°C. This substantial increase is the effect of the changing viscoelastic properties of PTFE due to temperature. We should note that the friction values in Figure 3-11 are obtained at the first instant at which a particular value of sliding velocity is achieved (note that the experiments are conducted with cyclic motion) so that for very low velocity the heat input is not sufficient to substantially change the temperature.

The heat flux generated by friction is proportional to the coefficient of friction, the average pressure and the velocity of sliding. Accordingly, the heat flux at large velocity (~500 mm/s) is several thousand times larger than the heat flux at very low velocity (≤ 1 mm/s). Thus, substantial frictional heating of the sliding interface occurs at large velocities which, in turn, substantially moderates the effects of low temperature on the viscoelastic properties of PTFE. The result is that the high velocity value of the coefficient of friction (f_{\max} in Fig. 3-11) increases by only approximately 50-percent in the temperature range of 20°C to -40°C. The subject of frictional heating is addressed in section 3.8.

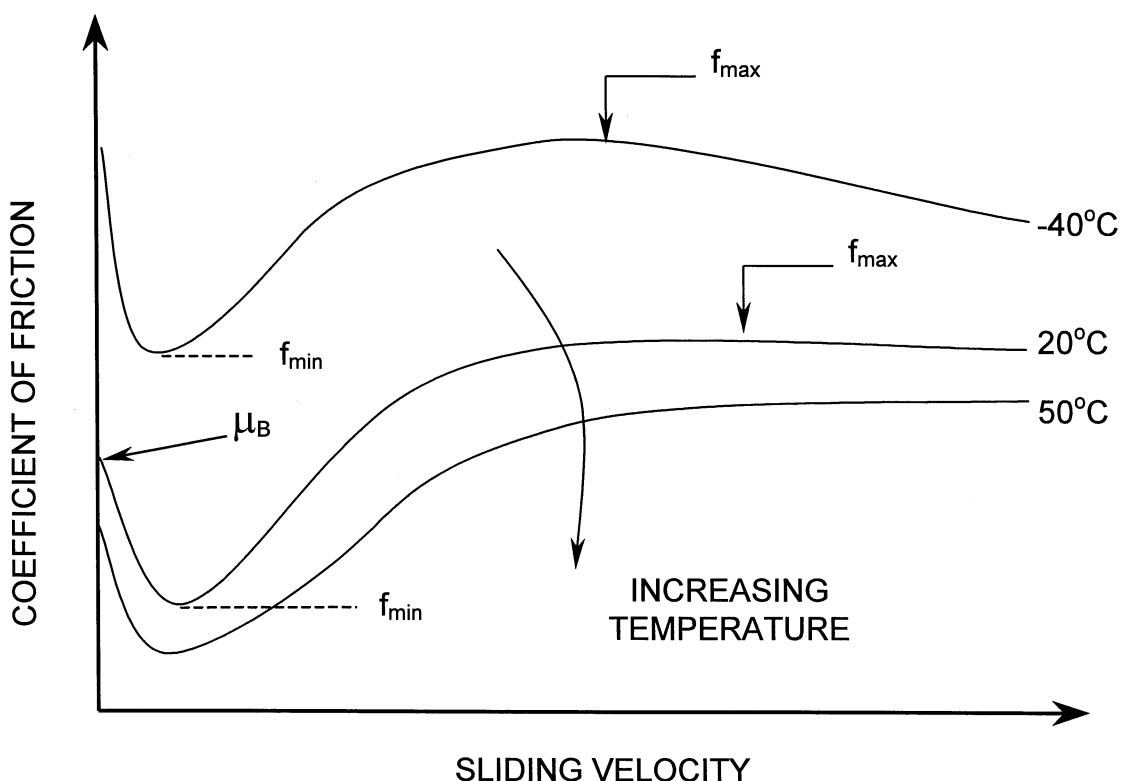


Figure 3-11 Effect of Temperature on the Frictional Properties of PTFE-Polished Stainless Steel Interfaces

3.6.3 Effect of Time of Loading (Load Dwell)

Since PTFE is a viscoelastic material we should expect the real area of contact and hence friction to depend on the load dwell (Bowden and Tabor, 1964). Indeed, experiments conducted with a steel sphere on a block of plastic demonstrated increases in both the real area of contact and the friction force over loading times of 6 to 1000 sec.

Testing of PTFE sliding bearings for the effect of load dwell has been conducted over much longer times, of up to 594 days. Paynter (1973) reported on tests conducted by the Glacier Company in England for dwells of up to 120 hours. Specific results are not reported other than that the static friction increased rapidly up to about 24 hours of dwell of load, and then leveled off. Paynter (1973) speculated (and this was repeated in Campbell and Kong, 1987) that such an increase is an anomaly since one would expect increasing time and increasing load to have the same effect-reduction in friction. He proceeded to suggest that the increase is likely caused by changes in the crystalline structure of PTFE.

Mokha et al. (1990) conducted testing on large specimens for load dwells of 0.5 hour and 594 days to produce nearly identical results on the static friction. Many more tests were conducted by these authors for load dwells of a few minutes to 120 hours (the result are presented in section 4 herein). The results on the static friction exhibit fluctuations that

can not be correlated to the load dwell. Rather, it was observed that static friction is higher in the first test conducted on a new specimen regardless of the load dwell. The static friction is lower in any subsequent test, again regardless of the load dwell. This may be explained by the existence of a film of PTFE on the stainless steel surface which was deposited in the previous tests.

It may be concluded that the time-dependent deformation of PTFE is nearly completed within a very short time interval, likely of the order of a few minutes or hours, resulting in a constant real area of contact. As discussed earlier, the experimental results on the dependency of the low velocity friction on normal load suggest that the real area of contact is approximately equal to the apparent area of the bearing. The results were obtained after some load dwell, which for the data of Mokha et al. (1988) was at least 10 minutes.

The question is whether it is possible to complete the time-dependent deformation of PTFE in such short time intervals and achieve a real area of contact that is constant. If a satisfactory explanation is found, we may conclude that it is likely to reach the condition of the real area of contact being equal to the apparent area. Then the observed dependency of the low velocity friction on normal load and the observed insignificance of load dwell on the static friction may be rationally explained.

One such explanation may be found by investigating the rate of deformation of PTFE under conditions of confined compression. We assume that PTFE can be reasonably modeled as a Kelvin viscoelastic material (Shames and Cozzarelli, 1992). Thus, the one-dimensional behavior of the material is described by

$$\sigma = E(\varepsilon + \tau \dot{\varepsilon}) \quad (3-11)$$

where σ = stress, ε = strain, E = elasticity modulus and τ = retardation time (a dot denotes differentiation with respect to time).

In the three dimensional theory of linear viscoelasticity it is usual to consider separately the viscoelastic behavior under conditions of pure shear and pure dilatation. This is handled by resolving the stress and strain tensors into their deviatoric and spherical parts, for each of which viscoelastic constitutive relations are written. The stress tensor decomposition is given by

$$\sigma_{ij} = s_{ij} + \delta_{ij}\sigma_{kk} / 3 \quad (3-12)$$

where s_{ij} = deviatoric part . Furthermore, the small strain tensor is given by

$$\epsilon_{ij} = e_{ij} + \delta_{ij}\epsilon_{kk} / 3 \quad (3-13)$$

where e_{ij} = deviatoric part of the strain tensor.

A three dimensional generalization of the viscoelastic constitutive equation (3-11) is

$$s_{ij} = 2 \{Q\} e_{ij} \quad (3-14)$$

$$\sigma_{ii} = 3K\varepsilon_{ii} \quad (3-15)$$

where $\{Q\}$ is the differential operator

$$Q = G \left\{ 1 + \tau \frac{\partial}{\partial t} \right\} \quad (3-16)$$

and K = bulk modulus and G = shear modulus. Note that in (3-14) to (3-16) we considered a material with elastic compressibility for bulk behavior and Kelvin-type viscoelasticity for multidimensional distortion. This behavior, while seemingly anomalous, is mathematically possible.

We now consider that a *creep test* is conducted on a column of Kelvin material. That is, a stress σ_0 is applied along direction 1 at time $t = 0$ and then maintained constant thereafter. For the case of uniaxial compression, all stresses other than σ_{11} are zero. The strain in direction 1 can be easily determined to be

$$\varepsilon_{11} = \frac{\sigma_0}{E} \left(1 - e^{-\frac{t}{\tau}} \right) \quad (3-17)$$

That is, the time dependent deformation of the column is dependent exponentially on the negative of the ratio of time to retardation time.

We consider now a block of Kelvin material compressed in a container under confined conditions so that $\varepsilon_{22} = \varepsilon_{33} = 0$. These would approximately be the conditions of a specimen partially retained in a recess and with large shape factor (small thickness, very large diameter) under compression. Solution of (3-11) to (3-16) results in for the strain

$$\varepsilon_{11} = \frac{3\sigma_0}{4G + 3K} \left\{ 1 - e^{-(1 + \frac{3K}{4G})\frac{t}{\tau}} \right\} \quad (3-18)$$

Evidently, deformation proceeds with a rate which is exponentially dependent on the negative of time and constant $\left(1 + 0.75 \frac{K}{G} \right) \frac{1}{\tau}$. This constant may be related to the Poisson's ratio so that estimates of its order may be made:

$$1 + 0.75 \frac{K}{G} = \frac{3(1 - v)}{2(1 - 2v)} \quad (3-19)$$

For PTFE $\nu \approx 0.46$ (du Pont, 1981), so that (3-19) gives a number of about 10. That is, the creep function of the confined material is proportional to $1 - \exp(-10t/\tau)$. Evidently, the confined material creeps at a substantially faster rate than the unconfined one. Experimental data on the creep of PTFE with and without retention in a recess demonstrate these substantially different rates of creep (Kauschke and Baigent, 1986; Campbell and Kong, 1987).

We have demonstrated that confined PTFE creeps at a much faster rate than unconfined PTFE. Therefore, it is likely that the condition of the real area of contact being approximately equal to the apparent area of the bearing is reached within very short time. If so, we have a rational explanation for (a) the observed insignificant effect of load dwell on the static friction, and (b) the observed dependency of the very low velocity sliding friction on the inverse of the normal load.

3.7 Friction in Bimetallic Interfaces

Bimetallic interfaces had a number of applications in structures. Specifically:

(a) Stainless steel in contact with bronze that was impregnated with lead has been used in the sliding isolation system of Koeberg Nuclear Power Station in South Africa (Pavot and Polust, 1979; Lee, 1993). The selection of this interface appears to have been based on considerations of the compatibility of the utilized metals. Rabinowicz developed in 1971 (see Rabinowicz, 1995) compatibility charts for metal combinations based on their solid and liquid solubility. Rabinowicz determined that two metals that can form alloy solutions or alloy compounds with each other have strong adhesion. Of the readily available and inexpensive metals, only iron and lead have no liquid solubility and very low solid solubility, hence they exhibit low adhesion. Stainless steel and bronze have been selected on the basis of preventing bimetallic corrosion. Lead is extruded from pockets within the bronze during the sliding process so that it and its oxide lubricate the interface.

Pavot and Polust (1979) reported friction coefficient values for this interface in the range of 0.15 to 0.22 for apparent pressures of 2 to 15 MPa, low and high sliding velocity and load dwells of up to 30 days. The interfaces were finally used under apparent pressure in the range of 2 to 8 MPa and the design was based on the assumption that the bearings obey Coulomb's law with a coefficient of friction in the range of 0.15 to 0.25.

Following 14 years in service, 60 sample bearings, which were stored in prestressed rigs in the same environment as the isolation bearings, were re-tested (Lee, 1993). Marked increases in the static (or breakaway) coefficient of friction have been recorded over the baseline test results. Specifically, the friction coefficient increased to a value of about 0.38, whereas in the baseline tests the friction was at about 0.22.

This increase, which occurred in the absence of any significant corrosion, is likely the result of an increase in the real area of contact due to creep.

(b)Stainless steel in contact with DU material has been very recently used in the seismic isolation bearings of a pair of highway bridges over the Corinth Canal in Greece (Constantinou, 1998). The DU material consists of bronze powder, which is sintered onto a steel backing. The porous structure of this material is impregnated with a mixture of lead and PTFE. On sliding, the lead and PTFE mixture is drawn from the porous bronze and lubricates the contact. The interface can sustain high pressures and exhibits low sliding friction following a typically high static (or breakaway) friction (Taylor, 1972).

DU bearings have been extensively used in automotive, machine and other industrial applications where load dwells are typically very short. Manufacturers of DU bearings for these applications warn on the significant effect of load dwell on the static friction of these bearings. For example, Garlock Bearings, Inc. (1987) provides the information that load dwell of few hours to few days may result in 50-percent to 200-percent increase in the static (breakaway) friction. Again these increases in the static friction are likely caused by increases in the real area of contact due to creep.

(c)Steel-on-steel, bronze-on-steel and steel-on-bronze interfaces have been used in the past, typically with lubricants such as grease and graphite, as bridge expansion bearings (Transportation Research Board, 1977). Steel-on-steel and bronze-on-bronze interfaces experienced cold welding, as it should have been expected given that identical metals exhibit very high adhesion. Corrosion has been reported as the main source of problems for the steel-on-steel and steel-on-bronze interfaces (Transportation Research Board, 1977; Jacobsen, 1977). Actually it is surprising that steel-on-bronze interfaces have been ever tried given that this interface may suffer severe bimetallic corrosion (Military Standards, 1976; British Standards Institution, 1990). Specifically, the British Standards Institution (1990) classified the additional corrosion of carbon and low alloy steel when in contact with copper, brass or bronze as moderate to severe.

(d)Lubricated bronze-steel interfaces are now commonly used for accommodating rotation in bridges. Bronze in these interfaces is impregnated with graphite in a variety of patterns. The graphite projects above the bronze approximately 1.5 mm and it spread upon load and movement application, thus lubricating the contact. The same interface has been used over 20 years ago in sliding bearings (Transportation Research Board, 1977). While this interface can maintain the solid lubricant much more effectively than when it is spread at the interface, eventually a condition is reached in which steel bears directly on bronze. Problems of corrosion and of significant increase in friction are then encountered. Transportation Research Board (1977) reports on such experiences, of which specific mention is made of a state which experienced a number of corrosion cases of galvanized steel-lubricated bronze interfaces. Again this should be expected since galvanized steel is coated with zinc which may suffer moderate to fairly severe additional corrosion when in contact with bronze (British Standards Institution, 1990).

(e) A number of bimetallic interfaces have been used or proposed for use in energy dissipation devices (Soong and Constantinou, 1994; Soong and Dargush, 1997; Constantinou et al., 1998). These are in the form either of graphite-impregnated bronze in contact with stainless steel or of brass in contact with steel (Grigorian and Popov, 1993). The latter is clearly susceptible to severe corrosion due to bimetallic contact (British Standards Institution, 1990) and the 1999 AASHTO (American Association of State Highway and Transportation Officials, 1999) strongly discourages its use. The graphite-impregnated bronze to stainless steel interface, while much more reliable in terms of corrosion resistance, can suffer from the aforementioned load dwell-creep induced increase in the static coefficient of friction.

It should be clear now that bimetallic interfaces that may be of use in sliding bearings or other elements in isolation systems (as the sliding interface) consist of stainless steel in contact with bronze which is impregnated with some form of solid lubricant. Field observations, laboratory experiments and data from industrial applications show potential for substantial increases of the static friction of these interfaces with load dwell. The likely explanation for this phenomenon is the very small real contact area in bimetallic interfaces, and thus the potential for increase in the area under prolonged loading.

3.8 Frictional Heating

3.8.1 Theory

To maintain sliding motion mechanical work must be done in order to overcome the friction forces. This work is converted into thermal energy, which is manifested as a temperature rise. Herein we attempt to quantify the temperature rise at the sliding interface based primarily on the classic work of Carslaw and Jaeger (1959).

The sliding contact problem of interest to us is illustrated in Figure 3-12. Body 1 (PTFE) is stationary, whereas body 2 (stainless steel) moves with known displacement history. The contact surface is the surface of the PTFE (presumed to be in full contact with the stainless steel). This surface represents the heat source, which has a heat flux distribution q . Portion q_1 of this heat flux enters the body 1, whereas portion q_2 enters the body 2. It is reasonable (and conservative in the estimation of the surface temperature) to assume that $q_1 = 0$ and $q_2 = q$. That is, the entire generated heat is supplied to body 2 (stainless steel). Detailed calculations of the heat partitioning problem (see American Society for Metals, 1992 for a review of frictional heating calculations) for a wide range of velocities of motion and contact area dimensions, confirm that for PTFE-stainless steel interfaces the heat partition factor q_1 / q is very small. The reason for this is the large values of the thermal conductivity and thermal diffusivity of stainless steel by comparison to those of PTFE. Table 3-1 presents the thermal properties of these materials (from American Society for Metals, 1992). Further information may be found in Linde (1993).

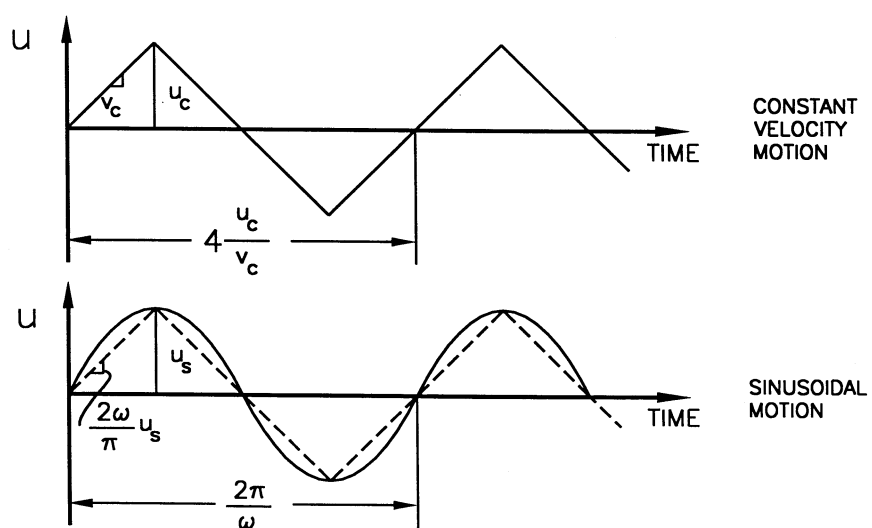
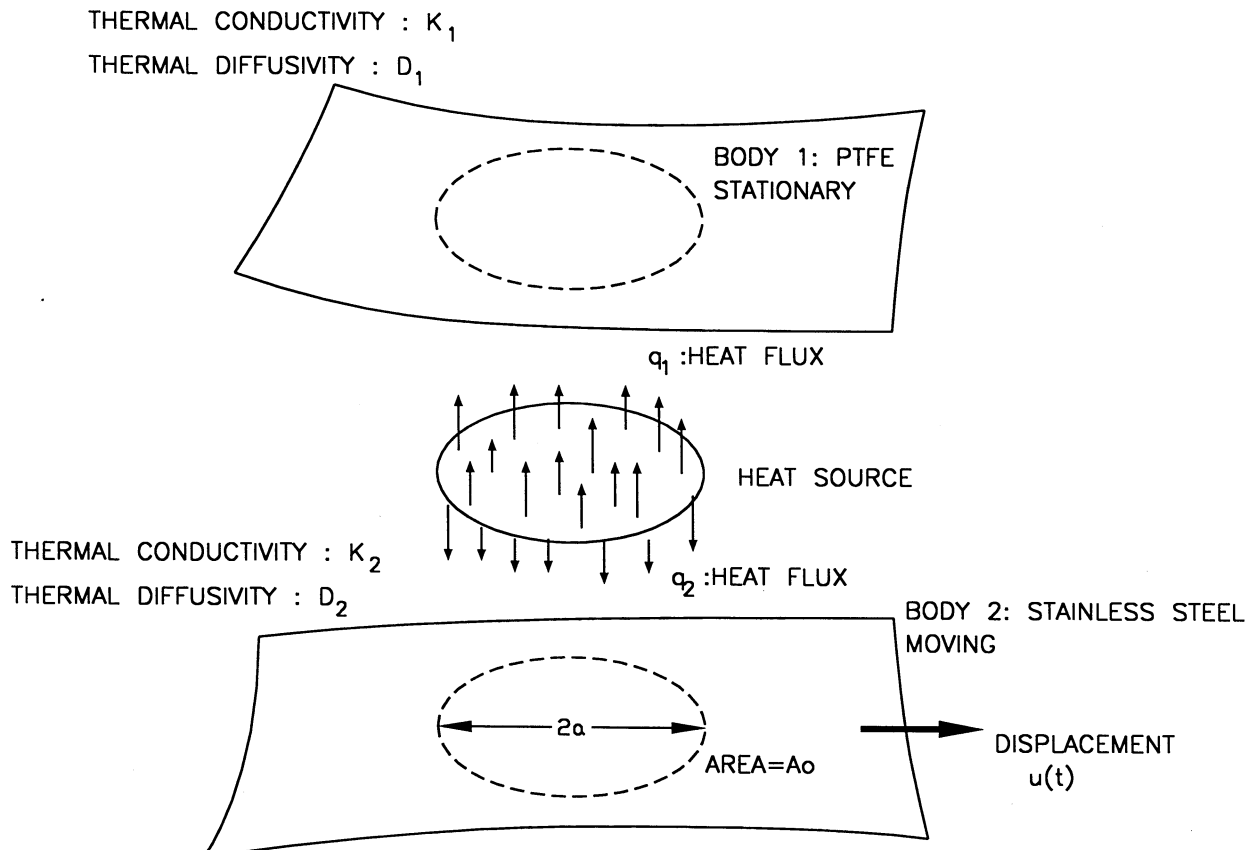


FIGURE 3-12 Schematic of Two Bodies in Sliding Contact

TABLE 3-1 Thermal Properties of PTFE and Stainless Steel

Material	Thermal Conductivity (k) W/ (m. $^{\circ}$ C)						Thermal Diffusivity (D) m 2 /s At 20 $^{\circ}$ C
	At 0 $^{\circ}$ C	At 20 $^{\circ}$ C	At 100 $^{\circ}$ C	At 300 $^{\circ}$ C	At 600 $^{\circ}$ C	At 1000 $^{\circ}$ C	
Unfilled PTFE	-	0.24	-	-	-	-	0.010 x 10 $^{-5}$
18%Cr, 8%Ni Steel	16.3	16.3	17	19	26	31	0.444 x 10 $^{-5}$
15% Cr, 10% Ni Steel	-	19	-	-	-	-	0.526 x 10 $^{-5}$

1 W = 1 N.m/s

Carslaw and Jaeger (1959) analyzed the problem of a semi-infinite solid with constant heat flux q at the free surface (see Figure 3-13 for illustration). The solution for the temperature rise as function of depth x and time t (note that this is a one-dimensional problem) is

$$T(x, t) = \frac{2q}{k} \left\{ \left(\frac{Dt}{\pi} \right)^{1/2} \exp\left(-\frac{x^2}{4Dt}\right) - \frac{x}{2} \operatorname{erfc}\left(\frac{x}{2D^{1/2}t^{1/2}}\right) \right\} \quad (3-20)$$

where k = thermal conductivity of the solid, D = thermal diffusivity of the solid and erfc = complementary error function. At the surface ($x = 0$) the temperature rise is

$$T_s = \frac{2q}{k} \left(\frac{Dt}{\pi} \right)^{1/2} \quad (3-21)$$

In utilizing this solution (particularly equation 3-21) for the problem of Figure 3-12 we recognize the following:

- (a) The solution is for a half-space with heat flux over the entire free surface, whereas the problem is for a body of finite plan dimensions and depth. However, when the interest is for the temperature generated by friction at the surface of a large contact area, the solution should be valid. Evidence for this may be found in the solution of the problem of a slab with prescribed heat flux at one surface (Carslaw and Jaeger, 1959, p. 113). While this solution is too complex to be of practical value, we can find that its leading term for the temperature rise at the surface is exactly that of (3-21).
- (b) The heat flux generated by friction is not, in general, constant but rather it exhibits dependencies on both time and space (dependency on y and z). This is due to dependencies of the friction force (per unit area) on the history of motion and on the

normal load distribution. To bypass this problem we shall utilize an average constant value of the heat flux so that the estimate for the temperature rise will be on an average over the apparent area of contact.

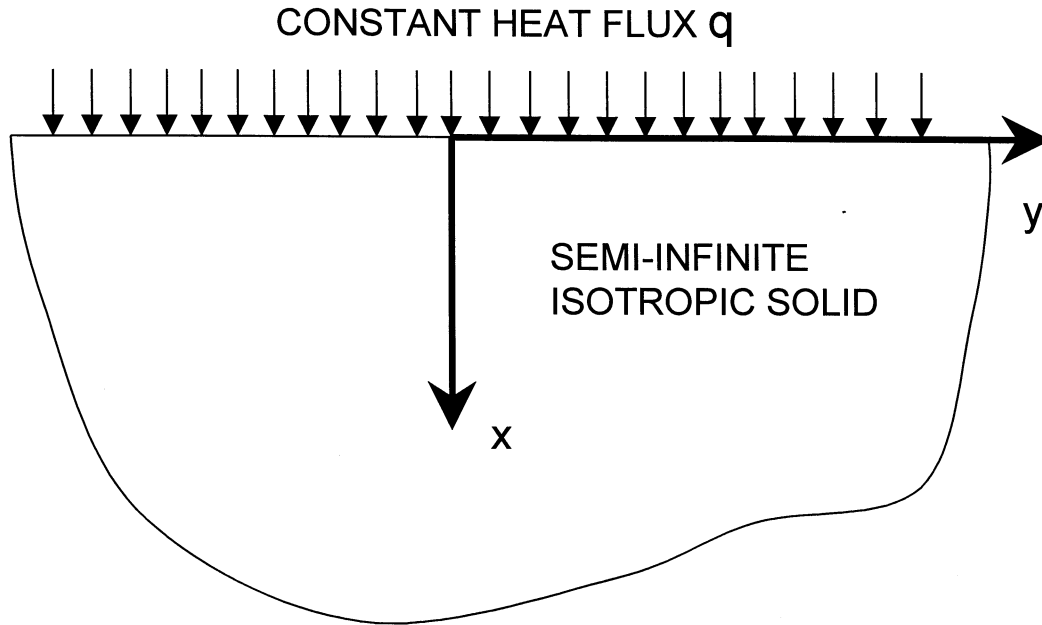


FIGURE 3-13 Semi-infinite Solid with Constant Heat Flux at $x=0$

- (c) We will consider motion of body 2 such that the amplitude is small by comparison to the radius of the apparent area of contact. Accordingly, we can assume that, on the average, body 2 is supplied with a constant heat flux over the duration of the motion. We will later relax this limitation and consider large amplitude motions.
- (d) We will consider short time intervals so that the solution for the heat applied over the entire free surface of a half-space is valid. Note that for very long time intervals heat will flow laterally to the cooler parts of the moving body, heat will be lost by radiation and convection, and eventually a stable condition may be reached.

Consider now that the motion is as illustrated in Figure 3-12, that is, as it would have been in a constant velocity test (sawtooth displacement). Time t is the total exposure time (for $u_c < a$), that is,

$$t = \frac{4u_c}{v_c} N \quad (3-22)$$

where N = number of cycles. Moreover, the average heat flux is equal to the energy dissipated in N cycles ($= 4N F_f u_c$) divided by the area A_0 and time t . That is,

$$q_{av} = \frac{F_f v_c}{A_o} = \mu p v_c \quad (3-23)$$

where F_f = friction force, μ = coefficient of sliding friction, and p = apparent pressure (assumed constant). Substituting (3-22) and (3-23) into (3-21) we obtain

$$T_s = 2.26 N^{1/2} \frac{\mu p u_c v_c}{k} \left(\frac{D}{u_c v_c} \right)^{1/2} \quad (3-24)$$

It should be noted that the dimensionless quantity $u_c v_c / D$ is the Peclet number. It is the ratio of the velocity of the surface to the rate of thermal diffusion into the moving body.

Consider now the case of sinusoidal motion of body 2 as illustrated in Figure 3-12. Using (3-21) with

$$q_{av} = \frac{2\mu p u_s \omega}{\pi} \quad (3-25)$$

and

$$t = \frac{2\pi N}{\omega} \quad (3-26)$$

we arrive at

$$T_s = 1.8 N^{1/2} \frac{\mu p u_s^2 \omega}{k} \left(\frac{D}{u_s^2 \omega} \right)^{1/2} \quad (3-27)$$

The usefulness of (3-27) is seen when the sinusoidal motion is replaced by an equivalent constant velocity motion as shown in Figure 3-12 with dashed line. That is, if we set $u_c = u_s$ and $v_c = 2u_s \omega / \pi$ (which indeed describe a reasonable representation of the sinusoidal motion by a constant velocity motion) in (3-24), we recover equation (3-27).

Equations (3-24) and (3-27) are similar in form to equations used by tribologists to estimate the flash temperature (American Society for Metals, 1992). The flash temperature is defined as the rise in temperature at the real area of contact. However, (3-24) and (3-27) are based on the use of the apparent area so that the calculated temperature is a representative average value of the temperature rise at the sliding interface. It is useful for assessing the structural effects of frictional heating on the stainless steel overlay (e.g., buckling) and in estimating average wear. Moreover, it can be compared with direct measurements of the temperature rise at some small depth inside the stainless steel plate (although the measurement is expected to be less than the actual average value at the surface). Furthermore, we expect the actual maxima and minima of the temperature rise to differ by relatively small amounts from the average temperature rise because in PTFE-polished steel interfaces the real area of contact is large and likely equal to the apparent area (see section 3.6).

The predictions of the presented theory are now compared with experimental results. Section 4.4 (to follow) describes tests conducted on unfilled PTFE-polished stainless steel interfaces (Type 304). Figure 4-1 illustrates the machine used and Appendix A presents a sample of experimental results. The imposed motion of the stainless steel plate consisted of an initial portion of 60 to 80 sec. duration with very low sliding velocity (e.g., in test UF-TEST43A of Appendix A the duration was 60 sec and average velocity was 0.42 mm/s). Subsequently, three and a quarter cycles of sinusoidal motion of specified frequency and amplitude were imposed. Measurements of temperature were made with a thermocouple embedded at the center of stainless steel plate at depth of 1.5 mm. The moving plate had a total depth of 16 mm.

We will first investigate the effect of the initial portion of the imposed motion on the surface temperature. Note that the tests described in section 4.4 were conducted in order to assess the effect of temperature on the frictional properties. There was a concern on whether this initial portion causes a substantial rise in the temperature of the interface. To estimate the rise in temperature we utilize (3-21) and (3-23). For test UF-TEST43A (see Appendix A) we have for the initial portion: $\mu = 0.028$ (measured), $v_c = 4.2 \times 10^{-4}$ m/s (average velocity), $t = 60$ sec, $p = 20.7 \times 10^6$ N/m². Values of thermal conductivity and thermal diffusivity for 18% Cr, 8% Ni steel at 20°C are used (Table 3-1). The result is $T_s = 0.28^\circ\text{C}$, that is, insignificant (the thermocouple did not record any temperature change – its accuracy on the visual display was 1°C).

Table 3-2 presents a comparison of measured and calculated maximum rise in temperature in a number of tests from Appendix A and a number of tests from Mokha et al. (1988). The latter tests were conducted with a similar testing arrangement using unfilled PTFE-polished stainless steel (Type 304) interfaces. The moving plate dimensions and the depth of installation of the thermocouple were identical to those in the tests of Appendix A. However, the specimens were large in size and lacked the supporting rotational element.

The comparison in Table 3-2 demonstrates that the calculation predicts reasonably well the measured temperature, although in some cases it overestimates and in other cases it underestimates the measured value. A source of discrepancies is the measurement. The actual distribution of temperature depends on the normal pressure distribution (and accordingly heat flux), which depends on the loading arrangement (existence of rotational element, leveling of surfaces, etc.) On the other hand the measurement is made at a single point and it is unknown whether this point is representative of the average conditions at the surface. Another possible contributor to errors in the measurement is the testing of two interfaces (see Fig. 4-1) and, therefore, it is possible that heat flux from the second interface affected the temperature at the thermocouple near the first interface. Calculations of the distribution of temperature with depth (see Figure 3-14) show this to be of significance only for the very slow test No. 94.

TABLE 3-2 Comparison of Measured and Calculated Maximum Rise in Temperature in Unfilled PTFE-Polished Stainless Steel (Type 304) Interfaces

Source	Test No.	Diameter of PTFE Specimen (mm)	N	u_s (m)	ω (r/s)	Apparent Pressure (MPa)	μ	Measured Temperature Rise ($^{\circ}$ C)	Calculated Surface Temp. Rise ($^{\circ}$ C)	Calculated Temperature Rise At x = 1.5 mm ($^{\circ}$ C)
Section 4.4 Appendix A	UF-TEST43A	95	3.25	0.0254	12.57	20.7	0.098	50	76.7	43.5
	UF-TEST44	95	3.25	0.0127	12.57	20.7	0.014	29	40.7	23.1
	UF-TEST94	95	3.25	0.0127	0.2	20.7	0.036	1	1.7	1.6
Mokha et al. (1988)	68	254	5	0.0500	2.0	20.7	0.065	51	49.5	42.0
	86	254	5	0.1016	3.77	13.8	0.069	66	97.6	77.7
	156	127	5	0.0510	2.0	20.7	0.067	37	52.1	44.2
	157	127	5	0.0510	3.14	44.9	0.046	51	97.2	78.9

Notes: All tests conducted with N cycles of sinusoidal motion.

1: Average value for N cycles

2: Measured at depth of 1.5 mm (accuracy of $\pm 1^{\circ}$ C)

3: Equation (3-27)

4: Equation (3-20) with q given by (3-25) and t given by (3-26)

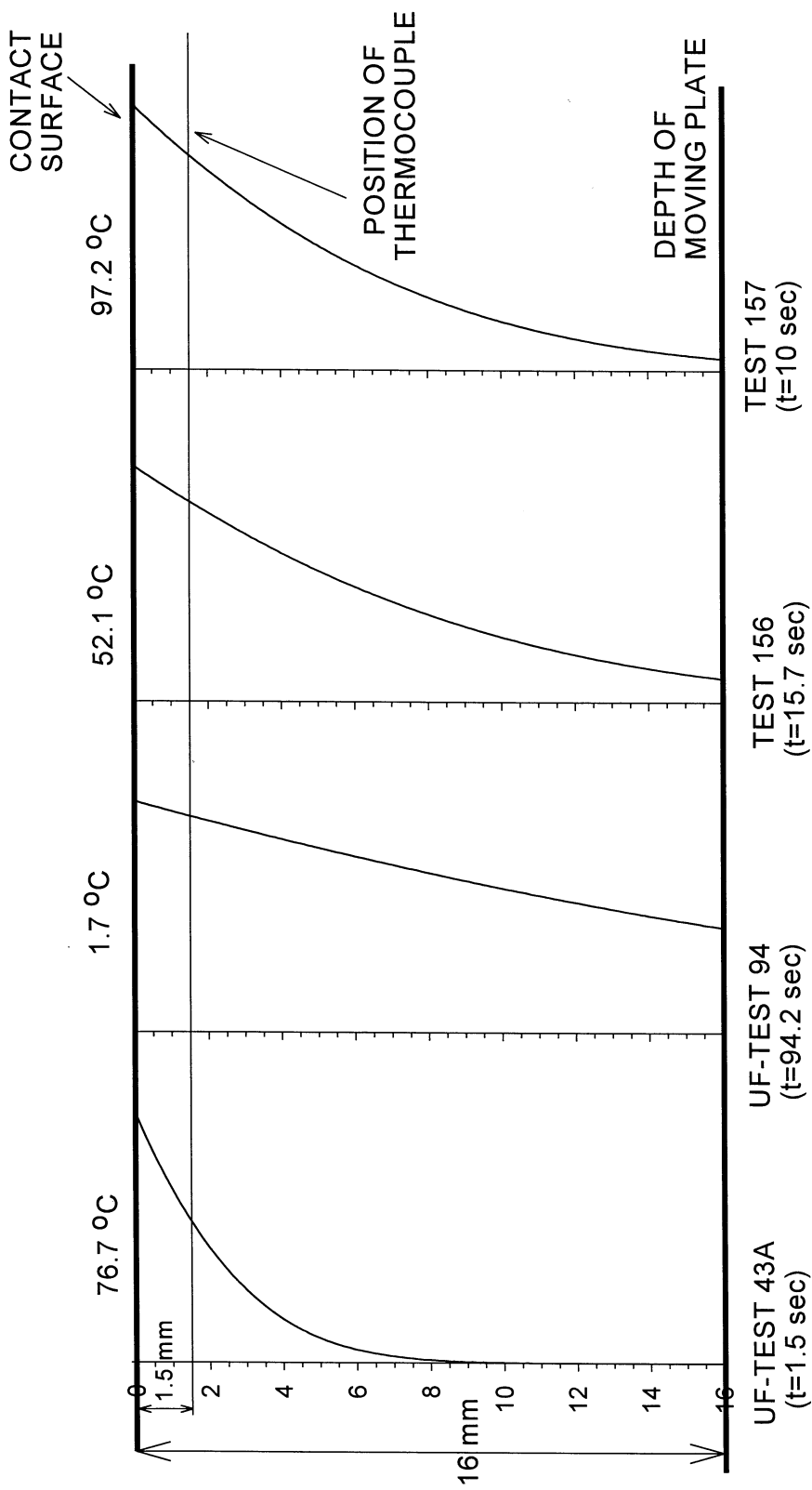


FIGURE 3-14 Calculated Distribution of Temperature Rise with Depth of Stainless Steel Plate at Conclusion of Testing

The presented solution (eq. 3-24 and 3-27) is valid when the amplitude of motion, u_c or u_s , is less (in theory much less) than the radius of the apparent contact area, a . Under these conditions, the average exposure time of any point within the apparent area is equal to the duration of the motion of body 2. One may note that for tests No. 86, 155 and 157 in Table 3-2, the amplitude of motion approached the radius of the specimen so that the conditions of continuous heat flux supply were not fully valid. It should be expected for these cases that the presented theory produces conservative results. Indeed, this is the case.

A more interesting situation is when the amplitude of motion is larger than the radius a of the apparent contact area. This is the typical situation in sliding seismic isolation bearings. To illustrate the difference between this case and the previously studied case of small amplitude motion consider that body 2 in Figure 3-12 moves at constant velocity v_c in a motion described by $u = v_c t$. The time during which any point on body 2 is exposed to heat flux is somehow less than $2a/v_c$ (it will be exactly that amount if the apparent area is square). We will show that the average exposure time is $\pi a/2v_c$. Now consider that the motion is as illustrated in Figure 3-12 with $u_c > a$. In each half cycle of motion there will be heat flux on the surface of body 2 for a duration $\pi a/2v_c$ followed by an interval of zero flux (the surface of body 2 moves beyond the heat source). That is, we have a case of intermittent heat flux, as if a heating element is periodically switched on and off. Apparently, the use of (3-24) or (3-27), which are based on the assumption of continuous heat flux, would yield a conservative estimate of the temperature rise.

We start the analysis of this problem by evaluating the average time that any point on body 2 is exposed to heat flux from the circular heat source. Consider the circular heat source to be described by $y^2 + z^2 = a^2$ and that motion is along the y -axis and is of constant velocity. The average exposure time is

$$t_{av} = \frac{1}{a} \int_{-a}^a \frac{(a^2 - z^2)^{1/2} dz}{v_c} = \frac{\pi a}{2v_c} \quad (3-28)$$

The distance traveled during this time is $\pi a/2$.

The average heat flux during the average exposure time is equal to the friction force times distance traveled and divided by the area of the heat source (πa^2) and the average exposure time. That is,

$$q_{av} = \mu p v_c \quad (3-29)$$

where μ = coefficient of friction and p = apparent pressure. We will again assume that this heat flux is supplied entirely to body 2.

Figure 3-15 (a) illustrates the configuration of the two bodies and the considered periodic constant velocity motion. Figure 3-15 (b) shows the resulting history of heat flux, whereas (c) shows the heat flux history shifted in time for ease in the analytical solution. Note that during the time intervals t_o , it is assumed that the heat flux is zero (as if the exposed to air surface of body 2 is insulated). In reality there is loss of heat due to convection and radiation, however, it is neglected as being insignificant.

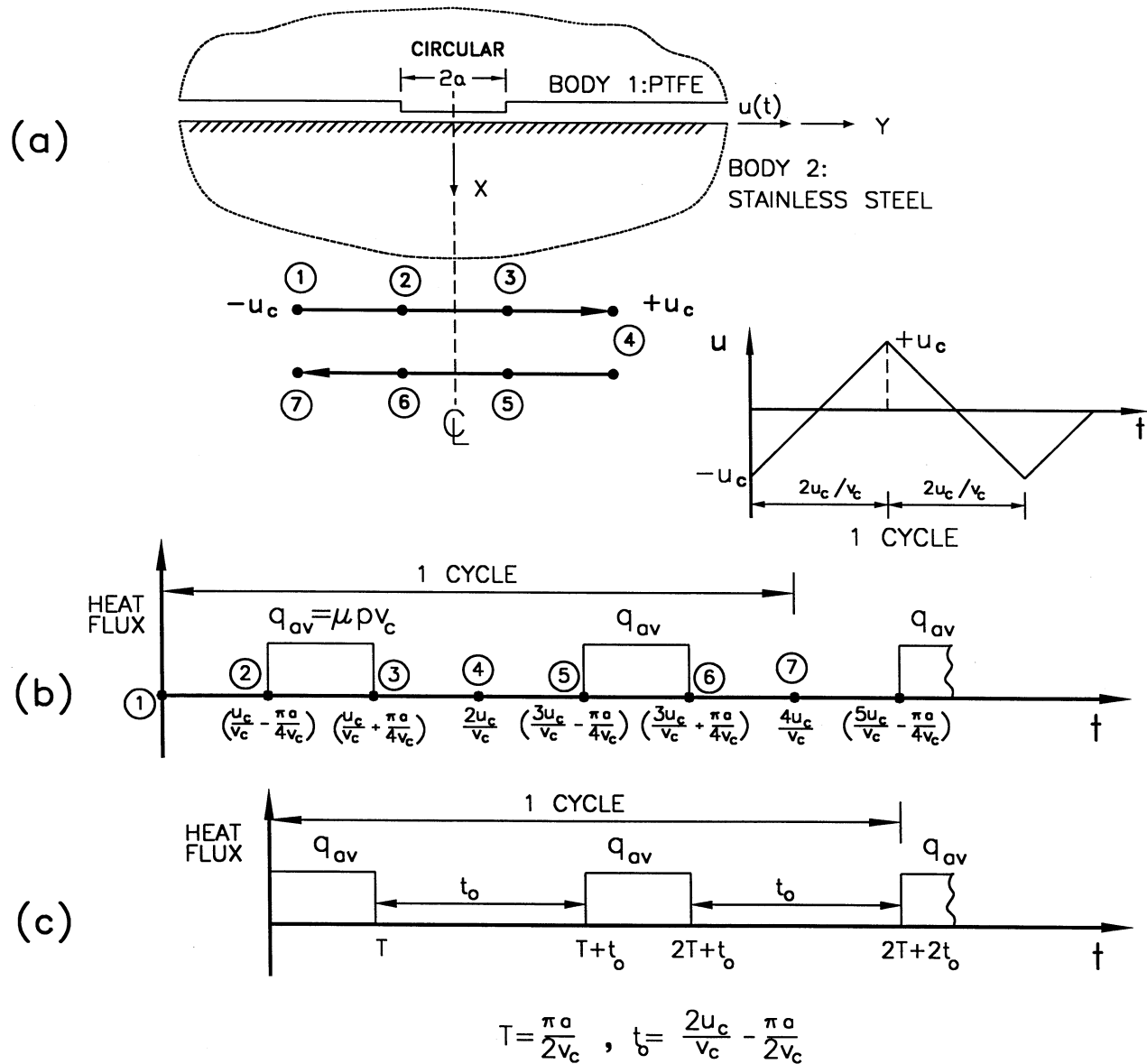


FIGURE 3-15 History of Heat Flux Input in Periodic Constant Velocity Motion of Large Amplitude

Carslaw and Jaeger (1959) presented the solution for the isotropic semi-infinite body subjected at $x = 0$ to constant heat flux, q , of duration T , that is, for what is shown in Figure 3-15(c) with t_0 being infinite. The solution for the temperature rise if $t < T$ is given by (3-20), whereas for $t > T$ the temperature rise is given by

$$T(x, t) = \frac{2qD^{1/2}}{k} \left\{ t^{1/2} \text{ierfc} \left(\frac{x}{2D^{1/2}t^{1/2}} \right) - (t-T)^{1/2} \text{ierfc} \left(\frac{x}{2D^{1/2}(t-T)^{1/2}} \right) \right\} \quad (3-30)$$

where

$$\text{ierfc}(x) = \int_x^{\infty} \text{erfc}(\zeta) d\zeta = \frac{e^{-x^2}}{\pi^{1/2}} - x \text{erfc}(x) \quad (3-31)$$

This function takes the value $1/\pi^{1/2}$ for $x = 0$. Accordingly, the solution for the surface ($x = 0$) temperature rise takes the simple form

$$T_s = \frac{2qD^{1/2}}{\pi^{1/2}k} \left\{ t^{1/2} - (t-T)^{1/2} \right\} \quad (3-32)$$

The solution for the intermittent heat flux of Figure 3-15(c) may be now constructed using (3-32):

For $t = 2T + t_0$ (first cycle)

$$T_{s1} = \frac{2q_{av}D^{1/2}}{\pi^{1/2}k} \left\{ (2T + t_0)^{1/2} - (T + t_0)^{1/2} + T^{1/2} \right\} \quad (3-33)$$

For $t = 4T + 3t_0$ (second cycle)

$$T_{s2} = \frac{2q_{av}D^{1/2}}{\pi^{1/2}k} \left\{ (4T + 3t_0)^{1/2} - (3T + 3t_0)^{1/2} + (3T + 2t_0)^{1/2} - (2T + 2t_0)^{1/2} \right\} + T_{s1} \quad (3-34)$$

For $t = 6T + 5t_0$ (third cycle)

$$T_{s3} = \frac{2q_{av}D^{1/2}}{\pi^{1/2}k} \left\{ (6T + 5t_0)^{1/2} - (5T + 5t_0)^{1/2} + (5T + 4t_0)^{1/2} - (4T + 4t_0)^{1/2} \right\} + T_{s2} \quad (3-35)$$

For $t = 8T + 7t_0$ (fourth cycle)

$$T_{s4} = \frac{2q_{av}D^{1/2}}{\pi^{1/2}k} \left\{ (8T + 7t_0)^{1/2} - (7T + 7t_0)^{1/2} + (7T + 6t_0)^{1/2} - (6T + 6t_0)^{1/2} \right\} + T_{s3} \quad (3-36)$$

For $t = 2nT + (2n-1)t_o$ (nth cycle)

$$T_{sn} = \frac{2q_{av}D^{1/2}}{\pi^{1/2}k} \left\{ [2nT + (2n-1)t_o]^{1/2} - [(2n-2)(T+t_o)]^{1/2} \right. \\ \left. + [(2n-1)T + (2n-2)t_o]^{1/2} - [(2n-2)(T+t_o)]^{1/2} \right\} + T_{s(n-1)} \quad (3-37)$$

Equations similar to (3-33) to (3-37), however much more complex, may be written for the temperature rise at depth $x > 0$ using (3-30). Moreover, a general solution for the problem of the semi-infinite body with heat flux $q(t)$ at $x = 0$ may be deduced from the solution of the problem of constant heat flux (eq. 3-20) and use of Duhamel's theorem (Carslaw and Jaeger, 1959):

$$T(x, t) = \frac{D^{1/2}}{\pi^{1/2}k} \int_0^t q(t-\tau) \exp\left(-\frac{x^2}{4Dt}\right) \frac{d\tau}{\tau^{1/2}} \quad (3-38)$$

In the light of these results we revisit Table 3-2 and attempt an explanation for the differences between calculated and measured temperatures. For the first four tests in this table the amplitude of motion is small by comparison to the radius of the heat source ($u_s/a \sim 0.25$ to 0.5). Under these conditions we expect the theory on which the calculations were based to be valid. Indeed, the calculation is within 20-percent or less of the measurement. For the remaining tests the ratio $u_s/a = 0.8$ and we have conditions approaching those of intermittent heat flux. Accordingly, we should expect the calculated temperatures to be more than the measured ones, and indeed this is the case.

To provide an example of surface temperature calculation for large amplitude, we consider test UF-TEST43A in Table 3-2 but assume three cycles with $u_s = 0.095$ m, that is, $u_s/a = 2.0$ (tests under such conditions have been recently conducted and reported in section 3.8.2). To perform calculations we first convert the harmonic motion to equivalent periodic constant velocity motion (see Fig. 3-12). That is, $u_c = u_s = 0.095$ m and $v_c = 2u_s \omega/\pi = 0.760$ m/s. Using $\mu = 0.098$ and $p = 20.7$ MPa, (3-29) gives for the average heat flux $q_{av} = 1,541,736$ W/m². The average duration of the heat flux $T = \pi a/2v_c = 0.0982$ sec., and the time between intermittent fluxes $t_o = 2u_c/v_c - T = 0.1518$ sec. (see Fig. 3-15). Using the same thermal properties (for temperature of 20°C) and (3-35) we calculate a surface temperature rise $T_s = 138.5^\circ\text{C}$. We can furthermore slightly reduce this estimate by using a higher value for the thermal conductivity that is appropriate for the absolute temperature of about 150°C (see Table 3-1).

It is interesting to note that a quick and conservative estimate of the temperature rise may be obtained by utilizing (3-21) with t being the total exposure time in the three cycles of test. That is, $t = 6T = 0.5892$ sec. The result is 172.6°C. On the other hand if we utilize the inapplicable solution for small amplitude motion (eq. 3-27) we calculate a temperature rise $T_s = 275.4^\circ\text{C}$, which is totally wrong.

Recapitulating, the temperature rise at the sliding contact of sliding bearings depends on:

- (a) The heat flux generated at the contact surface. In general, the heat flux is given by

$$q = \mu p \dot{u} \quad (3-39)$$

where \dot{u} = velocity of body 2 (see Fig. 3-12). Note that all quantities in (3-39) may be functions of time.

- (b) The heat flux partitioning between bodies 1 and 2. For unfilled PTFE-stainless steel interfaces it is appropriate to assume that all of the generated heat flux is supplied to the steel part.
- (c) The exposure time, that is, the duration of the heat flux.
- (d) The time between intermittent heat fluxes.

In large amplitude uni-directional periodic motion (as typically developed in testing of bearings), the heat flux exhibits periodic intermittent history as shown in Figure 3-15. However, the actual motion in an earthquake is multi-directional, in which the time between intermittent heat fluxes is generally longer than in uni-directional motions. To demonstrate this consider a motion that consists of six segments of constant velocity v_c , each with duration u_c/v_c , where u_c is the distance traveled in each segment. Figure 3-16 illustrates the time history of this motion when it is uni-directional and periodic along the y-axis. The same figure shows a schematic of the bearing in which the small circular area (of radius a) is the PTFE surface (shown moving with respect to the steel surface rather the other way around). The heat flux input at positions A (starting position) and B (extreme right, which is traversed twice) of the steel part are also shown in Figure 3-16. Note that as the contact area moves, the heat flux is supplied to a new portion of the steel surface resulting in different intermittent heat fluxes at different positions.

We consider next that the motion (again consisting of six segments, each of travel u_c , duration u_c/v_c and constant velocity v_c) is multi-directional as shown in Figure 3-17. Note that all positions of the contact area are fully traversed once, except for the starting position (A) which is fully traversed twice. The heat flux input at positions A and B is shown in Figure 3-17 and, as expected, has longer intermissions than that of the uni-directional motion.

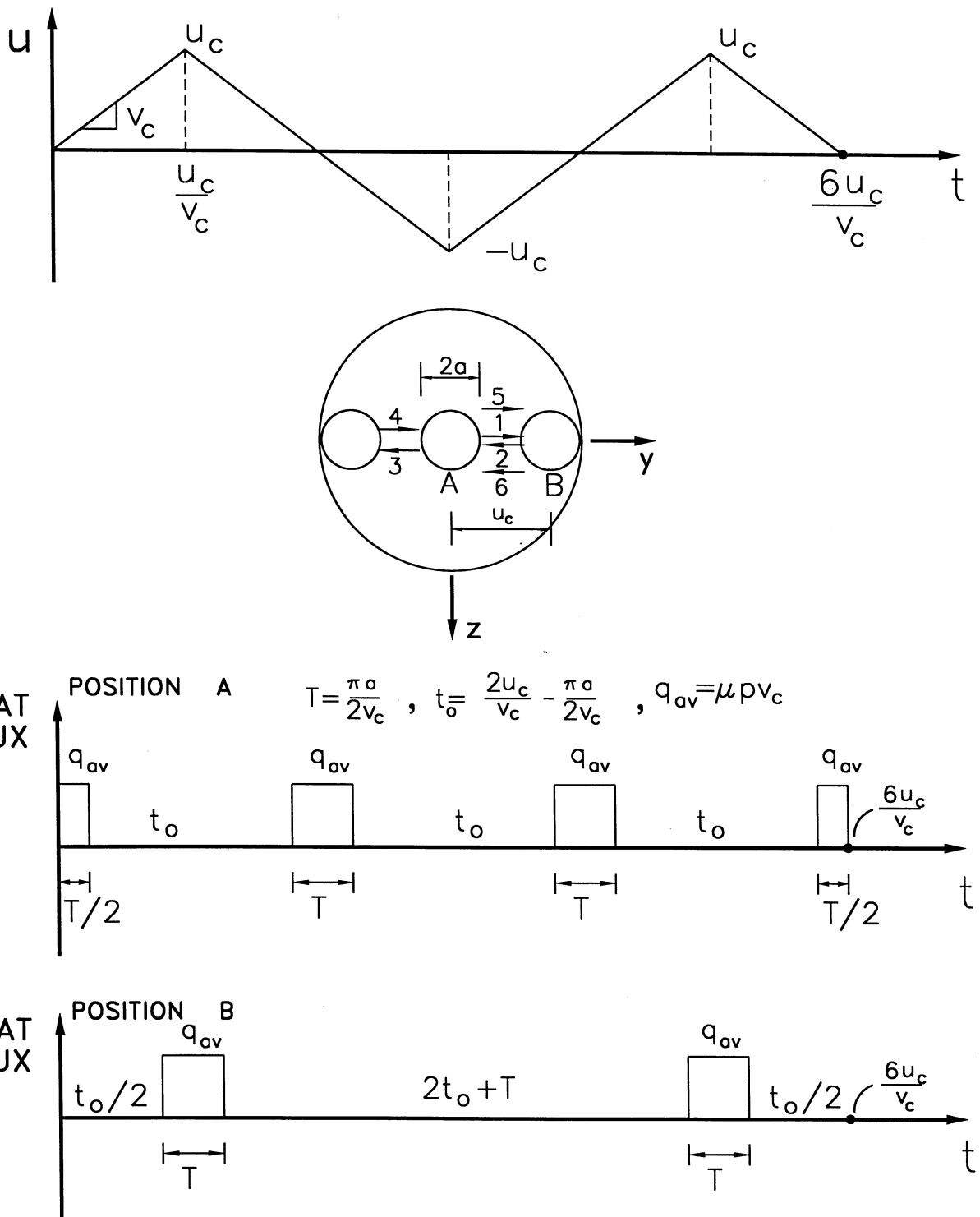


FIGURE 3-16 Heat Flux Input at Various Positions of Steel Body in Uni-directional Periodic Constant Velocity Motion

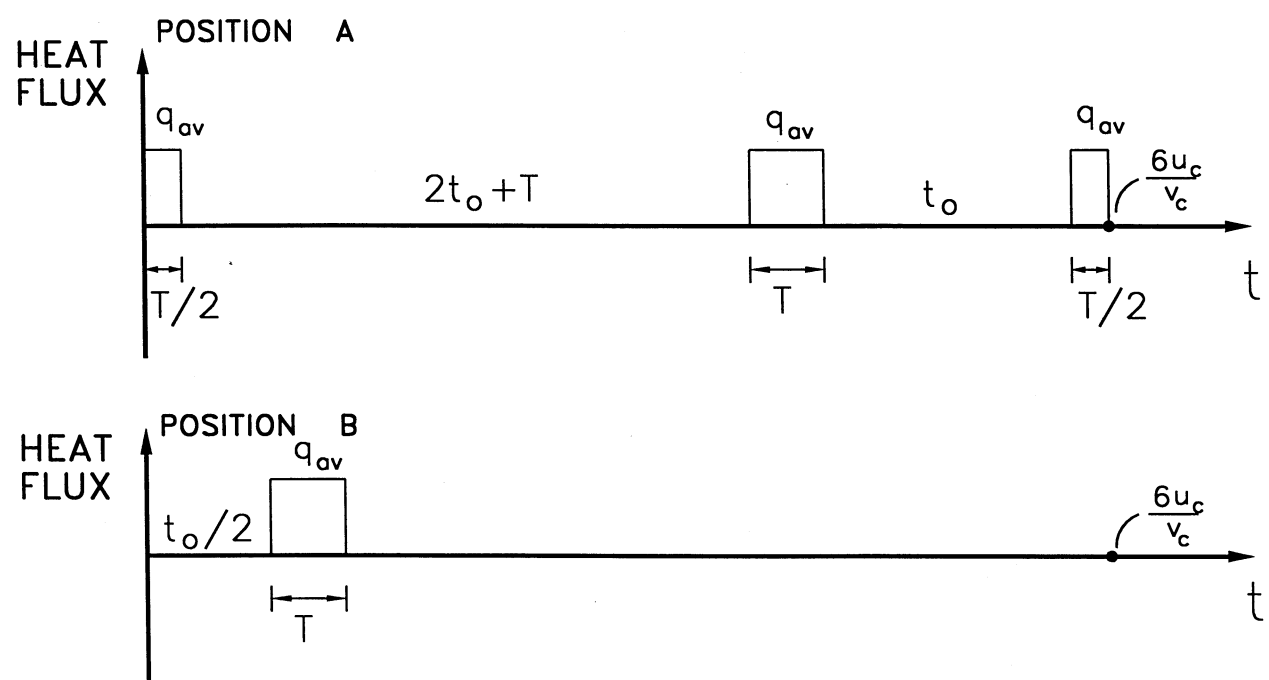
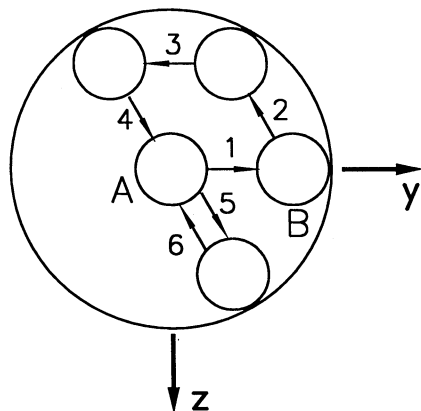


FIGURE 3-17 Heat Flux Input at Various Positions of Steel Body in Multi-directional Constant Velocity Motion

3.8.2 Test Results on Temperature Rise Histories due to Frictional Heating

A series of tests has recently been conducted for the specific purpose of measuring the temperature rise at the interface of sliding bearings (Wolff, 1999). The tests were conducted in the machine of Figure 3-3 utilizing flat sliding bearings. The sliding interface consisted of unfilled PTFE in contact with polished stainless steel. The apparent contact area had a diameter of 95.25 mm. Thermocouples were embedded in the stainless steel plate at depth of 1.5 mm. One thermocouple was located at the center of the bearing directly below the contact area.

T-type thermocouples with wire diameter of 0.025 mm were utilized in an attempt to increase the sensitivity of the instrument and obtain reliable measurements of temperature histories under conditions of high speed motion.

The tests consisted of five cycles of sinusoidal motion with amplitude of either 25.4 mm ($u_s/a = 0.54$) or 96.5 mm ($u_s/a = 2.03$). Frequency varied so that the peak velocity was in the range of 40 mm/s to 320 mm/s. The apparent bearing pressure was 13.8 MPa in the small amplitude tests and 12 MPa in the large amplitude tests.

Figure 3-18 presents the recorded histories of temperature at the central thermocouple in four small amplitude tests ($u_s = 25.4$ mm). In these small amplitude tests the conditions of continuous (uninterrupted) heat flux prevailed. This is observed in the monotonic increase of temperature with time as predicted by (3-20) and (3-21). Prediction of the temperature rise and drop following the conclusion of testing was made by use of (3-20) and (3-30), respectively, in which the heat flux was calculated by (3-25) using the measured coefficient of friction. Moreover, $x = 1.5$ mm, $k = 16.3$ W/(m·°C) and $D = 0.444 \times 10^{-5}$ m²/s, which are appropriate thermal properties for the stainless steel. Also in (3-30), T is the duration of testing (i.e., 20 sec in the test at frequency of 0.25 Hz, etc.) It is observed that the analytical prediction is good.

It is of interest to note that the recorded peak temperature rises in the four tests differ by small amounts despite the 8-fold difference in peak velocities. There are two reasons for this behavior. The first is revealed by examination of (3-27), which applies for this case. The temperature rise is proportional to the square root of the frequency when all other parameters are fixed (indeed this is the case for the tests at frequencies of 0.5, 1.0 and 2.0 Hz, in which the coefficient of friction was essentially the same). The second reason is that the temperature was recorded at a depth of 1.5 mm below the surface. Despite the small depth, the reduction of temperature with depth is significant in the higher velocity tests as revealed in the temperature profiles of Figure 3-14.

The peak surface temperatures could not be measured but could be analytically predicted and are shown in Figure 3-18. These temperatures are significantly higher than the recorded ones at the depth of 1.5 mm in the high velocity motions.

Figure 3-19 presents the recorded histories of temperature in three large amplitude tests ($u_s = 96.5$ mm). The conditions in these tests are those of intermittent heat flux for which

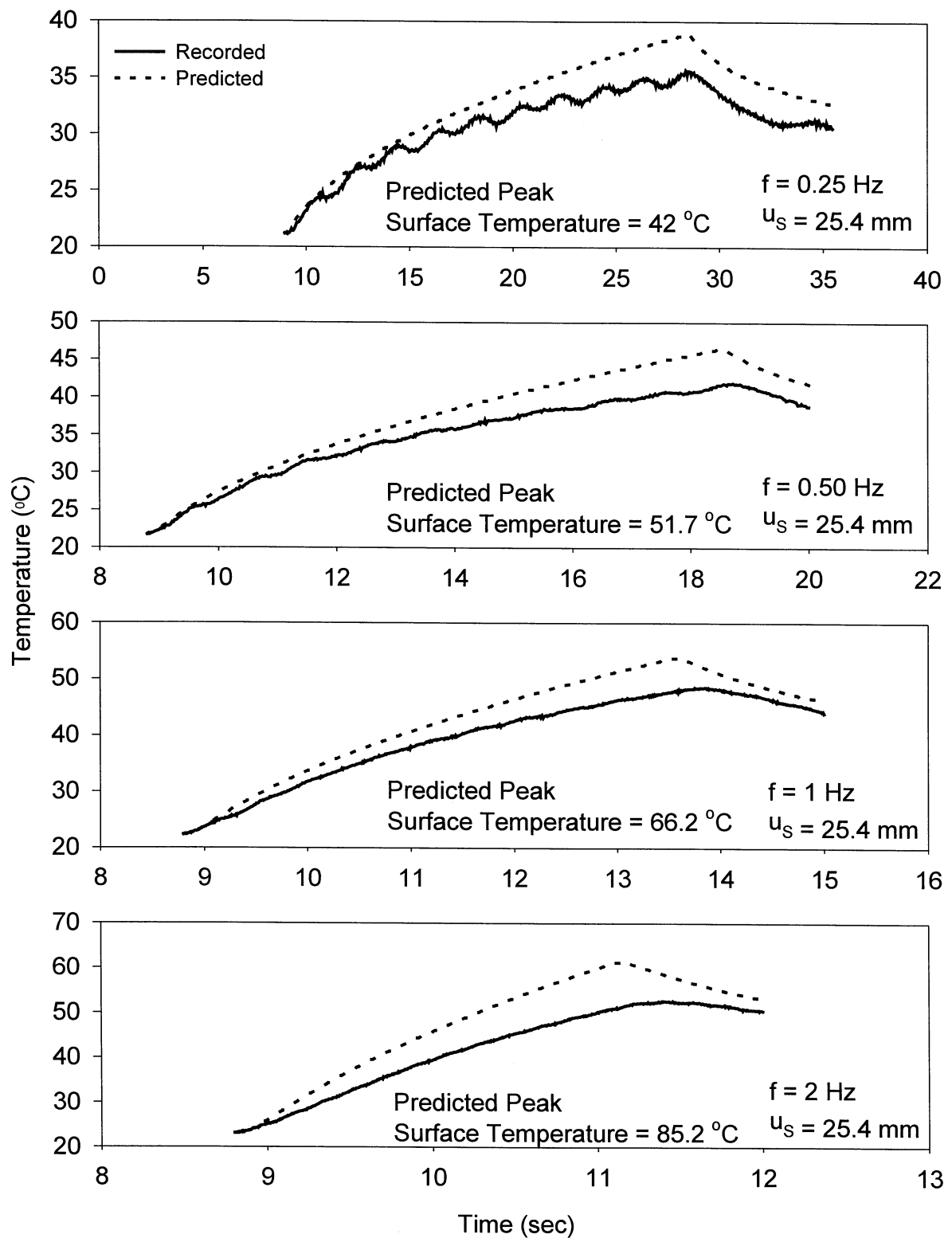


FIGURE 3-18 Recorded and Predicted Histories of Temperature at Middle Thermocouple (Depth of 1.5 mm) in Small Amplitude Tests

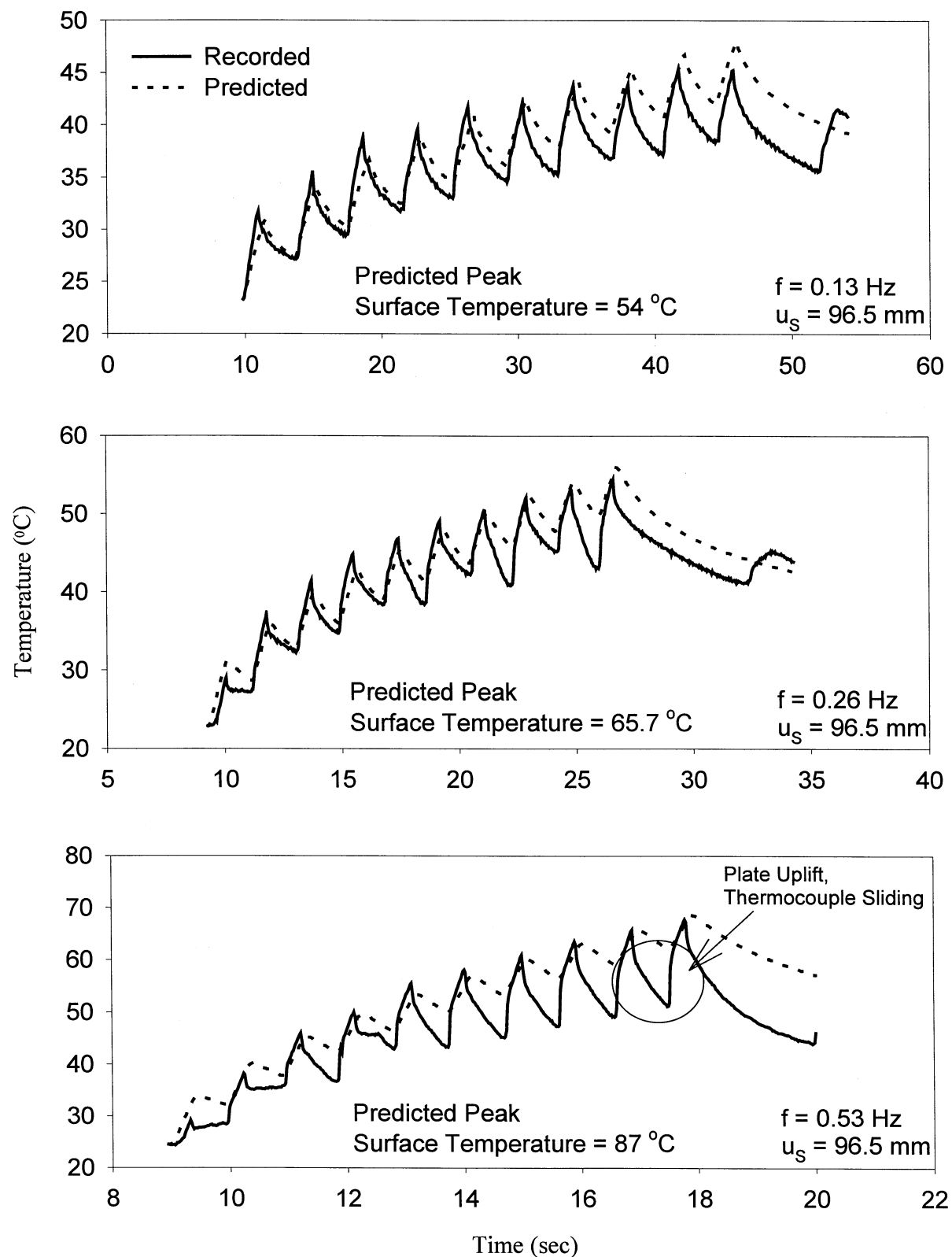


FIGURE 3-19 Recorded and Predicted Histories of Temperature at Middle Thermocouple (Depth of 1.5 mm) in Large Amplitude Tests

the history of temperature is predicted to have consecutive build-up and decay intervals. Indeed this is the recorded behavior.

Prediction of the temperature histories has been made by repeated use of (3-20) and (3-30) and superposition of the results. Again, the heat flux was calculated by (3-25) using the measured coefficient of friction. Moreover, the duration of each heat flux and the duration of each intermediate interval of zero heat flux were calculated on the basis of the theory presented in section 3.8.1. The thermal properties of $k = 16.3 \text{ W}/(\text{m}\cdot^\circ\text{C})$ and $D = 0.444 \times 10^{-8} \text{ m}^2/\text{s}$ were used for the stainless steel.

In discussing the accuracy of the analytical prediction, the following observations are made:

- The prediction is, in general, good in terms of both the peak temperature values and the trends in the histories of temperature.
- There is a small difference between analytical and experimental values of time at which the peak temperatures occur. This is the result of the calculation of the exposure time as an average time given by (3-28).
- There is a difference in the calculated and measured histories of temperature during the intervals of zero heat flux. This difference appears to increase with increasing frequency of motion. One reason for this difference is conservatism in the analytical solution, in which losses of heat due to radiation and the lateral conduction of heat (solution is for half space with heat flux at $x = 0$) are neglected. Another reason is related to limitations in the experimental setup. It has been observed that as the displacement approached its peak value, the stainless steel plate uplifted resulting in movement of the thermocouple and likely loss of contact. This behavior was more pronounced in the high frequency tests.

3.8.3 Example of Temperature Rise Calculation in Bi-directional Sliding Motion

The presented analytical solution for the temperature rise due to frictional heating may be used for arbitrary history of heat flux (though still restricted to the half space subject to heat flux at $x = 0$) either by utilizing the convolution integral of (3-38) or by repeatedly utilizing (3-20), (3-21), (3-30) and (3-32). The latter is equivalent to the use of (3-38) but with an incremental summation process involving gross time steps rather than "infinitesimal" time steps. This procedure is used for the prediction of the temperature rise at the surface of a large sliding bearing subjected to dynamic vertical load and high speed bi-directional motion.

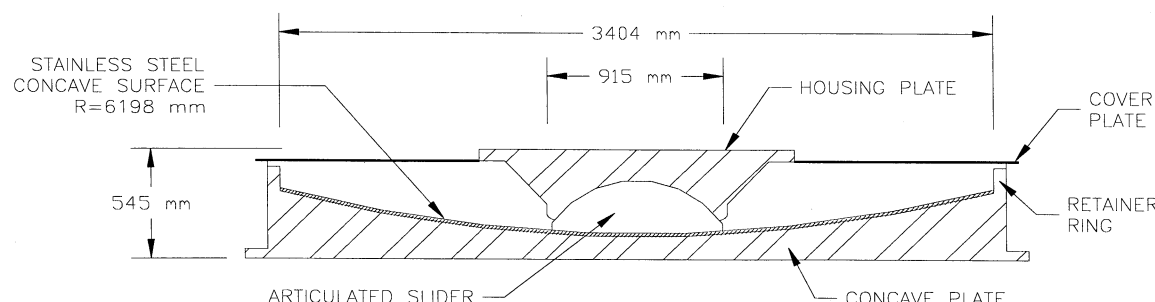


FIGURE 3-20 FPS Bearing for the Benicia-Martinez Bridge, California

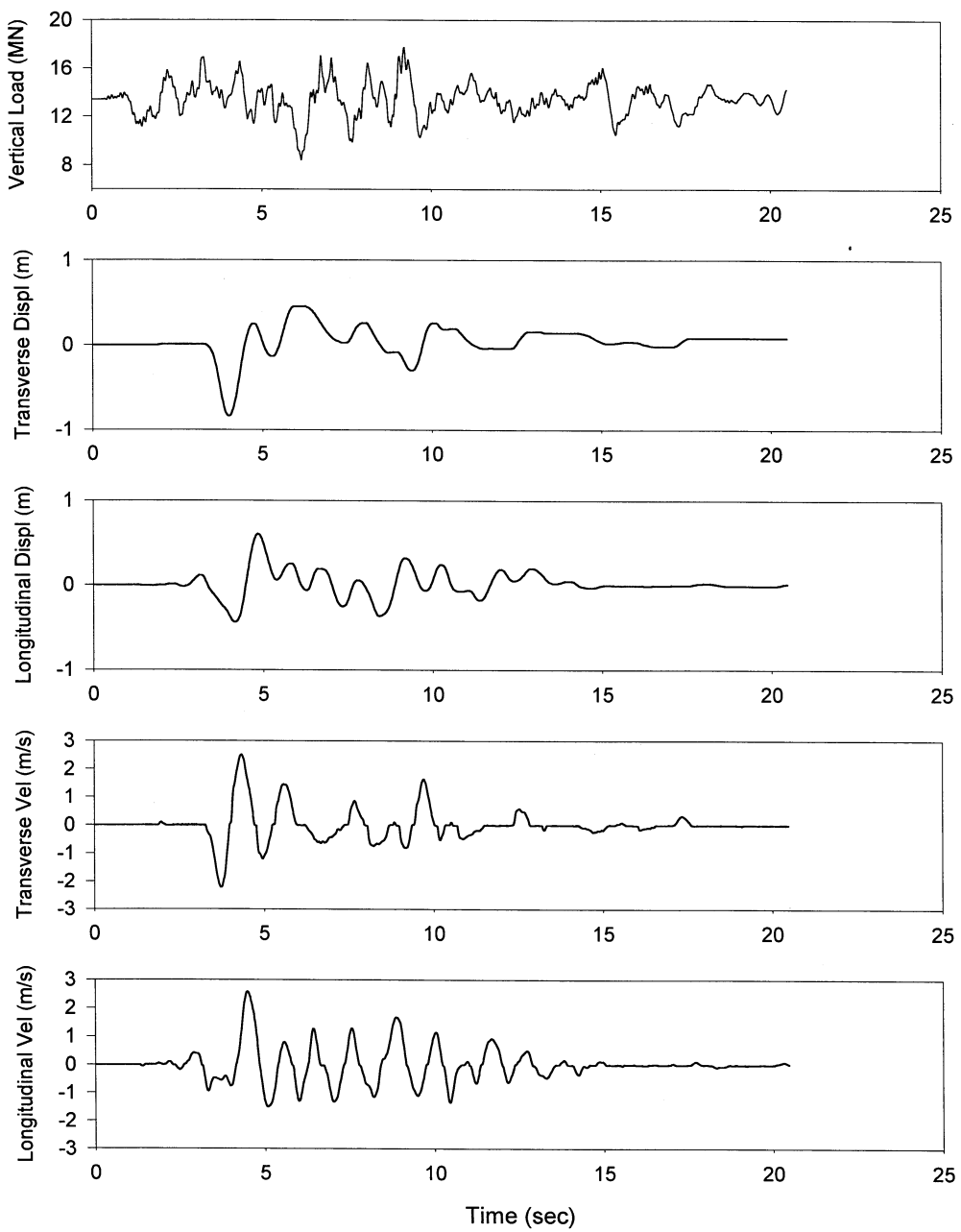


FIGURE 3-21 Calculated Histories of Vertical Load and Bi-directional Horizontal Motion of FPS Bearing for Benicia-Martinez Bridge, California

The presented example is for one of the FPS bearings to be used in the seismic rehabilitation of the Benicia-Martinez bridge in California (Mellon and Post, 1999). Figure 3-20 presents a schematic of this bearing and Figure 3-21 presents histories of the vertical load and bi-directional motion of the bearing as calculated in the dynamic analysis of the bridge. This bearing will be tested at the Caltrans Seismic Response Modification Device Test Facility at the University of California, San Diego (Benzoni and Seible, 1999). Despite the very large load, displacement and velocity capabilities of this testing machine, the bearing cannot be tested under the conditions depicted in Figure 3-21. Rather, the bearing will be tested with a one-directional motion within the peak velocity capability of the machine (currently at 1.65 m/s). In the establishment of the equivalent one-directional motion, the power input and heat flux input at the most traversed part of the bearing were considered. Particularly, calculations of the history of temperature rise in the calculated bi-directional motion and in the equivalent one-directional motion were important in establishing the equivalent one-directional motion.

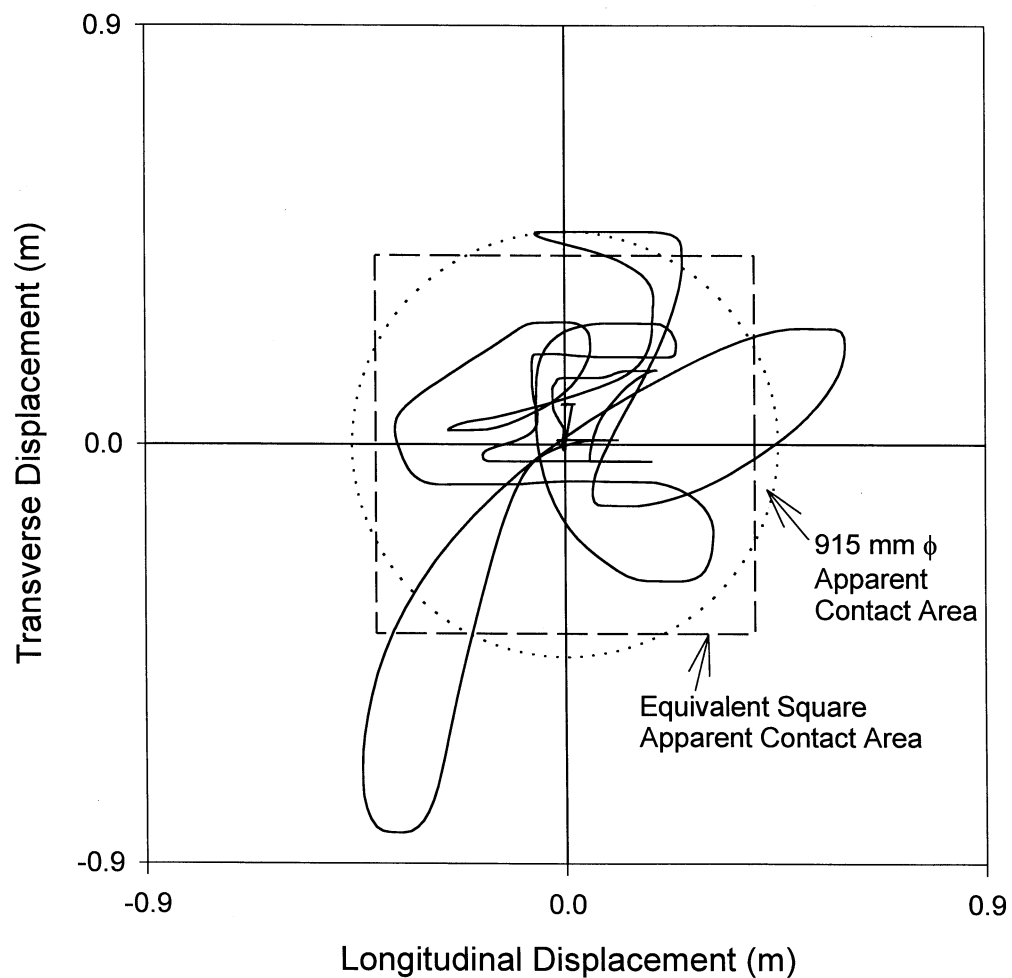


FIGURE 3-22 Displacement Path in Bi-directional Motion and Actual and Equivalent Apparent Contact Areas

To perform calculations for the temperature rise, one has to first identify the most traversed part of the bearing and then calculate the heat flux supplied to that part. Figure 3-22 shows the displacement path in the bi-directional motion. It is apparent that the most traversed part is the neighborhood of the center of the bearing. The heat flux generated at the sliding interface is given by (3-39) with p being the instantaneous apparent pressure, \dot{u} being the amplitude of the instantaneous velocity vector and μ being the coefficient of friction. The heat flux history has been calculated using the nominal value of the coefficient of friction ($= 0.06$) and it is shown at the top graph in Figure 3-23. This heat flux history is the one supplied at the instantaneous apparent contact area. The next step is to calculate the heat flux history at the selected fixed area of the steel part (in this case, the neighborhood of the bearing center).

The heat flux history at the selected fixed area of the steel part depends on the history of displacement and the size of the apparent contact area. In general, this heat flux history is similar to the history of heat flux supplied at the instantaneous apparent contact area except for some intervals of zero flux when the contact area moves away from the selected fixed area. Options for identifying the intervals of zero flux are:

- On the basis of calculations of average exposure times during each passage (in similarity to eq. 3-28). This is a complex procedure given that the velocity greatly varies and there is difficulty in the definition of the average exposure time.
- By simply defining the intervals of zero flux as those for which the resultant displacement u_r is larger than a , where a is the radius of the apparent contact area. This is a conservative approach since it neglects the effect of the diminishing width of the apparent contact area as u_r approaches a .
- By replacing the circular apparent contact area with an equal square area of which one side is always perpendicular to the direction of motion. This leads to the condition of zero heat flux when

$$u_r > \frac{\pi^{1/2} a}{2} \quad (3-40)$$

We prefer the use of this condition because of its simplicity. Of interest is to note that when the velocity is constant and equal to v_c , (3-40) results in an average exposure time given by

$$t'_{av} = \frac{\pi^{1/2} a}{v_c} \quad (3-41)$$

which is larger than what the more accurate (3-28) gives. The ratio $t'_{av}/t_{av} = 1.1284$ so that, for constant heat flux, the temperature rise is overestimated by $\sqrt{1.1284} = 1.062$. That is, this approach is slightly conservative.

The heat flux history at the bearing center was calculated on the basis of (3-40) and is shown in Figure 3-23. It should be noted that this history contains a small number of zero flux intervals due to the large radius of the apparent contact area by comparison to

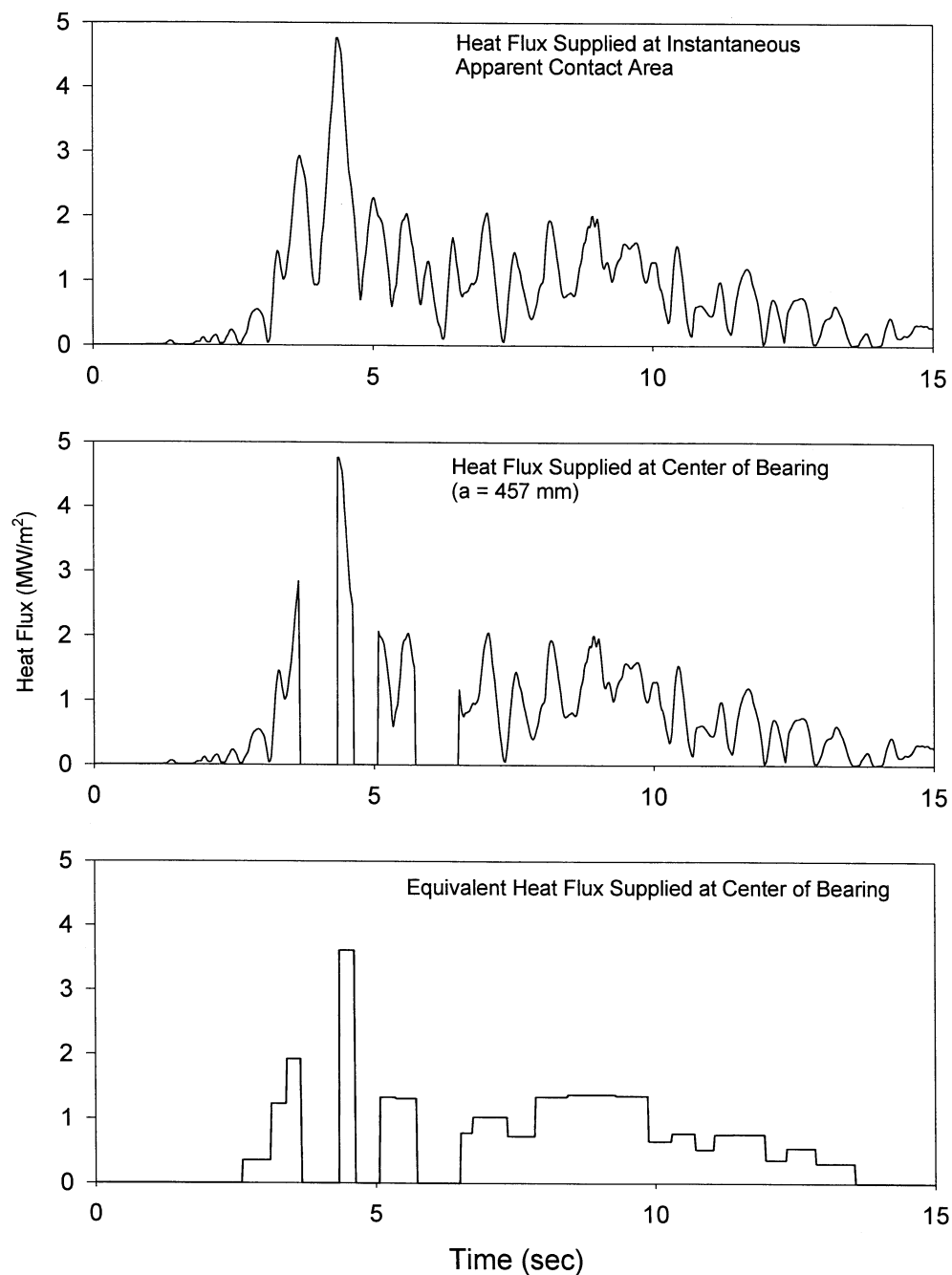


FIGURE 3-23 Histories of Heat Flux

the amplitude of motion. It is also evident that the part of the history that is critical for the temperature rise is the one beyond about the time of 7 sec, for which there is continuous heat flux supply.

The temperature rise can be calculated by use of the convolution integral of (3-38). More convenient, however, is the repeated use of (3-21) and (3-32) following replacement of the actual heat flux history with an equivalent series of rectangular heat flux pulses as shown in Figure 3-23 (a simple process that can be carried out with a spreadsheet program). In this case, each of the actual heat flux pulses was replaced by a rectangular pulse of the same "area". The calculation of the temperature rise at the surface was based on the use of (3-21) and (3-32) for each of the rectangular heat flux pulses and superposition of the results. Figure 3-24 shows the calculated history of temperature rise. The calculation was based on the thermal property values of $D = 0.444 \times 10^{-5} \text{ m}^2/\text{s}$ and $k = 18 \text{ W}/(\text{m}\cdot^\circ\text{C})$, which are approximately valid for a temperature of 200°C (that is, the average temperature conditions).

The temperature rise at a depth of 1.5 mm has also been calculated and it is shown in Figure 3-24. The calculation was based on the use of (3-20) and (3-30) for each of the rectangular heat flux pulses. The temperature rise at the depth of 1.5 mm is much less than that at the surface. This temperature is of little practical significance. Rather, the surface temperature is important since it is equal to the surface temperature of the bearing material, which is the one to use in assessing the potential for wear of the bearing material. However, the temperature at some small depth in the stainless steel is what could be measured and therefore what is available for verification of the predictions.

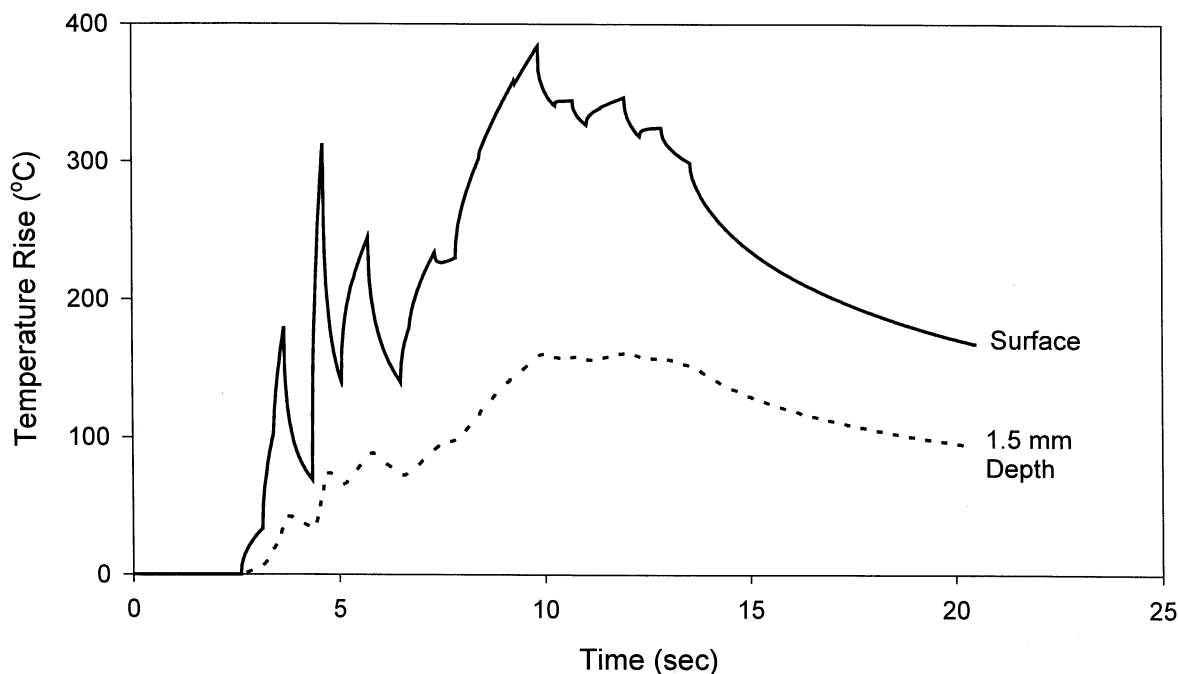


FIGURE 3-24 Predicted Histories of Temperature Rise at the Surface and at Depth of 1.5mm of Stainless Steel Overlay at its Center

3.8.4 Concluding Remarks on Frictional Heating

A theory has been presented to calculate the temperature rise at the contact surface and at small depths below the surface of sliding bearings. Important assumptions in this theory are that the heat generated at the contact is totally supplied to the steel part (i.e., the bearing material is a perfect thermal insulator), heat conduction is one-dimensional, loss of heat due to radiation and convection is negligible, conditions of half space prevail (a good assumption for large contact area and high speed motion) and that the true contact area is essentially the same as the apparent contact area. The latter assumption is based on the theory presented in section 3.6 which appears to be valid for PTFE and similar materials in contact with highly polished stainless steel.

The theory predicted well the temperature rise recorded in various experiments, although the experimental results were restricted to measurements of temperature at some small depth in the stainless steel and not at the surface. Nevertheless, the correlation of experimental data and calculated values provides some confidence in the use of this rather simple theory for the prediction of the temperature rise due to frictional heating in PTFE-stainless steel interfaces. It should be noted that because the temperature variations with time and space at the contact surface are greater than at the location of the thermocouples, the errors in prediction at the surface are likely to be larger than at the thermocouple locations.

It is important to note that large temperature increases are predicted at the contact surface of bearings subjected to high speed seismic motions. However, temperature increases at even small depths below the steel surface are significantly less. This fact should be considered when measurements of temperature are made by embedding thermocouples at small depths below the contact surface.

3.9 Summary

Friction is an extremely complex phenomenon of which the exact mechanism is not known. Rather, several mechanisms are believed to contribute in the generation of friction. One particularly important aspect of frictional behavior is that when solid materials come into contact, the true area of contact is, in general, less than the apparent contact area. The size of the true contact area depends on the materials in contact, the load and time.

In interfaces consisting of PTFE or similar soft materials and highly polished stainless steel, we have argued that the true area of contact is nearly equal to the apparent contact area. In support of this theory we have presented theoretical solutions on the rate of creep and experimental results on the dependency of friction on normal load and on the dependency of the breakaway (or static) friction on the load dwell. An important prediction of this theory is that load dwell does not have an effect on the breakaway friction except likely for short time intervals of the order of minutes or hours.

The macroscopic behavior of PTFE-stainless steel interfaces has been described and effects such as those of velocity of sliding, apparent bearing pressure and temperature have been discussed. Moreover, the so-called phenomenon of stick-slip has been described as the result of the flexibility of the testing arrangements and not as an intrinsic property of sliding bearings.

A major part of this section was devoted to the problem of frictional heating and an analytic solution for the temperature rise at the sliding interface has been presented. Experimental results confirmed approximately the validity of the theoretical solution.

SECTION 4

FRICTIONAL PROPERTIES OF PTFE-POLISHED STAINLESS STEEL INTERFACES

4.1 Introduction

This section is devoted to a presentation of the frictional properties of unfilled PTFE and one type of PTFE-based composite in contact with polished stainless steel. The effects of apparent pressure, sliding velocity, temperature, load dwell, corrosion of stainless steel, contamination and travel on the frictional properties are presented. The presented data have been collected from the literature or generated by authors when information was lacking. The presented data are primarily for unlubricated conditions with the effects of lubrication briefly presented last.

Most of the presented data have been generated by the authors at the University at Buffalo and by Professor Campbell's group at Queen's University, Kingston, Ontario, Canada (Campbell and Kong, 1989; Campbell and Fatemi, 1989; Campbell et al., 1991). The testing apparatuses used in these testing programs were very different, however specimen sizes and principal features of the apparatuses were similar. Specifically:

- (1) In the Queen's University testing apparatus a single sliding interface was used. Rollers were utilized below the sliding platform. Vertical load was developed with a hydraulic ram. Carefully placed load cells could monitor the friction force at the interface, excluding the inertia effects and the friction in the supporting rollers. Spherical bearings between the hydraulic ram and the sliding interface ensured concentric application of the normal load. The PTFE specimens had a 75 mm diameter.
- (2) In the University at Buffalo tests two different apparatuses were used. The first is illustrated in Figure 3-3. This machine is highly versatile. It can apply variable normal load, rotation of the tested bearing and horizontal movement. The machine can test a single bearing with the horizontal force been measured by a reaction load cell so that the inertia effects are eliminated. The tested sliding bearing included a rotational element (standard disc bearing with a soft adiprene disc) to ensure concentric application of the load and to accommodate rotation. The PTFE specimens had a 95 mm diameter, thickness of 3.2 mm and were recessed to a depth of 1.6 mm. The bearings were identical to those utilized in shake table testing (Tsopelas et al., 1994).

However, most of the results of the authors were produced with a different testing arrangement, which allowed for large load dwells and testing at low temperatures. Figure 4-1 illustrates this testing arrangement. It utilized two sliding interfaces, supported by disc bearings and which bear against a moving plate that is faced with stainless steel. The two sliding interfaces and the moving plate could be enclosed in

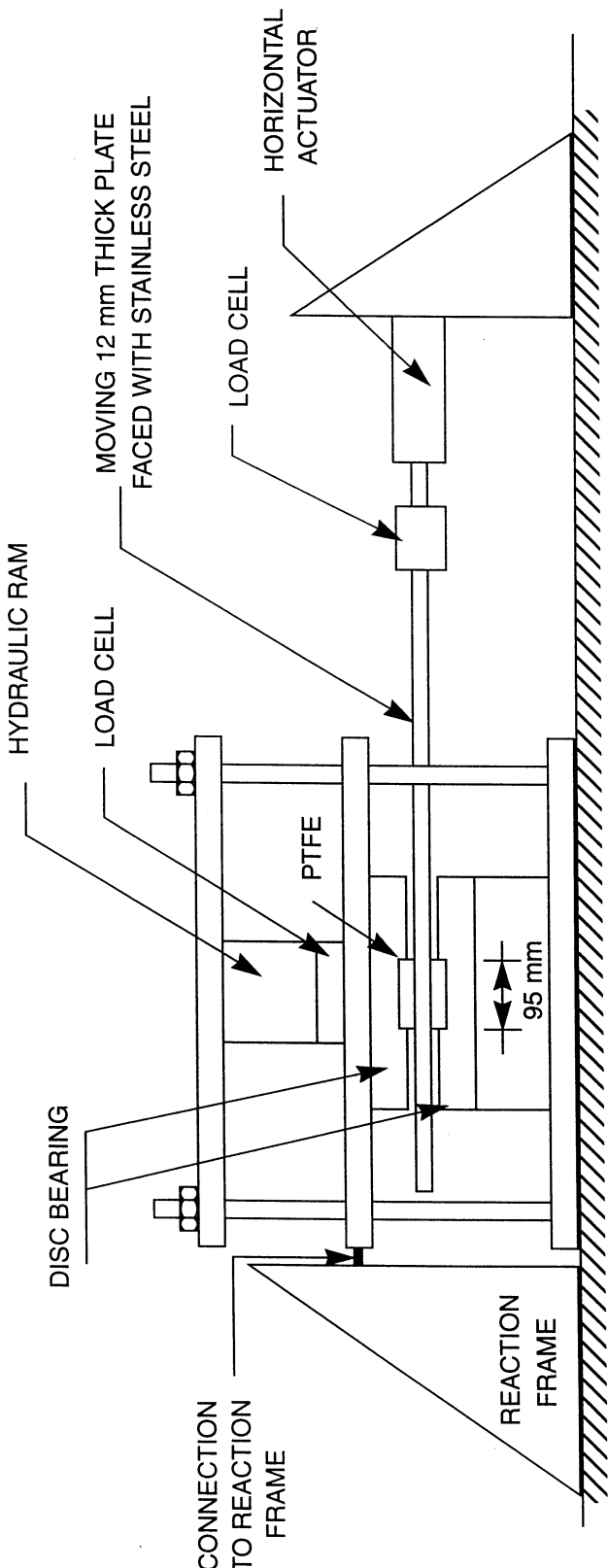


FIGURE 4-1 Testing Arrangement Used in Testing of Sliding Bearings

a styrofoam box which was filled with small sealed plastic bags containing solid carbon dioxide(dry ice)for low temperature testing. The temperature was monitored by a thermocouple embedded in the moving plate just below the stainless steel overlay.

In this testing arrangement the friction force was obtained from two sliding interfaces (presumably identical) and then divided by two to obtain the friction of a single interface. Moreover, the friction force was measured by the actuator load cell, the measurement of which included the inertia force of the moving plate. No correction was made for the inertia force since it was found to introduce negligible error (in the test under the least normal load and highest sliding velocity, the inertia force was about 2-percent of the friction force).

The arrangement of Figure 4-1 was also used in the testing of a PTFE-based composite which has been used in Friction Pendulum (FPS) bearings. We will denote this material as PTFE composite No. 1. It is identical to the material used in the shake table tests of Constantinou et al. (1993) and also utilized in many building applications of FPS bearings. In the testing, the two disc bearings in the arrangement of Figure 4-1 were replaced with the two housing plates of the FPS bearings used in Constantinou et al. (1993). These plates included the standard column with a spherical cavity and the articulated slider of the FPS bearings. However, the slider was machined flat in order to bear against the moving plate of the testing arrangement. The slider was 50 mm in diameter and was faced with the composite material at a thickness of 0.25 mm. This thickness is about three times smaller than the one utilized in applications of FPS bearings in building structures (U.S. Court of Appeals, LNG tank facility in Greece and San Francisco new International Airport Terminal). This material is not exactly the same as the one utilized in recent applications of FPS bearings in bridges.

4.2 Effect of Load Dwell on Breakaway (or Static) Friction

It is common practice to sustain load on PTFE bearings for some time prior to imposing sliding. Campbell and Kong (1989) and Campbell et al. (1991) used a 12 hour load dwell in all of their experiments. The 12 hour load dwell is required by the AASHTO Standard Specifications (American Association of State Highway and Transportation Officials, 1992). The origin of the 12 hour load dwell requirement is unknown. However, it appears to be related to data obtained at the factory of Glacier Bearings in 1971 and reported by Paynter (1973). Paynter provided a brief description based on his personal communication with the technical manager of Glacier Bearings. These load dwell tests were conducted on interfaces consisting of Glacier DZ material (reported as pure PTFE) in contact with polished stainless steel of surface roughness of about 0.05 to 0.10 μm on the arithmetic average scale, and at apparent pressure of 28 MPa. Load dwells of up to 24 hours are reported as having an effect, however, the extent of the effect is not reported. We note that the surface roughness of the stainless steel in these tests is approximately twice that utilized in the tests at Queen's University, Canada and at the University at Buffalo.

The authors have conducted a number of tests to assess the effect of load dwell on the static (breakaway) friction of PTFE bearings. Prior to these tests, Mokha et al. (1990) reported on the effect of load dwell on the frictional properties of such bearings. Mokha et al. (1990) observed nearly identical breakaway friction following 0.5 hours and 594 days of load dwell. In the tests reported herein we have utilized the testing arrangement of Figure 4-1 with 95 mm diameter unfilled PTFE specimens in contact with polished stainless steel (ASTM A240, Type 304) of surface roughness equal to 0.03 μm on the arithmetic average scale (R_a or CLA) (American Society of Mechanical Engineers, 1985). Testing was conducted at apparent pressure of 6.9 MPa using three different specimens and at apparent pressure of 20.7 MPa using one specimen. Ambient temperature during testing was about 20°C and relative humidity was in the range 25 to 30-percent. Lateral motion on the tested interfaces was imposed as a sine wave of frequency of 0.0318 Hz and amplitude of 12.5 mm so that the peak sliding velocity was 2.5 mm/s.

Table 4-1 presents the results in the case of apparent pressure of 6.9 MPa. The first specimen (actually pair of specimens) was loaded for 0.2 hours and then lateral motion was imposed. The specimen was then maintained under load for another 1.0 hour and the test was repeated. This process was repeated seven times for a cumulative loading time of 167.0 hours. Subsequently, new specimens were tested as presented in Table 4-1. The test results demonstrate that for new specimens (not previously tested), load dwells in the range of 0.2 to 118.4 hours results in static friction values that are unaffected by load dwell. There is, of course, some variability in the obtained results but not any systematic increase in the static friction with increasing load dwell (rather the opposite is observed).

TABLE 4-1 Test Results on Effect of Load Dwell on Static (Breakaway) Friction of Unfilled PTFE in Contact with Polished Stainless at Apparent Pressure of 6.9 MPa

Specimen	Cumulative Loading Time (hrs)	Static Friction Coefficient	Comments
1	0.2	0.116	Tests were conducted in the presented sequence without unloading of the interface.
	1.2	0.056	
	6.5	0.050	
	19.7	0.052	
	45.9	0.062	
	164.7	0.068	
	167.0	0.066	
2	118.4	0.095	Two high velocity tests were conducted immediately after the second and prior to the third test.
	128.9	0.031	
	153.3	0.073	
3	0.3	0.092	

Another observation in these tests is the marked reduction in the static friction following the first test. This is best illustrated in the recorded loops of Figure 4-2. It is likely caused by the depositing of a film of PTFE on the stainless steel plate in the previous tests.

In the tests at apparent pressure of 20.7 MPa only one specimen was tested. The results are presented in Table 4-2. The specimen was initially loaded for 0.2 hours and tested, and the process was repeated for various additional load dwells without unloading of the interface. The behavior is very similar to the one observed at the apparent pressure of 6.9 MPa, that is, friction is lower in the tests following the very first test. Subsequently, the specimen was unloaded and was allowed to relax overnight. Without cleaning the interface the specimen was reloaded for 24.2 hours and tested to obtain a higher static friction, close to the one obtained in the very first test. Later on, the same specimen was unloaded, cleaned from the PTFE film deposited on the slider and allowed to relax overnight. It was then reloaded for 50.2 hours and tested. The static friction coefficient was now measured to be higher (0.073) than in the very first test at load dwell of 0.2 hours (0.057).

TABLE 4-2 Test results on Effect of Load Dwell on Static (Breakaway) Friction of Unfilled PTFE in Contact with Polished Stainless Steel at Apparent Pressure of 20.7 MPa

Cumulative Loading Time (hrs)	Static Friction Coefficient	Comments
0.2*	0.057	*First test on new specimen
1.2	0.039	
6.0	0.043	
16.2	0.025	
29.4	0.030	
24.2**	0.047	**Same specimen as in first sequence.
118.7	0.045	However, interface was unloaded and allowed to relax overnight. Interface was not cleaned prior to re-loading.
139.8	0.031	
50.2***	0.073	***Same specimen as in previous tests.
118.9	0.045	Interfaces unloaded and allowed to relax overnight. Interface was cleaned prior to re-loading.

Figure 4-3 presents the recorded loops in the very first test and the two subsequent tests following unloading of the specimen. We may note in this figure that the true peak in the recorded friction in the first test may have been missed due to insufficient speed of data acquisition (it was rather low at 30 points per second, or about 1000 points for the duration of the imposed single cycle of movement). Nevertheless, the data on the static friction in the three tests of Figure 4-3 are within $\pm 30\text{-percent}$ of the value recorded in the first test. This range appears to be the result of natural variability in properties and measurement errors rather than the effect of load dwell (see also data in Table 4-1).

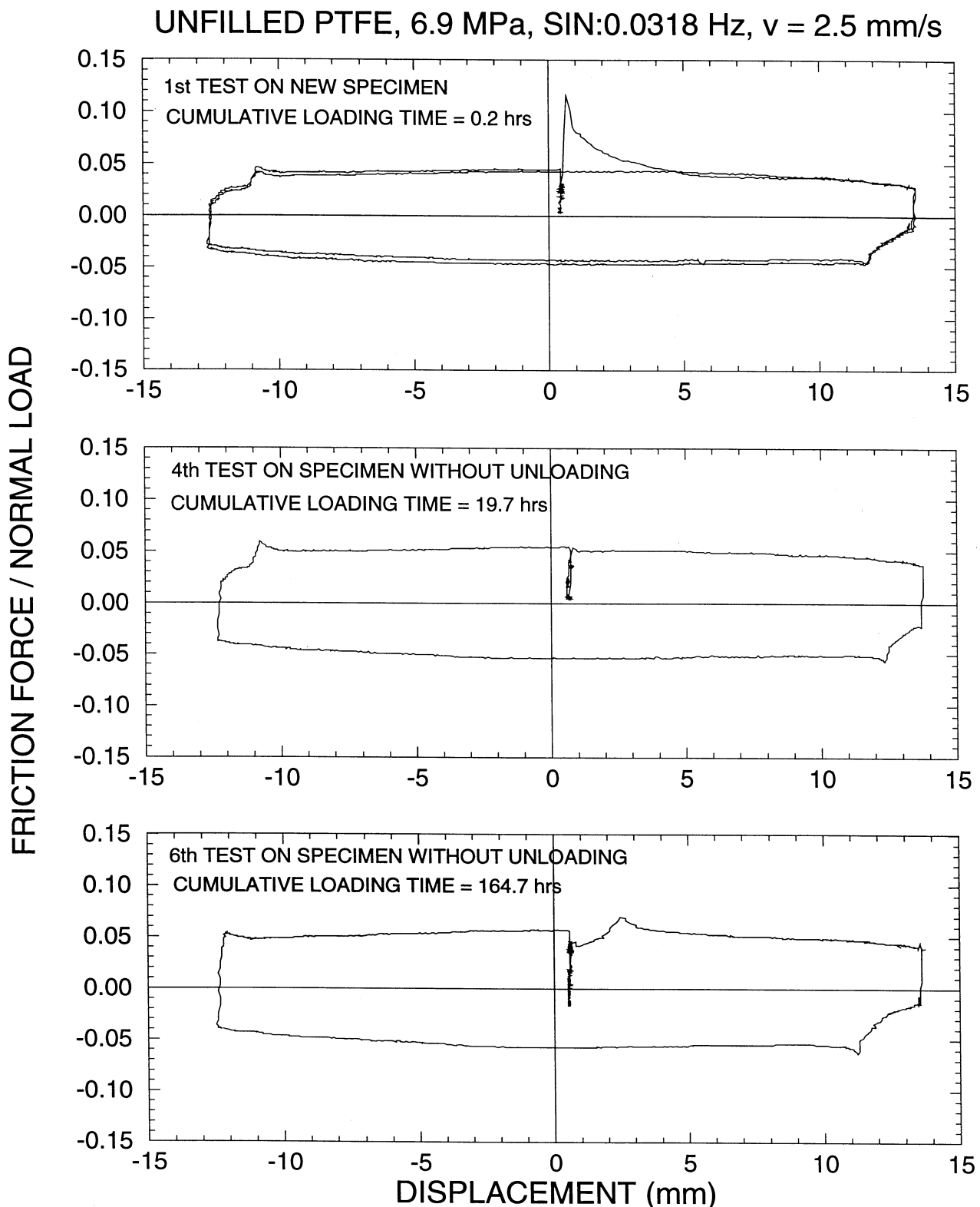


FIGURE 4-2 Recorded Loops of Friction Force Divided by Normal Load Versus Displacement in Load Dwell Tests at 6.9 MPa Apparent Pressure

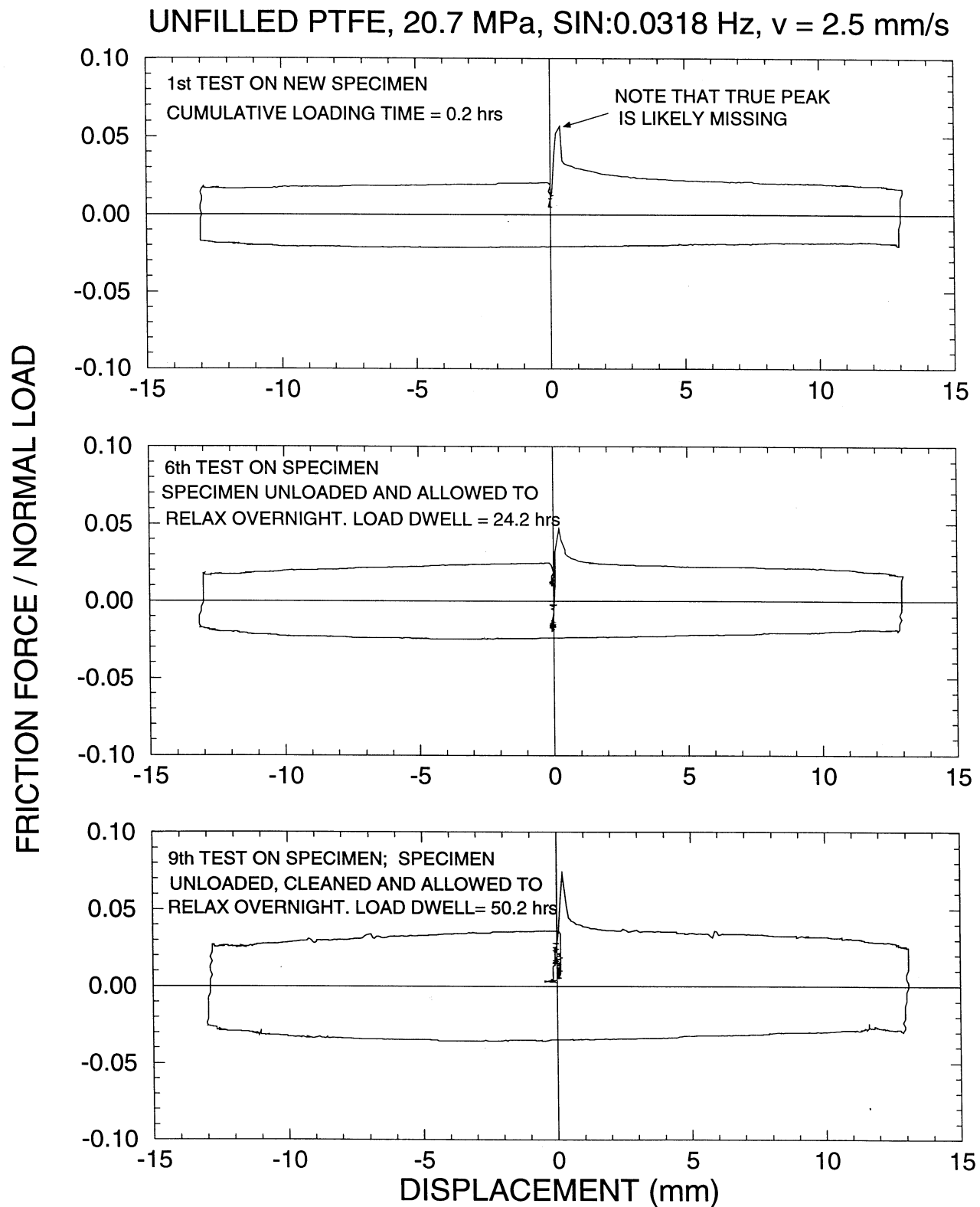


FIGURE 4-3 Recorded Loops of Friction Force Divided by Normal Load Versus Displacement in Load Dwell Tests at 20.7 MPa Apparent Pressure

The experimental data presented herein and the data from two tests by Mokha et al. (1990) indicate that, when considering the natural variability in the frictional properties obtained from different specimens or different tests of the same specimen and when considering likely measurement errors, the static friction of PTFE-polished stainless steel interfaces is unaffected by load dwell. Furthermore, we have provided in section 3 a rational explanation for this phenomenon. However, we should not consider that this issue has been settled. On this we note that the provided explanation is not based on direct observation (as it would have been one based on measurements of the real area of contact). Rather it is an assumption, which explains both the observed dependency of sliding friction on the inverse of normal load and the apparent insignificance of the effect of load dwell on the static friction. It would be appropriate that this problem is studied further by a different group of researchers (a good candidate for such work is the group at Queen's University in Canada).

4.3 Effect of Apparent Pressure and Sliding Velocity

Published data on the coefficient of friction of PTFE-polished stainless steel interfaces over a large range of sliding velocities are limited. The tests of Campbell and Kong (1989) have been limited to sliding velocities of 20 mm/s or less, apparently because this velocity range is relevant to the temperature and traffic induced movement of bridge bearings.

Tyler (1977), Mokha et al. (1988, 1990) and very recently Bondonot and Filiatral (1997) performed tests at high velocities of sliding, up to 0.8 m/s, apparent pressures in the range of 5 to 45 MPa, and with PTFE specimens having areas of approximately 12,500 mm² to 50,7000 mm². Testing was conducted by imposing either sinusoidal or constant velocity (sawtooth displacement) motion of specified displacement amplitude, d , and frequency, ω . This requires that immediately upon initiation of motion, a large sliding velocity be attained. For example, in the sinusoidal testing the imposed displacement history is $d \sin(\omega t)$, the velocity history is $\omega d \cos(\omega t)$, and the acceleration history is $-\omega^2 d \sin(\omega t)$. However, the actuator is at time $t = 0$ in a motionless state and it is required to achieve a velocity of ωd within an extremely short time interval. Accordingly, a large acceleration shock is imposed at the start of the experiment. The level of this acceleration largely depends on the available hydraulic power. The authors have measured this acceleration to be several times (between 2 and 13 times) the acceleration $\omega^2 d$ (i.e., see data in Mokha et al., 1988). For example, in a test at frequency of 2.0 Hz and amplitude of 70 mm (as in some of the tests conducted by Bondonot and Filiatral, 1997) quantity $\omega^2 d = 1.1$ g and the acceleration at the start of the experiment will exceed, and likely substantially exceed, 2.0 g.

Accelerations of this level on initiation of motion are unrealistic. For example, Figure 4-4 presents an example of histories of motion at isolation bearings from the tests of Constantinou et al. (1993) and Tsopelas et al. (1996). A 143 kN bridge model supported by four FPS bearings on top of flexible piers was tested at quarter length scale and half time scale. The input excitation is the 1952 Taft motion, component N21E scaled to a peak acceleration of 0.71 g and peak velocity of 0.54 m/s (in prototype scale). The

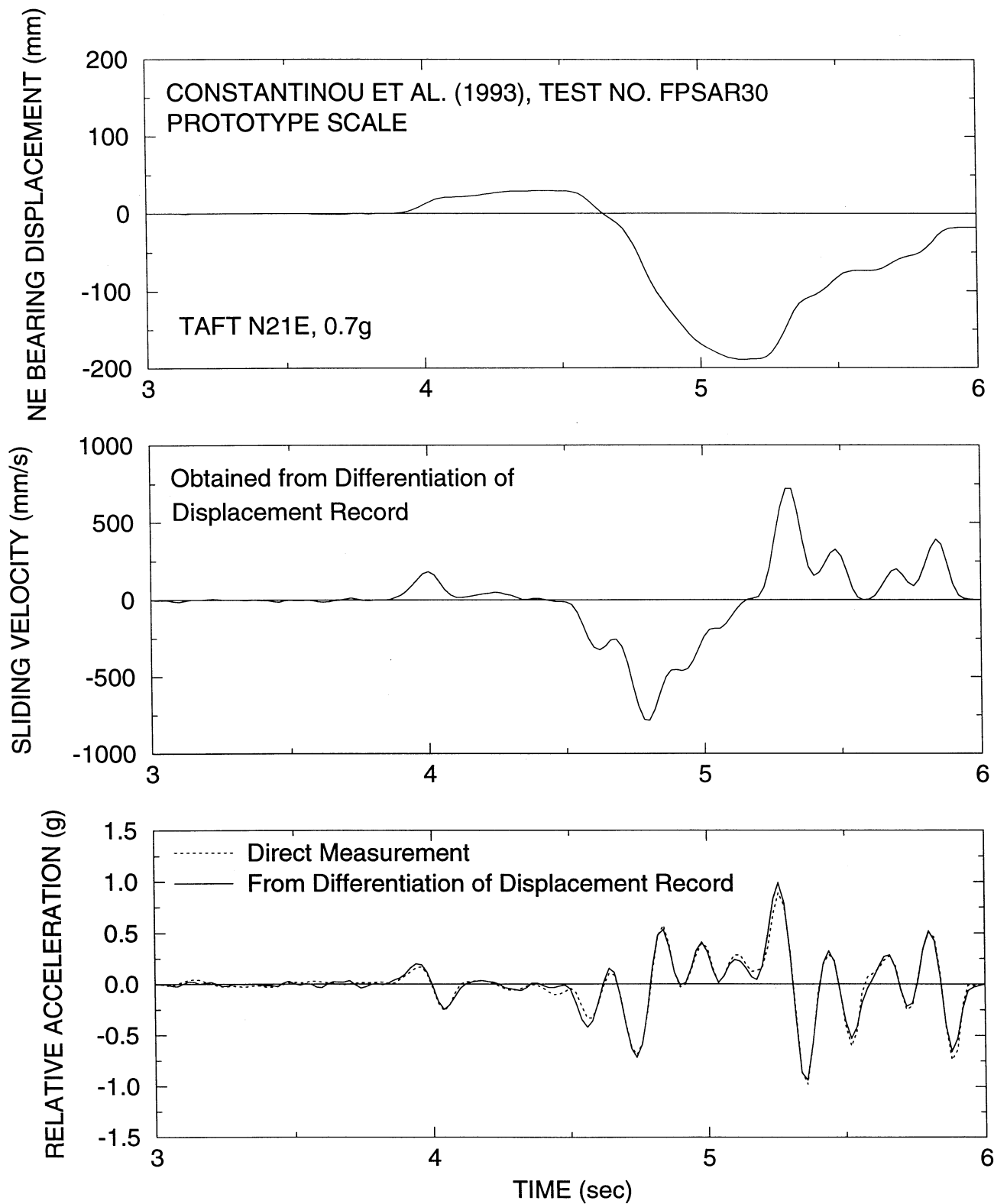


FIGURE 4-4 Recorded Response of Sliding Bearings in Shake Table Testing of a Model Bridge Structure by Constantinou et al. (1993)

record of bearing relative displacement was numerically differentiated to obtain the sliding velocity and the relative acceleration histories at the sliding interface. They are presented in Figure 4-4 after conversion to prototype scale. Moreover, a record of relative acceleration (obtained as the difference of records from accelerometers placed above and below the sliding interface) is shown to demonstrate the accuracy of the numerical differentiation. It may be observed that gross sliding occurs at 4 seconds from the start of the experiment. Following initiation of gross movement, a large sliding velocity of about 200 mm/s is reached within about 0.1 sec. However, the relative acceleration is only about 0.2 g. That is far less than the starting acceleration in displacement controlled, high frequency testing of sliding bearings.

While not evident in Figure 4-4, sliding at the interface of the isolation bearings occurred well before the time of 4 seconds. Figure 4-5 shows the responses of the bearings within the time frame of 2 to 4 seconds. Sliding displacements of about 0.5 mm are observed starting at the time of 2 seconds (actual measurement at the scale of the experiment was 0.14 mm with the instrument resolution being at 0.025 mm). The recorded shear force-displacement loop within this time frame clearly demonstrates sliding behavior with the breakaway friction coefficient being at about 0.08. By comparison the high velocity coefficient of sliding friction was about 0.10. Evidently, initiation of sliding occurs under truly quasi-static conditions. Specifically, the relative acceleration is very small and indistinguishable from noise.

We present a second example from the shake table testing of the same bridge model, but with a different sliding isolation system, namely that of Tsopelas et al. (1994, 1996). Figures 4-6 and 4-7 present the recorded response of one of four flat PTFE bearings (the isolation system consisted of these bearings and rubber restoring force devices) in a test with the S16E component of the Pacoima Dam record in the 1971 San Fernando earthquake. The record was scaled to 0.6 g peak acceleration and 0.73 m/s peak velocity in prototype scale. This earthquake component primarily consists of a high velocity shock and has near-source characteristics (the recording site was essentially at the surface projection of the rupture). As scaled, this record exhibited characteristics similar to many of the near-source records from the 1994 Northridge earthquake (Heaton et al., 1995).

We observe that initiation of motion (see close-up view in Figure 4-7) occurs at time of 3.8 seconds under again quasi-static conditions (a peak velocity of 12 mm/s is achieved within about 0.1 sec. with a peak relative acceleration of about 0.02 g). That is, the breakaway friction force is mobilized under nearly quasi-static conditions. Subsequently, and following momentary stops, conditions of high rate of motion may be achieved depending on the seismic demand. However, the experimental data show that the high initial value of the breakaway friction is not again mobilized. Rather, the prevailing friction force is the one under sliding conditions, which depends on the velocity of sliding.

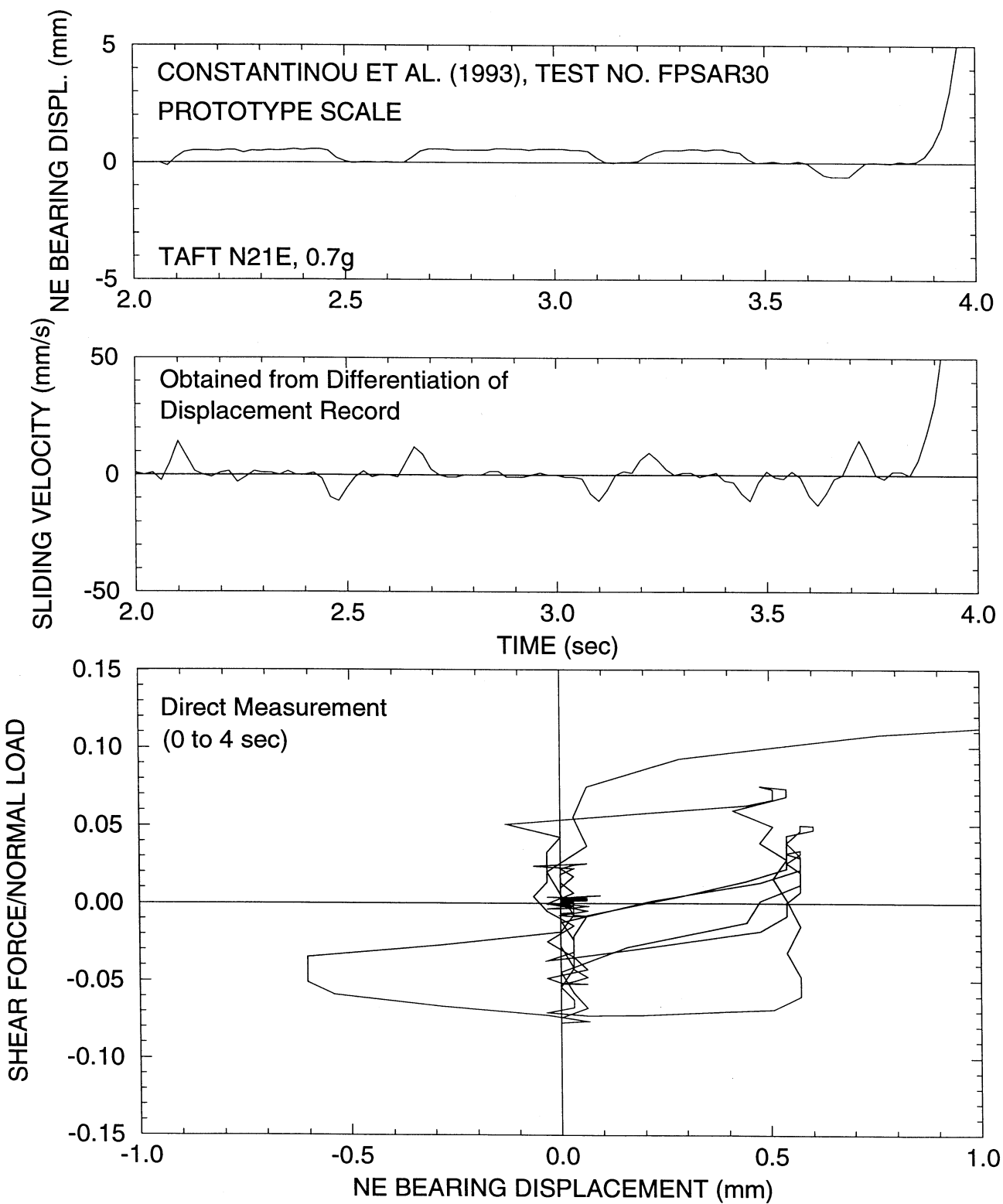


FIGURE 4-5 Close-up View of Recorded Response of Sliding Bearings in Shake Table Testing of a Model Bridge Structure by Constantinou et al. (1993)

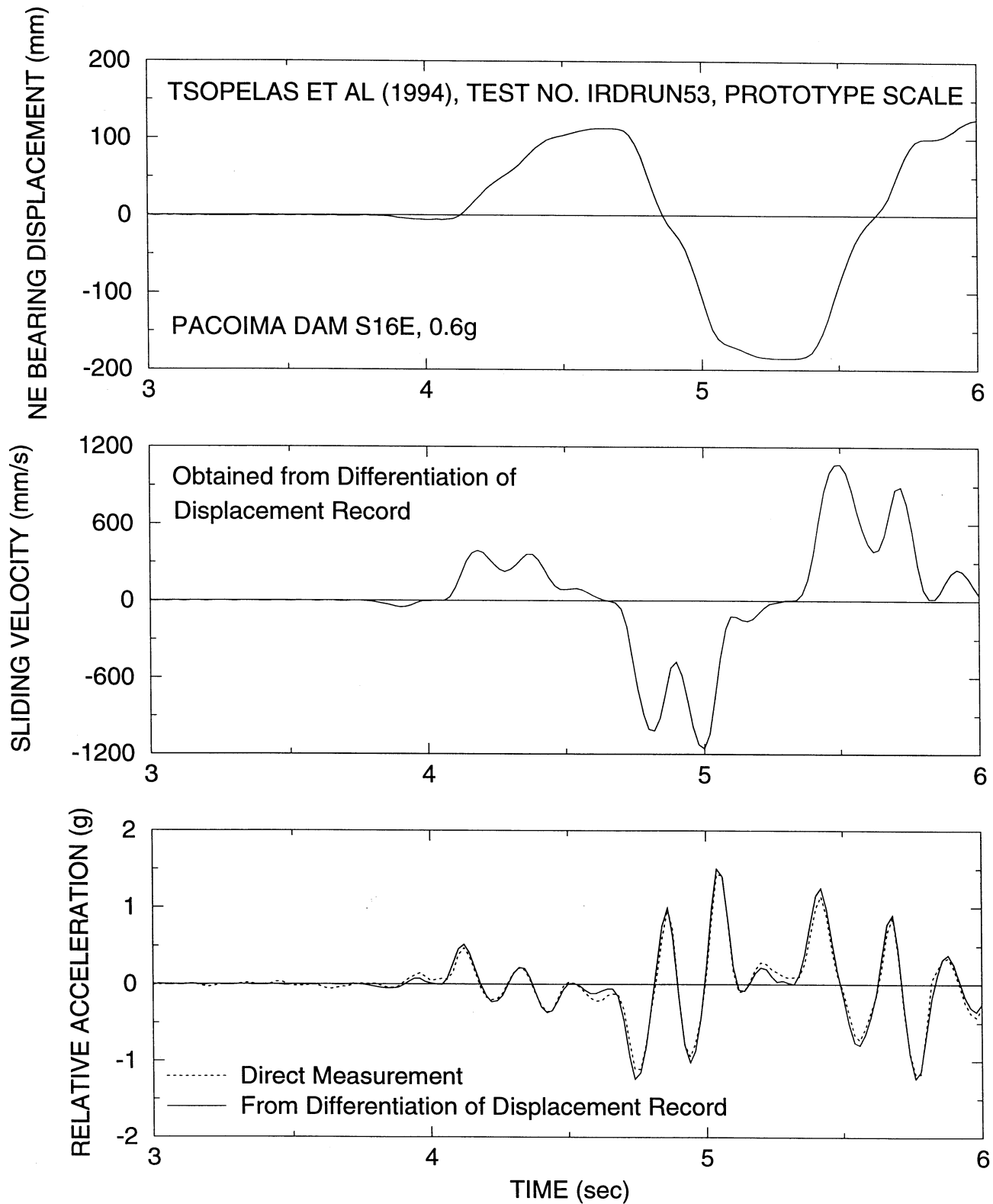


FIGURE 4-6 Recorded Response of Sliding Bearings in Shake Table Testing of a Model Bridge Structure by Tsopelas et al. (1994)

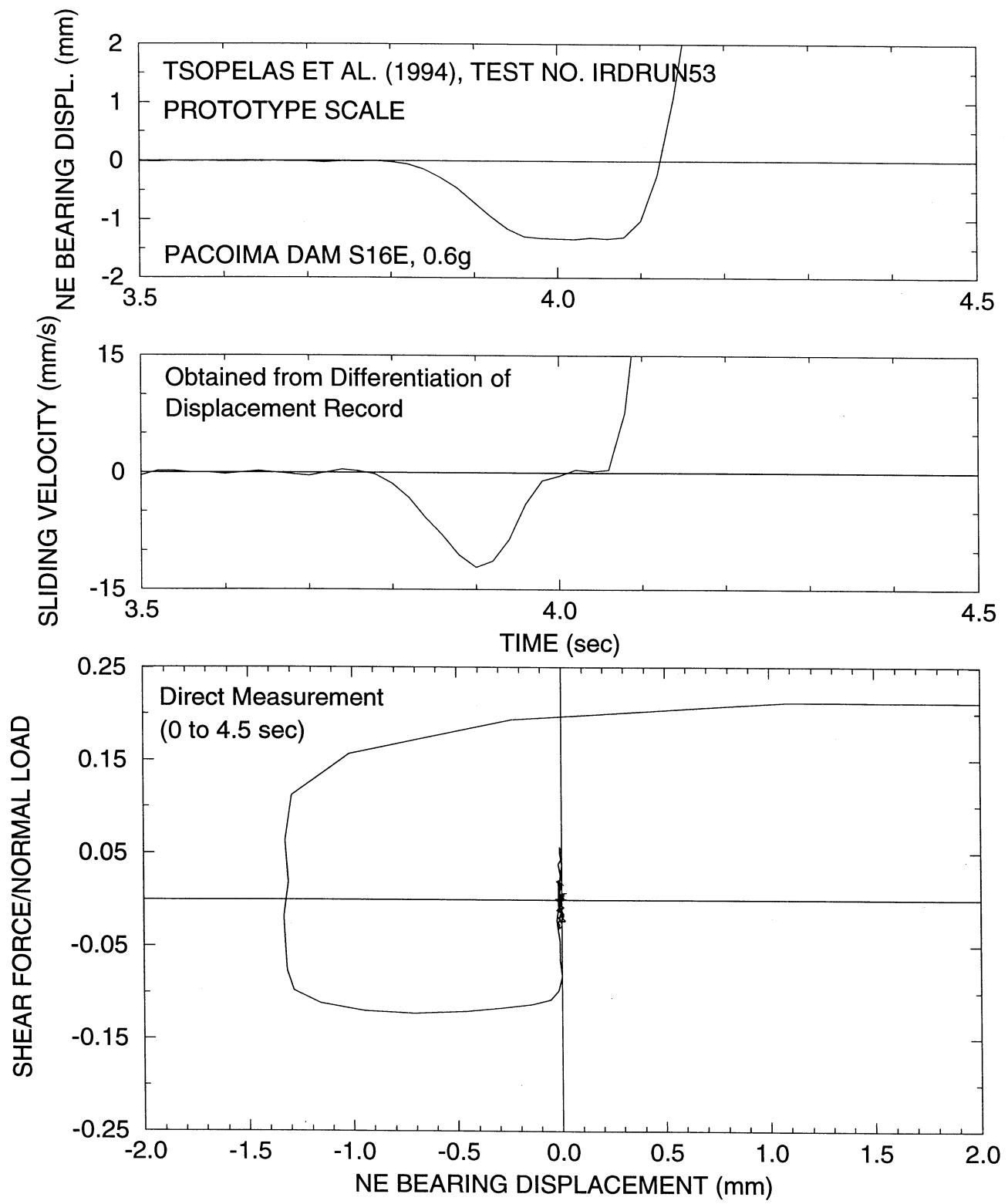


FIGURE 4-7 Close-up View of Recorded Response of Sliding Bearings in Shake Table Testing of a Model Bridge Structure by Tsopelas et al. (1994)

The effect of apparent pressure and sliding velocity on the coefficient of friction is as illustrated in Figure 3-8. Note that the breakaway friction coefficient (denoted as μ_B) is shown in this figure to be the value at nearly zero velocity of sliding. It is the value mobilized at initiation of motion under quasi-static conditions. The value of the sliding friction coefficient under very low sliding velocity is denoted in Figure 3-8 as f_{min} . Mokha et al. (1988, 1990) and Constantinou et al. (1990) reported values of the ratio μ_B/f_{min} for unfilled and glass filled PTFE in contact with polished stainless steel (surface roughness of 0.03 to 0.04 $\mu\text{m } R_a$) at temperature of about 20°C to be in the range of 1.3 to 4.4. Moreover, test data from Campbell et al. (1991) on a variety of PTFE-polished stainless steel interfaces indicate values of the ratio μ_B/f_{min} in the range of about 2.0 to 7.0.

Mokha et al. (1990) and Campbell et al. (1991) reported data on the frictional properties of woven PTFE, for which values of the ratio μ_B/f_{min} are again in the range of 2.0 to 3.0. However, data on the frictional properties of the PTFE composite used in FPS bearings (data are reported in section 4.4 herein where the effect of temperature is discussed) indicate small values of this ratio, typically of the order of 1.2. While the authors have observed this behavior in many test programs (Mokha et al., 1990; Constantinou et al., 1993; Al-Hussaini et al., 1994) they are unable to provide an explanation for the observed difference between this material and unfilled and woven PTFE.

Data in the literature on the frictional properties of PTFE bearings at large sliding velocities are few. Tyler (1977) was the first to report such data. While Tyler focused his study on the breakaway friction under high rate of motion (which is unrealistic), he also reported data on the sliding friction. These data are in general agreement with the data of Mokha et al. (1988, 1990) who conducted tests for a wider range of conditions.

Figure 4-8 presents data from Mokha et al. (1988) on the sliding coefficient of friction of unfilled PTFE in contact with polished ASTM A240, Type 304 stainless steel (surface roughness of 0.03 $\mu\text{m } R_a$) at temperature (this is the temperature at the start of the experiments) of about 20°C. The data reveal the dependency of this coefficient on the apparent pressure and velocity of sliding. However, the values of the coefficient of friction should not be regarded as absolute. Specifically, the shown values have been extracted from the first cycle of testing and it is known that the coefficient of friction may reduce with increasing travel depending on the conditions of testing. Moreover, the specimen size has an effect. Typically, slightly lower values are obtained in testing of very large specimens. It is likely that this is caused by uneven distribution and concentration of the bearing pressure which result from the high rotational stiffness of large bearings. Finally, there is variability in the recorded friction values that may be the result of yet unknown effects such as the type of stainless steel (the authors have observed small differences between types 304 and 316 stainless steels), humidity, etc.

Figure 4-9 presents data on the frictional properties of the PTFE composite used in FPS bearings from the tests of Constantinou et al. (1993) and Tsopelas et al. (1994). The values of the sliding coefficient of friction were obtained in shake table testing of a bridge model with either FPS bearings (Constantinou et al., 1993) or with flat sliding bearings (Tsopelas et al., 1994). The data were extracted from either displacement

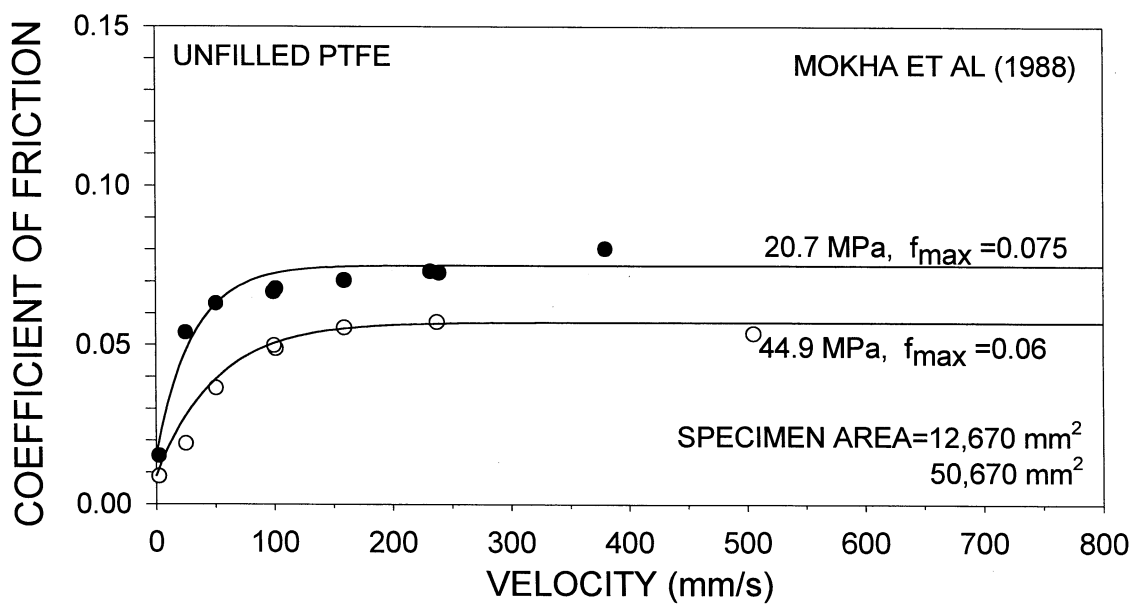
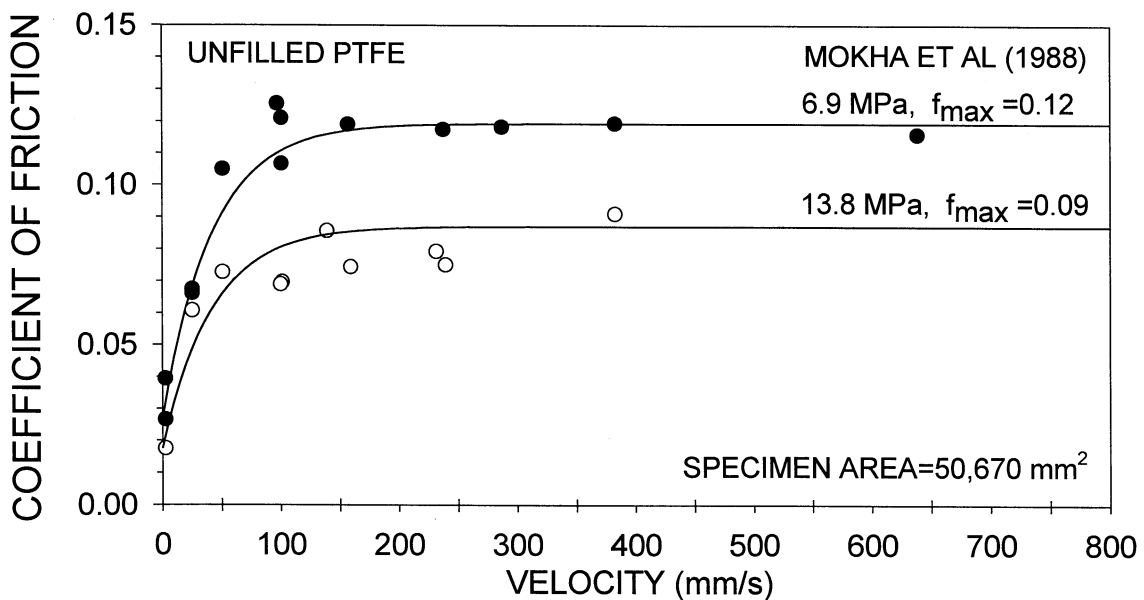


FIGURE 4-8 Coefficient of Sliding Friction of Unfilled PTFE-Polished Stainless Steel Interfaces ($0.03 \mu\text{m Ra}$). Ambient Temperature is about 20°C

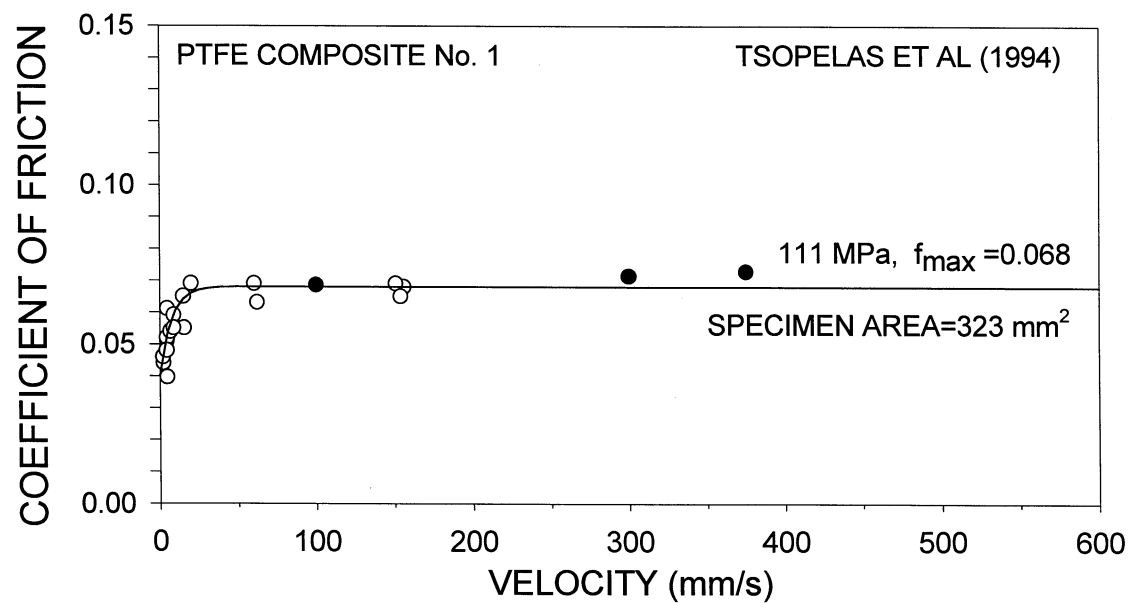
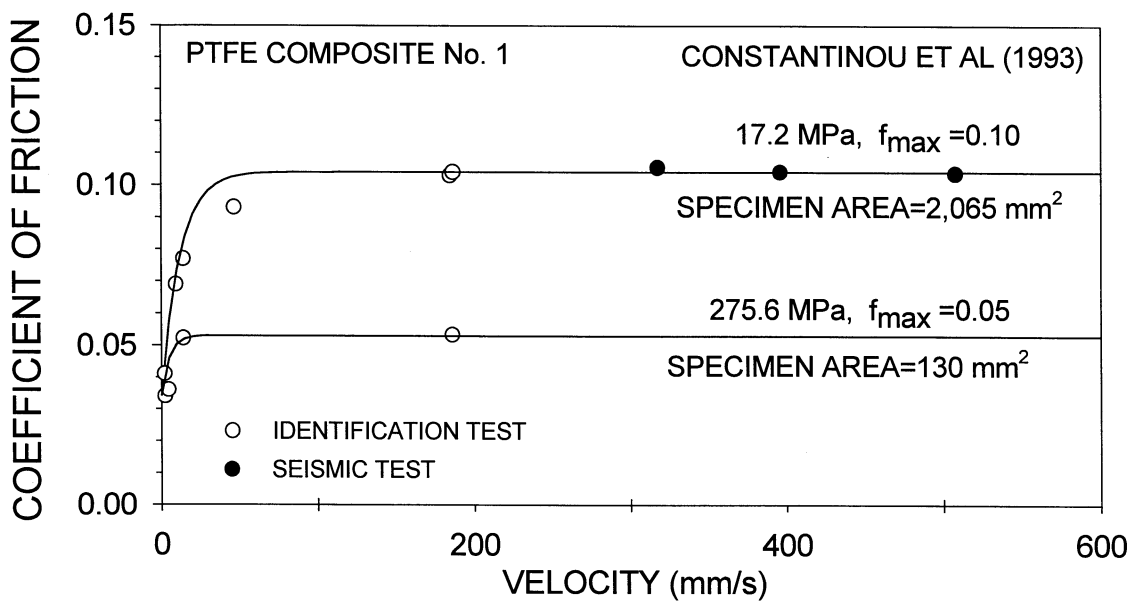


FIGURE 4-9 Coefficient of Sliding Friction of Composite No.1-Polished Stainless Steel Interfaces. Ambient Temperature is about 20°C (all tests conducted under normal load of about 35 kN)

controlled tests (open circle symbols) or seismic motion tests (dark symbols). In all tests the normal load on the bearings was about 35 kN. Again the presented values should be regarded as representative and not as absolute values.

In general, for a fixed value of the apparent pressure, the sliding coefficient of friction depends on the velocity, V, in a fashion that can be described by (Mokha et al., 1988; Constantinou et al., 1990).

$$\mu = f_{\max} - (f_{\max} - f_{\min}) \exp(-aV) \quad (4-1)$$

in which the meaning of f_{\max} and f_{\min} is illustrated in Figure 3-8 and a is a parameter with values of 20 to 30 s/m for unfilled PTFE and about 100 s/m or larger for the PTFE composite. Equation (4-1) with appropriate parameters (see Mokha et al. 1988; Constantinou et al., 1993, and Tsopelas et al., 1994) resulted in the curves shown in Figures 4-8 and 4-9. Indeed, (4-1) describes well the observed dependency of the sliding coefficient of friction on velocity.

Parameter a controls the transition of the coefficient of friction from its minimum value to its maximum value at high velocity of sliding. Figure 4-10 illustrates the effect of parameter a for two values of the ratio f_{\max}/f_{\min} , 2.5 and 5. The lower value of this ratio is representative of the PTFE composite, whereas the upper value is representative of the unfilled PTFE. This figure, as well as Figures 4-8 and 4-9, demonstrate that testing at a sliding velocity greater than about 150 mm/s will suffice to obtain the maximum value of the sliding coefficient of friction of all PTFE and PTFE-based materials under normal temperature conditions.

4.4. Effect of Temperature

Campbell et al. (1991) reported data on the effect of temperature on the breakaway and the low velocity sliding friction of unlubricated unfilled, glass filled and woven PTFE in contact with highly polished stainless steel at apparent pressure of 20.7 MPa. Table 4-3 presents the results of Campbell et al. (1991) as extracted by the authors from the graphs of Campbell et al. (1991). Quantity f_{\min} is the sliding coefficient of friction in the first cycle of movement. All tests were conducted at a peak sliding velocity of 1 mm/s. Evidently, temperature has a substantial effect on the breakaway and the low velocity sliding friction.

We have conducted tests on unfilled PTFE and the PTFE composite No. 1 over a wide range of sliding velocities and temperature in the range of 50°C to -50°C using the testing arrangement of Figure 4-1. Testing was conducted at apparent pressure of 20.7 MPa for the unfilled PTFE and of 69 MPa for the PTFE composite. The stainless steel utilized in these tests was ASTM A240, Type 304 with a measured surface roughness of 0.03 μm R_a .

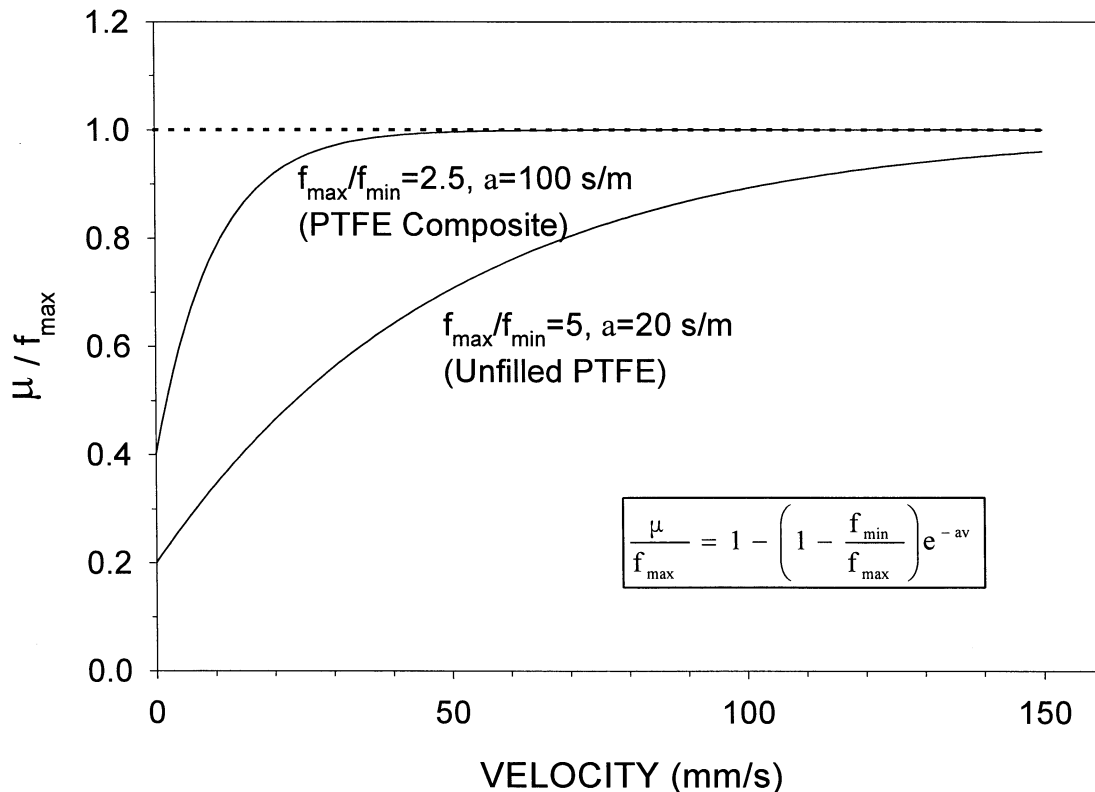


FIGURE 4-10 Effect of Parameter a on Variation of Coefficient of Friction with Velocity

TABLE 4-3 Effect of Temperature on the Breakaway and the Sliding Coefficient of Friction ($v = 1$ mm/s) of Unfilled PTFE in Contact with Highly Polished Stainless Steel at Apparent Pressure of 20.7 MPa (from Campbell et al., 1991).

Temperature °C	Breakaway Coefficient of Friction	Sliding Coefficient of Friction ($v = 1$ mm/s)
20	0.066	0.016
10	0.125	0.016
0	0.132	0.020
-10	0.149	0.039
-15	0.154	0.057
-20	0.136	0.074
-25	0.157	0.086

Appendix A contains a sample of experimental results from this testing program. Each page in this appendix presents the imposed displacement history, the recorded friction force history from two interfaces and the normalized friction force to normal load versus displacement loops for each experiment. Moreover, information on the materials (UF for unfilled PTFE and C1 for the composite PTFE No. 1), apparent pressure, frequency of harmonic motion and temperature at the start of each experiment is presented. The

imposed history of displacement is illustrated in Figure 4-11. It starts with an idle time in which data acquisition is performed for capturing the breakaway friction force in the case of unforeseen movement of the actuator. A build-up time of 60 to 80 sec. follows, in which a displacement amplitude, u_o , is reached under very low sliding velocity (less than 0.8 mm/s). During this part of the imposed motion, measurements of the breakaway and minimum sliding friction (f_{min}) could be made under truly quasi-static conditions. Subsequently, an idle time of 10 sec. was used to allow for stabilization of the temperature at the sliding interface. It was followed by two and a quarter or three and a quarter cycles of harmonic displacement history as shown in Figure 4-11.

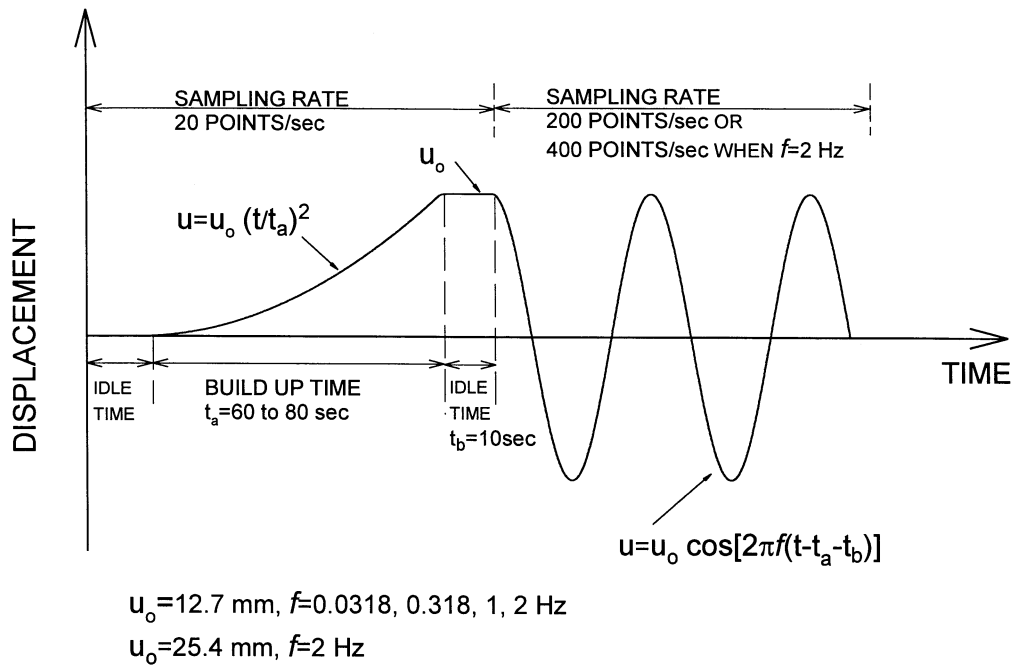


FIGURE 4-11 Imposed Displacement History in Testing of Sliding Interfaces for Determining Temperature Effects on Frictional Properties

Records of the frictional force from two interfaces were obtained in each test as shown in Appendix A. As seen in this appendix, the friction force histories are biased as a result of pre-loading in the horizontal actuator of the testing arrangement. The amount of pre-loading was determined from the average of the positive and negative normalized friction forces (divided by normal load, which slightly varied during testing) at zero displacement in the last cycle of imposed harmonic motion. With the value of the pre-load established, the normalized friction-displacement loops were adjusted to achieve symmetry as illustrated in Figure 4-12. These loops were then used to obtain the breakaway friction coefficient, the minimum sliding friction coefficient, f_{min} (at velocity less than 0.6 mm/s), and the sliding coefficient of friction at the first instant at which the largest velocity of sliding was attained (typically after 12.7 mm or 25.4 mm of travel) as shown in Figure 4-12.

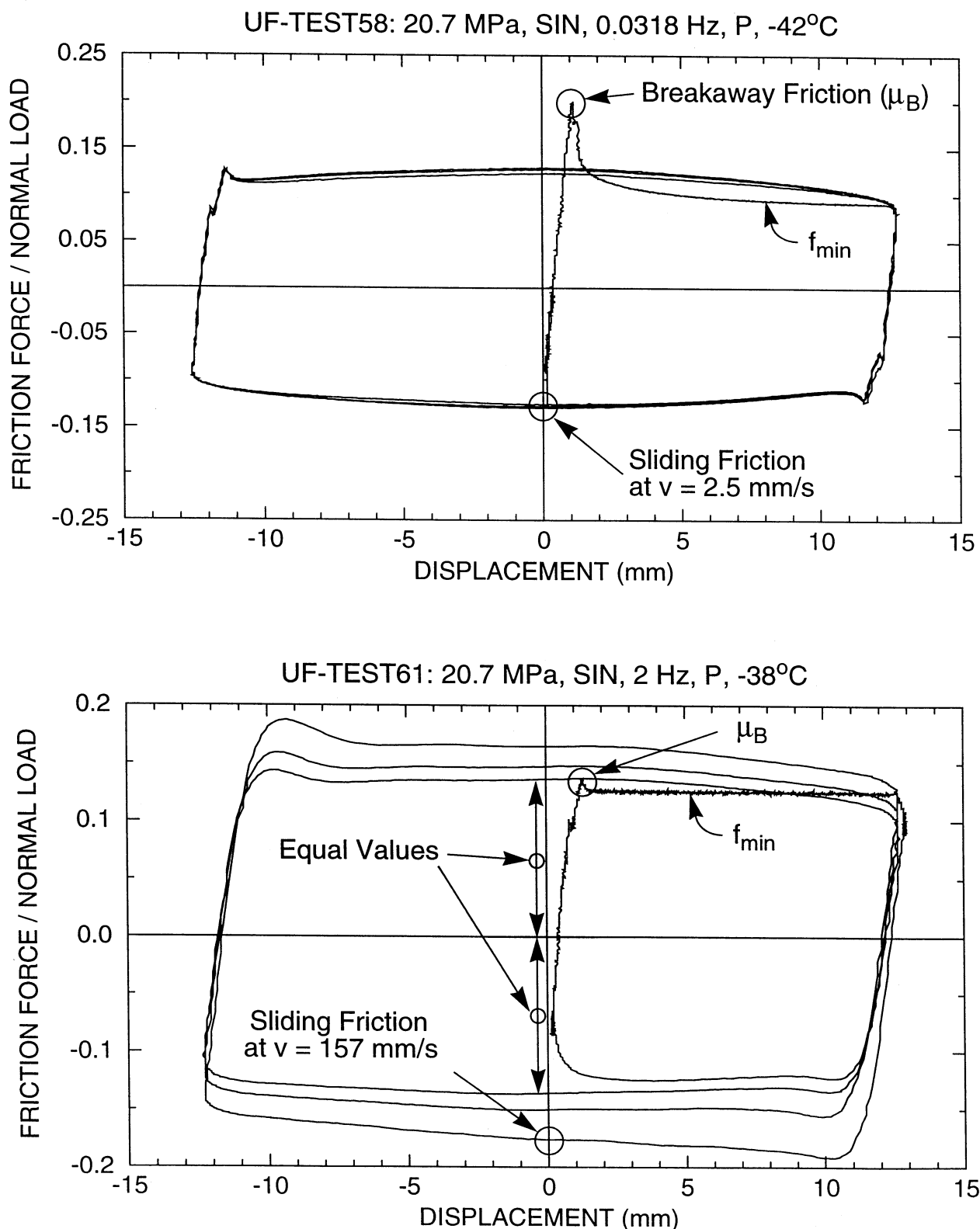


FIGURE 4-12 Example of Determination of Frictional Properties

Appendix A contains a complete set of results on the testing of unfilled PTFE at temperature of about -40°C (tests UF-TEST58 to UF-TEST62). Test No. 58 was conducted on new specimens of PTFE with a clean stainless steel plate. The specimens were loaded with a normal load of 147 kN at 4 p.m. on February 1, 1995 and were continuously maintained under load until testing on February 14, 1995 (load dwell of 311 hours). At 10 a.m. on that day the insulating box around the testing arrangement was filled with sealed bags containing solid carbon dioxide (dry ice). Following five hours of conditioning, the temperature was stable at -42°C and test No. 58 was conducted. At conclusion the temperature rose to -32°C . The specimen was left undisturbed for one more hour until the temperature reached -39°C and then test No. 59 was conducted (note that during testing the insulating box was filled with sealed bags of dry ice including some directly on the moving plate except for a 30 mm strip around the specimen). This procedure was repeated for a total of nine tests and then a new specimen was installed.

For testing at elevated temperatures, heating elements were installed around the testing arrangement and directly on the moving plate.

Testing of the unfilled PTFE material was conducted during the months of January and February 1995. During this period the average conditions in the laboratory were 22°C temperature and about 20-percent relative humidity. The PTFE composite material was tested in April and May 1995 when the conditions were 22°C temperature and 25 to 40-percent relative humidity. However, in the low temperature tests the relative humidity in the insulating box was extremely low.

It may be observed in Appendix A that at very low temperature and for the high frequency tests, the loops exhibit higher friction on reversal of motion during the first cycle. Particularly, the friction is highest at initiation of the harmonic portion of the imposed motion. It may be seen in Appendix A (e.g., tests UF-TEST 59 to UF-TEST 62) that the friction force on initiation of the harmonic motion is essentially constant and independent of the characteristics of the imposed motion (e.g., in these tests the peak velocity varied between 25 mm/s and 320 mm/s). It may be interpreted as breakaway friction following the brief (10 sec) stop (see Fig. 4-11), however, affected by the dynamic conditions at initiation of motion. In the presentation that follows the value of friction at initiation of motion (and at each reversal of motion) has not been used. Rather, the value at the first instant of peak velocity (see Fig. 4-12) is used for the following reasons:

- (a) The reported value is truly the sliding value at some known velocity and following some small travel.
- (b) There is interest in using (4-1) for describing the dependency of the sliding coefficient of friction on velocity. However, at low temperatures the maximum value of sliding friction, f_{\max} , occurs not at high velocities but rather at relatively low velocities (e.g., see Fig. 3-11) at which the friction on initiation of harmonic motion is essentially the same as the sliding value (e.g., see test UF-TEST 60).

- (c) The interest is primarily in establishing values of the ratio of parameter f_{\max} at various temperatures and at a reference temperature (20°C), which will be the λ -factors for temperature effect. In establishing these ratios we will utilize values of f_{\max} that occur at different velocities (a conservative approach). For example, consider that the λ -factor for temperature of -40°C is established from the ratio of the f_{\max} values at -40°C and 20°C . Based on the results of Appendix A for unfilled PTFE, the f_{\max} values are 0.178 at -39°C (test No. 60 at velocity of 80 mm/s) and 0.113 at 22°C (test No. 43A at velocity of 320 mm/s). The ratio is $0.178/0.113 = 1.58$. This is the value reported in this report. Alternatively, if we utilize the values at reversal of motion we have: at -40°C 0.189 (test No. 62) and at 22°C 0.118 (test No. 43A). The ratio is $0.189/0.118 = 1.60$, that is, essentially the same.

Figures 4-13 to 4-15 present data on the effect of temperature on the frictional properties of unfilled, unlubricated PTFE. Figure 4-13 present the breakaway friction as measured in the various tests. Temperatures are reported in the range of -40°C to 50°C . This is the temperature at the start of the experiment, rounded to the nearest multiple of ten. For each of the first tests in each sequence, the load dwell in hours is shown next to the data point. Each of the subsequent tests was conducted after a load dwell of less than one hour.

Figure 4-14 presents the measured breakaway friction, minimum sliding friction, f_{\min} , and sliding friction at three different velocities as function of the temperature at the start of each experiment. The figure demonstrates the substantial effect of temperature on the low velocity, f_{\min} , and breakaway friction and the much less effect on the high velocity friction. The latter is clearly the result of frictional heating. The values of friction in this figure are consistent with those reported by Campbell et al. (1991) (see Table 4-3). For example, data for the sliding coefficient of friction at very low velocity (f_{\min}) in Figure 4-14 are 0.016 to 0.03 at 20°C and about 0.09 (interpolated) at -25°C . Campbell et al. (1991) report values of 0.016 and 0.086, respectively.

Figure 4-15 presents the measured coefficient of friction as function of sliding velocity for various temperatures at the start of each experiment (rounded to the nearest multiple of ten). When data points for the same temperature are connected by a curve, as done in the figure for two cases, a clear picture of the effect of temperature emerges. For example, between the temperatures of 20°C and -40°C we observe a 4 to 5 times increase in the breakaway and low velocity sliding friction (f_{\min}) but only about a 1.6 times increase in the high velocity value (f_{\max}). Note that at some large enough velocity the temperature at the start of the experiment has a minor effect on friction - a result of frictional heating.

UNFILLED PTFE

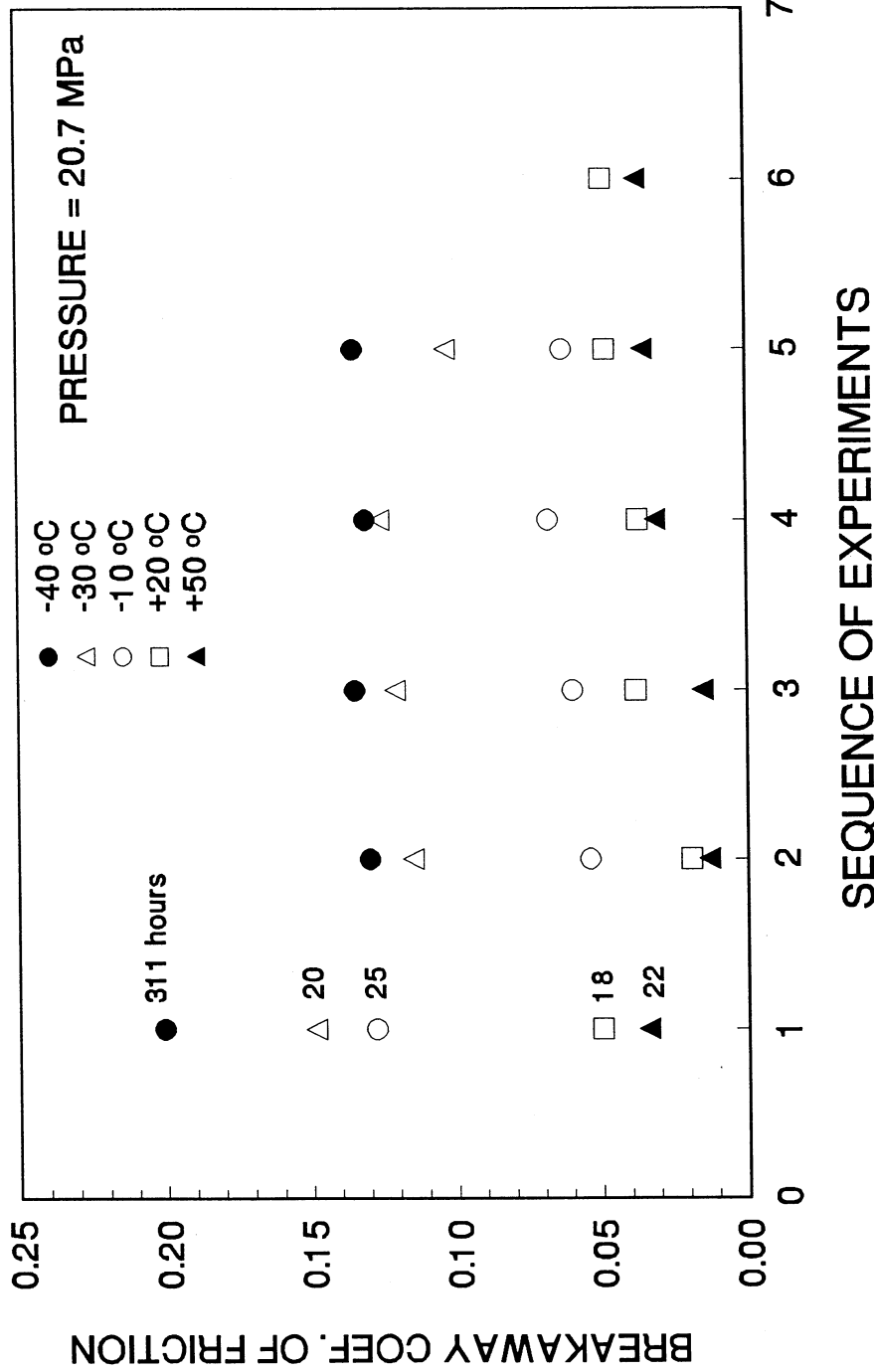


FIGURE 4-13 Breakaway (or Static) Friction of Unfilled PTFE-Polished Stainless Steel Interfaces as Function of Temperature and Sequence of Testing

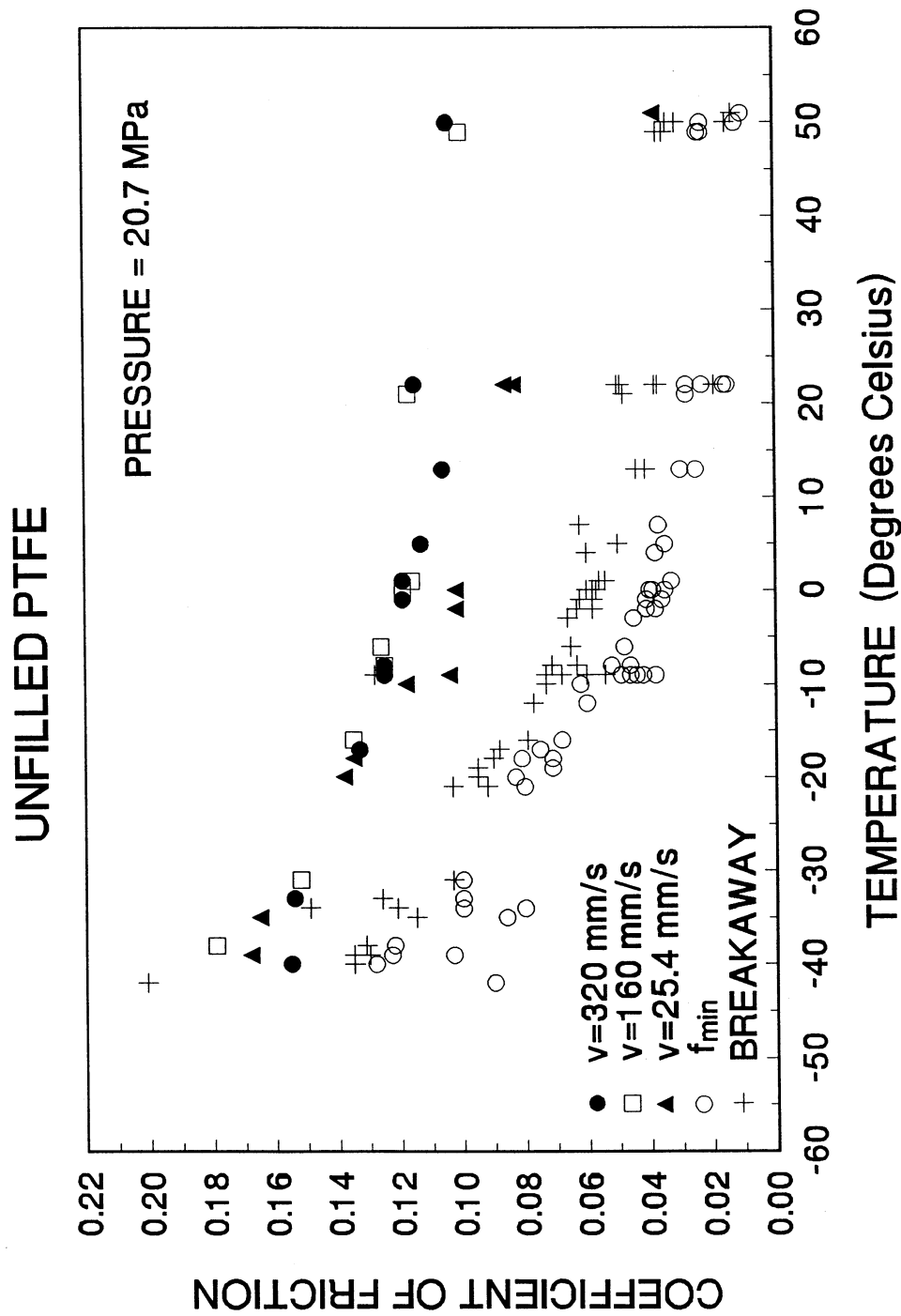


FIGURE 4-14 Friction of Unfilled PTFE-Polished Stainless Steel Interfaces as Function of Temperature

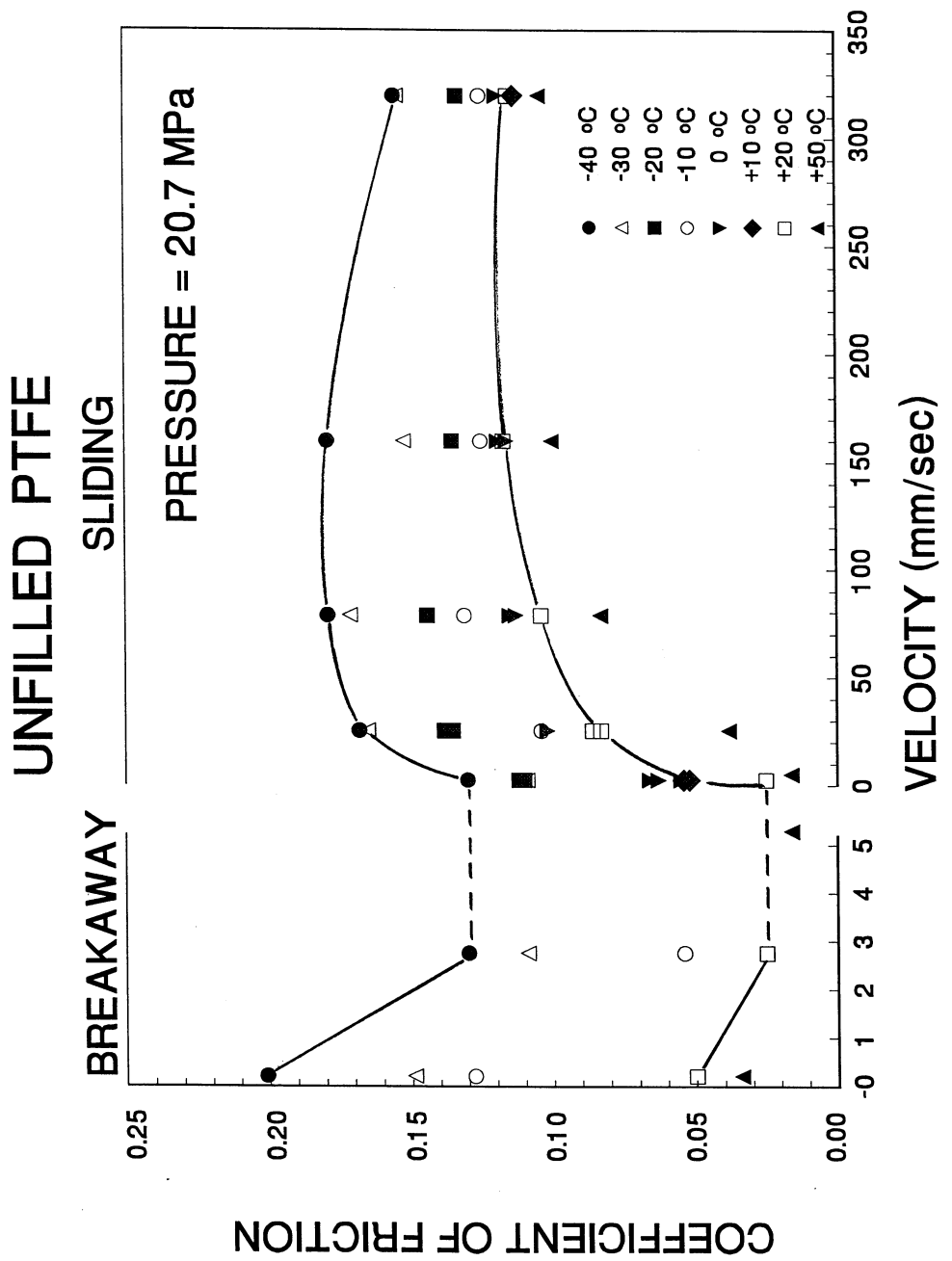


FIGURE 4-15 Friction of Unfilled PTFE-Polished Stainless Steel Interfaces at Various Temperatures as Function of Sliding Velocity

Since we have now a theory to predict the temperature rise due to frictional heating (section 3.8), it will be instructive to perform some representative calculations. Consider the test at which the f_{\max} value was determined at temperature of -40°C . In Figure 4-15, the data point is the one at velocity of about 80 mm/s. In this test, the imposed amplitude was 12.7 mm at frequency of 1 Hz. The value of f_{\max} was recorded after a quarter cycle of motion, that is, at time $t = 0.25$ sec. The motion is equivalent to one of constant velocity $v_c = 0.051$ m/s. Using $\mu = 0.18$, $p = 20.7$ MPa and thermal properties of steel that are appropriate for about -30°C (see Table 3-1 and Lide, 1993 for further information), and utilizing (3-21) and (3-29) we calculate a surface temperature rise of about 16°C . Repeating the calculation for the same temperature and the highest velocity (test at frequency of 2Hz and amplitude of 25.4 mm), we have $t = 0.125$ sec, $v_c = 0.20$ m/s, $\mu = 0.16$ and the surface temperature rise is about 35°C . That is, the temperature rise is large enough to affect the frictional properties.

Figures 4-16 to 4-18 present the data on the effect of temperature on the frictional properties of the PTFE-based composite. In comparing these to the results for unfilled PTFE we make two observations:

- (a) the breakaway friction is nearly the same as the low velocity sliding friction (f_{\min}), and
- (b) the effect of temperature is, in general, much less than in the case of unfilled PTFE.

An explanation for the lesser effect of temperature is related to the generated heat flux. Friction in the composite material is about half that of the unfilled PTFE, whereas the apparent pressure is 3.3 times larger. Given that the imposed motions were identical, the heat flux (see eq. 3-29) in the testing of the composite material was about 1.7 times more than in the testing of unfilled PTFE. However, the measurements of the temperature rise by the thermocouple embedded in the stainless steel plate were much less than those recorded, for identical motions, in the testing of unfilled PTFE. Therefore, there must have been a substantial heat flux towards the composite material, whereas in the case of unfilled PTFE nearly all of the generated heat was supplied to the stainless steel surface. Main reason for this must have been the very small thickness of the composite material (0.25 mm, which was selected on the basis of considerations for wear for the wear tests that followed the temperature testing). The results, therefore, for the composite material must be viewed in the light of this explanation. It is likely that the effect of temperature for thicker materials (as those expected to be used in bridge applications) is larger than what is shown in Figures 4-16 to 4-18.

COMPOSITE No. 1

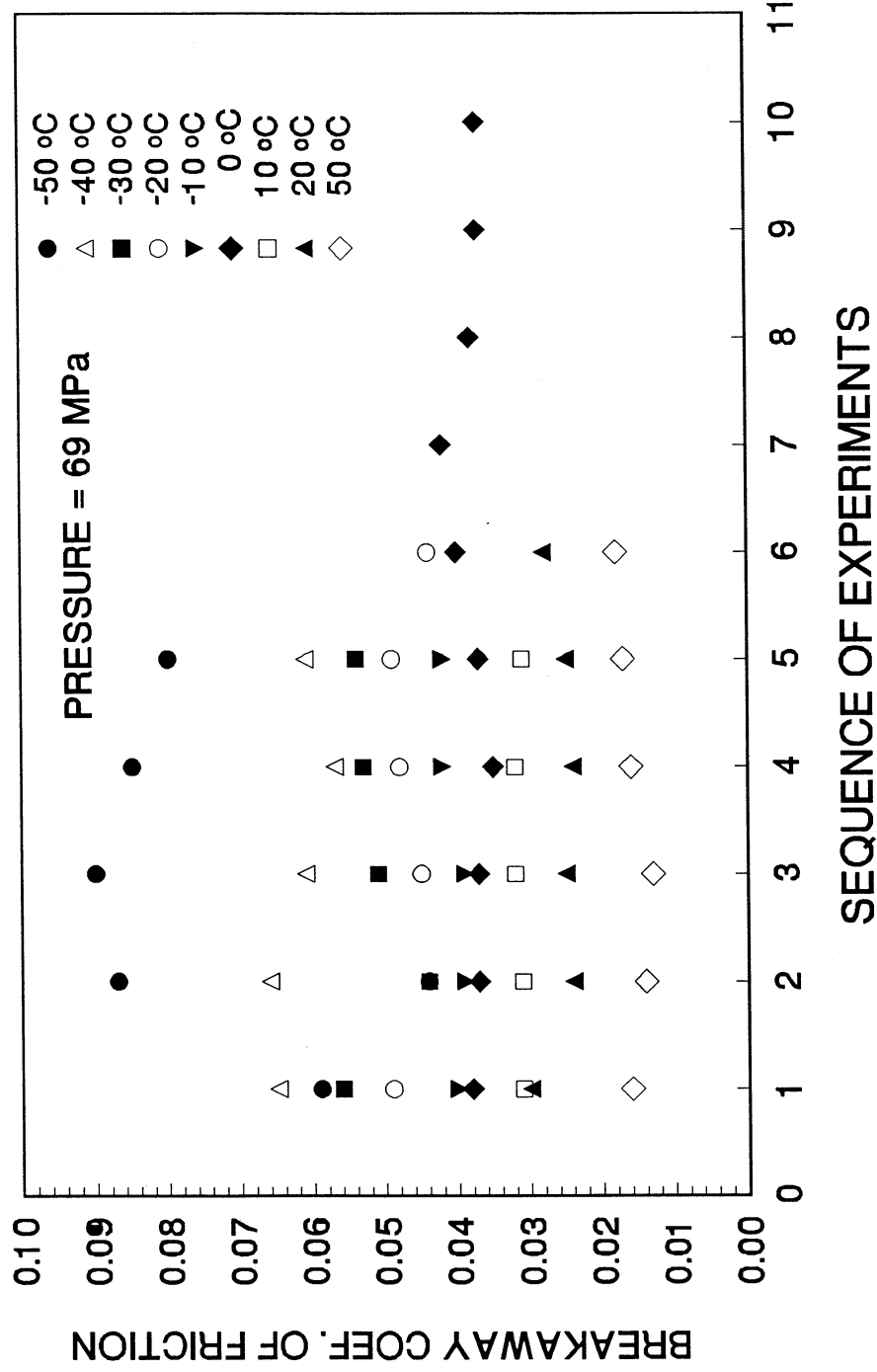


FIGURE 4-16 Breakaway (or Static) Friction of PTFE-based Composite-Polished Stainless Steel Interfaces as Function of Temperature and Sequence of Testing⁸⁹

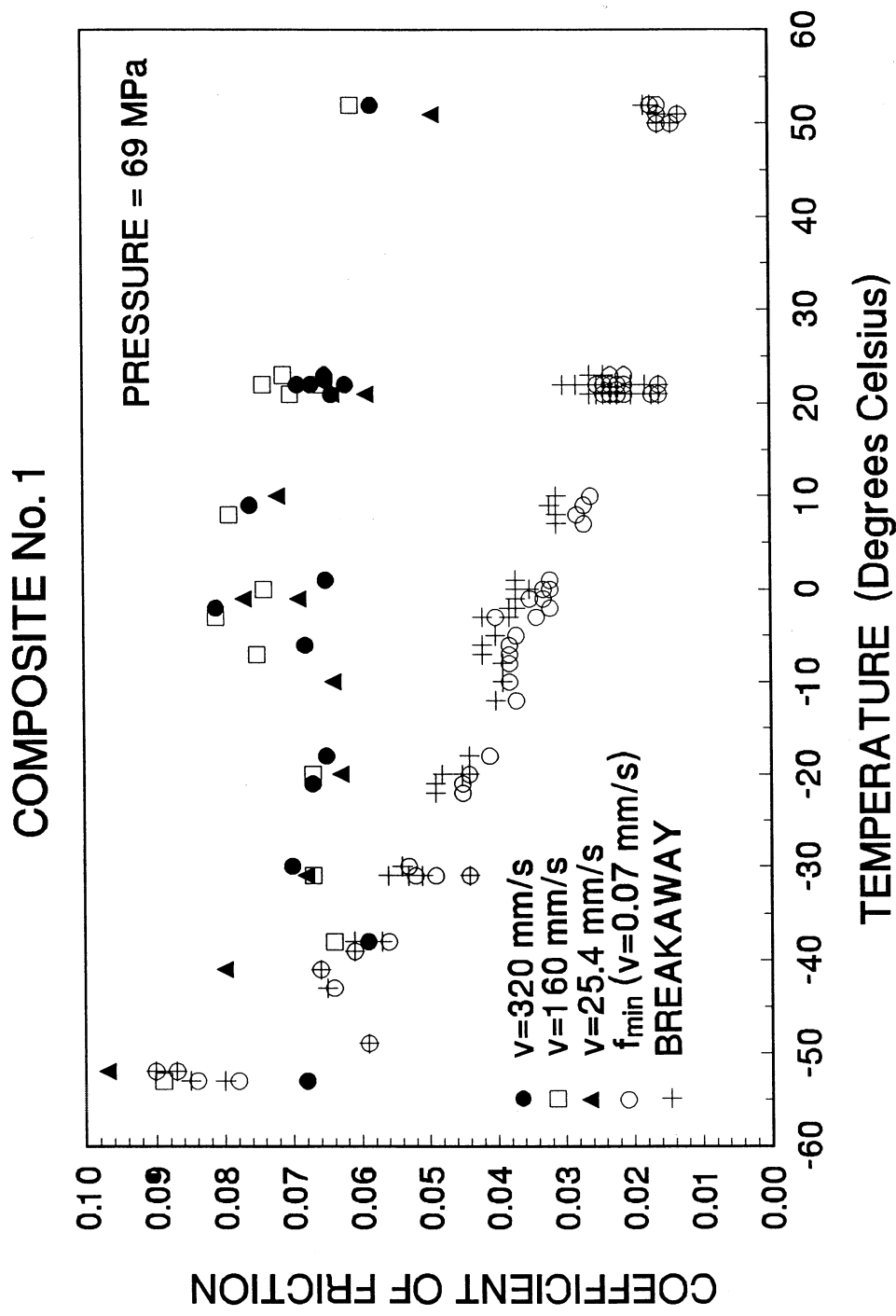


FIGURE 4-17 Friction of PTFE-based Composite-Polished Stainless Steel Interfaces as Function of Temperature

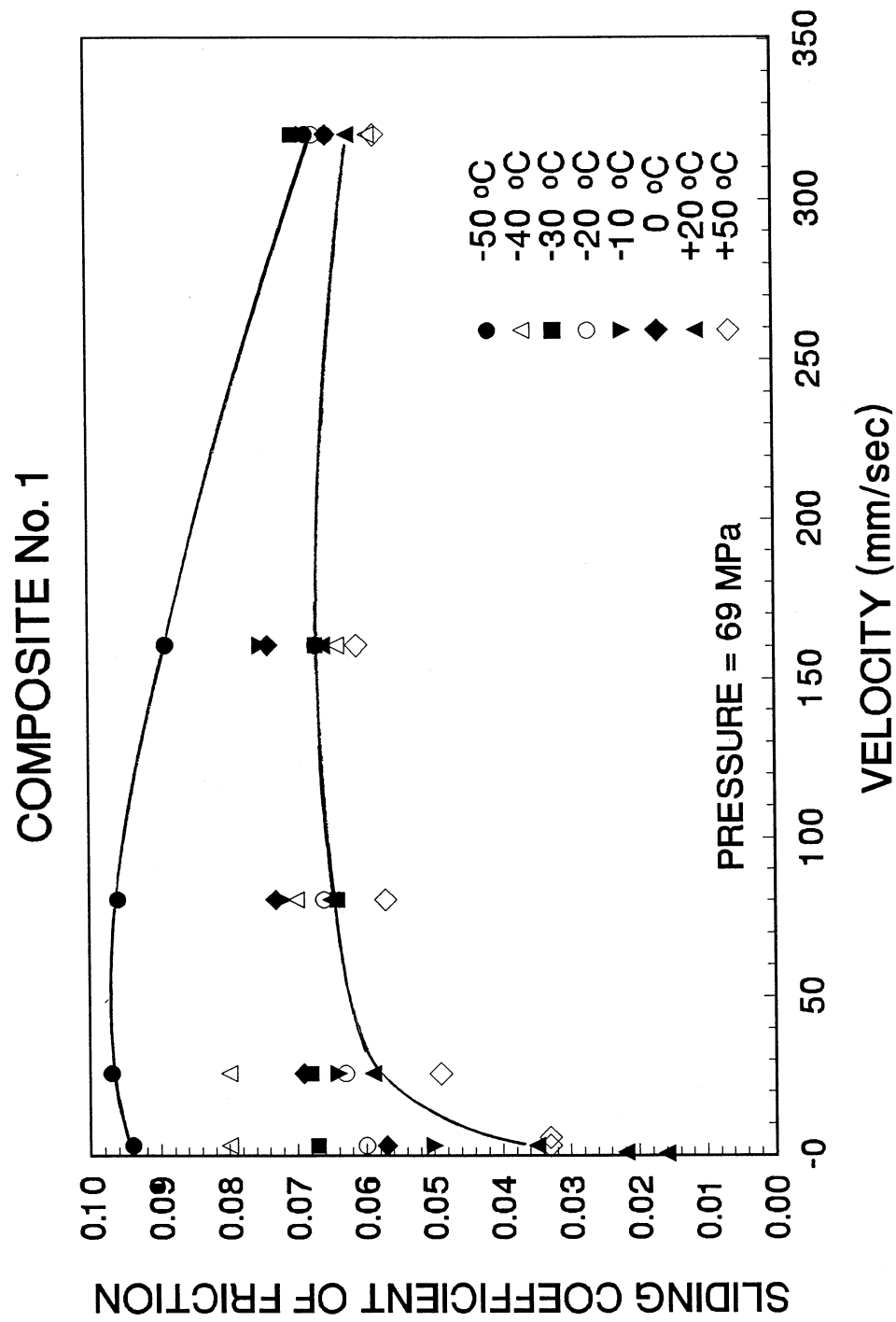


FIGURE 4-18 Friction of PTFE-based Composite-Polished Stainless Steel Interfaces at Various Temperatures as Function of Sliding Velocity

4.5 Effect of Cumulative Movement

A review of the literature on the effect of cumulative movement (travel) on the coefficient of friction of PTFE-stainless steel interfaces produces conflicting results. We start with the report of Campbell and Kong (1987) which is readily available in North America. The report contain two figures (Figs. 21 and 23) that show a substantial increase of the low velocity sliding friction with cumulative travel—approximately a 300-percent increase over a travel of 20 km. While not mentioned in the report, the results are for lubricated bearings and are of German origin. A more detailed presentation of such results may be found in Kauschke and Baigent (1986), who document the effect of travel of up to 20 km and temperature in the range of 20°C to –35°C on the low velocity (0.4 to 2.0 mm/s) sliding friction of lubricated PTFE-stainless steel bearings. The stainless steel (type X5CrNiMo 1810) is equivalent to ASTM 240, Type 316, and test results are presented for the stainless steel either been polished or as-rolled (i.e., rough).

Moreover, Kauschke and Baigent (1986) present results for unlubricated bearings, of which one set of results apply for Polyoxymethylene (a form of acetal plastic) in contact with PTFE (it is unfortunate that the results for this case are presented in Campbell and Kong, 1987 as Figure 7, without mentioning the nature of the interface) and another for polished, Type 316 stainless steel (respectively, Figs. 9 and 10 in Kauschke and Baigent, 1986). The former is of no interest whereas the second set of results apply for temperature of 21°C, apparent pressure of 30 MPa and travel of 2 km. For this travel the sliding coefficient of friction exhibits minor changes—the friction is in the range of 0.05 to 0.06.

Long (1969, 1974) reported on the effect of travel on the friction of unlubricated PTFE-polished stainless steel interfaces at apparent pressure of 24 MPa. The stainless steel was highly polished (0.05 µm arithmetic average). Periodic constant velocity motion was imposed at amplitude of 25 mm and velocity of 2.5 mm/s for a total travel of just over 5 km. Long reported the static coefficient of friction which in this case should be interpreted as the friction on reversal of motion. Excluding the higher value on initiation of motion (breakaway value), the reported value is essentially the same as the value of the sliding coefficient of friction. Long reports a breakaway friction value of 0.017, which drops to 0.010 after a short travel (50m), subsequently it stabilizes at 0.008 and ends at 0.007 after 5 km of travel.

The results of Long (1969, 1974) differ from those of German origin (reported by Kauschke and Baigent, 1986), in two respects:

- (a) Friction values for approximately the same conditions of apparent pressure (24 to 30 MPa) and sliding velocity (2.0 to 2.5 mm/s) are substantially different (about 0.05 in the German origin tests and about 0.01 in the tests of Long). This substantial difference may be the effect of specimen size (typically 75 mm diameter in the German tests, and about 20 mm in the tests of Long) and, foremost, the composition and surface condition of the stainless steel. Long (1969) actually obtained and tested

the German steel to find a higher surface roughness (about 0.18 μm arithmetic average) and substantially higher friction values than those of his tests.

- (b) The results of Long demonstrate a reduction of friction with increasing travel, whereas the results of German origin demonstrate the opposite. There is no obvious explanation for this difference. Possibilities are the effect of composition and surface roughness of stainless steel, and the effect of frictional heating. It is unknown whether, in either test program, the temperature was monitored at the sliding interface and measures were taken to prevent its rise (e.g., by conducting intermittent testing).

Regardless of these differences, both sets of results show rather small changes (whether increases or decreases) of the low velocity coefficient of friction with travel in the range of 2 to 5 km. However, more recently Campbell et al. (1991) reported test results on unfilled PTFE in contact with highly polished stainless steel at various apparent pressures and temperatures that show marked increases in the low velocity friction after short travel. Testing was conducted with 75 mm diameter specimens utilizing periodic constant velocity motion of 12.5 mm amplitude and 1 mm/s velocity. Typically, the coefficient of friction starts at a high value (the breakaway value), it drops and remains stable thereafter until the cumulative travel of about 10 m and subsequently increases. For example, at temperature of 20°C and apparent pressure of 20.7 MPa the friction is stable at 0.015 up to a travel of 10 m and it gradually increases to 0.025 at the travel of 15 m. Moreover, at temperature of -10°C the friction is nearly stable at 0.030 up to a travel of 5 m, rapidly increasing thereafter to a value of 0.072 at the travel of 25 m. These are disappointingly large increases over very short travel. Moreover, the results are in contradiction with the results of Long (1969, 1974) and the results of German origin as reported by Kauschke and Baigent (1986). Clearly, there is a need for further study of the effects of cumulative movement.

In an attempt to provide further information on the effect of cumulative movement we conducted testing of two interfaces, one of unfilled PTFE and the other of PTFE composite, up to travel of 500 m. The testing was conducted with the arrangement of Figure 4-1 and utilizing periodic constant velocity motion of 6.4 mm amplitude and velocity of either 0.8 or 2.4 mm/s. This range of velocities is consistent with the conditions of testing in earlier studies (about 2.0 to 2.5 mm/s in the German tests and in Long, 1969, and 1 mm/s in Campbell et al., 1991). Furthermore, it is consistent with field observations (Muller-Rochholz et al., 1986a, 1986b) and calculations.

At this point it is of interest to present a sample of such calculations. Bearing movement is primarily caused by traffic and secondarily by temperature changes. Extreme temperature changes are too rare to be of any significance in the calculation of cumulative movement. Rather, a more representative temperature change for such calculation is the difference between the average high and the average low temperatures over a specific period of time and a particular location. Utilizing widely available data for the United States (e.g., we utilized the USA Today Weather internet site, www.usatoday.com/weather), the difference between the monthly average high and

average low for most locations is approximately 20°F. It is reasonable to consider this value to be, on the average, the temperature change within a day. Considering steel girder bridges and a representative span of 100 feet (30.5 m), the cumulative movement in 30 years of service is about 90 m. This travel is insignificant by comparison to the one induced by traffic.

Estimating the bearing movement caused by traffic is difficult. However, for certain types of bridges one can easily obtain a reasonable estimate of the movement. Steel girder (I-beam) bridges are typically designed to have a beam depth, d , to span length, L , ratio of about 1/30 (here the span length is considered to be the distance between the inflection points under dead load). Moreover, the beams are designed to have a maximum deflection, Δ , under live load (including lateral distribution and impact) of about 1/1,000 of the span length (Xanthakos, 1994). To obtain the average bearing movement we exclude the lateral distribution and impact effect and approximately arrive at a value $\Delta/L = 1/1,500$. The relation between maximum support rotation, θ , and maximum deflection is $\theta = \alpha \Delta / L$ where α is approximately 3.0 for single span girders and less for continuous multi-span girders (for example, a two span equal length girder loaded in one span has an α of approximately 2.5). Moreover, the bearing movement has amplitude $u = \theta d/2$ (the amplitude will be approximately $0.75\theta d$ for composite girders).

A conservative estimate of the average bearing amplitude of movement in a single crossing is obtained when using $\alpha = 3.0$:

$$u = \frac{L}{30,000} \quad (4-2)$$

The cumulative movement u_T is

$$u_T = \left(\frac{L}{15,000} \right) \times C \times H \quad (4-3)$$

where C = number of crossings per hour and H = total number of hours. Furthermore, an estimate of the velocity of movement v can be obtained by considering that the time to traverse the span length L is L/v_T where v_T is the average speed of traffic. Accordingly,

$$v = \frac{v_T}{15,000} \quad (4-4)$$

Considering a typical span length of 100 feet (30.5 m) and an average speed of traffic of 60 km/h, we calculate $u \sim 1\text{mm}$ and $v \sim 1\text{mm/s}$. To estimate the cumulative movement we consider 30 years of service and 10 crossings per hour (these are crossings of the full traffic load) to obtain $u_T = 5.3\text{ km}$. This estimate depends largely on the assumed number of crossings per hour. Moreover, portion of this movement may be consumed as deformation of the bearing itself (rather than just sliding). Nevertheless, the conclusion is

that on the average the velocity of movement is of the order of 1 mm/s and the cumulative movement is large and of the order of several kilometers.

Testing for the effects of cumulative movement on friction was conducted with periodic constant velocity motion of 0.8 mm/s for a travel of about 260 m, followed by a motion at velocity of 2.4 mm/s for an additional travel of about 240 m. That is, the velocity is consistent with the expected average conditions in steel girder bridges, however, the cumulative movement is representative of about 3 years of service for such bridges. Testing of the PTFE composite was conducted first. The apparent bearing pressure was 69 MPa.

Figure 4-19 presents the results. These results were obtained as follows. The periodic constant velocity motion was interrupted and without unloading of the specimens:

- (a) Three cycles of periodic constant velocity motion of 0.8 mm/s were imposed and measurements of the sliding friction were made. This test was conducted in intervals following travel of between 5 and 25 m. The measured values of friction are shown in the figure with square symbols. Each of these tests was conducted immediately following the interruption of motion so that the sliding interface was at a temperature higher than the starting temperature of 24°C. Measurements of the temperature by the thermocouple embedded in the steel plate gave values of about 28°C.
- (b) A high velocity test was conducted at intervals following travel of 25 m. The test consisted of a displacement history as shown in Figure 4-11 with $u_0 = 12.7$ mm and frequency of 2 Hz. The test allowed for the measurement of the very low velocity sliding friction f_{min} and the sliding friction at velocity of 160 mm/s (as described in section 4.4). The measured values of friction are shown in the figure with circular and triangular symbols. Some of these tests were conducted after some idle time so that the temperature at the sliding interface, as monitored by the embedded thermocouple, was at about 24°C (dark symbols), whereas the rest were conducted without idle time so that the temperature at the start of each experiment was higher, typically about 28°C.

During testing and following a cumulative movement of about 125 m, it was detected that part of the normal load as applied by the hydraulic ram (see Fig. 4-1) was not directly transferred to the specimen. The cyclic motion was interrupted and without unloading of the specimen, the connection to the reaction frame was released (see Fig. 4-1). It resulted in a drop in the load measured by the load cell of the hydraulic ram by 15-percent (from 146.7 kN to 124.7 kN). Accordingly, the measured values of friction up to the cumulative movement of 125 m are about 83-percent of the actual values. That is, the starting value of the high velocity friction is not at 0.064, as shown in Figure 4-19, but rather should be at about 0.075. The problem was corrected by increasing the normal load to the appropriate value, connecting the loading plate to the reaction frame and restarting the experiment.

COMPOSITE No. 1 (PRESSURE = 69 MPa)

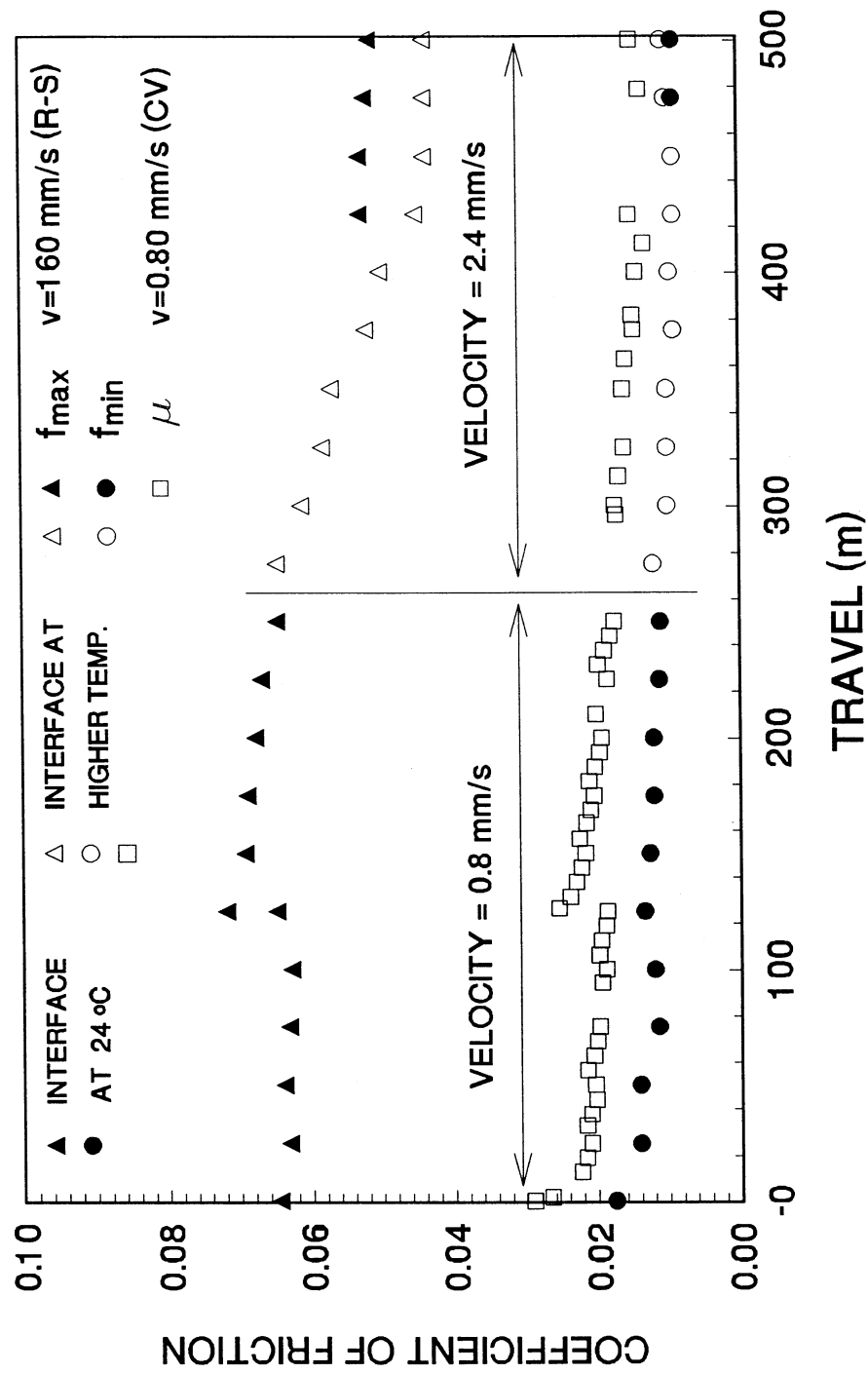


FIGURE 4-19 Effect of Cumulative Movement (Travel) on Sliding Coefficient of Friction of PTFE Composite in Contact with Polished Stainless Steel

The data, following correction for the aforementioned problem with the normal load path, demonstrate that the coefficient of sliding friction at very low velocity and at some representative high velocity reduce with increasing cumulative movement and appear stable after a 500 m travel. Specifically, the high velocity value (f_{\max}) starts at about 0.075 and stabilizes at about 0.052, that is, the reduction is about 30-percent.

A similar test was conducted on unfilled PTFE specimens at apparent pressure of 20.7 MPa. The results are presented in Figure 4-20. In this case, measurements of the sliding friction were obtained for a range of very low velocities and again at velocity of 160 mm/s. Moreover, all of the results were obtained at a temperature of about 24°C at the start of each experiment (that is, sufficient idle time was allowed until the embedded thermocouple recorded a temperature of about 24°C). Also, Figure 4-21 presents three recorded loops of normalized friction force versus displacement in the high velocity tests (per Fig. 4-11 and frequency of 2 Hz) following travel of 0.5, 254 and 510 m.

The results of Figure 4-20 demonstrate that the coefficient of sliding friction, in general, reduces with increasing travel and that after a travel of about 300 m it shows a mild tendency for increase. Moreover, we observe that the low velocity sliding friction exhibits fluctuations in the travel range of 0 to 40 m. That is, whereas the high velocity friction starts from a high value of 0.125 and within 40 m of travel it drops to a value of 0.100 (interestingly, this value is also attained after a travel of 510 m), the low velocity friction shows a sharp increase within a travel of about 15 m. Very interestingly, this is consistent with the results of Campbell et al. (1991).

Summarizing, available data on the low velocity friction of unfilled PTFE in contact with stainless steel are either of German origin and show a mild increase over a travel of 2 km or are of British origin (Long, 1969) and show a reduction over a travel of 5 km. It is likely that the difference is due to differences in the roughness and composition of the used stainless steel plates. Test results reported herein for unfilled PTFE and a PTFE composite material demonstrate a general reduction of both the high velocity and the low velocity sliding friction with increasing travel up to about 0.5 km.

It is likely that the high velocity friction increases beyond the starting value after about 1 to 2 km of cumulative movement. If we accept that the trend for the high velocity friction is the same as that of the low velocity friction (and this appears to be the case for unfilled PTFE see Fig. 4-20), we should expect about a 20-percent increase of the high velocity friction after about 2 km travel. This is based on the results of German origin (Kauschke and Baigent, 1986).

Certain phenomena were observed during testing which are interesting to report. In the testing of unfilled PTFE it was observed that, following a travel of 0.5 km, the PTFE surface contained very small dark particles, which could be removed by scratching of the surface. It is believed that they were either fine steel particles removed from the steel surface by rubbing or residuals of the abrasive used in polishing of the plate, or both. It is likely that these particles increase in density with increasing travel and eventually cause an increase in friction. If so, the problem could be lessened by the use of a high strength

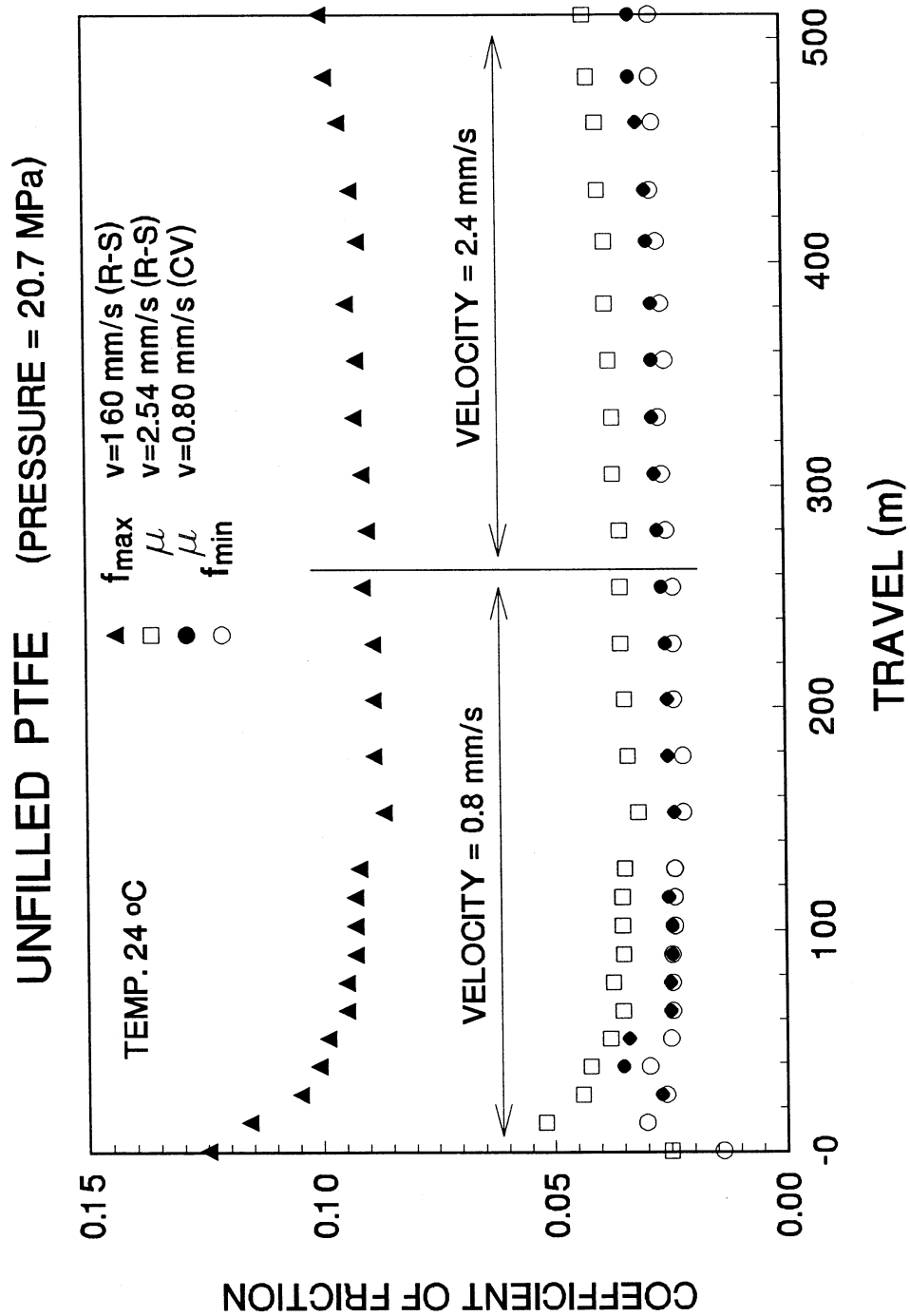


FIGURE 4-20 Effect of Cumulative Movement (Travel) on Sliding Coefficient of Friction of Unfilled PTFE in Contact with Polished Stainless Steel

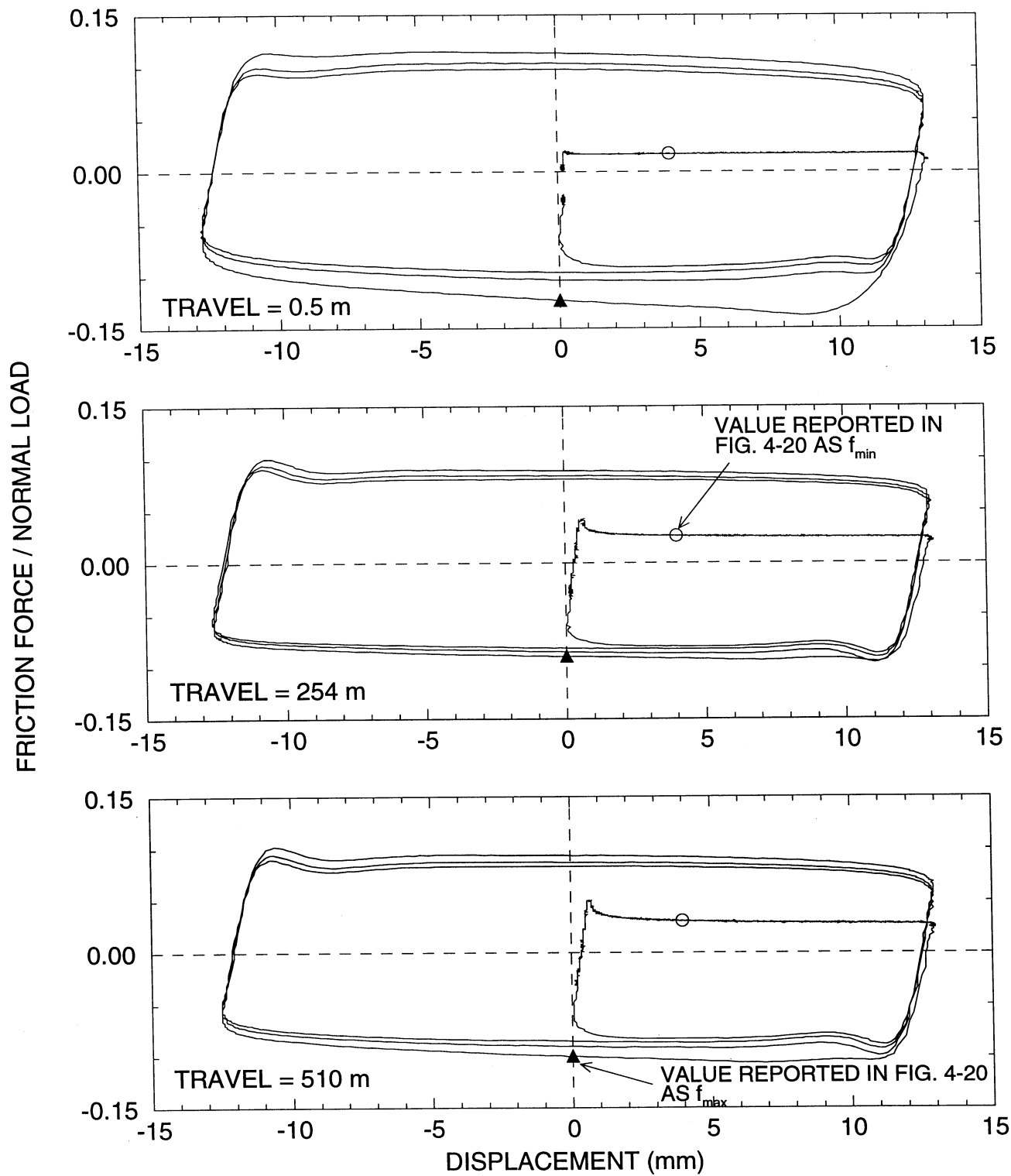


FIGURE 4-21 Recorded Loops of Friction Force/Normal Load vs Displacement of Unfilled PTFE-Polished Stainless Steel Interfaces Following Travel of 0.5 m to 510 m. Testing Conducted with Motion of Fig. 4-11 and Frequency of 2 Hz

and high degree of polish stainless steel which is also cleaned to removed all residuals of abrasives. Could this be the reason for the differences in the trends observed in the British and the German tests?

This phenomenon could not be observed in the testing of the PTFE composite because of its dark color. However, in this case observations on wear of the composite were made. The material was very thin, with a thickness of 0.25 mm. Figure 4-22 shows views of the material prior to and after testing. The disc on the right shows the material prior to testing. The one in the middle was tested extensively in high amplitude motion but the cumulative movement was only a few meters. It may be observed that the material is evenly distributed over the surface (flakes of material from the edges have been removed prior to taking the photograph). The disc on the left shows the material following a travel of 500 m (again flakes from the edges have been removed). It is interesting to note that the material exhibits uneven distribution. This was caused by transport of particles of the material and subsequent re-integration into the matrix of the composite during the low amplitude movement in the long travel testing. It appears that this mechanism is fundamental for this material (and likely also for woven PTFE) in reducing wear in small amplitude motion.

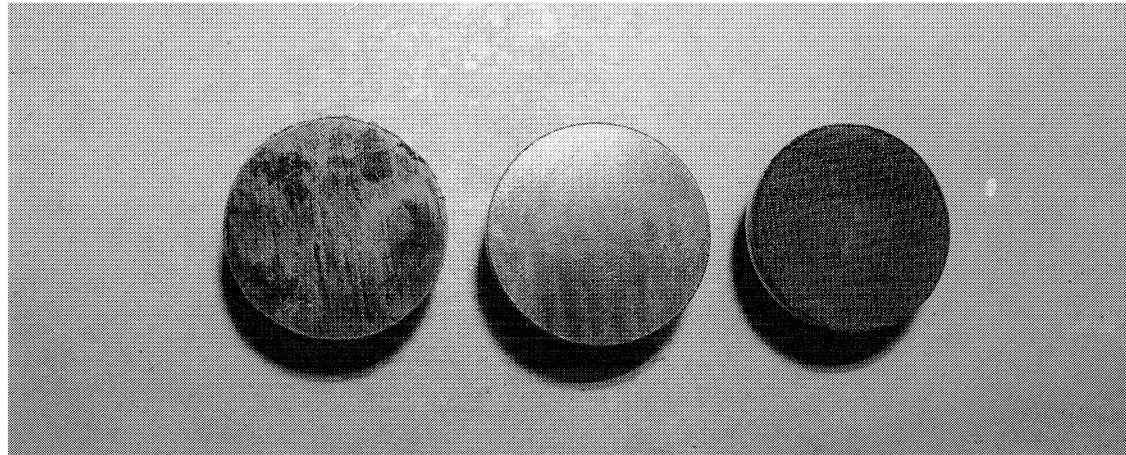


FIGURE 4-22 Views of PTFE Composite Material Following Travel of 500 m (left), Following Short Travel and High Amplitude Motion (center) and Prior to Testing (right)

4.6 Effect of Surface Roughness of Stainless Steel

The surface roughness of the stainless steel has an effect on friction. We have already mentioned of this effect as a likely contributor to the differences in the results obtained in Germany (reported by Kauschke and Baigent, 1986) and in England (Long, 1969; 1974). Moreover, Taylor (1972) documented the effect of surface roughness on the very low velocity friction in tests conducted on unfilled PTFE in contact with stainless steel at apparent pressure of 35 MPa, velocity of 0.02 mm/s and temperature of 20°C. He reported differences of the order of three to five times between the friction obtained with standard finish and with mirror finish stainless steel. The results of Long (1969) and Taylor (1972) are likely the reason for the near exclusive use today of mirror finish stainless steel in PTFE sliding bearings.

Despite that mirror finish stainless steel (surface roughness of about 0.03 μm arithmetic average) is almost exclusively used today, results on the effect of roughness of friction (and particularly the high velocity friction) are of interest if we assume that the effects of corrosion are equivalent to those of roughness. We will address the subject of corrosion of stainless steel in section 4.7. Herein we will assume that the stainless steel may suffer corrosion to a degree that depends on time and the severity of the environment. We will further assume that the corrosion is uniform on the surface of the stainless steel. Accordingly, we may relate corrosion to surface roughness, and thus assume that corrosion is equivalent to an increase in the surface roughness.

We have conducted testing of unfilled PTFE and the PTFE composite in contact with stainless steel (ASTM 240, type 304) having surface roughness of 0.03, 0.30 and 0.50 μm R_a . The lowest roughness is that in the lay direction of a sheet commercially polished to mirror finish (or No. 8). The middle roughness is that of an as-rolled sheet of stainless steel. The maximum roughness was created on the as-rolled sheet by further uniform roughening utilizing a wire brush.

Testing was conducted using the motions shown in Figure 4-11. Load dwell prior to imposing the motion was generally less than one hour, whereas the temperature at the start of each experiment was about 24°C. Apparent pressures in the two cases were 69 MPa and 20.7 MPa, respectively.

Figures 4-23 and 4-24 present the results on the coefficient of sliding friction as measured at the first instant at which the indicated velocity was reached (that is, after a travel equal to the amplitude of the imposed motion as demonstrated in Fig. 4-12). For each of the three cases of roughness, a new specimen of unfilled PTFE was used. However, the same specimen of PTFE composite was used in all of the conducted tests. Most of the tests were conducted without unloading the specimen and cleaning of the interface. That is, in these tests the stainless steel was coated with PTFE from the previous test. However, selected tests (particularly in the case of the highest roughness) were repeated with prior cleaning of the interface. The test data for these cases are shown in the figures with dark symbols, whereas the rest of the data are shown with open symbols.

The results in Figures 4-23 and 4-24 demonstrate an increase of the sliding friction with increasing roughness. The increase is substantial at very low velocity of sliding and is, in general, consistent with the observations of Taylor (1972). This increase is likely caused by:

- (a) The introduction of a component of friction due to plowing of the PTFE by the rough stainless steel, and
- (b) The effects of increased number of wear particles trapped between the sliding surfaces.

Of interest is to note in Figures 4-23 and 4-24 that the effect of surface roughness on the sliding friction reduces with increasing velocity of sliding. This phenomenon is particularly pronounced for unfilled PTFE, for which the high velocity sliding friction (f_{max}) is nearly unaffected by the roughness. An explanation for this phenomenon is related to the effect of third body particles (wear debris) which dominate friction at high velocities of sliding. The effect of third body particles is limited, hence friction attains a constant value beyond some large velocity (except for the effect of frictional heating). High roughness results in the generation of more wear particles, of which, however, the effects are minor at large sliding velocities.

As seen in Figure 4-24 the effect of surface roughness on the sliding friction of the PTFE composite is more than that of unfilled PTFE in the high velocity range. The data have been carefully examined to identify likely contributors to this effect. For example, it was observed that the tests were conducted over a period in which the relative humidity in the laboratory was either at about 20-percent or at about 45-percent. However, even when some of the data were ignored still the effects of roughness remained at the level depicted in Figure 4-24. It is likely that the third body particle effects for this interface are not as important as for the unfilled PTFE due to the woven nature of the material (significant part of the wear debris is re-integrated in the matrix of the material). Accordingly, some other mechanism (likely plowing) may be responsible for this phenomenon.

4.7 Corrosion of Stainless Steel

Stainless steels are alloys containing iron, at least 10-percent chromium and some ten to fifteen other elements that can provide a range of corrosion resistance. There are five major families of stainless steels: Ferritic, Austenitic, Martensitic, Precipitation-Hardening and Duplex. Of these, austenitic stainless steels of the AISI (American Iron and Steel Institute) types 304 and 316 are used in sliding bearings (Davison et al., 1987).

The mechanism of corrosion protection of stainless steel differs from that of most metals, including that of carbon steel. Unlike other metals, stainless steels do not form a layer of true oxide. Rather, they form a passive film, which is likely a film of continuous, nonporous, self-healing hydrated oxide. When this film is maintained, the stainless steels exhibit outstanding corrosion resistance. This film forms immediately in the presence of oxygen.

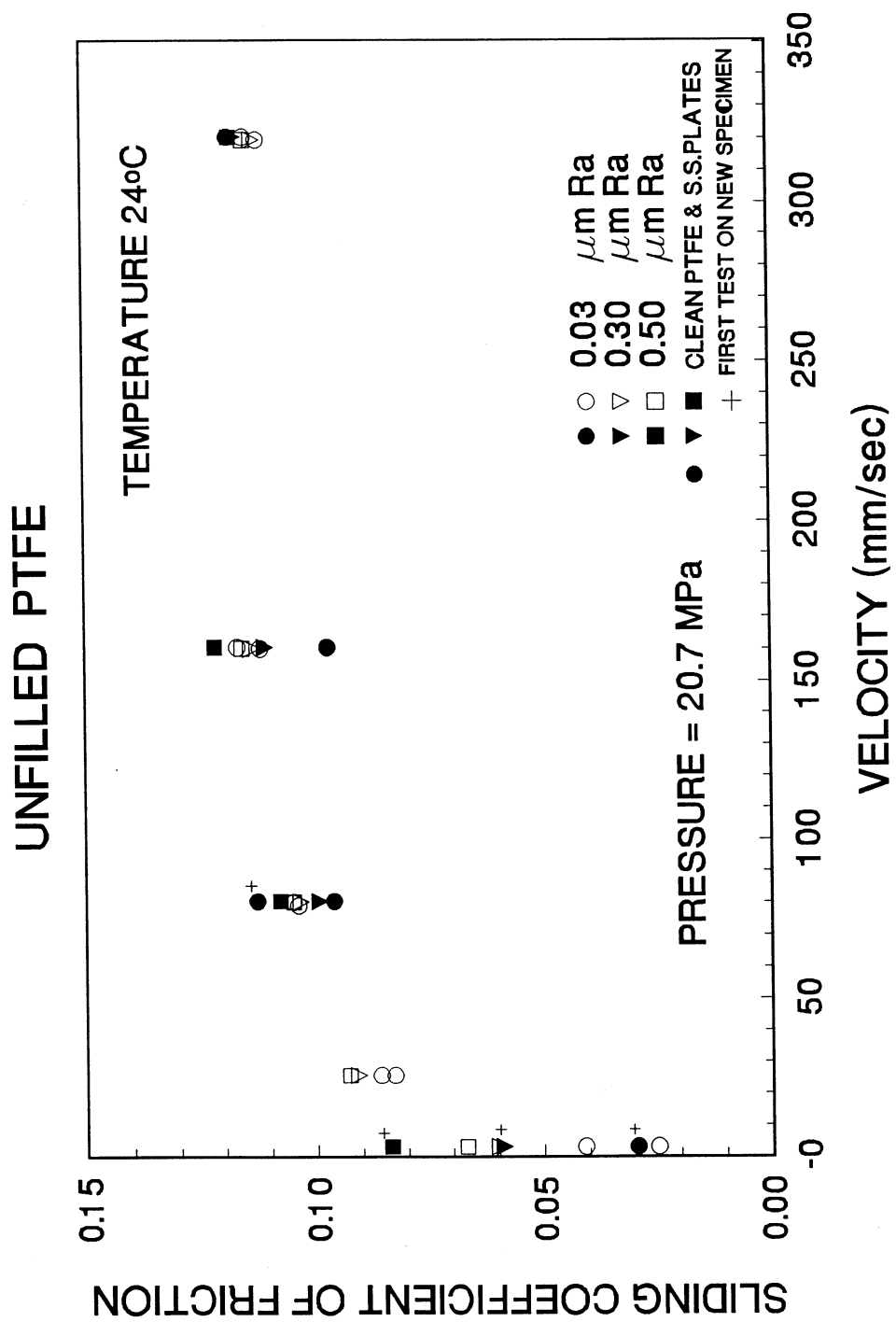


FIGURE 4-23 Effect of Surface Roughness of Stainless Steel on the Sliding Friction of Unfilled PTFE

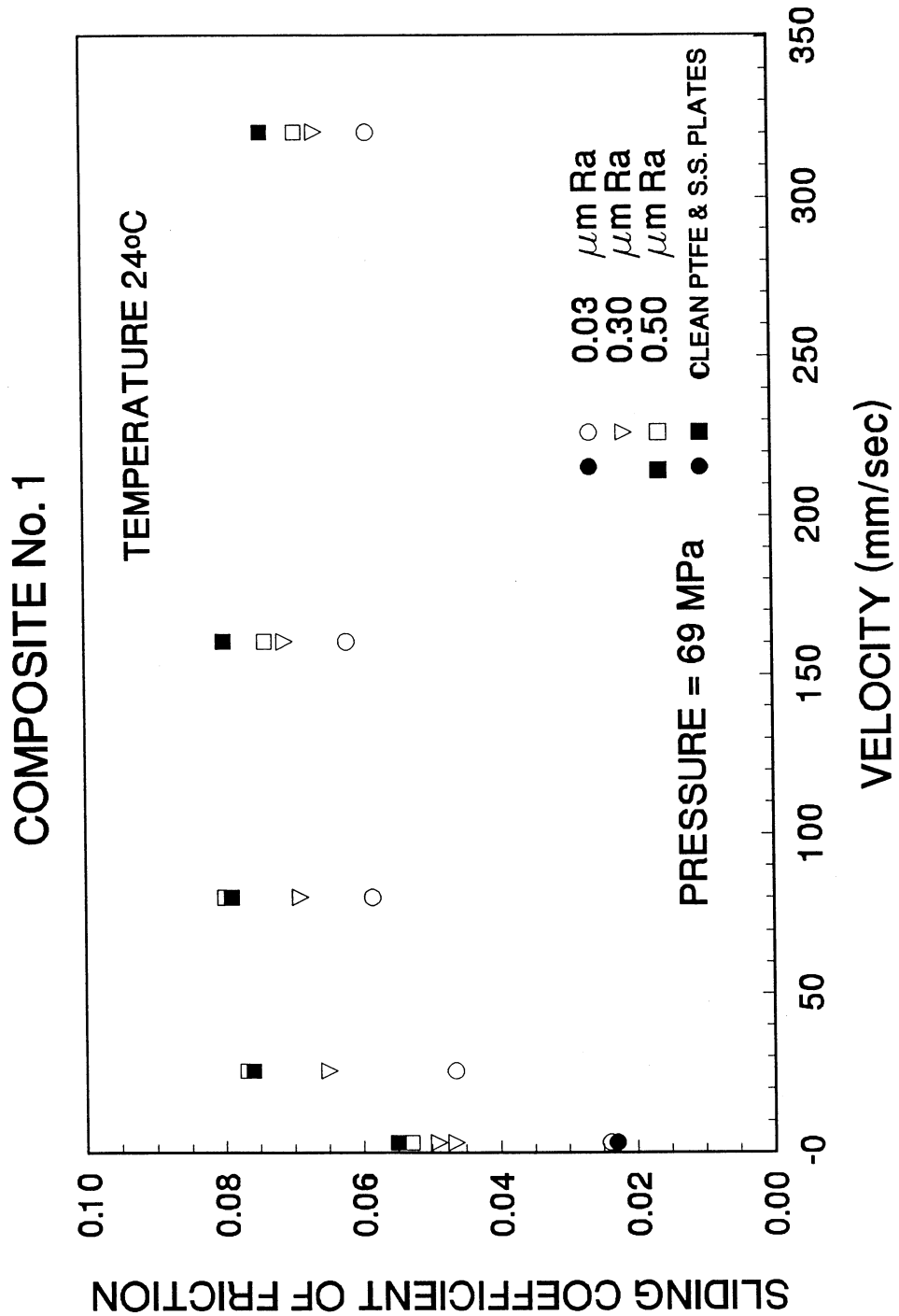


FIGURE 4-24 Effect of Surface Roughness of Stainless Steel on the Sliding Friction of PTFE Composite

The basic elements of stainless steels that are important for corrosion resistance are chromium for forming the passive film and molybdenum, which in combination with chromium is effective in stabilizing the passive film in the presence of chlorides. Moreover, carbon is detrimental to corrosion resistance through its reaction with chromium.

AISI type 304 austenitic stainless steel is the most commonly used stainless steel because of its high ductility, ease in fabrication, availability and good corrosion resistance. However, type 316 which contains molybdenum and particularly type 316L with low carbon content have superior corrosion resistance and should be utilized in sliding bearings in environments in which chlorides abide.

The corrosion of stainless steel may take various forms (Davison et al., 1987). However, the most common one is pitting which is associated with local discontinuity of the passive film. Typically, chloride is the responsible agent for initiation of pitting. On the other hand, uniform corrosion of a stainless steel is very rare and, typically, such an occurrence indicates error in the stainless steel selection.

Data on the corrosion resistance of stainless steels are presented in Davison et al. (1987). However, the most comprehensive collection of data that are of interest in sliding bearings may be found in International Nickel Company (1970). This collection of data is specifically for austenitic stainless steels in atmospheric environments. The data are typically in the form of qualitative statements on the appearance of stainless steels following lengthy exposure in known environments. Table 4-4 presents information from International Nickel Company (1970) for types 304 and 316 austenitic stainless steels.

The information in Table 4-4 reveals that:

- (a) Corrosion of stainless steel in atmospheric environments is possible. However, it is typically in the form of light rust stains over small part of the surface.
- (b) Type 316 stainless steel has significantly better corrosion resistance than type 304 in all environments.
- (c) Industrial-chemical environments may cause unacceptable corrosion to type 304 stainless steel due, apparently, to the existence of chlorides.

Of interest is to note in Table 4-4 the case of specimens exposed to industrial environment under sheltered and unsheltered conditions. The sheltered specimens were kept under roof so that rain could not wash away deposits that accumulated over the 12 years of observation of the specimens. The unsheltered specimens were boldly exposed so that rain regularly removed deposits. These specimens remained un-attacked, whereas the sheltered ones experienced corrosion. The reason for this significant difference is that, for the covered specimen, the accumulated deposits depleted the stainless steel of oxygen and prevented the restoration of the passive film.

TABLE 4-4 Information on Performance of Austenitic Stainless Steels in Various Atmospheric Environments

Location	Environment	Duration (Years)	Condition	
			Type 304	Type 316
New York City	Industrial-Urban	26	No rust stains	-
		23	-	No rust stains
Niagara Falls, NY	Industrial-Chemical	6	Covered with rust, pitted	Slight rust spots, slightly pitted
Panama Canal	Tropical	8	-	No rust, no pitting
Bayonne, NJ	Industrial* (sheltered)	12	Pitted to depth of 0.18 mm	Pitted to depth of less than 0.025 mm
Bayonne, NJ	Industrial* (not sheltered)	12	No rust, no pitting	No rust, no pitting
Kure Beach, NC	Marine	15	Spotted with slight rust stain over 15% of surface	Extremely light rust stain over 15% of surface

*Likely chemical environment

This observation raises a concern on whether sliding bearings should be sealed for preventing contamination. The authors strongly believe that bearings should be sealed for the following reasons: (a) to prevent contamination (note that heavy contamination depletes the stainless steel of oxygen) and, (b) to prevent exposure of the surface to de-icing salts (chlorides). Moreover, the stainless steel surface should be facing downwards to prevent contamination from within the bearing (e.g., from falling rust debris from the carbon steel parts of the bearings). Therefore, the ideal situation for sliding bearings for the prevention of corrosion over prolonged time intervals is the use of type 316 stainless steel (preferably 316L) in a configuration with the stainless steel facing down and with a seal that prevents contamination but allows flow of air. The flow of air is important both for the supply of oxygen to the stainless steel and for the prevention of moisture condensation which promotes corrosion of the carbon steel parts of the bearing.

The superiority of type 316 stainless steel is documented in a number of other environments. Particularly, Romanoff (1957) documents extensive data on the underground corrosion of some 37,000 specimens for exposures of up to 18 years. While not directly relevant to sliding bearings, the data are highly informative. Specifically, type 304 and 316 stainless steels exposed for 14 years in soil containing 2-percent sodium chloride exhibited significantly different corrosion—the type 316 remained un-attacked, whereas the type 304 developed significant pitting.

Despite the wealth of information on the corrosion of stainless steels, there is lack of data to relate corrosion to friction and particularly the high velocity friction. In order to

provide some quantitative information on this problem we have to relate the information on the appearance of stainless steel to some relevant quantity, such as surface roughness. When this is accomplished, data such as those of Figures 4-23 and 4-24 may be utilized in assessing the effect of corrosion on friction.

The authors were able to obtain some information from observations made on sliding bearings they have tested. The bearings were faced with type 304 austenitic stainless steel that was welded on a carbon steel plate. The bearings were extensively tested over a period of 9 years and were stored disassembled in the laboratory. One of these bearings (total of four) exhibited light rust stains over the perimeter of the stainless steel sheet for a distance of about 20 mm from the edge. The rust stains covered an area of about 15-percent of the stainless steel surface. It is likely that the observed corrosion was the result of contamination of the perimeter of the stainless steel plate by iron particles due to grinding performed on the carbon steel plate. Nevertheless, the area with light rust stains appeared to touch as having a rougher surface. Measurements of surface roughness gave a value of about $0.30 \mu\text{m}$ on the arithmetic average. The rest of the surface, as well the entire surface of the other three bearings, was rust free and had a measured surface roughness of about $0.03 \mu\text{m}$ arithmetic average after 9 years of exposure.

We have made the assumption that a surface roughness of $0.3 \mu\text{m}$ arithmetic average is representative of the surface condition of type 304 stainless steel after 30 years of exposure in atmospheric industrial/urban (but not chemical) environment under conditions that prevent contamination and direct exposure to salts. Note that the assumption may be very conservative because (a) actual observations for 26 years exposure in such an environment (see Table 4-4) report no rust stains, and (b) even when rust stains develop, they are over a small portion of the surface and do not represent uniform corrosion as we have assumed.

Moreover, entirely arbitrarily we assume that a surface roughness of $0.5 \mu\text{m}$ arithmetic average is representative of the condition of type 304 stainless steel under the condition described above except that the environment is industrial/chemical.

Based on these assumptions, Table 4-5 has been prepared. It presents assumed values of the surface roughness of type 304 stainless steel for various environmental conditions and methods of installation of the stainless steel plate. Of these values only the value of $0.3 \mu\text{m}$ (underlined in the table) is supported by actual measurements. The values in the table may be very conservative. However, they represent a starting point for assessing the effects of corrosion on friction. Moreover, they reflect the effects of environmental conditions and methods of installation, as they are understood from the study of the mechanisms of corrosion of stainless steel.

Based now on the proposition in Table 4-5 and the friction values in Figures 4-23 and 4-24, Table 4-6 has been prepared. It presents suggested factors for increasing the high velocity friction (f_{\max}) of unlubricated unfilled PTFE and PTFE composites in contact with type 304 austenitic stainless steel after 30 years of exposure in various environments. In arriving at these factors, use was made of the data in Figures 4-23 and

4-24 at velocities of about 75 mm/s. The factor should be less (closer to unity) at velocities exceeding 75 mm/s.

TABLE 4-5 Suggested Surface Roughness Values (in μm arithmetic average) of Type 304 Austenitic Stainless Steel (originally polished to roughness of 0.03 μm arithmetic average) After 30 Years of Exposure Within Unlubricated Sliding Bearings

Environment	Installation Method of Stainless Steel Plate in Sliding Bearing			
	Sealed Facing Down	Sealed Facing Up	Unsealed Facing Down	Unsealed Facing Up
Rural	0.10	0.30	0.30	Unacceptable* Installation
Industrial/ Urban	<u>0.30</u>	0.40	0.40	Unacceptable Installation
Marine	0.40	0.50	0.50	Unacceptable Installation
Industrial/ Chemical	0.50	>0.50	>0.50	Unacceptable Installation

*Installation method is unacceptable due to potential for significant contamination.

Austenitic type 316 stainless steel exhibits corrosion resistance far superior than that of type 304 stainless steel. Accordingly, factors for adjusting the friction for the effects of corrosion should be less than those in Table 4-6. As a starting point we may assume values that are the average of what is in Table 4-6 and unity (e.g., factor of 1.20 for type 304 and factor of 1.10 for type 316).

TABLE 4-6 Proposed Factors for Increasing the High Velocity Sliding Coefficient of Friction (f_{\max}) of Unlubricated Unfilled PTFE and PTFE Composites in Contact with Type 304 Austenitic Stainless Steel After 30 Years of Exposure in Various Environments

Environment	Installation Method of Stainless Steel Plate in Sliding Bearing		
	Sealed Facing Down	Sealed Facing Up	Unsealed Facing Down
Rural	1.10	<u>1.20</u>	<u>1.20</u>
Industrial/ Urban	<u>1.20</u>	1.30	1.30
Marine	1.30	<u>1.40</u>	<u>1.40</u>
Industrial/ Chemical	1.40	>1.40	>1.40

Underlined values are based on actually measured values of friction at velocity of 75 mm/s. The factor is less (closer to unity) at velocities exceeding 75 mm/s.

4.8 Effect of Contamination

The contamination of the sliding interface is known to cause an increase in friction. A number of experimental studies have documented this phenomenon, which is apparently caused by the introduction of an additional component of friction due to third body effects (see section 3.3) and due to abrasion of the stainless steel.

Long (1969) reported satisfactory performance of unfilled PTFE bearings following deliberate contamination of the PTFE with dust. Neither the satisfactory performance nor the amount of contamination are quantified, other than that the bearing was subjected to cumulative travel of about 5.7 km. Likely the contamination was light and of very small particle size so that it was absorbed by the soft PTFE. Of interest is that Long (1969) reports that it was impossible to contaminate the sliding interface while the bearing was under load and it was necessary to disassemble the bearing and introduce the contamination. Moreover, Long (1969) reported on a substantial increase in the static (breakaway) coefficient of friction (approximately 6-fold, from 0.017 to 0.100) when heavy contamination with dry cement dust was introduced.

Jacobsen (1977) reported similar results. Tests were conducted on unfilled PTFE-stainless steel interfaces (the type of stainless steel and its surface condition were not reported) at an apparent pressure of 6.5 MPa and slow constant velocity motion (4 mm/s) to obtain a static (breakaway) value of friction of 0.05 and a sliding value of 0.06 after about 950 m of travel. The same specimen was contaminated at the interface with sand particles (the amount is not given) and tested at an apparent pressure of 4.3 MPa. The static friction was measured at 0.27 and the sliding value at 0.14 after about 870 m of travel. In another test on unfilled PTFE at an apparent pressure of 4.1 MPa, the static friction of the uncontaminated interface was 0.08 whereas the one of the contaminated one with sand particles was 0.29.

Moreover, Jacobsen (1977) reported test results on woven PTFE in contact with bronze. At an apparent pressure of 13.8 MPa, the static friction was at 0.065 for the uncontaminated specimen and at 0.125 for the contaminated one (sand particles). However, with repeated sliding the value of the sliding friction reduced to the value of the uncontaminated specimen after about 130 m of travel. Apparently, the sand particles worked their way between the woven fibers and, thus, their effect was lessened.

Tyler (1977) conducted testing on contaminated and uncontaminated lubricated, dimpled PTFE-stainless steel interfaces at large velocity of sliding (375 mm/s). The contamination was in the form of cement dust, the amount of which was not reported. Substantial increases in the sliding friction were recorded, which were about 10 to 15-fold.

Lastly, Campbell and Fatemi (1989) and Campbell et al. (1993) reported on the results of a systematic study of the effect of contamination on the friction of lubricated, dimpled PTFE bearings. Tests were conducted at apparent pressure of 30 MPa, following load dwells of 12 hrs and by imposing motion at velocity of 1 mm/s. Contamination in the

form of cement dust was introduced at various degrees of concentration (reported in weight of contaminant per unit area of interface) and results were obtained on the initial (static or breakaway) friction and the sliding friction for 200 cycles of movement. Substantial increases in friction were recorded for heavy contamination. For example, increases in the initial (breakaway) friction of about 15 times were recorded with contamination of 0.239 mg/mm^2 (for the tested 75 mm diameter specimen, this amounts to about 1 gram of cement dust).

Moreover, Campbell and Fatemi (1989) conducted tests with a contaminated stainless steel surface over the portion not in contact with PTFE, as the actual situation may be in the field. In these tests, the tested bearings were subjected to eccentric loading in order to enhance infiltration of the contaminant. Moreover, the contaminant was continuously replenished on the stainless steel surface during testing. These tests demonstrated little, if any, infiltration of the sliding interface by the contaminant. Accordingly, friction was practically unaffected.

It is clear that contamination, when artificially introduced in the sliding interface, has significant effects on friction. While for unlubricated bearings this effect has been measured at very slow sliding velocities or under conditions of breakaway, it is likely that large increases in friction will also occur at large velocities of sliding. Intuitively, we expect the increase in the high velocity sliding friction of contaminated unlubricated PTFE-stainless steel interfaces to be less than the corresponding increase in the low velocity sliding friction. The reason is that the significance of the third body contribution to friction (see section 3.3) from contaminants is somewhat less at high velocities due to the large third body contribution to friction from the agglomerates of PTFE debris. Nevertheless, the increase is expected to be more than any of the previously described other effects, such as wear, temperature, corrosion, etc.

Contamination of the sliding interface is possible when bearings are disassembled at the construction site. It is, thus, a problem that can be prevented by exercising quality control at the construction site. Simply, sliding bearings should be delivered assembled, lightly pre-compressed and locked by side plates.

The results of Campbell and Fatemi (1989), Campbell et al. (1993) and previously by Long (1969) demonstrate that contamination of the sliding interface of sliding bearings in service is unlikely, even in the presence of significant load eccentricity. Nevertheless it would be prudent to assume some small increase in friction due to in-service contamination that depends on the method of installation of the stainless steel surface. For example, if the stainless steel surface is installed facing up, it will likely collect over the years some contamination on its surface, which may migrate within the sliding interface during movement of the bearing under the action of service loads.

4.9 Effect of Lubrication

Lubrication of the PTFE-stainless steel interface reduces the coefficient of friction. The lubricant, typically in the form of grease, is stored in dimples under hydrostatic pressure from where it is extruded to the sliding interface. Dimpling is important for prolonging the effective life of the lubricant (Campbell and Kong, 1987). Dimples cover approximately 30-percent of the apparent contact area. Grease consists of primarily oil or synthetic fluid (approximately 80-percent or more), a thickening agent (typically soap at approximately 10-percent) and additives (antioxidants, anticorrosion agents, etc. at less than 10-percent).

In unlubricated PTFE-stainless steel interfaces, the friction at low velocity of sliding is primarily the result of shearing at the junctions. Moreover, at high velocity of sliding significant contributions to the sliding friction are provided by third body effects (agglomerates of wear debris) and the viscoelastic deformation of PTFE (see section 3). For these interfaces it is also likely that the real area of contact (that is, the area of the junctions) is approximately equal to the apparent area of contact (see sections 3.6.1 and 3.6.3).

For dimpled, lubricated PTFE-stainless steel interfaces there is total separation of junctions by the lubricant over the area of the dimples (approximately 30-percent of the apparent area). For the rest of the area the conditions are not exactly known, but it is reasonable to assume that major part of the load is carried by junctions which are separated by a very thin film of lubricant. The result is substantial reduction in the friction. For a wide range of values of apparent pressure and velocity of sliding, the sliding coefficient of friction for highly polished stainless steel and for normal temperature is of the order of 0.02 or less.

Campbell and Kong (1989), Campbell and Fatemi (1989) and Campbell et al. (1993) reported on the results obtained in the testing of lubricated, dimpled PTFE-stainless steel interfaces for a variety of conditions of temperature (20° and -25° C), surface roughness of stainless steel (0.03 and $0.34 \mu\text{m} R_a$), apparent pressure (10 to 45 MPa) and velocity of sliding (up to 20 mm/s). Moreover, the effects of contamination have been studied as discussed herein in section 4.8. Selected results from these carefully conducted experiments are presented in Tables 4-7 and 4-8. A number of interesting observations can be made about the results of these tables:

- (a) Friction is velocity dependent. At normal temperature, fresh conditions (highly polished stainless steel) and large velocity of sliding, the coefficient of sliding friction in the first cycle of movement is of the order of 0.02 (see Table 4-7). The observed substantial increase of friction with velocity, which is by about a two-fold within the range of 1 to 20 mm/s velocity, is of unclear origin. A likely explanation is that the increase is caused by third body effects (PTFE wear particles).
- (b) The coefficient of friction reduces to a very low value following some movement. As seen in Table 4-8 for normal temperature conditions and highly

TABLE 4-7 Coefficient of Sliding Friction of Lubricated Unfilled PTFE-Stainless Steel Interfaces (data from Campbell and Kong, 1989). Values of Friction are for First Cycle of Movement

Apparent Pressure (MPa)	Temperature 20° C		Temperature -25° C		Surface Roughness of Stainless Steel (μm R _a)
	Friction at v=1 mm/s	Friction at v=20 mm/s	Friction at v=1 mm/s	Friction at v=20 mm/s	
10	0.0068	0.0172	0.0251	0.0526	0.03
15	0.0092	0.0258	0.0197	0.0673	
25	NA	0.0181	0.0420	0.0489	
30	NA	0.0175	0.0139	0.0505	
45	0.0079	0.0160	0.0340	0.0395	
10	0.0132	0.0530	0.0528	0.0770	0.34
15	0.0280	0.0381	0.0259	0.0559	
25	0.0118	0.0191	0.0307	0.0515	
30	0.0095	0.0218	0.0166	0.0467	
45	0.0125	0.0185	0.0225	0.0595	

TABLE 4-8 Coefficient of Sliding Friction of Lubricated Unfilled PTFE-Stainless Steel Interfaces after 50 Cycles of Movement (2 m of travel) and Velocity of 20 mm/s (from Campbell and Kong, 1989)

Apparent Pressure (MPa)	Surface Roughness of Stainless Steel (μm R _a)	Coefficient of Sliding Friction	
		Temp. 20° C	Temp. -25° C
10	0.03	0.0064	0.0290
15		0.0028	0.0223
25		0.0035	0.0230
30		0.0044	0.0238
45		0.0030	0.0163
10	0.34	0.0310	0.0434
15		0.0233	0.0365
25		0.0136	0.0370
30		0.0107	0.0212
45		0.0078	0.0209

polished stainless steel, the friction attains values of the order of 0.003 but it could be somewhat higher at velocities relevant to seismic motions. It may be assumed that such values would prevail under fresh bearing conditions and following some small cumulative movement as a result of thermal and traffic effects. It is apparent that this reduction of friction after some small movement is the result of the spreading of lubricant from the dimples to the stainless steel plate.

- (c) There is a substantial effect of low temperature and of increased stainless steel surface roughness on the coefficient of friction. From the data in Tables 4-7 and 4-8 at the highest tested velocity, there is an increase of the coefficient of sliding friction of the order of 1.5 to 8.0 for temperatures in the range of 20 to -25° C, and an increase of the order of 1.0 to 8.0 for roughness in the range of 0.03 to 0.34 $\mu\text{m R}_a$.

By contrast, the same temperature range of 20 to -25°C causes sliding friction to increase by a factor of only 1.7 in unlubricated specimens that were otherwise comparable, as shown in Figure 4-15. Also the effect of surface roughness on the coefficient of sliding friction is very small (by about a factor of 1.1) for the same range of roughness and velocities of motion (see Fig. 4-23). The substantially greater effect of temperature on the friction of lubricated than of the unlubricated PTFE bearings could be explained on the basis of frictional heating, which is much less in the lubricated bearings due to the very low friction. Moreover, the effect of the stainless steel surface roughness could be explained on the basis of a change in the lubrication regime, which for the rougher surface is one with a smaller number of contact areas separated by a lubrication film.

Despite the significant effects of low temperature and high roughness, the coefficient of sliding friction of lubricated PTFE bearings is low. As seen in Table 4-8 (following some small movement), the friction values are generally less than 0.04. This would have been a very good performance of lubricated bearings if it were possible to maintain the lubricant in its original condition. It is known that the lubricants used in PTFE bearings harden with time and that replenishing the lubricant is extremely difficult (Campbell and Kong, 1987; Kauschke and Baigent, 1986). As suggested by Kauschke and Baigent (1986) it should be realized that lubricated PTFE bearings have limited lifetime and that provisions should be made to replace the PTFE sheets with the lubricant when such need arises.

4.10 Summary

Available and newly generated data on the frictional properties of interfaces consisting of PTFE or PTFE-based composites in contact with stainless steel and of certain bimetallic interfaces have been presented and discussed in detail. Data on the effects of load dwell, apparent bearing pressure, velocity, temperature, cumulative movement (travel), roughness of stainless steel, corrosion of stainless steel, contamination and lubrication are presented.

It should be noted that the results presented are representative of the behavior of these interfaces, they demonstrate the effects of the aforementioned parameters and they provide first order data for use in research studies, preliminary designs and the development of specifications. They should not be viewed as definitive.

@Seismicisolation¹¹⁴

Telegram Channel: @Seismicisolation

SECTION 5

SYSTEM PROPERTY MODIFICATION FACTORS

5.1 Introduction

The properties of seismic isolation bearings vary due to the effects of wear, aging, temperature, history of loading, etc. The exact state of the bearings at the time of seismic excitation cannot be known. However, it is possible to establish maximum and minimum probable values of important properties (i.e., characteristic strength and post-yielding stiffness, see Fig. 2-1) within the lifetime of the structure. The analysis can then be conducted twice using the bounding values of properties. In general, the maximum force and displacement responses will be obtained in these analyses.

In principle, the probable maximum and minimum property values could be established on the basis of statistical analysis of the variability of the properties and the likelihood of occurrence of relevant events, including that of the considered seismic excitation. This is an admittedly difficult problem. However, it is relatively easier to assess the effect of a particular phenomenon on the properties of a selected type of bearing, either by testing (e.g., effect of temperature on friction coefficient in sliding bearings) or by a combination of testing, rational analysis and engineering judgement (e.g., effect of aging). This leads to the establishment of system property modification factors, that is, factors which quantify the effect of a particular phenomenon on the nominal properties of an isolation bearing, or system in general.

5.2 The Concept of System Property Modification Factor

Consider that a nominal value of a property of an isolation system is known. It could be that this value is assumed (on the basis of experience from previous testing) during the analysis and design phase of the project or it is determined in the prototype bearing testing. Typically, this nominal value applies for specific conditions, such as fresh bearing conditions, temperature of 20°C and the relevant conditions of vertical load, frequency or velocity and strain or displacement. Let this value be P_n .

The minimum and maximum values of this property, P_{\max} and P_{\min} respectively, are defined as the product of the nominal value and a series of System Property Modification Factors, or λ -factors as follows:

$$P_{\max} = \lambda_{\max} \cdot P_n \quad (5-1)$$

$$P_{\min} = \lambda_{\min} \cdot P_n \quad (5-2)$$

where

$$\lambda_{\max} = \lambda_{\max,1} \cdot \lambda_{\max,2} \cdot \lambda_{\max,3} \cdots \quad (5-3)$$

$$\lambda_{\min} = \lambda_{\min,1} \cdot \lambda_{\min,2} \cdot \lambda_{\min,3} \cdots \quad (5-4)$$

Each of the $\lambda_{\max,i}$, $i = 1, 2, \dots$ factors is larger than or equal to unity, whereas each of the $\lambda_{\min,i}$, $i = 1, 2, \dots$ is less than or equal to unity. Moreover, each of the λ -factors is associated with a different aspect of the isolation system, such as wear, contamination, aging, history of loading, temperature, etc.

As an example, consider the effect of temperature on the friction coefficient of a sliding bearing. The range of temperature over the lifetime of the structure is first established for the particular site or general geographic area of the project. This range need not be the one of the extreme (lowest and highest) temperatures. Rather, it could be a representative range determined by the responsible professional (more appropriately, this range could be included in the applicable specifications). Say this range of temperature is -10°C to 50°C . Testing is then performed at the two temperatures and the λ -factors are established as the ratio of the coefficient of friction at the tested temperature to the coefficient of friction at the reference temperature (say 20°C). Factor $\lambda_{\min,t}$ will be based on the data for the highest temperature (50°C), whereas $\lambda_{\max,t}$ will be based on the data for the lowest temperature (-10°C).

As another example, consider the effect of wear on the friction coefficient. On the basis of the geometric characteristics of the bridge (span, girder depth, etc.), average vehicle crossing rate and lifetime of the structure, the cumulative travel is determined (see section 4.4). Test data are then utilized to establish the λ -factors for wear (or travel). Typically, $\lambda_{\max,tr}$ is the ratio of the friction coefficient determined in high velocity testing following and prior to a test at the appropriate velocity ($\sim 1\text{mm/s}$) for a total movement equal to the calculated cumulative travel. The $\lambda_{\min,tr}$ is determined in a similar manner but for a total movement less than the calculated cumulative travel for which the coefficient of friction attains its least value (see section 4.4 for representative test data).

5.3 System Property Adjustment Factors

The system property modification factors are associated with different aspects of the isolation system and combined on the basis of (5-3) and (5-4). While each one of these factors describes the range of effect of a particular aspect, their multiplication results in a combined factor of which the value may be very conservative. That is, the probability that several events (such as lowest temperature, maximum travel, maximum corrosion, etc.) occur simultaneously with the design-basis earthquake is very small.

It is necessary that some adjustment of the system property modification factors be applied to reflect the desire degree of conservatism. This adjustment should be based on a statistical analysis of the property variations with time, the probability of occurrence of joint events and the significance of the structure. It is also desirable to apply this adjustment with the simplest possible procedure.

Such a procedure is based on system property adjustment factors, a , such that the adjusted value of the λ -factor is given by

$$\text{adjusted } \lambda_{\max} = 1 + (\lambda_{\max} - 1) \cdot a \quad (5-5)$$

$$\text{adjusted } \lambda_{\min} = 1 + (1 - \lambda_{\min}) \cdot a \quad (5-6)$$

That is, the property adjustment factor is multiplied by the amount by which the λ -factor differs from unity and the result is added to unity to yield the adjusted λ -factor. It is evident that the adjustment factor can take values in the range of 0 to 1. The value $a = 0$ results in an adjusted λ -factor of unity (that is, variations in properties are disregarded - least conservative approach). The value $a = 1$ results in no adjustment (that is, the maximum variations are considered to occur simultaneously - most conservative approach).

The following tentative system property adjustment factors have been proposed by the authors:

- | | |
|------|-----------------------|
| 1 | for critical bridges |
| 0.75 | for essential bridges |
| 0.66 | for all other bridges |

These values are based on engineering judgement and a desire to employ the most conservative design approach for critical bridges. It is expected that as experience develops over the years of observation of the performance of seismically isolated bridges and other structures, and more data are collected on the variations of properties, more refined values of system property adjustment factors could be established.

5.4 Proposed System Property Modification Factors for Sliding Bearings

The following system property modification factors have been established on the basis of the test data of section 4, the interpretation of the nature of friction presented in section 3, and consensus by the members of the T-3 Task Group who developed the 1999 AASHTO Guide Specifications for Seismic Isolation Design (American Association of State Highway and Transportation Officials, 1999). The factors apply on the nominal value of the coefficient of friction under conditions of relevance in the dynamic analysis of seismically isolated bridges (that is, conditions of high velocity motion). The proposed values are presented in tables for a range of conditions relating to the environment, service conditions, installation details and materials.

Three material interfaces are identified in these tables:

- (a) **Unlubricated PTFE.** This category includes unlubricated interfaces consisting of highly polished austenitic stainless steel in contact with PTFE or similar composite materials (such as those used in FPS bearings).

- (b) **Lubricated PTFE.** This category includes lubricated interfaces consisting of highly polished austenitic stainless steel in contact with unfilled PTFE. Lubrication is applied by grease, which is stored in dimples.
- (c) **Bimetallic Interfaces.** This category includes interfaces consisting of stainless steel in contact with bronze (or similar metals and alloys) and without or with solid lubricants such as graphite, lead, PTFE, etc. The basic feature of this interface is the bimetallic contact, which may be significantly affected by load dwell. Moreover, this interface does not include dissimilar metals, which promote additional corrosion such as carbon and low alloy steels in contact with copper alloys. The authors believe that such interfaces should be avoided.

5.4.1 Effect of Aging

For stainless steel-PTFE interfaces, whether lubricated or not, the proposed factors are based on data on the effect of surface roughness on the coefficient of friction which are reported in section 4. When data were not available (see Table 4-6), appropriate values have been assumed on the basis of engineering judgement.

For bimetallic interfaces, the proposed factors are based on data on the effect of load dwell reported in section 3.7 after adjustment for the likely effects of corrosion.

The proposed values are for the λ_{\max} factor, denoted as $\lambda_{\max, a}$ are presented in Table 5-1. The $\lambda_{\min, a}$ is equal to unity.

Moreover, the following comments apply:

- (a) The exposure time is 30 years.
- (b) For interfaces consisting of PTFE, whether lubricated or not, the stainless steel is austenitic, type 304. Lower values may be justified for austenitic, type 316 stainless steel as discussed in section 4.7.
- (c) Table 5-1 distinguishes between sealed and unsealed bearing conditions, with the latter case associated with higher values of $\lambda_{\max, a}$. It is presumed that unsealed bearing conditions allow exposure to water and salt, thus promoting further corrosion.
- (d) While Table 4-6 distinguishes between three installation methods and four environmental conditions, the table below has been condensed to include two installation methods and two environmental conditions. These conditions are normal, which include rural and urban environments, and severe, which include marine and industrial environments.
- (e) The factors for lubricated PTFE do not adequately address the problem of drying up of the lubricant. If that occurs, the values in Table 5-1 are likely low by a factor of 2.

**TABLE 5-1 System Property Modification Factor for Effects of Aging
($\lambda_{\max, a}$) on the Coefficient of Friction of Sliding Bearings**

Interface	Unlubricated PTFE		Lubricated PTFE		Bimetallic Interfaces	
	Sealed	Unsealed	Sealed	Unsealed	Sealed	Unsealed
Installation Method						
Normal Environment	1.1	1.2	1.3	1.4	2.0	2.2
Severe Environment	1.2	1.5	1.4	1.8	2.2	2.5

5.4.2 Effect of Contamination

The proposed factors on the effect of contamination in Table 5-2 are for $\lambda_{\max, c}$, whereas the value of $\lambda_{\min, c}$ is 1.0. The values are based on the data presented in section 4.8. Contamination is considered only while the bearings are in service, whereas contamination due to disassembly of the bearings at the construction site is not considered. Moreover, unsealed bearings with the stainless steel surface facing up are considered susceptible to contamination, the effects of which may be significant. Accordingly, such installation method is disallowed. It should be noted that seals are envisioned as elements that prevent contamination but allow for the flow of air so that the stainless steel is supplied with oxygen and moisture condensation is prevented (see also section 4.7).

In the acceptable methods of installation, the effect of contamination is expected to be minor. Accordingly, the $\lambda_{\max, c}$ factor for contamination is proposed to be in the range of 1.0 to 1.1. The exception is the case of lubricated PTFE bearings when unsealed. Under these conditions, contamination is likely to cause hardening of the lubricant and significant increase of friction. The proposed factor of 3.0 reflects this reality and intends to discourage the use of unsealed lubricated PTFE bearings.

It should be noted in Table 5-2 that a value of $\lambda_{\max, c}$ equal to 1.1 is proposed for sealed bearings with the stainless steel facing down. In this case it is presumed that some contamination is likely from falling rust or paint particles from the carbon steel plate of the bearing above the stainless steel surface. When this plate is protected against corrosion, either by galvanizing or by painting for 30-year lifetime, the factor is proposed to be 1.0.

5.4.3 Effect of Wear (Travel)

The proposed factors for the effect of wear (travel or cumulative movement) are based on the data presented in section 4.5. The data indicate that the coefficient of friction of sliding bearings reduces following short cumulative movement and subsequently increases following larger travel. The amount of increase depends on the roughness of the stainless steel and the composition of the sliding interface.

TABLE 5-2 System Property Modification Factor for Effects of Contamination ($\lambda_{\max, c}$) on the Coefficient of Friction of Sliding Bearings

Installation Method	Unlubricated PTFE	Lubricated PTFE	Bimetallic Interfaces
Sealed with Stainless Steel Surface Facing Down	1.0	1.0	1.0
Sealed with Stainless Steel Surface Facing Up, Bearing Galvanized or Painted for 30 Years	1.0	1.0	1.0
Sealed with Stainless Steel Surface Facing Up	1.1	1.1	1.1
Unsealed with Stainless Steel Surface Facing Down	1.1	3.0	1.1
Unsealed with Stainless Steel Surface Facing Up	Not Allowed	Not Allowed	Not Allowed

The proposed factors for wear are based on data for unfilled PTFE in contact with highly polished stainless steel. These data show trends that are similar to those observed for the tested PTFE composite material (see Figures 4-19 and 4-10). In general, data are limited or lacking on the effect of wear for the commonly used sliding interfaces at travels exceeding about 2 km. Accordingly, the proposed factors are limited to the travel of 2 km. It is believed that manufacturers of sliding bearings should establish λ -factors for wear of their products under the commonly used conditions of their application (e.g., thickness of bearing material, roughness of stainless steel and apparent bearing pressure).

The 1999 AASHTO Guide Specifications for Seismic Isolation Design (American Association of State Highway and Transportation Officials, 1999) specify $\lambda_{\min, tr}$ values of unity. In reality, the $\lambda_{\min, tr}$ is less than unity for some interfaces, although this may not be of much practical significance. The authors believe that appropriate values of $\lambda_{\min, tr}$ are about 0.8 to 0.9 for unlubricated PTFE bearings and unity for lubricated PTFE bearings. There is insufficient information for proposing a value for bimetallic interfaces.

Table 5-3 includes the proposed $\lambda_{\max, tr}$ values. The incompleteness of the table denotes the lack of data on the effect of wear and the necessity for testing.

TABLE 5-3 System Property Modification Factor for Effects of Wear (Travel) ($\lambda_{\max, tr}$) on the Coefficient of Friction of Sliding Bearings

Cumulative Travel (m)	Unfilled PTFE	Lubricated PTFE	Bimetallic Interfaces
1000	1.0	1.0	NA
2000	1.2	1.0	NA
>2000	NA	NA	NA

5.4.4 Effect of Temperature

Test results presented in sections 4.4 and 4.9 demonstrate the effect of temperature on the friction coefficient of sliding bearings. In general, the coefficient of friction increases with reducing temperature at the start of the experiment. The increase in friction is dependent on the frictional heating during the interval between the start of the experiment and the time at which the measurement is made. Even when this time interval is very short, substantial frictional heating in high velocity motions causes considerable alleviation of the effects of low temperature.

The proposed factors for unfilled PTFE interfaces are based on the test results of the authors, which are presented in section 4.4. These factors are believed to be also appropriate for the PTFE-composite interface under the conditions of testing described in section 4.4 despite the fact that the results show a lesser effect of temperature on the friction properties of this interface. As explained in section 4.4, the very small thickness of the material used in the tests may have affected the heat flux partitioning at the interface and, thus, the tests may have not revealed the full effect of low temperatures.

The proposed factors for lubricated bearings are based on the data reviewed in section 4.9 (from Campbell and Kong, 1989) and which are presented in Tables 4-7 and 4-8.

Table 5-4 presents the proposed $\lambda_{\max, t}$ factor values. They are based on the reference temperature of 20°C. Moreover, for unlubricated and lubricated PTFE interfaces, values of $\lambda_{\min, t}$ equal to 0.9 and 0.8, respectively are proposed for the temperature of 50°C.

TABLE 5-4 System Property Modification Factor for Effects of Temperature ($\lambda_{\max, t}$) on the Coefficient of Friction of Sliding Bearings

Temperature (°C)	Unlubricated PTFE	Lubricated PTFE	Bimetallic Interfaces
20	1.0	1.0	NA
0	1.1	1.3	NA
-10	1.2	1.5	NA
-30	1.5	3.0	NA
-40	1.7	NA	NA
-50	2.0	NA	NA

5.5 Other Applications of System Property Modification Factors

System property modification factors may be used to establish the nominal properties of isolation systems at the relevant conditions of their application from data obtained under different conditions. This is typically the case when full-scale isolation bearings cannot be tested at the actual conditions of their application due to limitations of the available testing equipment.

Effects that may be accounted for by the use of system property modification factors are those of apparent bearing pressure, velocity of movement (for sliding systems) and frequency of movement (for elastomeric systems). These effects can be studied in scaled bearing tests and the appropriate system property modification factors can be established on the basis of the test results, application of principles of mechanics and engineering judgement. These factors should be used without adjustment (that is, they should be used with a system property adjustment factor equal to unity).

The 1999 AASHTO Guide Specifications for Seismic Isolation Design (American Association of State Highway and Transportation Officials, 1999) specify only a λ -factor for the effects of velocity on the coefficient of friction of sliding systems. However, the Guide Specifications imply that a λ -factor for velocity can be used for elastomeric bearings (see section A.2.2.2 of Guide Specifications). In this case, velocity is related to frequency since testing is performed with sinusoidal motion of specified amplitude and frequency. It is also implied that λ -factors for the effects of velocity on the post-yielding stiffness and characteristic strength of elastomeric systems can be utilized.

5.6 System Property Modification Factors for Elastomeric Isolation Systems

The 1999 AASHTO Guide Specifications for Seismic Isolation Design (American Association of State Highway and Transportation Officials, 1999) define system property modification factors for the effects of aging, temperature, wear (or travel) and scragging in elastomeric isolation systems.

It is recognized that elastomeric bearings are produced in a variety of compounds and that λ -factor values will significantly depend on the particular compound used. Moreover, published experimental data on elastomeric bearings are scarce, a fact that significantly complicates the establishment of λ -factor values. The proposed values in the 1999 AASHTO Guide Specifications for Seismic Isolation Design are primarily based on a proposal of these authors, which was based on the limited understanding of the behavior of these bearings as described in section 2.2.

5.6.1 Effect of Aging

On the basis of the review of data and the discussion in section 2.2, it is believed that aging causes an increase in both the post-yielding stiffness and the characteristic strength of elastomeric bearings. Over a period of approximately 30 years, this increase is believed to be of the order of 10-percent for the low damping natural rubber bearings and higher for the high damping natural rubber bearings. As discussed in section 2.2, large differences between unscragged and scragged properties (and recovery of these properties) imply that the chemical processes continue following curing of the elastomer. Therefore, such large differences between unscragged and scragged properties suggest potential for aging. Accordingly, a proposal has been advanced to relate the effects of aging to the difference between the unscragged and scragged properties. Somewhat arbitrarily, a large difference has been defined to be one in which the unscragged properties (post-yielding stiffness or characteristic strength) are at least 25-percent higher

than the scragged properties. Consequently, Table 5-5 has been developed in which the λ -factor values of 1.1 and 1.2 are based on the limited data reviewed in section 2.2, whereas the value of 1.3 is based on engineering judgement.

**TABLE 5-5 System Property Modification Factor for Effects of Aging
($\lambda_{\max, a}$) on the Properties of Elastomeric Bearings**

Natural Rubber Compound	Factor for Post-Yielding Stiffness	Factor for Characteristic Strength
Low Damping	1.1	1.1
High Damping with Small Difference between Unscragged and Scragged Properties	1.2	1.2
High Damping with Large Difference between Unscragged and Scragged Properties	1.3	1.3

5.6.2 Effect of Scragging

Elastomeric bearings typically exhibit higher characteristic strength and stiffness when subjected to testing for the first time. The properties under these conditions are termed virgin or unscragged properties. Subsequent testing under the same conditions results in stable but lower strength and stiffness properties, which are termed the scragged properties. As an example, Figure 5-1 presents force-displacement loops from the testing of a small scale high damping elastomeric bearing (Kasalanati and Constantinou, 1999).

It has been assumed in the past that during testing certain internal structures of rubber are severed so that the scragged properties prevail and become permanent. It is now recognized that recovery of rubber bearings to their virgin (unscragged) stage occurs. For example, test results reported in Cho and Retamal (1993) and Murota et al. (1994) demonstrate that significant recovery occurs within short periods of time. The existence of recovery suggests that chemical processes continue in the bearing following its vulcanization. It is thus likely that full recovery occurs in sufficient time, with the duration of the process being dependent on the rubber compound and the extent of its curing.

If we accept that full recovery occurs, then the bearings exhibit two distinct behaviors on the basis of only the phenomena of scragging and recovery. The properties can be established by testing of the bearings, as for example, in the small bearing for which the results are shown in Figure 5-1. In this case, one 3-cycle test at the relevant load, frequency and displacement (top left plot in Figure 5-1) is sufficient to establish the two sets of properties.

When the nominal properties of an isolation system are based on the scragged conditions of the bearings, then a system property modification factor may be utilized in establishing

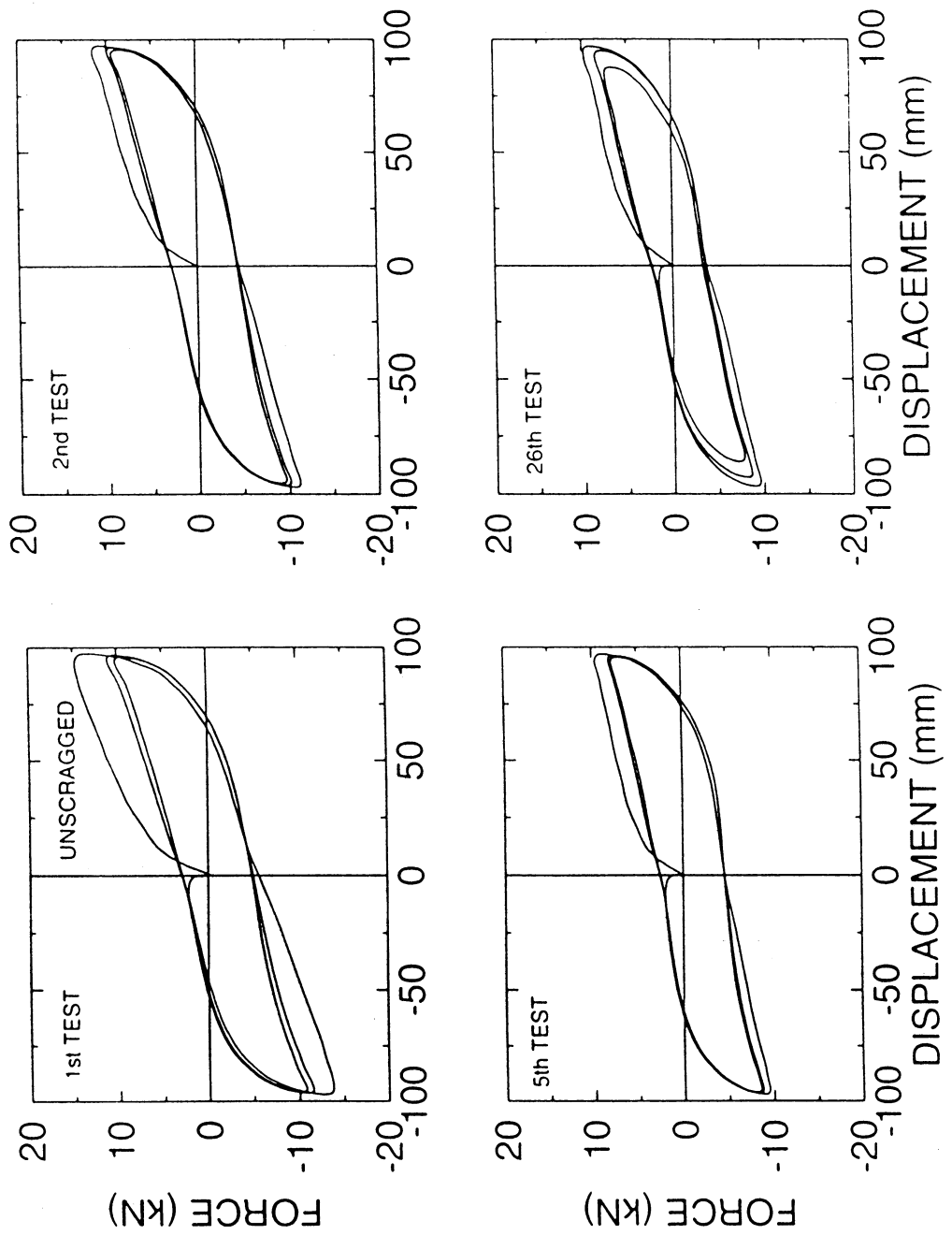


**FIGURE 5-1 Lateral Force-Lateral Displacement Loops of a Small Scale High Damping Elastomeric Bearing
(all test are at frequency of 1.0 Hz)**

the contribution of recovery to the upper bound properties of the system. Accordingly, a $\lambda_{\max, \text{scrag}}$ factor is defined for the properties of characteristic strength and post-yielding stiffness. However, few published results are available in a form that can be used to extract the appropriate λ -factors for scragging.

It is generally recognized that low damping rubber bearings do not exhibit much difference between unscragged and scragged properties. This suggests that the additives in rubber and the curing process used to enhance damping are responsible for this increased difference of unscragged and scragged properties in high damping rubber bearings. It also presents the opportunity to relate the extent of the difference between the two properties to the effective damping of the bearings.

The authors have observed in the testing of small scale high damping rubber bearings (e.g., Kasalanati and Constantinou, 1999) that $\lambda_{\max, \text{scrag}}$ for both the characteristic strength and the post-yield stiffness is of the order of 1.2 or less when the effective damping in the bearings (defined as the equivalent damping in the 1999 AASHTO Guide Specifications but for a single bearing) is less than about 0.15. They also observed that improperly cured bearings exhibit much higher damping and much higher ratio of unscragged to scragged properties. Also the data reported in Cho and Retamal (1993) shows a large $\lambda_{\max, \text{scrag}}$ factor for the characteristic strength. The bearings had effective damping in the range of 0.15 to 0.20.

On the basis of these limited data, the members of the T-3 Task Group decided to propose the $\lambda_{\max, \text{scrag}}$ factors in Table 5-6.

TABLE 5-6 System Property Modification Factor for Effects of Scragging-Recovery ($\lambda_{\max, \text{scrag}}$) on the Properties of Elastomeric Bearings

Natural Rubber Compound	Factor for Post-Yielding Stiffness	Factor for Characteristic Strength
Low Damping	1.0	1.0
High Damping with Effective Damping ≤ 0.15	1.2	1.2
High Damping with Effective Damping > 0.15	1.8	1.5

The scragging and recovery of high damping elastomeric bearings has been recently re-examined by researchers at the University of California, Berkeley (Thompson et al., 2000). Based on newly conducted tests and examination of available data on 34 bearings fabricated by 5 manufacturers using 10 different compounds, the following were concluded:

- (a) Recovery occurs within a short period following scragging.

- (b) The λ -factor for scragging appears to be better correlated to the shear modulus of the elastomer rather than the damping ratio.
- (c) Values of λ -factor for accounting for the effects of scragging on the effective shear modulus are in the range of 1.4 to 2.1 for elastomers with third-cycle shear modulus at 100-percent strain below 0.7 MPa (100 psi), and in the range of 1.2 to 1.5 for elastomers with third-cycle shear modulus greater than 0.7 MPa (100psi).

The values of scragging factor proposed by Thompson et al. (2000) apply to the effective shear modulus, whereas the 1999 AASHTO Guide Specifications specify λ -factors for the post-yielding stiffness and the characteristic strength. Actually, the T-3 Task Group originally considered the use of the effective shear modulus but finally opted for the use of the post-yielding stiffness and the characteristic strength because they provide for a generic description of the behavior of most isolation bearings. However, the various parameters may be related as follows:

$$G_{\text{eff}} = G + \frac{Q_b}{A_r \gamma} = G + \frac{(Q_b/N)(N/A_r)}{\gamma} \quad (5-7)$$

where G_{eff} = effective shear modulus, G = shear modulus based on the post-yielding stiffness ($=K_b T/A_r$, T = total rubber thickness), Q_b = characteristic strength (see section 2), N = gravity load on the bearing, A_r = bonded rubber area, and γ = amplitude of shear strain in the rubber. Note that quantity N/A_r is the average bearing pressure.

On the basis of (5-7) and the λ -factors in Table 5-6, one may calculate a scragging factor for the effective shear modulus equal to 1.2 when the λ -factor values of 1.2 and 1.2 are used for the post-yielding stiffness and characteristic strength, respectively. Moreover, a scragging factor for the effective shear modulus equal to 1.7 to 1.8 is calculated when the λ -factor values of 1.8 and 1.5 are respectively used and a wide range of parameters is utilized ($\gamma = 1.0$ to 2.0 , $G = 0.35$ to 0.7 MPa, $N/A_r = 7$ to 11 MPa, $Q_b/N = 0.02$ to 0.04). The calculated values are lower by about 10 to 20-percent of the values proposed by Thompson et al. (2000). Therefore, it would be prudent to modify the values of $\lambda_{\max, \text{scrag}}$ in Table 5-6 for both the post-yielding stiffness and characteristic strength as proposed by Thompson et al. (2000):

- (a) For high-damping elastomers with third-cycle effective shear modulus at 100-percent shear strain greater than 0.7 MPa, 1.5.
- (b) For high-damping elastomers with third-cycle effective shear modulus at 100-percent shear strain less than 0.7 MPa, 2.0.

5.6.3 Effect of Temperature

It is well known that low temperatures cause increase in both the stiffness and strength of elastomeric bearings. Roeder et al. (1987) presented a comprehensive review of this effect. In general, the effect of low temperature consists of the instantaneous thermal stiffening, which is achieved within the time needed for thermal equilibrium, and the crystallization stiffening, which is time-dependent. Figure 5-2 illustrates the typical low-temperature behavior of elastomers. Time t_1 depends on the size of the bearing, and particularly its height. On the basis of the results of Roeder et al. (1987), time t_1 may be of the order of 12 to 24 hours for large size elastomeric bearings such as those used in seismic isolation applications. Time t_2 is dependent on the elastomeric compound and temperature and is relatively short – of the order of a few hours. When crystallization stiffening begins, the material stiffens with time because of reorientation of its molecular structure. However, crystallization is reversible when temperature is increased.

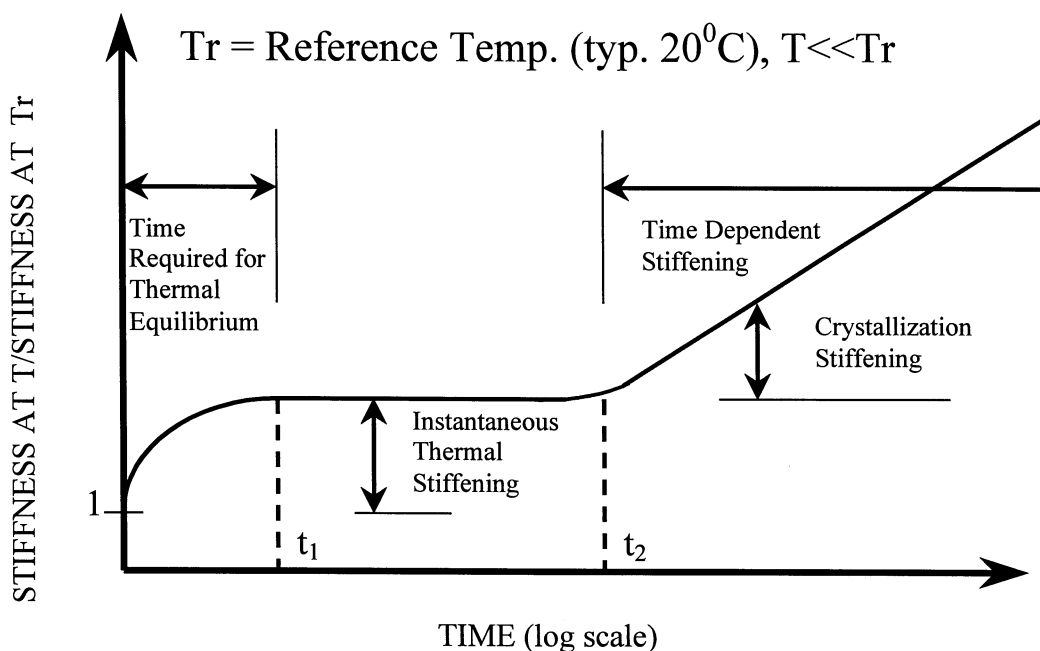


FIGURE 5-2 Time-dependent Low Temperature Behavior of Elastomers

Furthermore, another phenomenon, called glass transition, occurs when the temperature is below the glass transition temperature, which is a characteristic of the elastomeric compound. When glass transition occurs, the elastomer becomes brittle and many of its mechanical and physical properties undergo significant and rapid changes. Natural rubber has a glass transition temperature of about -55°C .

Roeder et al. (1987) concluded that thermal stiffening in elastomeric bearings (that is, the effect of low temperature for relatively short time intervals) is likely to be a serious problem in Alaska, limited parts of the continental United States, and much of Canada.

Moreover, they concluded that crystallization is a problem when temperature drops below 0°C.

It is clear that the mechanical properties of elastomeric bearings are affected by low temperatures and the duration of exposure to these temperatures. It is unfortunate that all of the studies (which these authors were able to review) on the effect of low temperature on the properties of elastomeric seismic isolation bearings have neglected the significance of the duration of exposure. Some of the studies neglect to report the duration of exposure, whereas others report a single approximate exposure time.

Skinner et al. (1993) report on the effect of low temperature on the properties of a tested lead-rubber bearing in New Zealand. The exposure time is not reported. Also only the peak force (force at the maximum displacement of testing) is reported from which only the effective stiffness can be calculated. For the strain of 0.5 and frequency of 0.9 Hz, the effective stiffness exhibited increases by factor of 1.4 and 1.2 at the temperature of -35 and -15°C, respectively, with respect to the reference temperature of 18°C. Moreover, at 45°C the factor was 0.9.

Nakano et al. (1993) reported data on the effective stiffness and effective damping of one lead-rubber and one high damping rubber bearing which were cooled at the temperature of about -18°C and subsequently tested. Measurements were made at various temperatures up to 5°C as the bearings warmed up during testing. The exposure time for each of the reported temperatures was extremely short (not reported but presumed to be of the order of a few minutes). Nevertheless, these test data are useful and used herein to establish λ -factors for high damping rubber bearings.

Kim et al. (1996) reported results on the low temperature properties of one lead-rubber and one low damping elastomeric bearing. The bearings were cooled to -60°C for at least three days and subsequently tested. Records of force-displacements loops and values of characteristic strength and post-yielding stiffness are reported for various temperatures as it was increased during warming up of the bearing to the temperature in the laboratory. Testing was conducted at a range of rubber shear strains and frequency of 0.1 Hz. This is a well documented set of results, which is used herein to establish λ -factors for temperature effects on lead-rubber bearings. However, the reader is cautioned that the results may have been affected by the history of cooling (first lengthy exposure at a very low temperature and then very quick warming up to the temperatures of testing).

On the basis of the results of Nakano et al. (1993) and Kim et al. (1996), Table 5-7 was prepared. The data for lead-rubber bearings are for grade 3 natural rubber, whereas those for the high damping rubber apply for a material with effective damping of less than 15-percent and with moderate difference between unscragged and scragged properties.

TABLE 5-7 System Property Modification Factor for Effects of Temperature ($\lambda_{\max, t}$) on the Properties of Elastomeric Bearings

Temperature (°C)	Factor for Post-Yielding Stiffness		Factor for Characteristic Strength	
	LRB	HDRB	LRB	HDRB
20	1.0	1.0	1.0	1.0
0	1.1	1.2	1.2	1.2
-10	1.1	1.4	1.4	1.4
-30	1.3	2.0 ¹	1.8	2.3 ¹

1: extrapolated value LRB = Lead-rubber Bearings

HDRB = High Damping Rubber Bearings

The data in Table 5-7 differ slightly from the λ -factor values in the 1999 AASHTO Guide Specifications for Seismic Isolation Design. The values in the 1999 AASHTO Guide Specifications were decided on the basis of consensus by the members of the T-3 Task Group. The values in the specifications reflect a desire to extend the description of high damping rubber bearings, which again and somewhat arbitrarily are distinguished on the basis of the difference between unscragged and scragged properties.

5.7 Generation of Heat in Elastomeric Bearings during Testing

The tests on elastomeric bearings at low temperatures described in section 5.6.3 were conducted at a range of conditions of strain, pressure and frequency. A question then arises on the significance of the test conditions on the obtained results. Particularly, the effect that the frequency of testing has on the generation heat in the bearing and the resulting rise in temperature needs to be investigated. The reader should recall the significance of velocity in the frictional heating of sliding bearings (see section 3.8).

5.7.1 High Damping Rubber Bearings

When high damping rubber bearings are subjected to motion, heat is produced in the rubber itself. The mechanism of heat generation is mechanical in origin, and likely based on viscous action and friction between intertwined rubber molecules. When heat is generated in the solid, the equations of heat conduction are (Carslaw and Jaeger, 1959)

$$\frac{\partial^2 T}{\partial x^2} + \frac{\partial^2 T}{\partial y^2} + \frac{\partial^2 T}{\partial z^2} - \frac{1}{D} \frac{\partial T}{\partial t} = -\frac{A_o}{k} \quad (5-8)$$

where T = temperature, k = thermal conductivity of the material, D = thermal diffusivity of the material and A_o = rate of heat production per unit volume per unit time.

The generated heat is practically independent of the space variables since it is primarily dependent on the shear strain, which is practically the same for the entire volume of rubber. Moreover, if we neglect radiation of heat and heat conduction through the end

plates of the bearings, we conclude that the temperature is independent of the space variables.

Also,

$$A_o = \tau \frac{dy}{dt} \quad (5-9)$$

where τ = shear stress in rubber and γ = shear strain in rubber. Therefore, (5-8) reduces to

$$\frac{dT}{dt} = \frac{D}{k} \tau \frac{dy}{dt} \quad (5-10)$$

or

$$\rho c \frac{dT}{dt} = \tau \frac{dy}{dt} \quad (5-11)$$

in which the ratio k/D has been replaced by its equivalent ρc , where ρ = mass density of the material and c = specific heat of the material. Integration yields

$$T(t) = \frac{1}{\rho c} \int_{0}^{\gamma(t)} \tau dy \quad (5-12)$$

or

$$T(t) = \frac{1}{\rho c V} \int_{0}^{u(t)} F du \quad (5-13)$$

where V = volume of rubber, F = lateral force on the bearing and u = lateral displacement of the bearing.

It is recognized that the integral in (5-13) is the area enclosed by the lateral force - displacement loop of the bearing. The temperature rise is dependent on frequency only indirectly through its effect on the lateral force. This effect is typically small and testing at reduced frequencies should not affect the quality of the test results at low temperatures. Yet at some low frequency, the conduction of heat through the end plated should start having an effect, so that the temperature rise will not be as much as calculated on the basis of (5-13).

We proceed with calculating estimates of the temperature rise during testing. Consider cyclic motion at amplitude u_{max} . For the idealized bilinear hysteretic behavior shown in Figure 2-1, the temperature rise per cycle is easily calculated on the basis of (5-13) to be

$$T_c = \frac{4Q_b(u_{max} - u_y)}{\rho c A_r T_r} \quad (5-14)$$

where u_y = yield displacement, A_r = rubber area and T_r = total rubber thickness. More conveniently, (5-14) is written as

$$T_c = \frac{4p(\gamma_{max} - \gamma_y)}{\rho c} \cdot \left(\frac{Q_b}{N} \right) \quad (5-15)$$

in which p = average bearing pressure, N = vertical load on the bearing, γ_{max} = rubber shear strain at the displacement amplitude and γ_y = rubber shear strain at the yield displacement.

Considering typical values of $p = 7\text{MPa}$, $\gamma_{max} = 1.5$, $\gamma_y = 0.07$, $Q_b/N \leq 0.05$, and $\rho c \approx 2 \times 10^6 \text{ N}/(\text{m}^2 \text{ }^\circ\text{C})$, we calculate $T_c \leq 1\text{ }^\circ\text{C}$, which is insignificant. Accordingly, we conclude that the heat generated during testing of high damping rubber bearings is too small to affect the results.

The estimated temperature rise per cycle of less than $1\text{ }^\circ\text{C}$ is very small. It agrees, however, very well with the results of Nakano et al. (1993) who reported values of about $0.6\text{ }^\circ\text{C}$ per cycle during a 50-cycle test.

5.7.2 Lead-Rubber Bearings

In lead-rubber bearings, the heat is primarily generated in the lead core from where it flows vertically and radially in the steel end and shim plates. Additionally, there is generation of heat in the rubber itself, which is typically small, except likely when the rubber is at very low temperatures.

It is known that the energy dissipated per cycle and the characteristic strength of lead-rubber bearings reduce with increasing number of cycles. The reduction is substantial in the first few cycles when the motion is of high speed. For example, Figure 5-3 presents the energy dissipated per cycle in a large size lead-rubber bearing which was tested under dynamic conditions. The figure shows both the measured dissipated energy and the estimated contribution to the dissipated energy by the lead core. For the estimation, it was assumed that the rubber contributes to the equivalent viscous damping ratio of the bearing (per definition of the 1999 AASHTO Guide Specifications) an amount equal to 0.04.

Evident in this figure is a substantial reduction in energy dissipation per cycle in the initial cycles, followed by a near stabilization of the energy dissipated per cycle. A brief interruption of the testing and restart, results in an almost complete recovery to the original energy dissipation per cycle. These observations clearly demonstrate that the reduction in the energy dissipation per cycle is the result of heating of the lead core. The core may reach nearly constant temperature conditions after a number of cycles due to

equalization of the generated heat to the heat lost by conduction through primarily the steel plates and secondarily the rubber. The near complete recovery after the 2-minute interruption of testing demonstrates the significance of the conduction of heat.

Analysis of the problem of the temperature rise in lead-rubber bearings requires the solution of a problem on the conduction of heat in a composite circular cylinder. An appropriate model would be the one shown in Figure 5-4 with zero initial temperature and with heat production at a variable rate $A_0(t)$ per unit time per unit volume in the region $0 \leq r < a$, $-l < z < l$ for $t > 0$. This problem is very difficult to treat analytically. Much easier to treat is the infinitely long composite cylinder (problem of Fig. 5-4 with l extended to infinity) and constant heat rate but the solution is very complicated to be of much practical value (see p. 347 in Carslaw and Jaeger, 1959).

Some insight and useful information may be obtained by solving selected simplified problems which may adequately describe the physical problem under certain restrictions. To select these simplified problems, it is important to review some thermal and other properties of the materials in lead-rubber bearings. Table 5-8 presents a collection of such properties obtained from several sources (American Society of Metals, 1991; American Society of Metals, 1992; Lide, 1993; Hofmann, 1970). Important in these data is that the thermal properties of lead are practically unaffected by temperature up to the melting point. The reduction in the energy dissipation per cycle is the result of the reduction in the "effective yield stress" of lead with increasing temperature. The yield stress of lead cannot be accurately measured due to the tendency of the material to creep. However, the ultimate strength (which is somehow related to the "effective yield stress") can be measured and some representative data are shown in Table 5-8 (from Hofmann, 1970 after adjustment for the effects of rate of strain). Another important observation is that rubber has a much lower thermal conductivity and thermal diffusivity than either lead or steel. Accordingly, it may be assumed that heat conducts entirely through the steel shin plates and the steel end plates of the bearing.

It is reasonable to assume that for a short time interval after the start of the experiment, heat conduction through the steel shim plates and steel end plates is negligible. Accordingly, the heat generated in the lead core is entirely consumed for the rise of its own temperature. On the average, this temperature rise is given by (5-13), where V = volume of lead. For the tested bearing (Fig. 5-3), $V = 8.137 \times 10^{-3} \text{ m}^3$, $\rho c = 1.465 \times 10^6 \text{ N}/(\text{m}^2 \text{ }^\circ\text{C})$ (see Table 5-8 for lead), whereas the energy dissipated per cycle is 311,600 N-m for the first cycle and 256,000 N-m for the second cycle (see Fig. 5-3). For an ambient temperature of 20°C , the calculated temperature of the lead core is about 46°C at the end of the first cycle and about 68°C at the end of the second cycle. Now assume that the "effective yield stress" of lead is related to its ultimate strength, so that the energy dissipated per cycle is proportional to the ultimate strength of the lead. Then the reduction of the energy dissipated per cycle shown in Figure 5-3 is consistent with the calculated temperature in the lead core and the strength data for lead in Table 5-8.

Let us consider now that heat conduction through the steel shim and end plates prevails. This is likely the condition of the tested bearing after about three cycles of motion. The

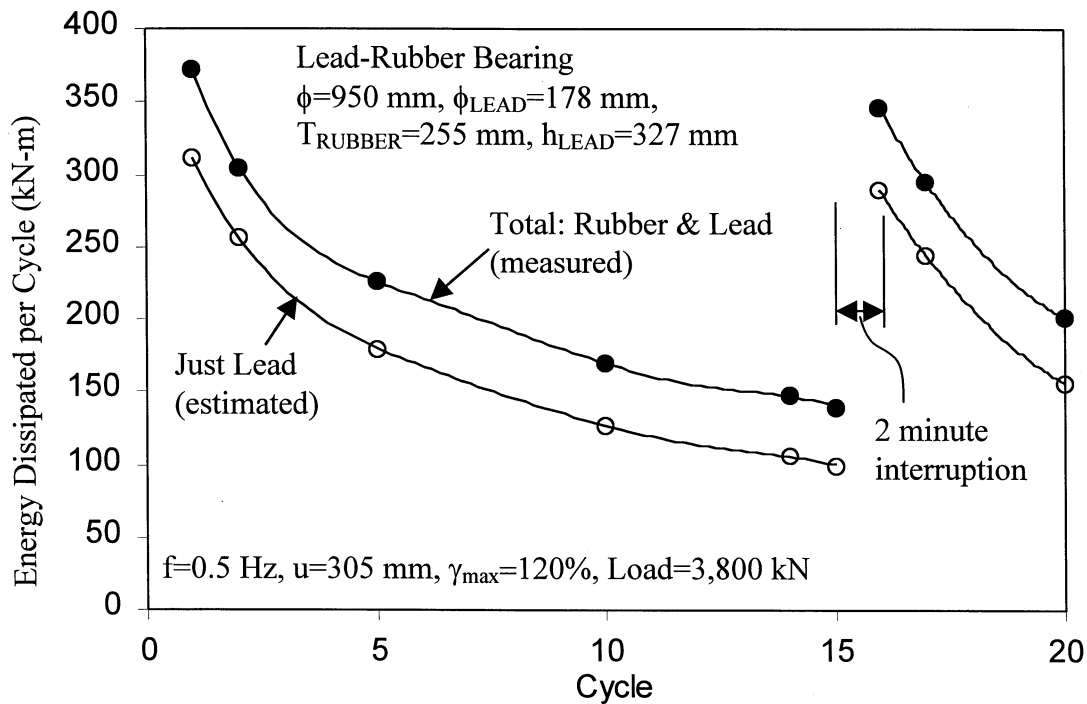


FIGURE 5-3 Energy Dissipation Per Cycle in a Lead-Rubber Bearing

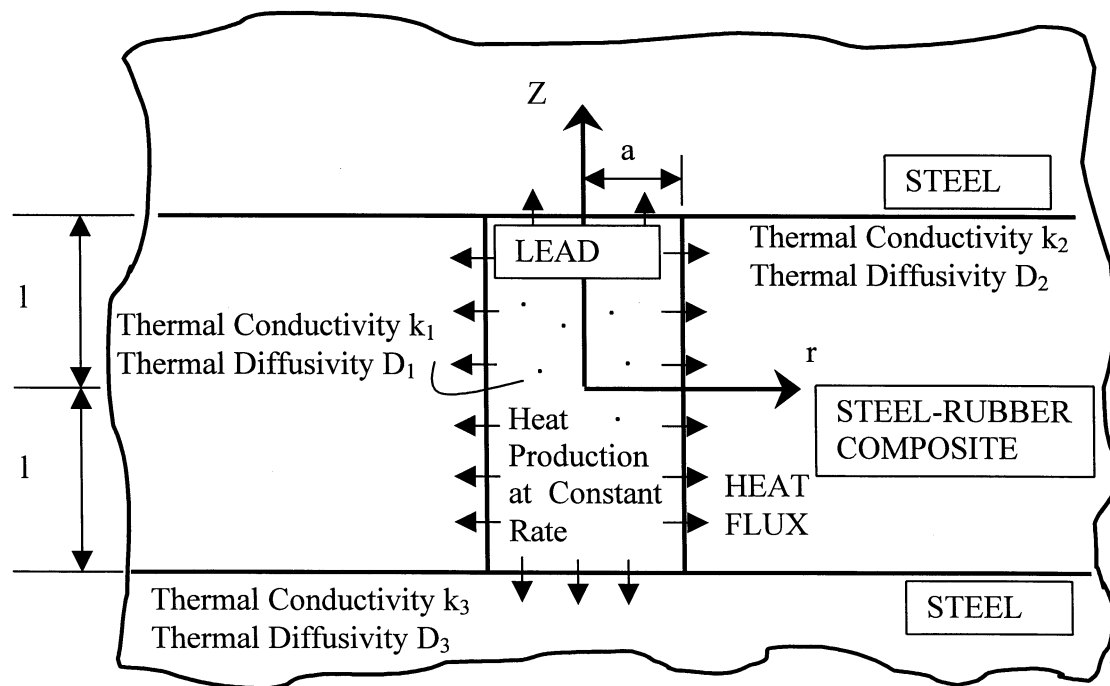


FIGURE 5-4 Appropriate Model for Problem of Heat Conduction in Lead-Rubber Bearings

TABLE 5-8 Thermal and Other Properties of Lead, Steel and Rubber

Temperature (°C)	-25	25	75	125	225	327 (melting of lead)
Thermal Conductivity k, W/(m °C)						
Lead (99.99% pure)	36	35.3	34.7	34	32.8	31.4
Rubber	-	~0.16	-	-	-	-
Carbon Steel (<0.5% C)	-	~54	~53	~51	~47	~44
Thermal Diffusivity D, m²/s						
Lead (99.99% pure)	-	2.42x10 ⁻⁵	2.34x10 ⁻⁵	2.29x10 ⁻⁵	2.14x10 ⁻⁵	~2x10 ⁻⁵
Rubber	-	~1.2x10 ⁻⁵	-	-	-	-
Carbon Steel (<0.5% C)	-	~1.48x10 ⁻⁵	-	-	-	-
Specific Heat c, J/(g °C)						
Lead (99.99% pure)	0.127	0.129	0.131	0.132	0.137	0.142
Rubber	-	~1.7	-	-	-	-
Carbon Steel (<0.5% C)	-	~0.45	-	-	-	-
Density ρ, g/cm³						
Lead (99.99% pure)	-	11.36	11.30	11.24	11.17	~11.00
Rubber	-	1.3	-	-	-	-
Carbon Steel (<0.5% C)	-	7.9	-	-	-	-
Ultimate Strength (MPa)						
Lead (99.99% pure) at strain rate ≥ 0.02 sec⁻¹	-	~18	~10	~7.4	~4	~0

temperature of the lead core is nearly uniform over its volume and equal to that of the steel plates at the areas of contact with lead. The temperature rise of the lead core is proportional to the heat flux Q at the steel-lead interface as shown in Figure 5-4. Let the total thickness of the shim plates be t_s ($t_s = 72$ mm for the tested bearing), the radius of the lead core be a , and the “effective yield stress” of lead be σ_L . Then

$$T \sim Q \sim \frac{\sigma_L \cdot \pi \cdot a^2 \cdot u \cdot f}{(2\pi a^2 + 2\pi a \cdot t_s)} \sim \frac{1}{1 + t_s/a} \quad (5-16)$$

where u = amplitude of motion and f = frequency (see Fig. 5-3). The important conclusion from (5-16) is that the radius of the lead core affects the temperature rise, and therefore, it affects the reduction of the energy dissipation per cycle. For example, consider two identical lead-rubber bearings with $t_s = 72$ mm and one with $a = 89$ mm (as in the tested one) and the other with $a = 50$ mm. The temperature rise in the second bearing will be about $(1+72/89) / (1+72/50) = 0.74$ times the temperature rise in the first one.

The effects of the frequency of testing (or strain rate) may now be approximately assessed as follows:

- (1) The rate of strain affects the effective yield properties of lead and, thus, indirectly the energy dissipated per cycle and the characteristic strength. In general, the effect is not important for rates of strain above about 0.02 (sec) $^{-1}$ (Skinner et al., 1993; Hofmann, 1970).
- (2) In the initial stages of testing (one or two cycles), when heat conduction through the steel end and shim plates is minor, the energy dissipated per cycle and the characteristic strength are primarily unaffected by the frequency of testing. This is due to the weak dependence of the temperature rise per cycle on the frequency of testing.
- (3) In the later stages of testing, when heat conduction through the steel end and shim plates prevails, the energy dissipated per cycle and the characteristic strength should be somewhat affected by the frequency of testing. The reason for this is that the heat flux to the steel parts is proportional to the frequency, whereas the temperature is proportional to the heat flux and the square root of time. That is, the temperature rise in the bearing is somewhat related to the square root of the frequency.

On the basis of these results, it appears that the data of Kim et al. (1996) on the low temperature properties of lead-rubber bearings have not been significantly affected by the frequency of testing. Since the mechanical properties were extracted from the initial loops, when heat conduction through the steel parts was minor, the frequency of testing did not significantly affect the temperature rise and, accordingly, the properties.

5.8 Summary

We have presented in this section the concept of system property modification factors and proposed values of these factors for sliding and elastomeric isolation bearings. It is important to note that it is expected from manufacturers of isolation hardware to conduct testing and establish the values of system property modification factors for their products. There is urgent need to develop standards to which this testing and interpretation of results should adhere. It should also be mentioned that the responsibility for testing and interpreting the results is a delicate issue. It seems that self-policing is unlikely to work and that some agency should take the responsibility of reviewing and approving the results of manufacturers. Moreover, certain factors should not be established by the manufacturers but rather be determined by committees on the basis of laboratory results, field observations and judgement. Particularly, factors related to aging and contamination are the most difficult to establish and cannot be determined in a single test.

This section includes also a description of system property adjustment factors. It is appropriate that some study is conducted to relate these factors to the variability in the properties of seismic isolation bearings and the probability of occurrence of independent events.

SECTION 6

CONCLUSIONS

This report presented the concept of system property modification factors, which are utilized in the 1999 AASHTO Guide Specifications for Seismic Isolation Design for establishing bounding values of properties of isolation bearings. The concept is simple and rational. However, the determination of values of some of these factors, such as that for aging, requires knowledge of the behavior of the materials used in the construction of these bearings and the understanding at the microscopic level of complex phenomena such as that of friction. Accordingly, a major part of the report was devoted to the subject of aging and the description of the phenomenon of friction at the microscopic and macroscopic levels. Moreover, the problem of frictional heating was addressed and an analytic solution was presented for the temperature rise at sliding interfaces. Partially confirmed in experiments, this solution was used in the interpretation of results.

Each section of this report contains a summary, where the interested reader is referred to for brief information on the presented material. Herein, we present a list of subjects that were treated in this report and for which further studies are warranted:

- (1) The aging of seismic isolation hardware is an important subject which so far has not received appropriate attention. Field data on aging are scarce and the validity of the methods used for accelerated aging are open to serious question. It is important that the basic mechanisms for aging and other related phenomena are understood.
- (2) The mechanism of friction in sliding seismic isolation bearings is not fully understood. One topic of importance is the effect of load dwell on the breakaway friction in interfaces consisting of PTFE or PTFE-based materials in contact with polished stainless steel. While we have argued and provided some theoretical and experimental evidence that load dwell does not affect the breakaway friction, it is appropriate that additional studies are conducted.
- (3) Frictional heating is of importance in the design of sliding seismic isolation bearings. The presented theory predicts large interface temperature rises in high velocity motions. It would be of interest to conduct experiments and measure the temperature at the surface, rather than at some depth. This would require the use of novel temperature measurement techniques.
- (4) The effect of low temperature on the properties of sliding and elastomeric isolation bearings is not well documented. Particularly, for elastomeric bearings the combined effects of low temperature and duration of exposure require documentation. Similarly in sliding bearings, the effect of the duration of exposure to low temperatures is unknown.
- (5) The effect of cumulative movement on the frictional properties of sliding interfaces needs to be documented for large travel. Similarly, the effect of large cumulative

movement on elastomeric seismic isolation bearings (and not of small size rubber coupons) is completely unknown. Indirect information exists from the observation of the performance of standard bridge bearings.

- (6) The problem of heating of lead-rubber bearings when subjected to seismic motion (or testing) is both challenging to solve analytically and interesting for assessing the behavior of these bearings and for interpreting experimental results.
- (7) Further studies on the phenomena of scragging and recovery in elastomeric bearings are needed to assess both the extent of recovery and the time it requires. Interesting is to study low modulus compounds, including low damping ones. There is a recent interest in the use of such compounds for achieving large effective period with compact bearing design. The behavior of these compounds is now in question given the recent results of Thompson et al. (2000).
- (8) Bimetallic sliding interfaces are the least studied and also the least used interfaces. The authors believe that these interfaces are unreliable and inappropriate for use in isolators. Field observations provide evidence for this. However, some study and full documentation of the existing information for these interfaces is appropriate.
- (9) A study should be conducted to relate the system property adjustment factors to the variability in the properties of seismic isolation bearings and the probability of occurrence of the various events considered in the bounding analysis.
- (10) There is an urgent need to develop standards for the establishment of system property modification factors. Moreover, there is a need for some agency to take responsibility for the review and approval of the testing and interpretation of results by manufacturers of seismic isolation hardware.

SECTION 7 REFERENCES

- (1) Al-Hussaini, T. M., Zayas, V. A. and Constantinou, M. C. (1994), Seismic Isolation of Multistory Frame Structures Using Spherical Sliding Isolation Systems", Report NCEER-94-0007, National Center for Earthquake Engineering Research, Buffalo, NY.
- (2) American Association of State Highway and Transportation Officials (1999), "Guide Specifications for Seismic Isolation Design", Washington, D.C.*
- (3) American Association of State Highway and Transportation Officials (1992), "Standard Specifications for Highway Bridges", 15th Edition, Washington, D.C.
- (4) American Society for Metals (1991), *Properties and Selection: Non-ferrous Alloys and Special-Purpose Materials*, ASM Handbook, Vol. 2, Metals Park, Ohio.
- (5) American Society for Metals (1992), *Friction, Lubrication, and Wear Technology*, ASM Handbook, Vol. 18, Metals Park, Ohio.
- (6) American Society of Mechanical Engineers (1985), "Surface Texture (Surface Roughness, Waviness, and Lay)", Standard ANSI/ASME B46.1-1985, New York, NY.
- (7) Benzoni, G. and Seible, F. (1999), "Design of the Caltrans Seismic Response Modification Device (SRMD) Test Facility", Proceedings of U.S.-Italy Workshop on Seismic Protective Systems for Bridges, Multidisciplinary Center for Earthquake Engineering Research, Buffalo, NY.
- (8) Bondonot, G. and Filliatrault, A. (1997), "Frictional Response of PTFE Sliding Bearings at High Frequencies", J. Bridge Engng., ASCE, Vol. 2, No. 4, 139-148.
- (9) Bowden, F. P. and Tabor, D. (1950), *The Friction and Lubrication of Solids: Part I*, Oxford University Press, Oxford, UK.
- (10) Bowden, F. P. and Tabor, D. (1964), *The Friction and Lubrication of Solids: Part II*, Oxford University Press, Oxford, UK.
- (11) Bowden, F. P. and Tabor, D. (1973), *Friction; an Introduction to Tribology*, Heinemann, UK.
- (12) British Standards Institution (1990), "Commentary on Corrosion at Bimetallic Contacts and its Alleviation", PD 6484:1979, London, UK.

* The 1999 Guide Specifications for Seismic Isolation Design were developed in 1997, adopted by the 52 AASHTO member states in 1998 and published in 1999.

- (13) Campbell, T. I. and Fatemi, M. J. (1989), "Further Laboratory Studies of Friction in TFE Slide Surface of a Bridge Bearing", Report ME-89-06, Ministry of Transportation and Communications, Ontario, Canada.
- (14) Campbell, T. I. and Kong, W. L. (1987), "TFE Sliding Surfaces in Bridge Bearings", Report ME-87-06, Ministry of Transportation and Communications, Ontario, Canada.
- (15) Campbell, T. I. and Kong, W. L. (1989), "Laboratory Studies of Friction in TFE Slide Surfaces of Bridge Bearings", Report ME-89-04, Ministry of Transportation and Communications, Ontario, Canada.
- (16) Campbell, T. I., Pucchio, J. B., Roeder, C. W. and Stanton, J. F. (1991), "Frictional Characteristics of PTFE Used in Slide Surfaces of Bridge Bearings", Proc. 3rd World Congress on Joint Sealing and Bearing Systems for Concrete Structures, Toronto, Ontario, Canada, Vol. 2 of Preprints (published by the National Center for Earthquake Engineering Research, Buffalo, NY), 847-870.
- (17) Carslaw, H. S. and Jaeger, J. C. (1959), *Conduction of Heat in Solids*, 2nd Edition, Oxford University Press, London, UK.
- (18) Cho, D.M. and Retamal, E. (1993). "The Los Angeles County Emergency Operations Center on High Damping Rubber Bearings to Withstand an Earthquake Bigger than the Big One." Proc. ATC-17-1 Seminar on Seismic Isolation, Passive Energy Dissipation, and Active Control, March, San Francisco, CA, Applied Technology Council, Redwood City, CA.
- (19) Clark, P. W., Kelly, J. M. and Aiken, I. D. (1996), "Aging Studies of High-Damping Rubber and Lead-Rubber Seismic Isolators", Proc. 4th U.S.-Japan Workshop on Earthquake Protective Systems for Bridges, published by the Public Works Research Institute, Ministry of Construction, Japan as Technical Memorandum No. 3480, 75-89.
- (20) Constantinou, M. C. (1998), "Application of Seismic Isolation Systems in Greece", Proc. Structural Engineers World Congress, San Francisco, CA, July.
- (21) Constantinou, M. C., Mokha, A. S. and Reinhorn, A. M. (1990a), "Experimental and Analytical Study of a Combined Sliding Disc Bearing and Helical Steel Spring Isolation System", Report NCEER-90-0019, National Center for Earthquake Engineering Research, Buffalo, NY.
- (22) Constantinou, M., Mokha, A. and Reinhorn, A. (1990b), "Teflon Bearings in Base Isolation. II: Modeling", J. Structural Engng., ASCE, Vol. 116, No. 2, 455-474.

- (23) Constantinou, M. C., Soong, T. T. and Dargush, G. F. (1998), *Passive Energy Dissipation Systems for Structural Design and Retrofit*, Monograph, Multidisciplinary Center for Earthquake Engineering Research, Buffalo, NY.
- (24) Constantinou, M. C., Tsopelas, P., Kim, Y-S. and Okamoto, S. (1993), “NCEER-Taisei Corporation Research Program on Sliding Seismic Isolation Systems for Bridges: Experimental and Analytical Study of a Friction Pendulum System (FPS), Report NCEER-93-0020, National Center for Earthquake Engineering Research, Buffalo, NY.
- (25) Davison, R. W., DeBold, T. and Johnson, M. J. (1987), “Corrosion of Stainless Steels”, in Metals Handbook, 9th Edition, Vol. 13, *Corrosion*, American Society for Metals, Metals Park, Ohio.
- (26) Den Hartog, J. P. (1931), “Forced Vibrations with Combined Coulomb and Viscous Friction”, Trans. ASME, Vol. 53 (APM-53-9), 107-115.
- (27) Du Pont (1981), “Teflon-Mechanical Design Data”, E. I. du Pont de Nemours & Co., Polymer Products Department, Wilmington, Delaware.
- (28) Garlock Bearings, Inc. (1987), “DU Self-Lubricating Bearings”, Catalog 781-C, Thorofare, New Jersey.
- (29) Grigorian, C. E. and Popov, E. P. (1993), “Slotted Bolted Connections for Energy Dissipation”, Proc. Seminar on Seismic Isolation, Passive Energy Dissipation, and Active Control, ATC-17-1, Applied Technology Council, Redwood City, CA, Vol. 2, 545-556.
- (30) Heaton, H. T., Hall, J. F., Wald, D. J. and Halling, M. W. (1995), “Response of High-rise and Base-isolated Buildings to a Hypothetical Mw 7.0 Blind Thrust Earthquake,” Science, Vol. 267, 206-211.
- (31) Hofmann, W. (1970), *Lead and Lead Alloys*, Springer-Verlag, Berlin.
- (32) Hwang, J. S., Chang, K. C. and Lee, G. C. (1990), “Quasi-Static and Dynamic Sliding Characteristics of Teflon-Stainless Steel Interfaces”, J. Structural Engineering, ASCE, Vol. 116, No. 10, 2747-2762.
- (33) International Nickel Company (1970), “Corrosion Resistance of the Austenitic Chromium-Nickel Stainless Steels in Atmospheric Environments”, Chromium-Nickel Stainless Steel Data, Section III, Bulletin B, Suffern, NY.
- (34) Jacobsen, F. K. (1977), “TFE Expansion Bearings for Highway Bridges”, Report FHWA-IL-PR-71, Illinois Department of Transportation, Springfield, Illinois, April.

- (35) Kasalanati, A. and Constantinou, M.C. (1999), "Experimental Study of Bridge Elastomeric and Other Isolation and Energy Dissipation Systems with Emphasis on Uplift Prevention and High Velocity Near-Source Seismic Excitation", Report No. MCEER-99-0004, Multidisciplinary Center for Earthquake Engineering Research, Buffalo, NY.
- (36) Kauschke, W. and Baigent, M. (1986), "Improvements in the Long Term Durability of Bearings in Bridges, Especially of PTFE Slide Bearings", Proc. 2nd World Congress on Joint Sealing and Bearing Systems for Concrete Structures, American Concrete Institute, Detroit, Michigan, Publication SP-94, Vol. 2, 577-612.
- (37) Kim, D.K., Mander, J.B. and Chen, S.S. (1996), "Temperature and Strain Effects on the Seismic Performance of Elastomeric and Lead-rubber Bearings," Proc. 4th World Congress on Joint Sealing and Bearing Systems for Concrete Structures, American Concrete Institute, Farmington Hills, Michigan, Publication SP-164, Vol. 1, 309-322.
- (38) Kojima, H. and Fukahori, Y. (1989), "Performance and Durability of High Damping Rubber Bearings for Earthquake Protection", distributed by Bridgestone Corp., Japan with other documentation on its seismic isolation products.
- (39) Krim, J. (1996), "Friction at the Atomic Scale", Scientific American, Vol. 275, No. 4, 74-80, October.
- (40) Lee, D. E. (1993), The Base Isolation of Koeberg Nuclear Power Station 14 Years after Installation", Proc. Post-SMiRT Conference Seminar on Isolation, Energy Dissipation and Control of Vibrations of Structures, Capri, Italy, August.
- (41) Lee, D. J. (1981), "Recent Experience in the Specification, Design, Installation, and Maintenance of Bridge Bearings", Proc. World Congress on Joint Sealing and Bearing Systems for Concrete Structures, American Concrete Institute, Detroit, Michigan, Publication SP-70, Vol. 1, 161-175.
- (42) Lide, D. R. (1993), editor, *Handbook of Chemistry and Physics*, 74th Edition, CRC Press, Boca Raton, Florida.
- (43) Long, J. E. (1969), "The Performance of PTFE in Bridge Bearings", Civil Engineering and Public Works Review, UK, May, 459-462.
- (44) Long, J. E. (1974), *Bearings in Structural Engineering*, J. Wiley & Sons, New York.
- (45) Makison, K. R. and Tabor, D. (1964), "The Friction and Transfer of Polytetrafluoroethylene", Proc. Royal Society A, Vol. 281, 49-61.
- (46) Makris, N. and Constantinou, M. C. (1991), "Analysis of Motion Resisted by Friction: II. Velocity-Dependent Friction", Mech. Struct. & Mach., Vol. 19(4), 501-526.

- (47) Malik, A. H. (1991), "Replacement of Twenty-Year Old Elastomeric Bearings", Proc. 3rd World Congress on Joint Sealing and Bearing Systems for Concrete Structures, Toronto, Ontario, Canada, Vol. 2 of Preprints (published by the National Center for Earthquake Engineering Research, Buffalo, NY), 1109-1120.
- (48) Manning, D. and Bassi, K. (1986), "Bridge Bearing Performance in Ontario", Proc. 2nd World Congress on Joint Sealing and Bearing Systems for Concrete Structures, American Concrete Institute, Detroit, Michigan, Publication SP-94, Vol. 2, 1017-1050.
- (49) Mayrbaurl, R. M. (1986), "High Cycle Bearing Tests for the Manhattan Bridge", Proc. 2nd World Congress on Joint Sealing and Bearing Systems for Concrete Structures, American Concrete Institute, Detroit, Michigan, Publication SP-94, Vol. 1, 343-370.
- (50) Mellon, D. and Post, T. (1999), "Caltrans Bridge Research and Applications of New Technologies", Proceedings of U.S.-Italy Workshop on Seismic Protective Systems for Bridges, Multidisciplinary Center for Earthquake Engineering Research, Buffalo, NY.
- (51) Military Standards (1976), "Dissimilar Metals", MIL-STD-889B, July, Department of Defense.
- (52) Mokha, A. S. , Constantinou, M. C. and Reinhorn, A. M. (1990a), "Experimental Study and Analytical Prediction of Earthquake Response of a Sliding Isolation System with a Spherical Surface", Report NCEER-90-0020, National Center for Earthquake Engineering Research, Buffalo, NY.
- (53) Mokha, A., Constantinou, M. and Reinhorn, A. (1990b), "Teflon Bearings in Base Isolation. I: Testing", J. Structural Engng., ASCE, Vol. 116, No. 2, 438-454.
- (54) Mokha, A., Constantinou, M. C. and Reinhorn, A. M. (1988), "Teflon Bearings in Aseismic Base Isolation: Experimental Studies and Mathematical Modeling", Report NCEER-88-0038, National Center for Earthquake Engineering Research, Buffalo, NY.
- (55) Mokha, A., Constantinou, M. C. and Reinhorn, A. M. (1991), "Further Results on Frictional Properties of Teflon Bearings", J. Structural Engineering, ASCE, Vol. 117, No. 2, 622-626.
- (56) Muller-Rochholz, J. F. W., Fiebrich, M. and Breitbach, M. (1986a), "Measurement of Horizontal Bridge Movements due to Temperature, Wind and Traffic", Proc. 2nd World Congress on Joint Sealing and Bearing Systems for Concrete Structures, American Concrete Institute, Detroit, Michigan, Publication SP-94, Vol. 1, 409-418.

- (57) Muller-Rochholz, J. F. W., Fiebrich, M. and Breitbach, M. (1986b), "Short Time Field Measurements on Bearings of a Steel Bridge", Proc. 2nd World Congress on Joint Sealing and Bearing Systems for Concrete Structures, American Concrete Institute, Detroit, Michigan, Publication SP-94, Vol. 1, 453-464.
- (58) Murota, N., Goda, K., Suzuki, S., Sudo, C. and Suizu, Y. (1994). "Recovery Characteristics of Dynamic Properties of High Damping Rubber Bearings." Proc. 3rd U.S.-Japan Workshop on Earthquake Protective Systems for Bridges, January, Berkeley, CA, Report No. NCEER-94-0009, National Center for Earthquake Engineering Research, Buffalo, NY.
- (59) Nakano, O., Nishi, H., Shirono, T. and Kumagai, K. (1993), "Temperature-Dependence of Base-Isolated Bearings", Proc. 2nd U.S.-Japan Workshop on Earthquake Protective Systems for Bridges, Technical Memorandum No. 3196 , Public Works Research Institute, Tsukuba Science City, Japan.
- (60) Nelson, W. (1990), *Accelerated Testing*, J. Wiley & Sons, New York.
- (61) Pavot, B. and Polust E. (1979), "Aseismic Bearing Pads", *Tribology International*, Vol. 13, No. 3, 107-111.
- (62) Paynter, F. R. (1973), "Investigation of Friction in PTFE Bridge Bearings", *The Civil Engineer in South Africa*, August, 209-217.
- (63) Predicting Bearing Wear (1968), Reprint No. 34, *The Journal of Teflon*, E. I. du Pont de Nemours and Company, Wilmington, Delaware.
- (64) Rabinowicz, E. (1995), *Friction and Wear of Materials*, J. Wiley & Sons, Inc., New York.
- (65) Roeder, C.W., Stanton, J.F. and Taylor, A.W. (1987), "Performance of Elastomeric Bearings", Report No. 298, National Cooperative Highway Research Program, Transportation Research Board, Washington, D.C.
- (66) Romanoff, M. (1957), "Underground Corrosion", National Bureau of Standards, Circular 579, Department of Commerce, Washington, DC.
- (67) Sarkar, A. D. (1980), *Friction and Wear*, Academic Press, London, UK.
- (68) Shames, I. H. and Cozzarelli, F. A. (1992), *Elastic and Inelastic Stress Analysis*, Prentice Hall, Englewoods Cliffs, New Jersey.
- (69) Skinner, R.I., Robinson, W.H. and McVerry, G.H. (1993), *An Introduction to Seismic Isolation*, John Wiley and Sons, Chichester, UK.

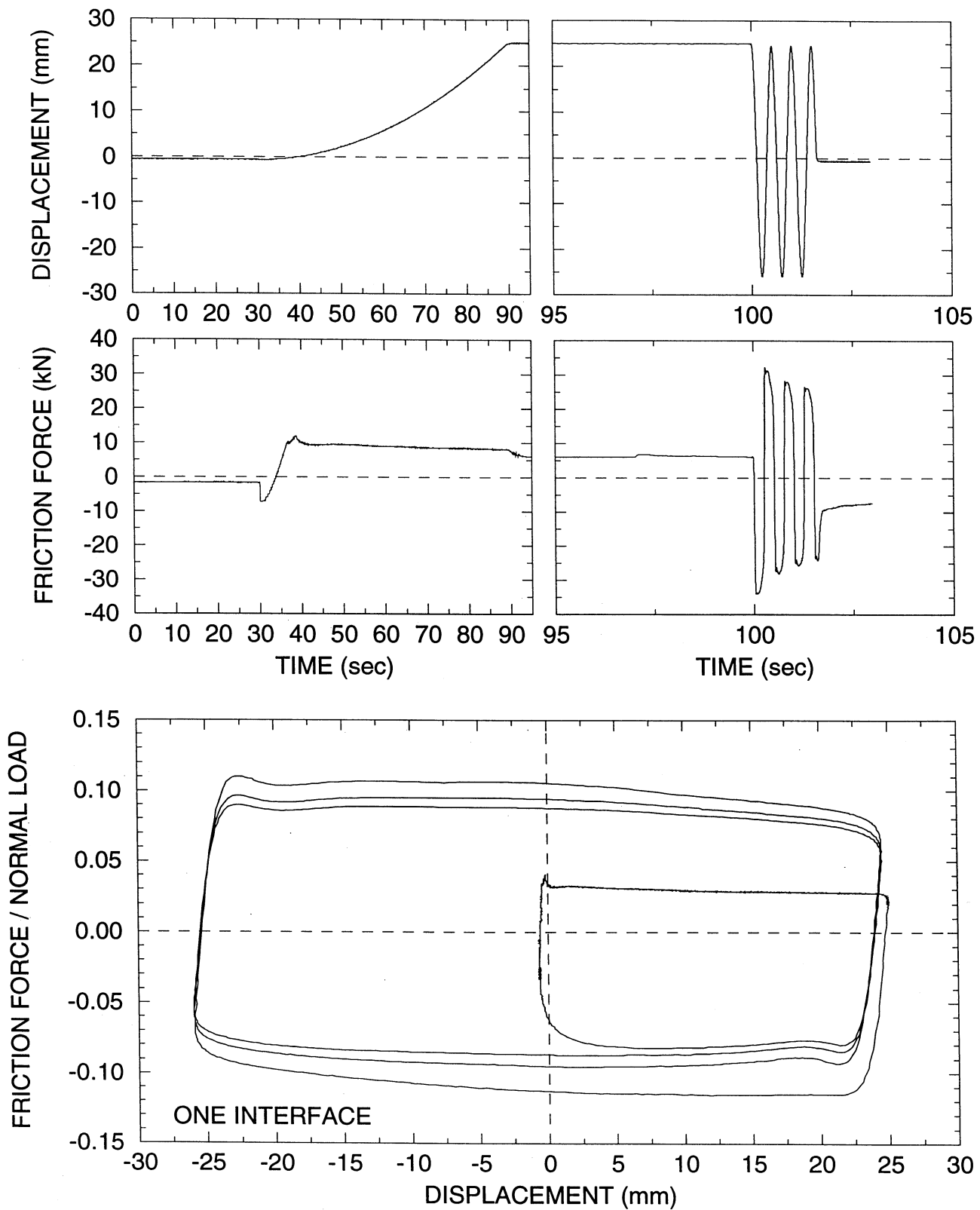
- (70) Soong, T. T. and Constantinou, M. C. (editors) (1994), *Passive and Active Structural Vibration Control in Civil Engineering*, CISM Course and Lectures No. 345, Springer-Verlag, Wien- New York.
- (71) Soong, T. T. and Dargush, G. F. (1997), *Passive Energy Dissipation Systems in Structural Engineering*, J. Wiley & Sons, London, UK.
- (72) Stanton, J. F. and Roeder, C. W. (1982), "Elastomeric Bearings Design, Construction, and Materials", NCHRP Report 248, Transportation Research Board, Washington, D.C.
- (73) Stevenson, A. and Price, A. R. (1986), "A Case Study of Elastomeric Bridge Bearings After 20 Years Service", Proc. 2nd World Congress on Joint Sealing and Bearing Systems for Concrete Structures, American Concrete Institute, Detroit, Michigan, Publication SP-94, Vol. 1, 113-136.
- (74) Tabor, D. (1981), "Friction-The Present State of Our Understanding", J. Lubrication Techn., ASME, Vol. 103, 169-178.
- (75) Taylor, A. W., Lin, A. N. and Martin, J. W. (1992), "Performance of Elastomers in Isolation Bearings: A Literature Review", Earthquake Spectra, Earthquake Engineering Research Institute, Oakland, CA, Vol. 8, No. 2, 279-303.
- (76) Taylor, M. E. (1972), "PTFE in Highway Bridge Bearings", Report LR 491, Transport and Road Research Laboratory, Department of the Environment, UK.
- (77) Thompson, A. C. T., Whittaker, A. S., Fenves, G. L. and Mahin, A. A. (2000), "Property Modification Factors for Elastomeric Seismic Isolation Bearings", Proc. 12th World Congress on Earthquake Engineering, New Zealand.
- (78) Thompson, J. B., Turrell, G. C. and Sandt B. W. (1955), "The Sliding Friction of Teflon", SPE Journal, Vol.11(4), 13-14.
- (79) Transportation Research Board (1977), "Bridge Bearings", NCHRP Report 41, Washington, DC.
- (80) Transportation Research Board (1989), "Pot Bearings and PTFE Surfaces", Research Results Digest, No. 171, Washington, DC, September.
- (81) Tsopelas, P., Constantinou, M. C., Kim, Y-S. and Okamoto, S. (1996), "Experimental Study of FPS System in Bridge Seismic Isolation", Earthquake Engineering and Structural Dynamics, Vol. 25, 65-78.
- (82) Tsopelas, P., Constantinou, M. C., Okamoto, S., Fujii, S. and Ozaki, D. (1996), "Experimental Study of Bridge Seismic Sliding Isolation Systems", Engineering Structures, Vol. 18, No. 4, 301-310.

- (83) Tsopelas, P., Okamoto, S., Constantinou, M. C., Ozaki, D. and Fujii, S. (1994), "NCEER-Taisei Corporation Research Program on Sliding Seismic Isolation Systems for Bridges: Experimental and Analytical Study of Systems Consisting of Sliding Bearings, Rubber Restoring Force Devices and Fluid Dampers", Report NCEER-94-0002, National Center for Earthquake Engineering Research, Buffalo, NY.
- (84) Tyler, R. G. (1977), "Dynamic Tests on PTFE Sliding Layers under Earthquake Conditions", Bulletin of the New Zealand National Society for Earthquake Engineering, Vol. 10, No. 3, September, 129-138.
- (85) Wolff, E. (1999), "Frictional Heating in Sliding Bearings and an Experimental Study of High Friction Materials," M.S. Thesis, University at Buffalo, Buffalo, NY.
- (86) Xanthakos, P. P. (1994), *Theory and Design of Bridges*, John Wiley & Sons, New York.
- (87) Yoshizawa, H. and Israelachvilli, J. (1993), "Fundamental Mechanisms of Interfacial Friction. 2. Stick-Slip Friction of Spherical and Chain Molecules", J. Phys. Chem., Vol. 97, 11300-11313.

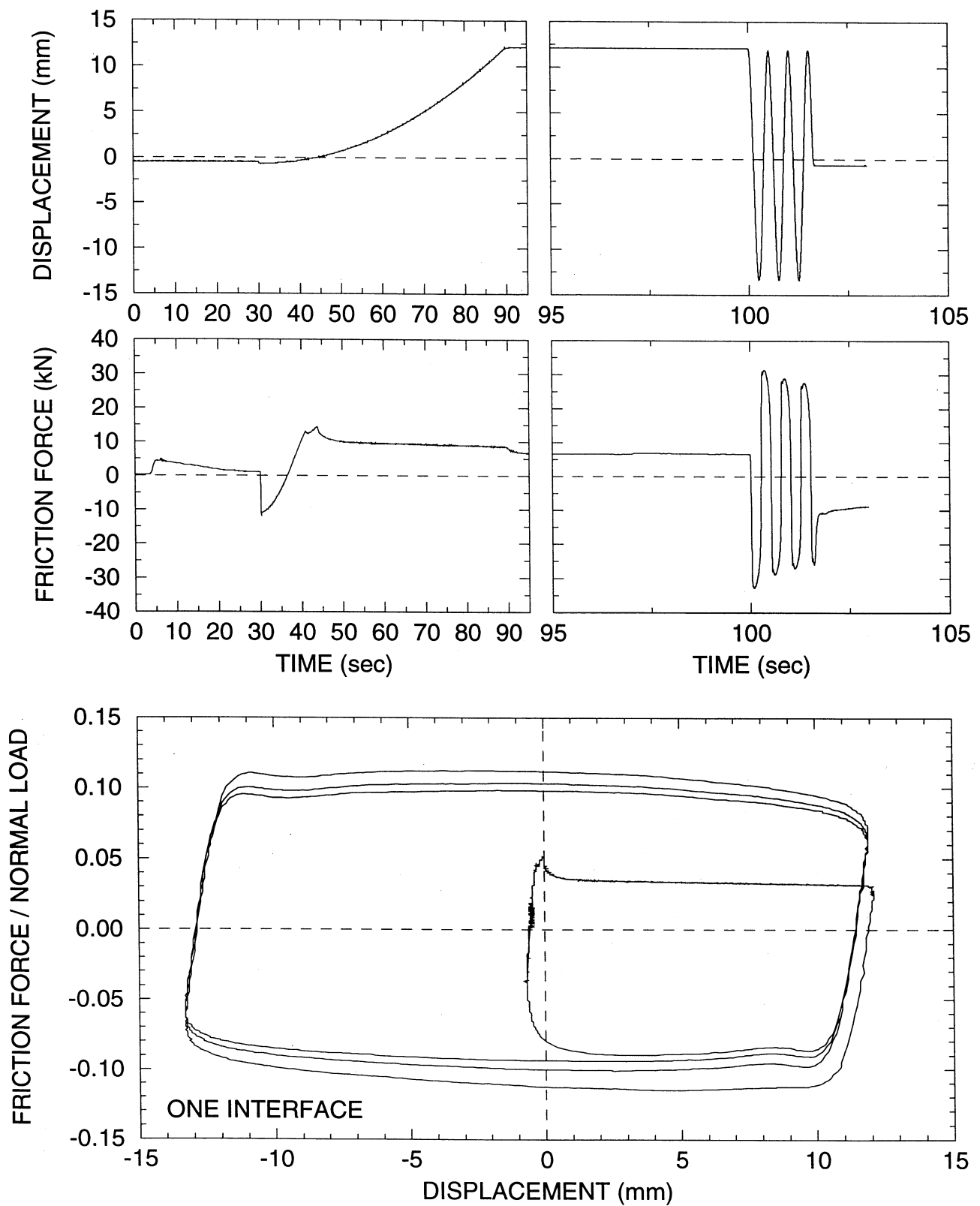
APPENDIX A

Sample of Experimental Results in Testing of Sliding Interfaces for Determining Temperature Effects on Frictional Properties

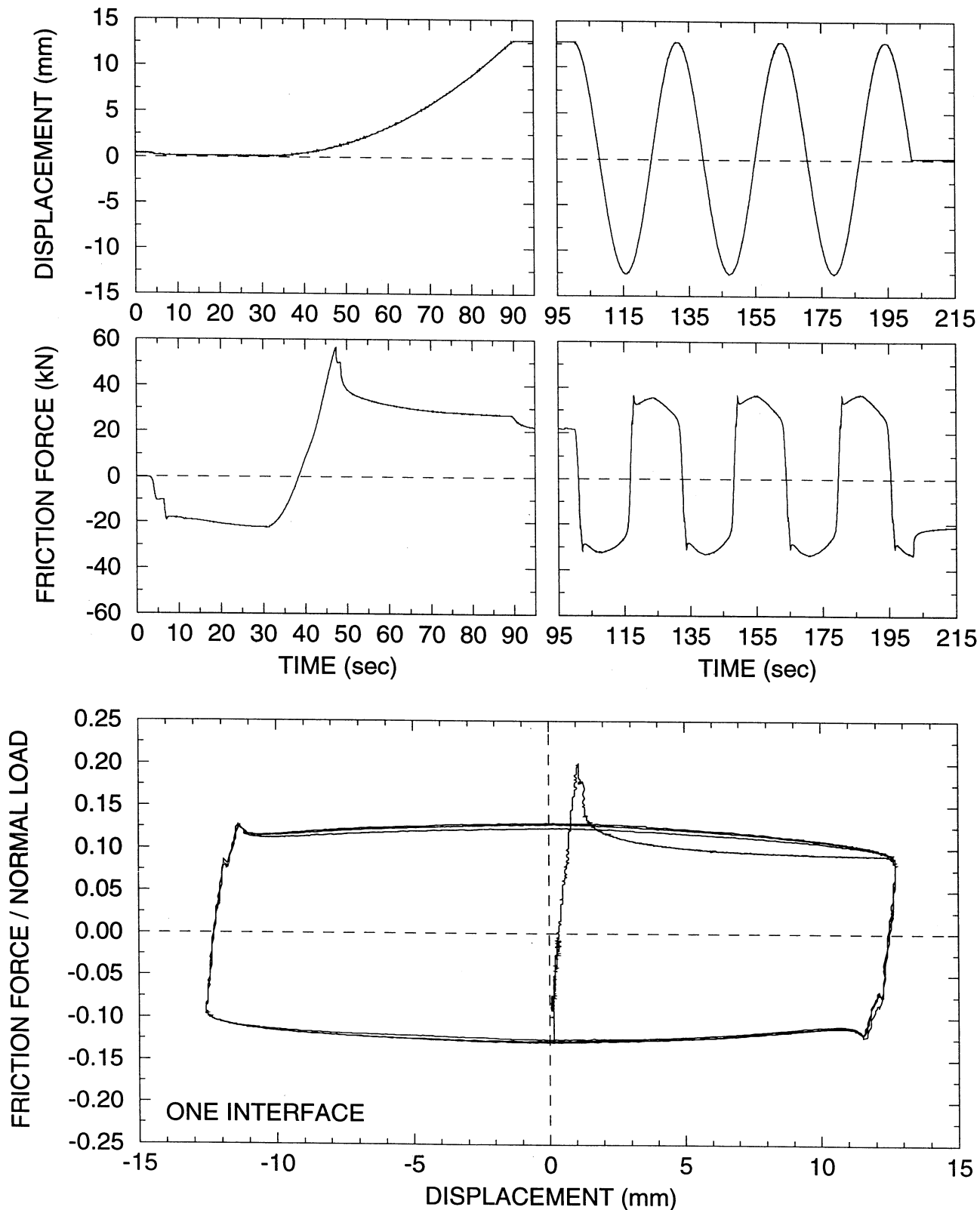
UF-TEST43A: 20.7 MPa: SIN: 2 Hz: P: 22 C



UF-TEST44: 20.7 MPa: SIN: 2 Hz: P: 21 C



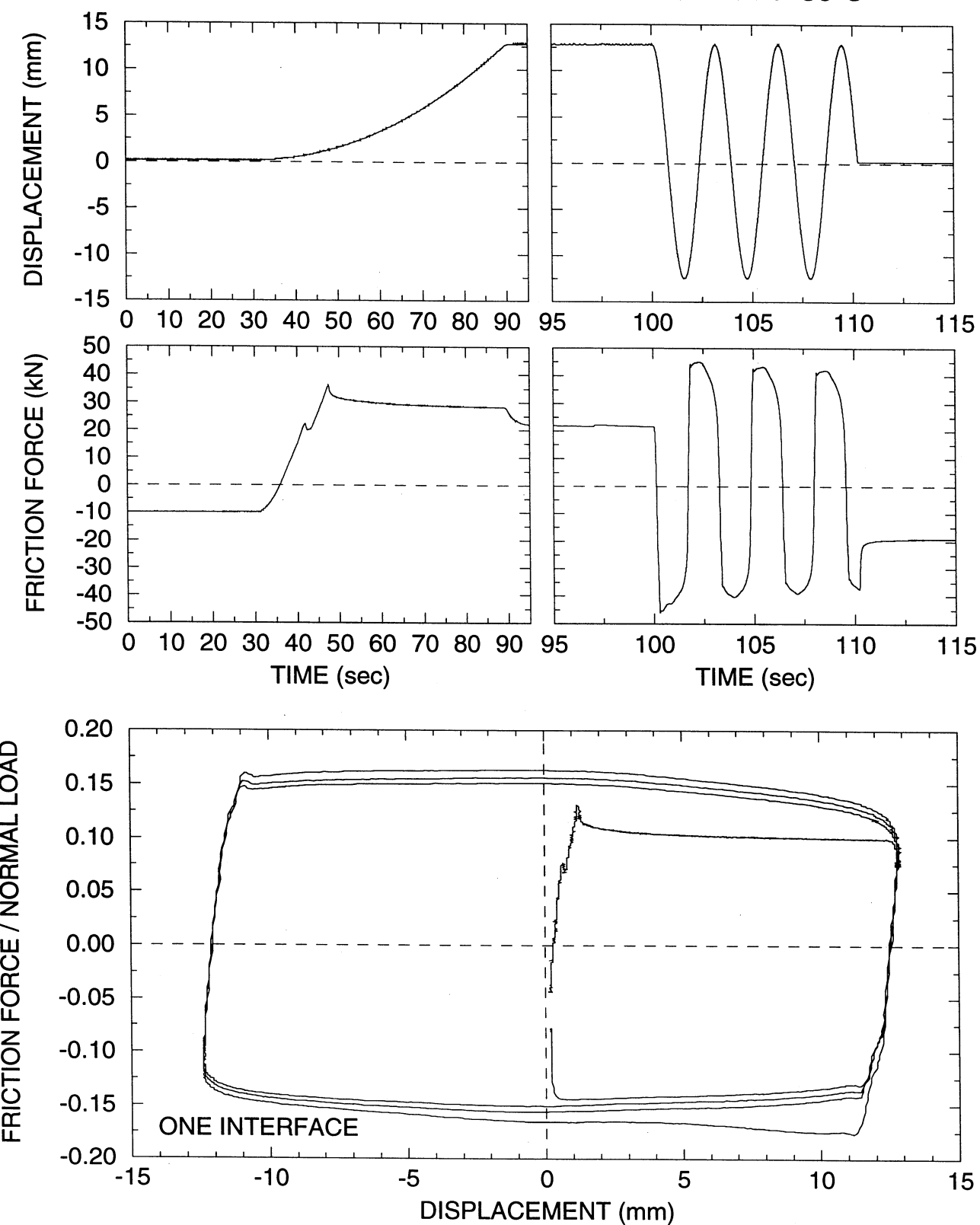
UF-TEST58: 20.7 MPa: SIN: 0.0318 Hz: P: -42 C



@Seismic¹⁵¹isolation

Telegram Channel: @Seismicisolation

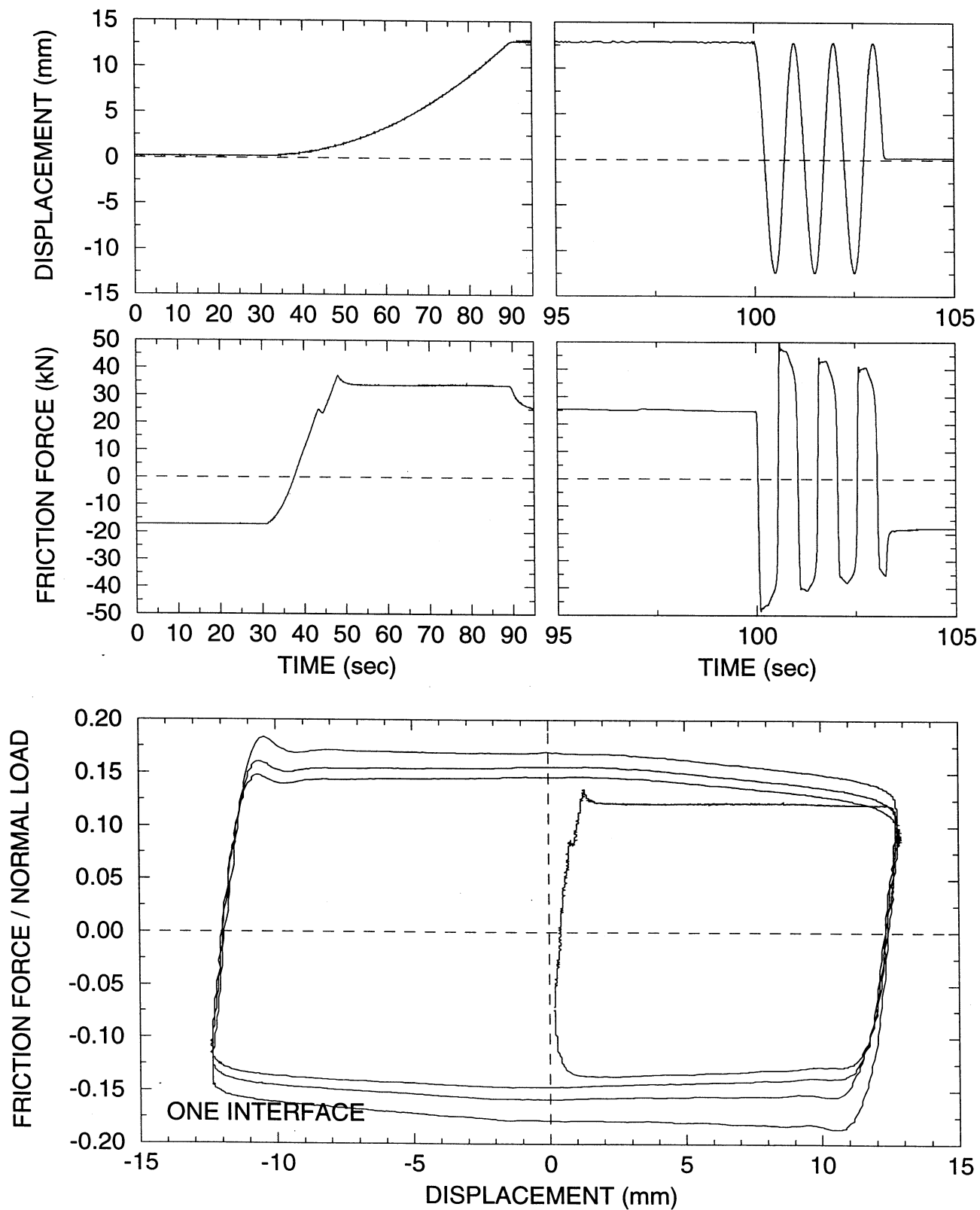
UF-TEST59: 20.7 MPa: SIN: 0.318 Hz: P: -39 C



@Seismic¹⁵²isolation

Telegram Channel: @Seismicisolation

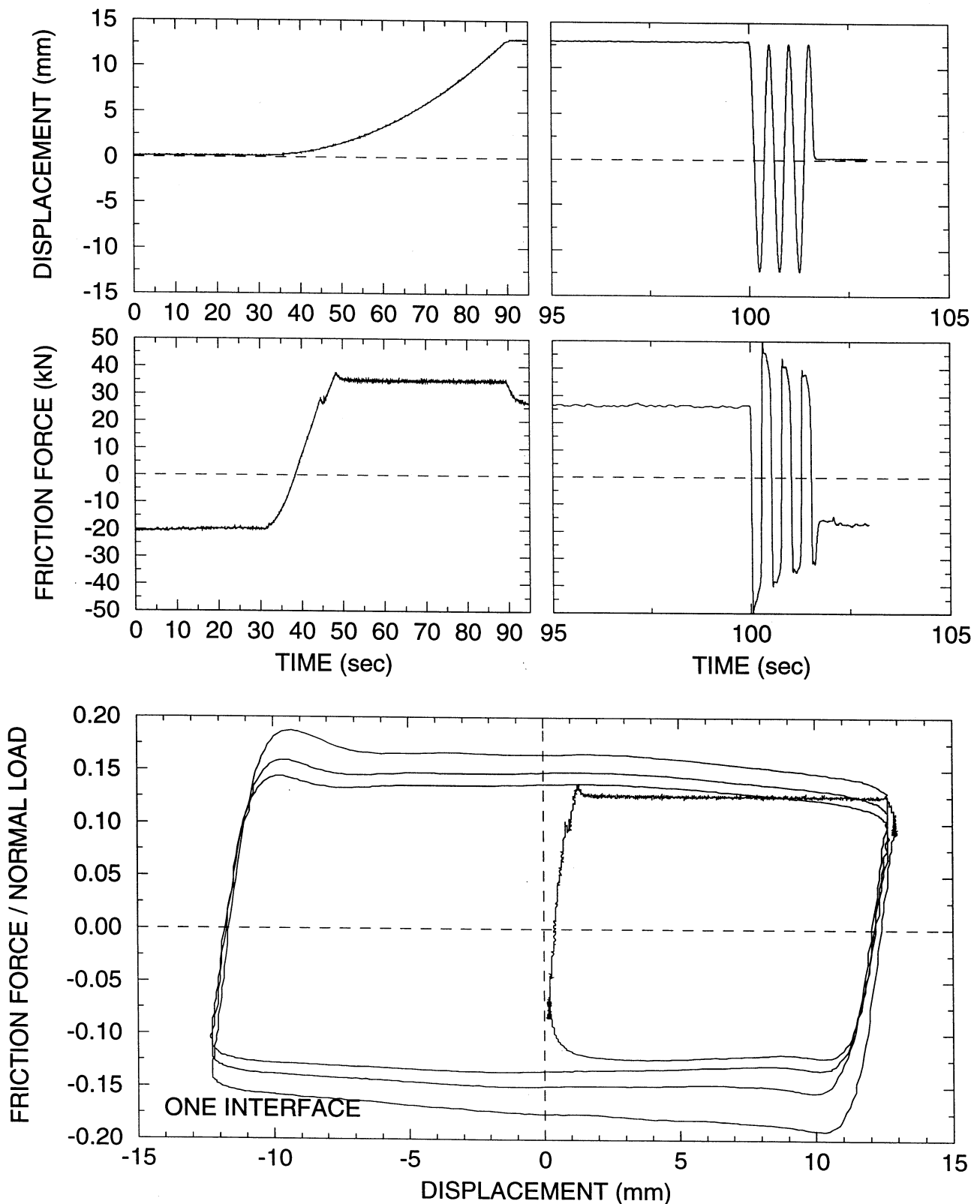
UF-TEST60: 20.7 MPa: SIN: 1 Hz: P: -39 C



@Seismic¹⁵³isolation

Telegram Channel: @Seismicisolation

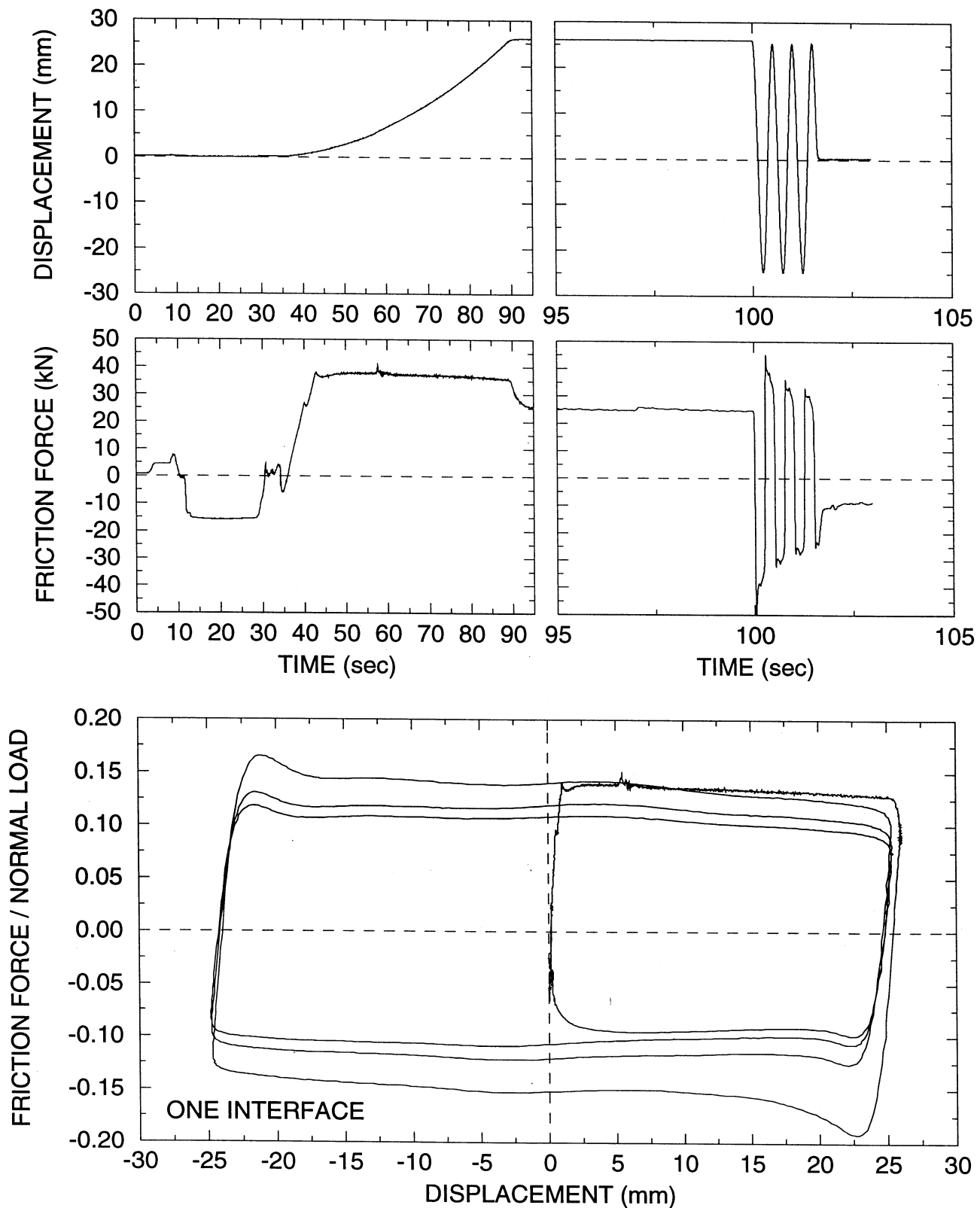
UF-TEST61: 20.7 MPa: SIN: 2 Hz: P: -38 C



@Seismic¹⁵⁴isolation

Telegram Channel: @Seismicisolation

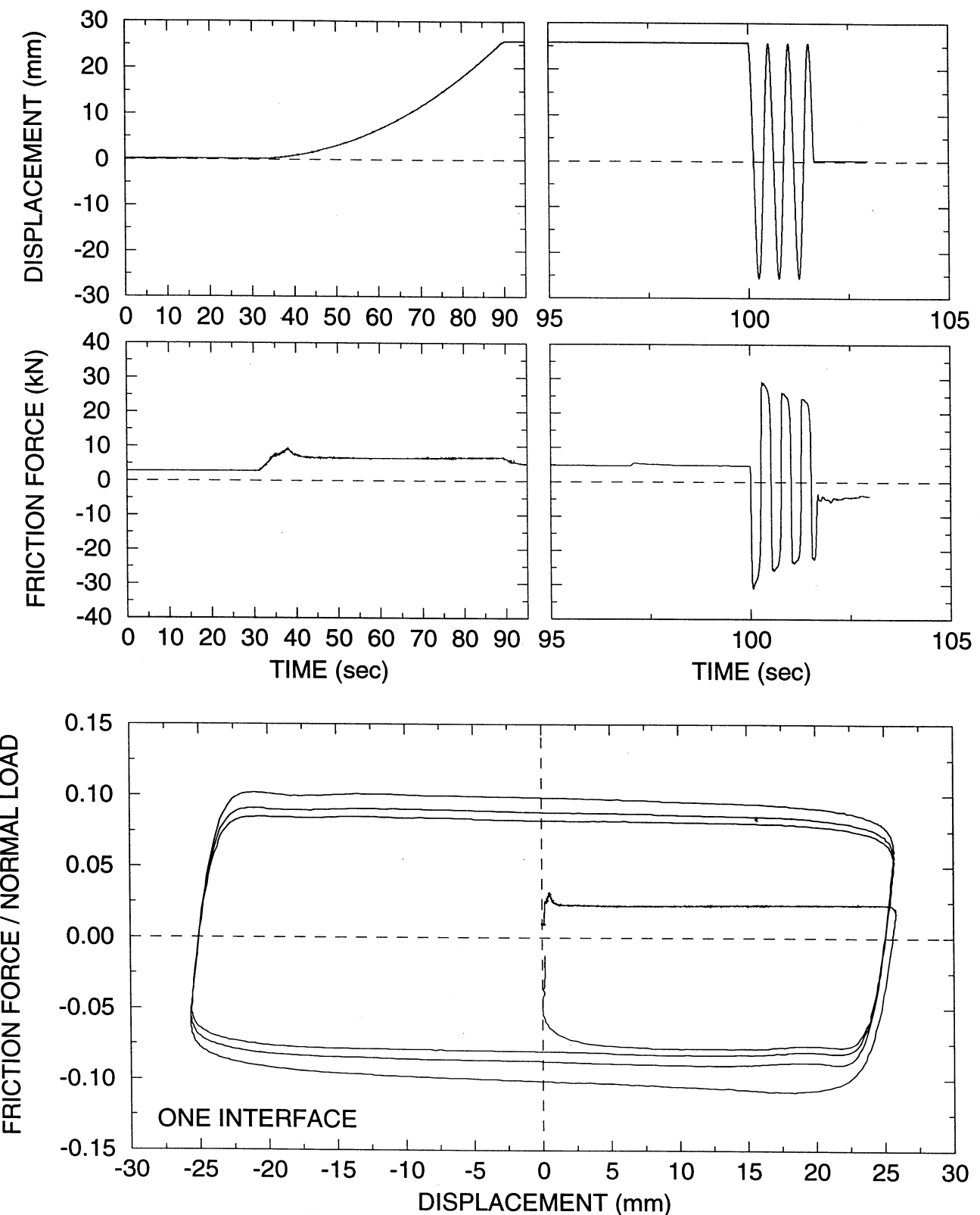
UF-TEST62: 20.7 MPa: SIN: 2 Hz: P: -40 C



@Seismic¹⁵⁵isolation

Telegram Channel: @Seismicisolation

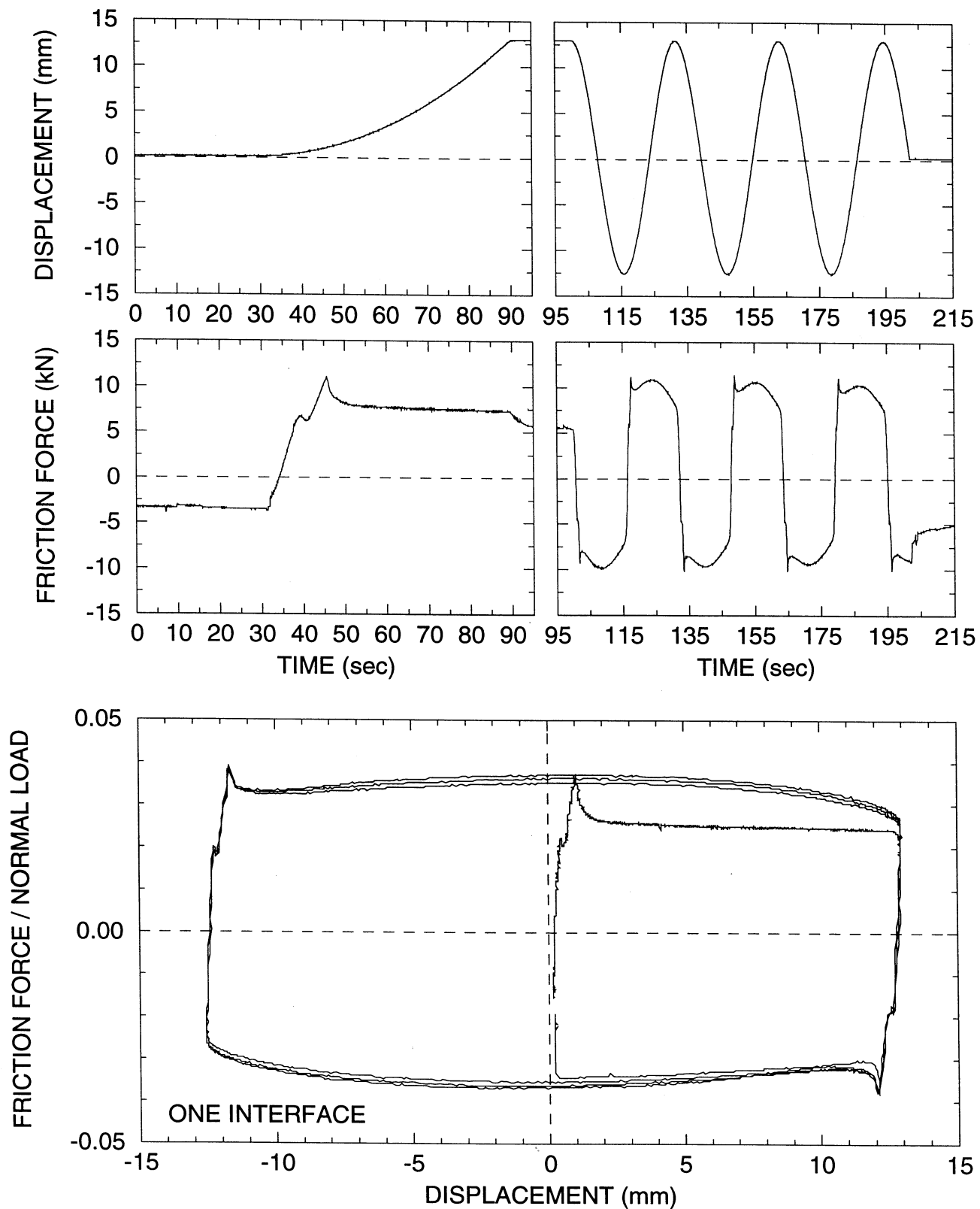
UF-TEST92: 20.7 MPa: SIN: 2 Hz: P: 50 C



@Seismic¹⁵⁶isolation

Telegram Channel: @Seismicisolation

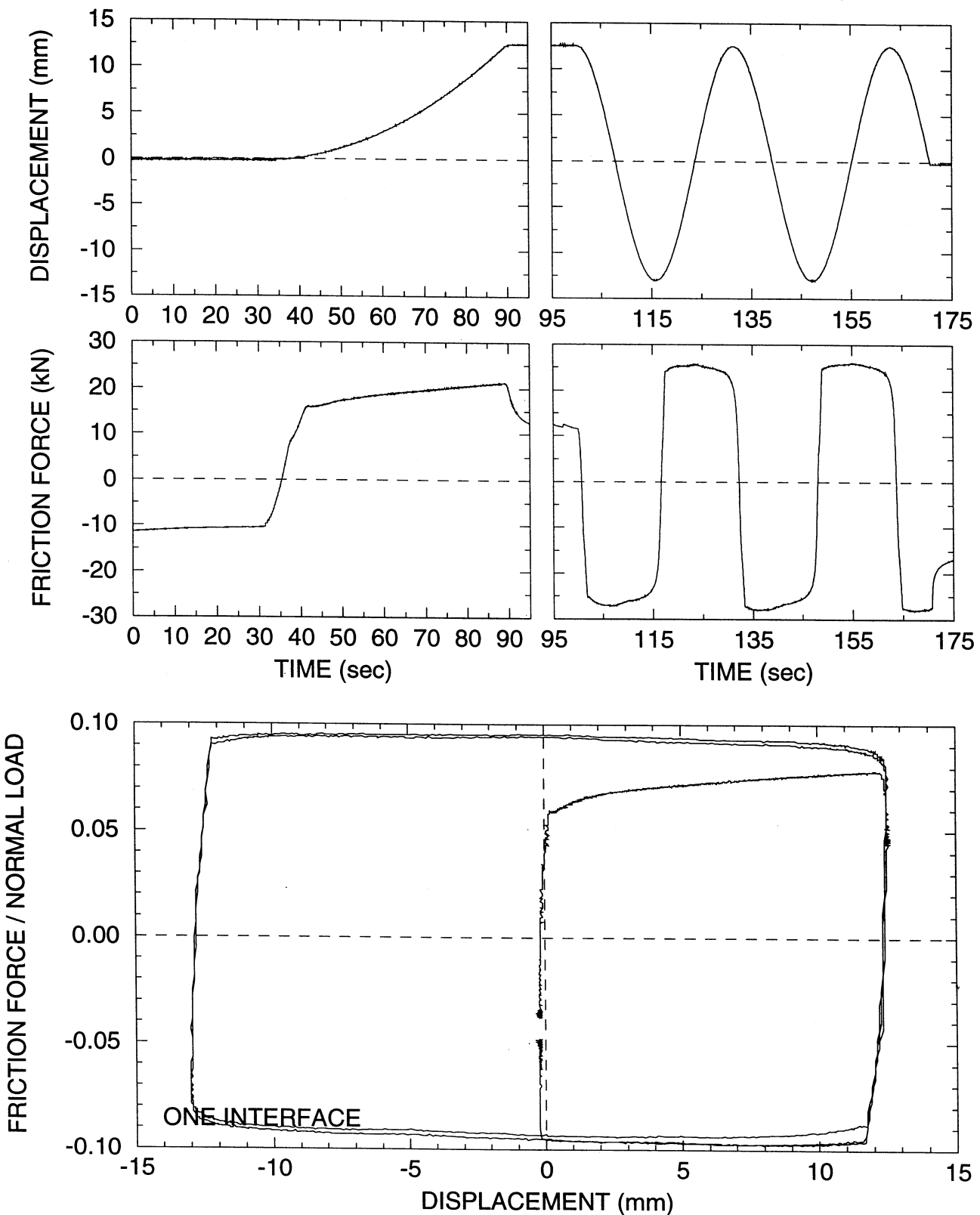
UF-TEST94: 20.7 MPa: SIN: 0.0318 Hz: P: 49 C



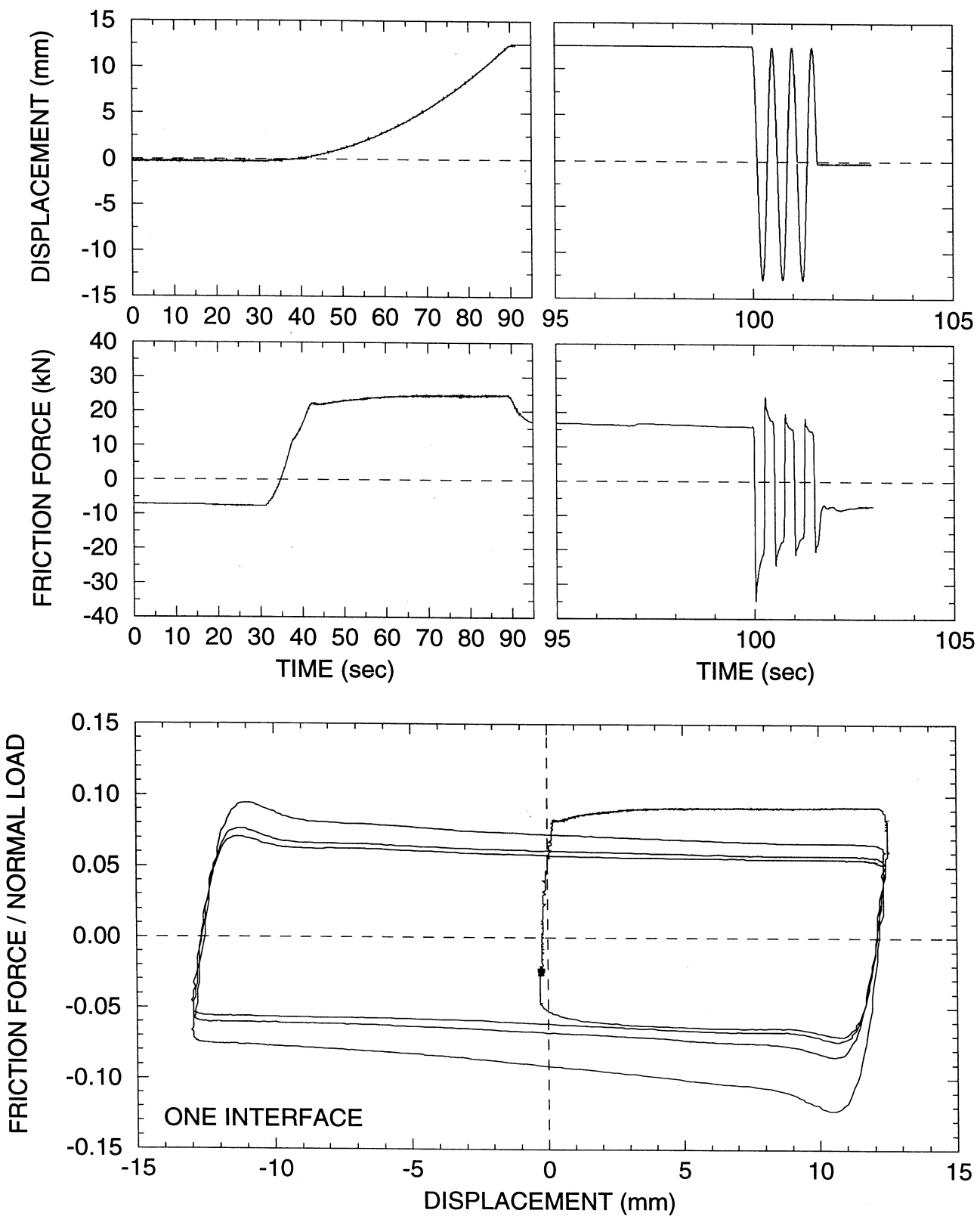
@Seismic¹⁵⁷isolation

Telegram Channel: @Seismicisolation

C1TEST11: 69 MPa: SIN: 0.0318 Hz: P: -49 C



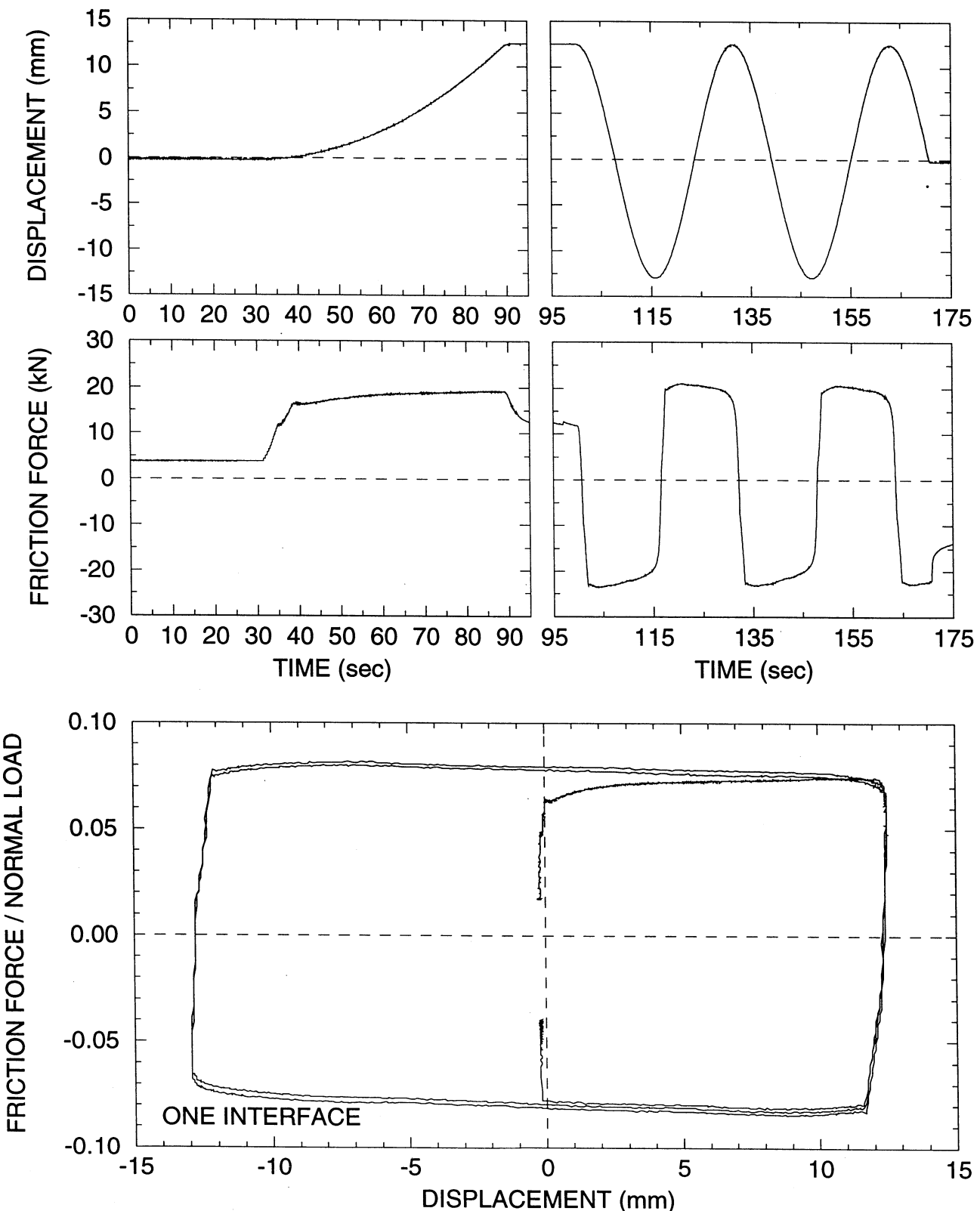
C1TEST14: 69 MPa: SIN: 2 Hz: P: -53 C



@Seismic¹⁵⁹isolation

Telegram Channel: @Seismicisolation

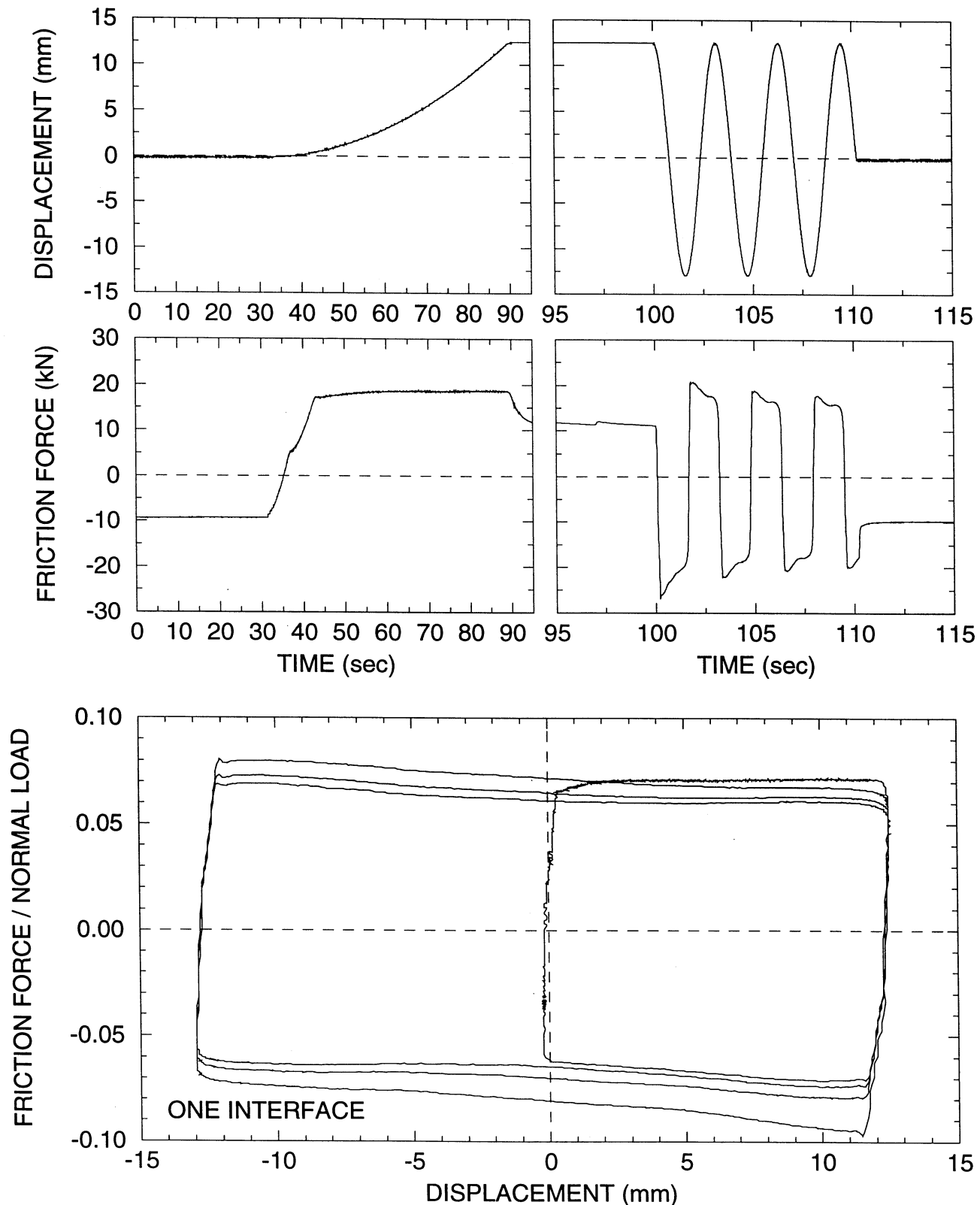
C1TEST16: 69 MPa: SIN: 0.0318 Hz: P: -43 C



@Seismic¹⁶⁰isolation

Telegram Channel: @Seismicisolation

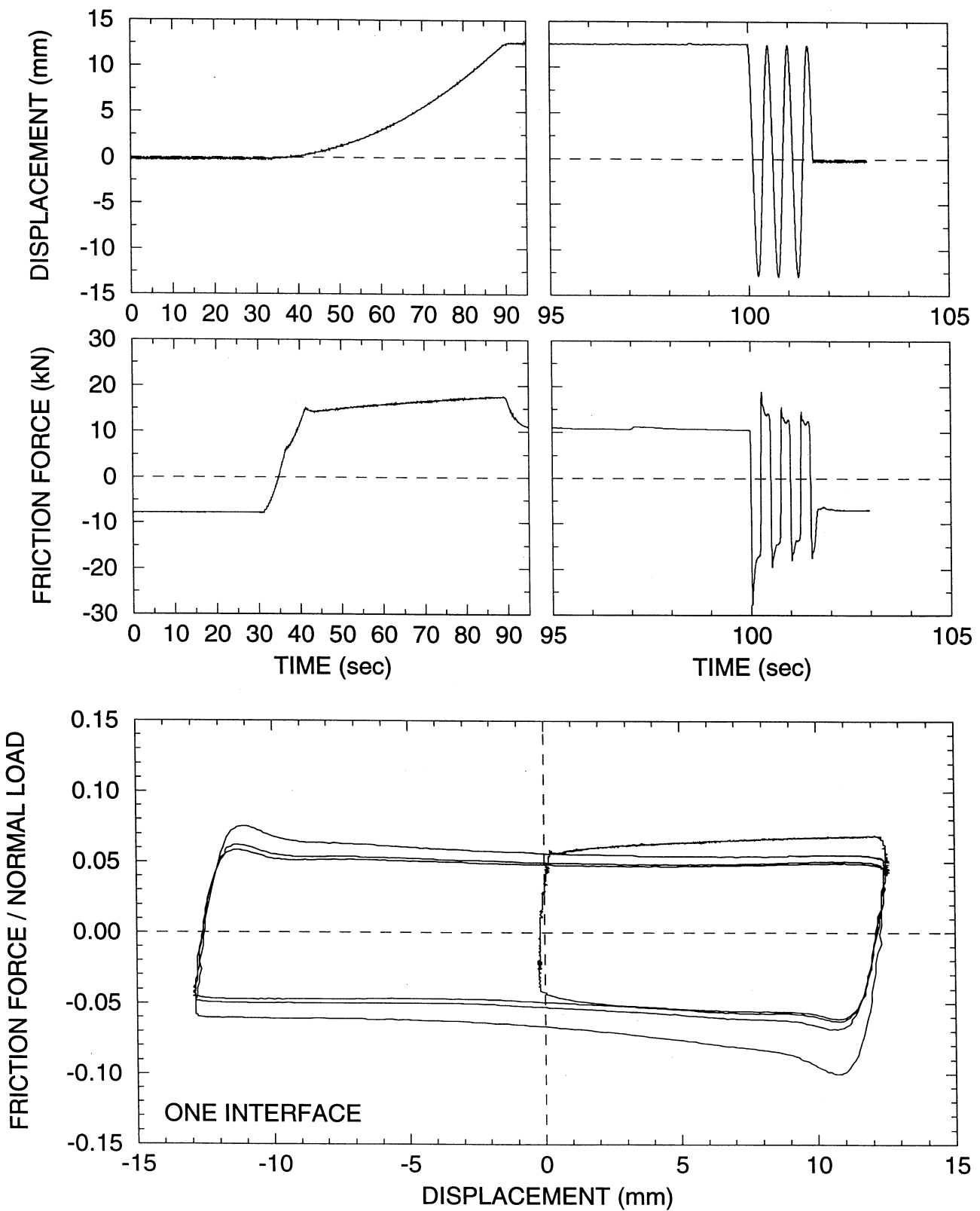
C1TEST17: 69 MPa: SIN: 0.318 Hz: P: -41 C



@Seismic¹⁶¹isolation

Telegram Channel: @Seismicisolation

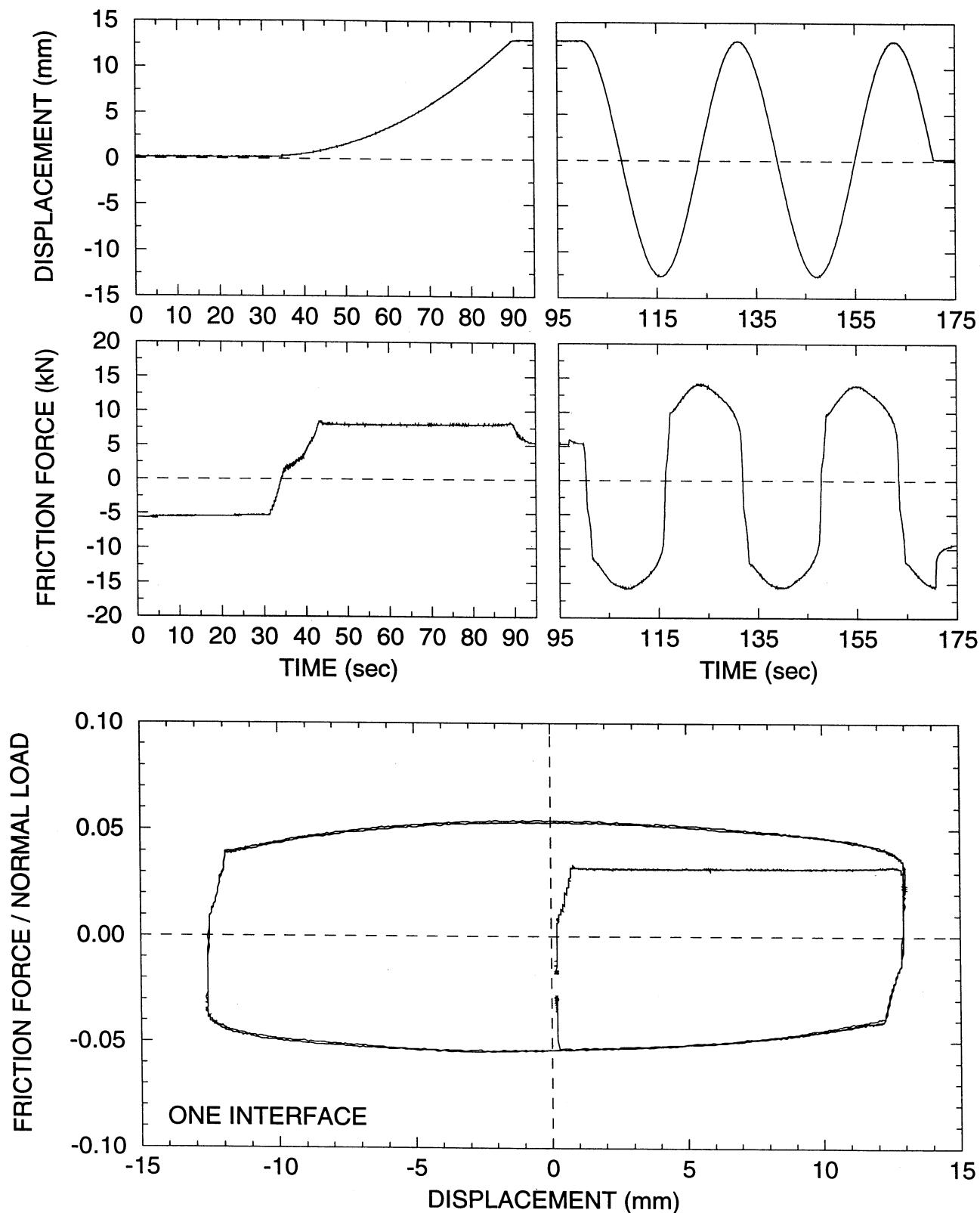
C1TEST19: 69 MPa: SIN: 2 Hz: P: -38 C



@Seismic¹⁶²isolation

Telegram Channel: @Seismicisolation

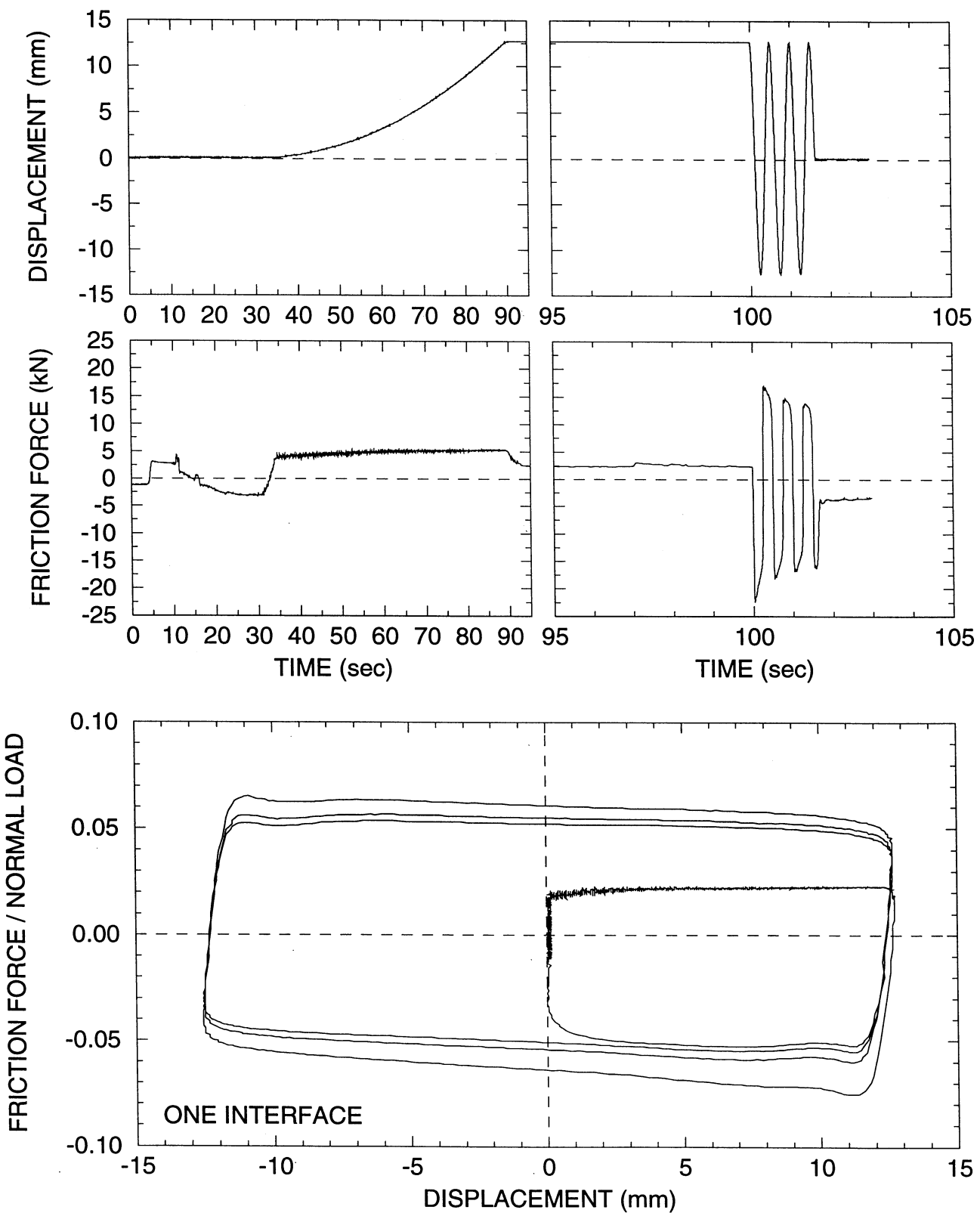
C1S3T192: 69 MPa: SIN: 0.0318 Hz: P: 24 C



@Seismicisolation¹⁶³

Telegram Channel: @Seismicisolation

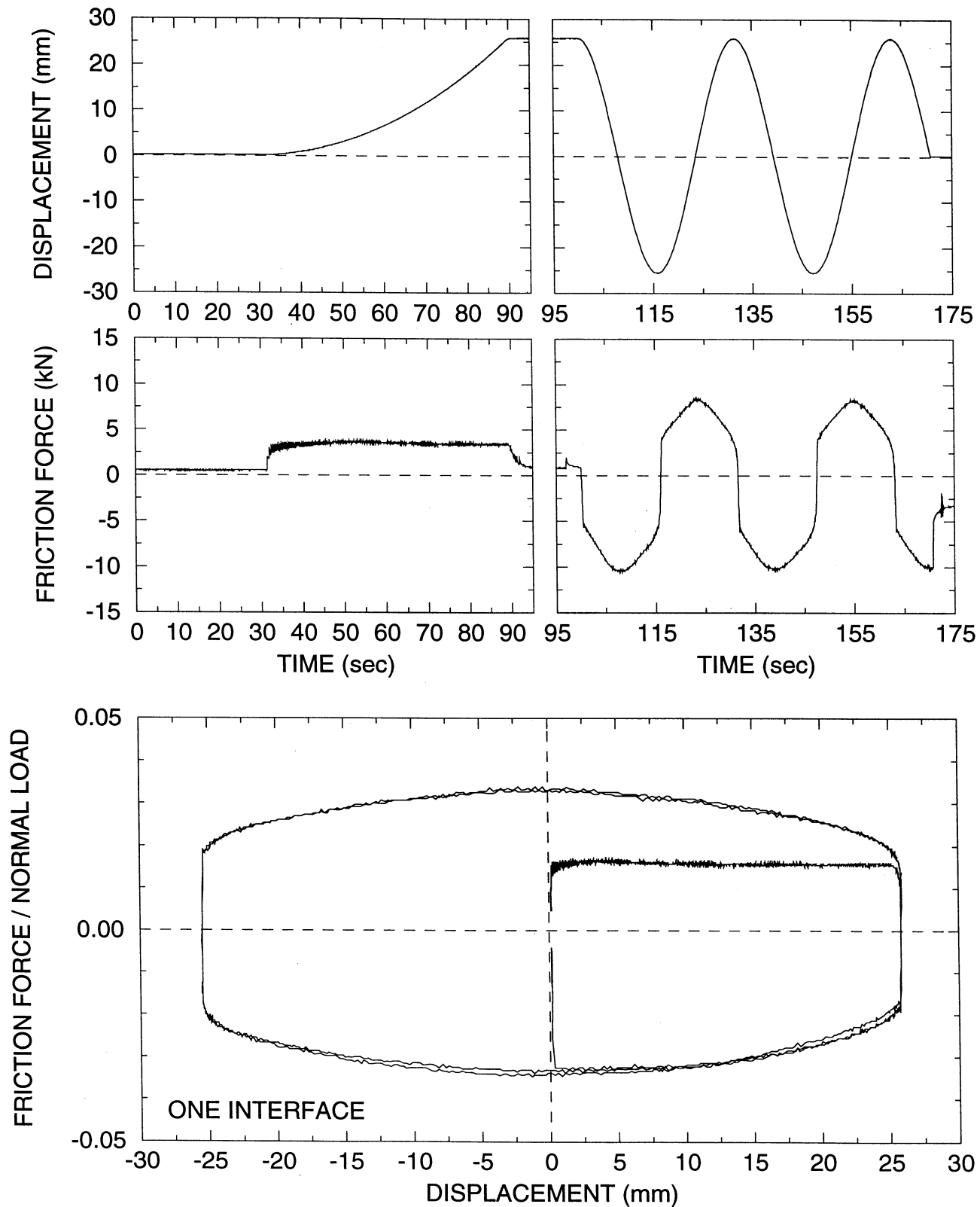
C1TESW86: 69 MPa: SIN: 2 Hz: P: 23 C



@Seismic¹⁶⁴isolation

Telegram Channel: @Seismicisolation

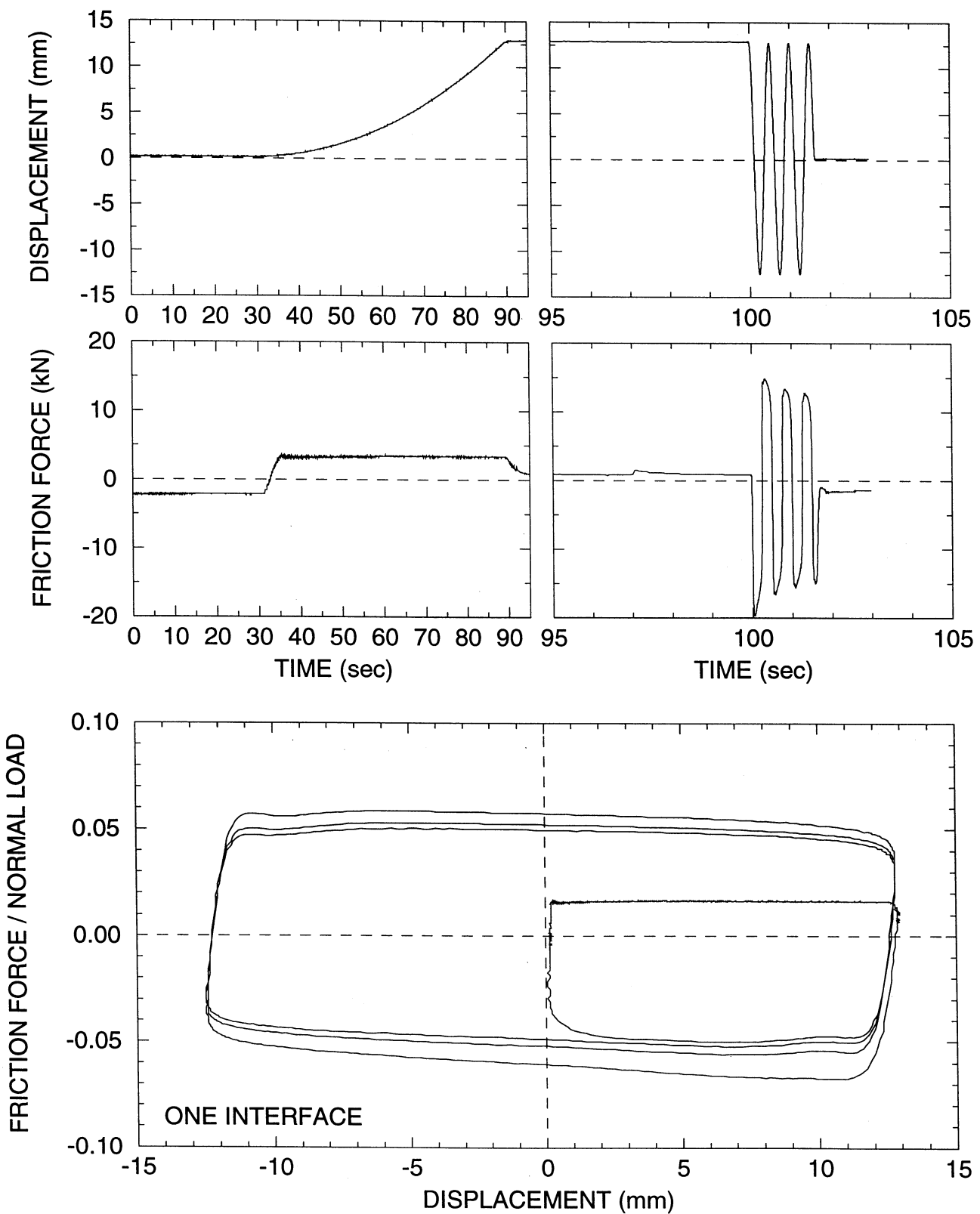
C1TEST68: 69 MPa: SIN: 0.0318 Hz: P: 50 C



@Seismic¹⁶⁵isolation

Telegram Channel: @Seismicisolation

C1TEST72: 69 MPa: SIN: 2 Hz: P: 52 C



@Seismic¹⁶⁶isolation

Telegram Channel: @Seismicisolation



ISSN 1520-295X

@Seismicisolation

Telegram Channel: @Seismicisolation